FIELD AND LABORATORY EXPERIMENTS IN ROCK MECHANICS

A thesis submitted for the degree of

DOCTOR OF PHILOSOPHY

in

The Australian National University

by

EARL R. HOSKINS Jr.

Department of Geophysics and Geochemistry
Research School of Physical Sciences
Institute of Advanced Studies

July 1967

FIELD AND LABORATORY EXPERIMENTS IN ROCK MECHANICS

CONTENTS

STATEMENT

Two of the published papers submitted as a portion of this thesis were done in collaboration with Professor Jaeger. In these studies I did the experimental work, Professor Jaeger derived the equations given in the appendix to appendix 3 and the discussion was developed jointly. All of the other work presented in this thesis is entirely my own apart from assistance given by

(i) Mr E. Pederson and Mr A. Powell who prepared the rock specimens tested in the laboratory experiments;

(ii) Mr W. McIntyre and Mr J.H. Angus and other technical staff of the Research School of Physical Sciences workshop who constructed some of the various pieces of apparatus used in these experiments;

(iii) Mr G. Milburn who prepared the thin and polished sections of rock.

Their help is gratefully acknowledged.

Acknowledgements are also due to Mt. Isa Mines Ltd. for their generous hospitality and assistance with the underground stress measurements.

It is a pleasure to record my thanks to Professor J.C. Jaeger for originally suggesting this study and for his helpful advice and criticism throughout his supervision of this work.

Earl R Hoskins

Earl R. Hoskins

LIST OF TABLES

LIST OF FIGURES

Chapter I

INTRODUCTION

The basic work undertaken in this thesis was a rock mechanics investigation of a portion of the Mt Isa mine, Mt Isa, Queensland, Australia. Both "in situ" measurements and laboratory tests were made. During the course of this study it was often necessary to develop or at least investigate the various measurement, analysis, and testing techniques in the laboratory under controlled conditions in uniform experimental materials before they could be applied with any confidence to the unkown and variable conditions and materials found at Mt. Isa. This development and testing work is presented as an integral part of the thesis, as the Mt Isa experiments could not proceed until the development work was done, and the analysis of the Mt Isa work depends in large measure upon these laboratory investigations.

The term "rock mechanics" has recently been defined by the Committee on Rock Mechanics of the Geological Society of America in the following manner:

> "Rock mechanics is the theoretical and applied science of the mechanical behaviour of rock; it is that branch of mechanics concerned with the response of rock to the force fields of its physical environment."[1]

---

[1] W.R. Judd, State of Stress in the Earths Crust (Elsevier, 1964) page 7.

Workers in the subject, then, whether physicists, geophysicists, geologists, or engineers, are concerned primarily with two problems:

(1) determining the force fields of a particular physical environment, and

(2) measuring, understanding and perhaps predicting the response of the rock present to some specified change in these force fields.

These two problems must be solved whether one is working on the mechanism of deformation of a fine grained monomineralic rock at high temperatures and pressures, trying to predict the occurrence of the next major earthquake in an active fault zone, or designing a mining extraction sequence.

Rock mechanics as a science is quite young, certainly less than a century old. As an art it has been practiced by definition since the stone age. The overwhelming majority of scientific papers and publications on the subject have appeared in the last 20 years and the definition of the subject given above was written only in 1963. Because the field is so new our fund of basic rock mechanics knowledge is still fragmentary and imperfect. Much of the applied rock mechanics work that is being done today must of necessity be based on poorly tested assumptions concerning both the force fields existing in nature and the response of rock to these and other induced force fields.

This particular rock mechanics investigation at Mt Isa was intended to be fairly complete and it included both measurements of the stress field acting in this portion of the mine and measurements of the strength and elastic properties of the various rocks that are present. At nearly every step of the investigation it was necessary to retreat into the laboratory to make more basic investigations under controlled conditions. The first portion of the thesis, Chapters II through V, describes laboratory experiments on the failure of rocks under complex polyaxial stresses. The rock surrounding an underground excavation is certainly not in a state of uniform uniaxial or triaxial compression or tension. The stress perpendicular to the surface of the opening is zero, (or really one atmosphere, approximately 14.7 psi. This will be taken as zero in both the laboratory and underground strength and stress measurements reported in this thesis). The other two principal stresses may be either tensile or compressive and may bear nearly any relationship to each other. The failure criteria commonly used in rock mechanics have, however, in the main been derived from laboratory tests in which two of the stresses in a sample are held equal while the third stress is varied until the specimen fails. It has often been assumed (c.f. Brace [1964], and Obert and Duvall [1967]) that the intermediate principal stress has little or no effect on the failure strength of rock.

The experiments reported in Chapters II through V show that this assumption can be wrong, especially in stress fields similar to those around an underground opening.

Chapters VI through VIII deal with laboratory investigations of several stress measurement systems. These were full scale tests in which large blocks of rock were loaded to specified stress levels and held there while the different stress measurement techniques were tried in the blocks. The results of the tests were then compared with the known applied stresses. Full scale tests such as these were necessary because they were the only way that it was possible to study directly such problems as the effect of creep on flatjack measurements, or the effect of a stress component acting parallel to the borehole axis on strain rosette relief techniques. The laboratory tests made it possible to study the use of flatjacks to measure an "in situ" modulus for rock and also to empirically determine which of the different techniques of determining elastic moduli of rock gives the best value to use in analyzing the borehole deformation gage and borehole strain rosette relief measurements. In addition of course, many minor practical problems in equipment, techniques, and analysis were found and solved in the full scale laboratory tests and this made the underground work simpler and more efficient.

Chapters IX through XII deal with the underground work at Mt Isa and the laboratory investigations of the properties of the

rocks collected at Mt Isa. The three stress measurement techniques studied in the laboratory were used at Mt Isa and the results are analyzed, compared, and discussed in Chapter X. Chapter XI gives a comparison, of the "in situ" and laboratory determined values of elastic moduli. The strength of the Mt Isa rocks determined by both the conventional uniaxial and triaxial tests, and some of the more complex systems given in Chapters II through V, have been given in Chapter XII, and a general failure surface has been developed for the Mt Isa "silica-dolomite".

Some of the work presented in this thesis was published as soon as it was completed. To avoid unnecessary duplication and bulk this work is introduced and briefly reviewed in short chapters in the body of the thesis and reprints of the papers are included as appendices.

Chapter II

THE FAILURE OF THICK WALLED HOLLOW CYLINDERS OF ISOTROPIC ROCK

Introduction

A series of experiments on thick-walled hollow cylinders of rock subjected to separately controlled and varied internal and external pressure and axial load were performed. The immediate object of this work was to experimentally map the "failure surface" in principal stress space of three different rocks to see firstif such a unique surface does exist in each case and second, if it does exist, how closely it conforms to the various "failure surfaces" predicted by the commonly used failure criteria such as Mohr, Griffith or the modified Griffith theory of McClintock-Walsh. Hollow cylinders were used because nearly any principal stress relationship at failure can be attained with this system. The specimens are easily prepared and only minor modifications need be made to the usual simple triaxial testing equipment in order to perform these tests. The stresses in the sample are not homogeneous in this system, however, and must be calculated by elastic or elastic-plastic theory from the applied pressures and axial load. Also, since the stresses are inhomogeneous, stress gradients exist which in themselves may affect the measured failure strength. In addition the effect

of end conditions or friction at the platens may be of more importance than in conventional triaxial compression tests on solid cylinders. These problems are very real and can not yet be completely resolved. It is most important to make investigations of this type, however, as rock in nature and around engineering works does not necessarily fail under uniform triaxial compression or extension stresses. Stress gradients on some scale will nearly always be present and no two of the three principal stresses at a point of failure will in general be equal. It is clearly impossible to study the effect of stress gradients or the relative value of the intermediate principal stress on the failure of rock unless experimental systems are used which allow these to be varied.

The term "failure surface" is here used in the same sense as "yield surface" is in ductile materials, c.f. Nadai [1950, §28], except that most of these tests were performed in the brittle range of behaviour of the materials so that failure was mostly by fracturing with only minor amounts of yielding. This "failure surface" then is the locus of all possible combinations of principal stresses which cause the specimen to fail and may be expressed, $\sigma_1 = f(\sigma_2, \sigma_3)$. This has frequently been simplified to $\sigma_1 = f(\sigma_3)$, or in other words, it has been stated that the intermediate principal stress, σ_2, has no significant effect on the failure strength. This simplification has long been known

not to hold for the yield of ductile metals, c.f. Taylor and Quinney [1931] and it has also been shown that it is not always valid for the brittle fracture of rocks or cast iron, Robertson [1955], Grassi and Cornet [1949]. Variation of the intermediate principal stress appears to affect the strength of the rocks in the present series of experiments by upwards of several hundred per cent in some cases. Throughout this thesis compressive stresses will be reckoned positive and $\sigma_1 \geq \sigma_2 \geq \sigma_3$. The term triaxial will be restricted to the condition $\sigma_1 > \sigma_2 = \sigma_3$ or the conventional confined compression test. Polyaxial will be used to describe states of stress in which $\sigma_1 \neq \sigma_2 \neq \sigma_3$.

Previous Work

Hollow cylinders of rock with axial load and external pressure have been studied by Adams [1912], King [1912], Bridgman [1918], Robertson [1955], Obert and Stephenson [1965] and Jaeger and Hoskins [1966], (the work being included in Chapter III and appendix 2 of this thesis). Hobbs [1962] and Pomeroy and Hobbs [1962] have worked on coal. Bellamy [1960] has tested hollow cylinders of concrete and Wu et al [1963] and Broms et al [1965] describe similar tests on soil materials.

Thin-walled and thick-walled tubular specimens of ceramics, graphite, and various metals with some combinations of either internal or external pressure and axial tension, torsion, or

compression have been extensively studied to determine their behaviour under combined stresses. Much of this work has been summarized by Nadai [1950, Chapter 17].

Böker [1951] and Handin, Higgs, and O'Brien [1960] have performed experiments on solid cylinders of marble with combinations of axial stress, torque, and confining pressure. Handin, Heard, and Magourik [1967] have tested thin walled hollow cylinders of limestone, dolomite, and glass with combinations of internal pressure; external pressure, torque and axial stress at several strain rates and temperatures.

Paul [1961], Marin [1966] and Jaeger [1966] have given recent theoretical discussions of the shape of the failure surface for brittle materials.

Stresses in a Hollow Cylinder

Let the external radius of the cylinder be b, the internal radius a, the internal pressure P_i, the external pressure P_e, and the differential axial force applied by the testing machine P. The radial and tangential stresses σ_r and σ_θ at any radius r, based on elastic theory are, Jaeger [1962]

$$\sigma_r = \frac{b^2P_e - a^2P_i}{b^2 - a^2} - \frac{a^2b^2(P_e-P_i)}{r^2(b^2-a^2)} \qquad (1)$$

$$\sigma_\theta = \frac{b^2P_e - a^2P_i}{b^2 - a^2} + \frac{a^2b^2(P_e-P_i)}{r^2(b^2-a^2)} \qquad (2)$$

The axial stress σ_z for the test geometry and apparatus used in these experiments is:

$$\sigma_z = \frac{P}{(b^2-a^2)\pi} + \frac{P_e b^2}{(b^2-a^2)} - \frac{P_i a^2}{b^2-a^2} \qquad (3)$$

The distribution of radial and tangential stress through the cylinder walls for the two limiting conditions $P_i = 0$ and $P_e = 0$ is shown in Figures 1(a) and (b). King [1912] has described the types of failure to be expected for different relative values of σ_r, σ_θ and σ_z based on maximum shear stress failure criterion. Jaeger [1966] discusses the various possible cases in some detail.

In some of these experiments, conducted with relatively high internal and external pressures, the stress distribution in the cylinders is probably not very well described by the equations of classical elasticity. Robertson [1955] has discussed and used equations based on simple plasticity first derived by Beliaev and Sinitskii for the stress distributions in hollow cylinders with external pressure and axial load. There are numerous treatments of the expansion of elastic-plastic cylindrical tubes in connection with autofrettaging and pressure vessel design, c.f. Hill [1950, Chapter 5]. MacGregor et al [1948] present a theory for the partial yielding of thick walled cylindrical tubes under internal pressure, external pressure, and axial load using von Mises yield condition. Wu et al [1963] give a solution for the stresses in a hollow cylinder using a Mohr-Coulomb yield criterion.

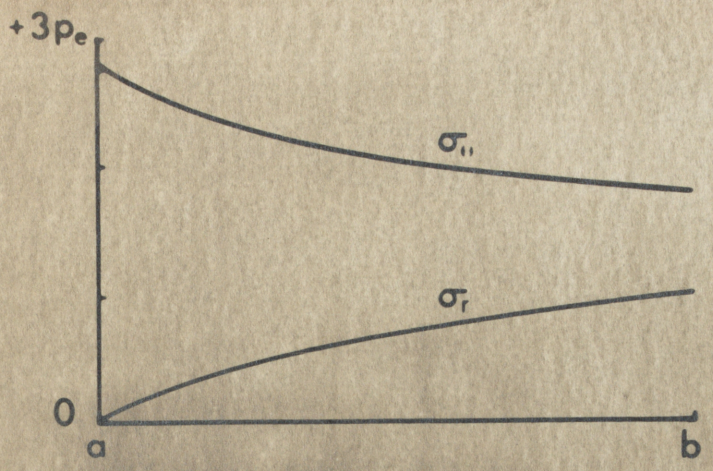

(a)

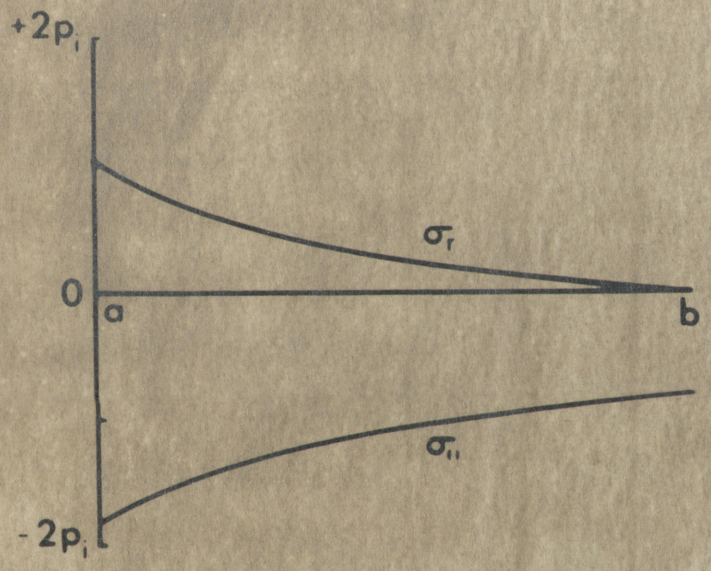

(b)

Fig. 1 (a) Stress distribution in hollow cylinders 5 cm outside diameter by 2.5 cm inside diameter with external pressure only, a, inner surface to b, outer surface.

(b) Stress distribution in hollow cylinders 5 cm outside diameter by 2.5 cm inside diameter with internal pressure only, a, inner surface to b, outer surface.

The problem here is that the magnitudes of the stresses calculated from the applied pressures and loads in the elastic-plastic solutions depend on the yield criterion chosen and it is the form of the yield criterion that we are attempting to find with these experiments. It should be recognized that neither rocks nor very many other materials are perfectly elastic or elastic-plastic up to the point of rupture. Elastic theory was used to calculate the stresses in the experiments because it is the most reasonable mathematical approximation to the behaviour of these materials in most of the tests.

Apparatus and Materials

The testing apparatus is shown diagrammatically in Figure 2. It basically consisted of a simple triaxial pressure cell and piston. The piston was hollow to allow the internal pressure to be applied and controlled independently. The rock specimens were 5 cm outside diameter, 2.5 cm inside diameter and 12 cm long. They were jacketed both internally and externally with soft rubber tubing. Pressure was controlled through separate outlets on a hydraulic bench with needle valves and a screw press. Additional differential axial load was applied by an Avery 500 ton compression testing machine. Sheets of dry paper cut to shape were placed on the ends of the specimen and a thin layer of graphite

placed between the paper and the anvils of the testing apparatus in an attempt to eliminate frictional restraints at the ends of the specimen. Several lubricants were investigated before settling on this procedure. The main object was to find a material which would not inhibit any radial deformations that the specimen tried to take without introducing other modifications of the stress distribution near the ends of the specimen or intruding as a liquid into the ends of the specimen. Bowden and Tabor [1964, Chapter VII] give values for the coefficient of sliding friction of various ionic brittle solids on steel from 0.4 to 0.9. They give a coefficient of sliding friction for graphite on steel of approximately 0.1 so that the graphite should be effective in reducing radial frictional restraints. The paper was placed between the rock and the graphite to preclude the slight possibility of the graphite intruding into any open pores, grain boundaries, or cracks in the ends of the specimens under the (up to 6.5 kb) end pressures reached in some of these tests. It is assumed that the paper has no significant strength and that it does not modify the stress distribution at the ends of the hollow cylinder. Tests have been performed on solid cylinders of the same three rocks under confining pressure and with several different end lubricants and the results of these tests are given in appendix 1. The presence of the paper and graphite

layer does not appear to affect the strength of solid cylinders of these rocks. Comparison tests were made on specimens with clean (wiped with acetone), dry, bare ends in direct contact with dry, hardened, steel end pieces of the same diameter. The axial load was applied through a spherical seat in all cases.

Due to the complicated geometry of the system the actual strain rates achieved are not accurately known. Additional load from the testing machine was applied to give axial strain rates of between 10^{-6} and 10^{-7} sec^{-1} during the linear portions of the stress strain curve.

The three rock types tested were:

(1) Bowral "trachyte". This is the commercial name for a rock that has been more accurately described by Joplin [1964] as an altered micro-syenite. It is an even-grained, isotropic igneous rock consisting predominantly of orthoclase and aegerine-augite 1 mm in grain size with minor amounts of quartz, calcite, and altered ferro-magnesian minerals.

(2) Gosford Sandstone. A very uniform, isotropic, fine-grained, weakly cemented, quartz sandstone with a sugary texture.

(3) Carrara Marble. A uniform medium to fine-grained isotropic essentially pure calcite marble. The grain size varies from piece to piece of this material but a single block with average grain size of about 0.2 mm was used for all of the specimens in these experiments.

Failure Criteria

Nadai [1950], Jaeger [1962], [1963], and [1966] and Marin [1966] have given reviews of the various commonly used failure criteria for brittle materials. Of these the octahedral shear stress or distortional energy failure criterion and the three stress dimensional generalizations of Griffith and modified Griffith failure criteria predict the dependence of the ultimate strength of a sample on the relative value of the intermediate principal stress. The distortional energy or octahedral shear stress criteria much used for the yield of metals under combined stresses predicts the same strengths in tension and compression. In terms of invariants the yield strength depends only on the invariants of stress deviation and not on the invariants of stress. Since the measured strength of rock is lower in tension than in compression, the distortional energy criterion cannot be expected to be applicable to rocks unless all three principal stresses are of the same sign. In practice the rock must deform plastically as only then does its strength appear to be independent of the stress invariants.

Murrell [1963] and [1966] and Jaeger [1966] have given and discussed a three dimensional treatment of Griffith theory. The "failure surface" derived on this basis is a paraboloid of revolution, symmetrical about the line $\sigma_1 = \sigma_2 = \sigma_3$ and passing

through the origin. In terms of principal stresses the equation of this surface is

$$(\sigma_1-\sigma_2)^2 + (\sigma_2-\sigma_3)^2 + (\sigma_3-\sigma_1)^2 = 24\ T_o\ (\sigma_1+\sigma_2+\sigma_3) \qquad (4)$$

where T_o is the uniaxial tensile strength. From this it can be shown that the uniaxial compressive strength, C_o, should be $-12T_o$. The intersection of this surface with any given stress plane can easily be found. For example, the intersection of the surface with the plane representing the condition $\sigma_3 = 0$ is an ellipse

$$(\sigma_1-\sigma_2)^2 + \sigma_2^2 + \sigma_1^2 = 24T_o(\sigma_1+\sigma_2) \qquad (5)$$

Hollow cylinders tested with external pressure and axial load only are tests in which $\sigma_3 = 0$ at failure (assuming failure occurs on the inner surface). If this three dimensional Griffith criterion is valid then these hollow cylinder test results should fall on this ellipse.

Jaeger [1966] has proposed regarding the triaxial test results as a fundamental measure of a rock's properties. In other words, the triaxial results give the intersection of the failure surface with the $\sigma_2 = \sigma_3$ plane for that particular rock regardless of failure mechanism or mechanisms acting. A complete failure surface might then be generated by rotating a curve fitted to the triaxial test results about the line $\sigma_1 = \sigma_2 = \sigma_3$. It was simpler and more illustrative for the purposes of this investigation to rotate the individual triaxial results point by

point to the particular sections plotted. Using Jaeger's notation this is done by means of equations (6) and (7)

$$\sigma_{1_T} + 2\sigma_{3_T} = \sigma_1 + \sigma_2 + \sigma_3 \qquad (6)$$

$$2(\sigma_{1_T} - \sigma_{3_T})^2 = (\sigma_2 - \sigma_3)^2 + (\sigma_3 - \sigma_1)^2 + (\sigma_1 - \sigma_2)^2 \qquad (7)$$

where σ_{1_T} and σ_{3_T} are the maximum stress at failure and the confining pressure from the conventional triaxial tests. If the triaxial points are rotated to the $\sigma_3 = 0$ section of the failure surface for example they should fall on the same curve as the hollow cylinder tests conducted with $P_i = 0$ if this criterion is valid.

The McClintock-Walsh modification of Griffith theory to account for the effects of friction in the Griffith cracks under compressive stresses can similarly be rotated and made into a three stress dimensional criterion. In two stresses it can be written

$$\sigma_1\left[(1+\mu^2)^{\frac{1}{2}}-\mu\right] - \sigma_2\left[(1+\mu^2)^{\frac{1}{2}}+\mu\right] = 4T_o\left[1+\sigma_c/T_o\right]^{\frac{1}{2}} - 2\mu\sigma_c \qquad (8)$$

where μ is the coefficient of sliding friction in the crack surfaces and σ_c is the stress required to close enough of the cracks far enough to bring the friction mechanism into play. Assuming this criterion to be valid when $\sigma_2 = \sigma_3$ a three stress dimensional extension of the criterion can then be made by rotating it about the $\sigma_1 = \sigma_2 = \sigma_3$ axis. The failure surface thus formed is a portion of a cone and this cone can be terminated in the tensile

stress region by a paraboloid the $\sigma_2 = \sigma_3$ section of which is determined by the original Griffith theory. The magnitude of σ_c, the stress required to close the cracks, has been variously taken as $-3T_o$ by McClintock and Walsh [1962], zero by Brace [1960] and $-4.19T_o$ (an experimentally determined value) by Murrell [1966]. There are two difficulties here, one, the crack length and shape are not accurately known and two, complete closure is apparently not required. $-T_o$ was used in the present work not implying any fundamental relationship but merely as a small convenient quantity which seems to fit the trachyte data. The coefficients of friction, μ, for each of the three rocks used were experimentally determined using the techniques given by Jaeger [1959] for sliding friction on experimentally formed fracture surfaces and were found to be trachyte = 0.80, sandstone = 0.66, and marble = 0.90. These values are constant over the range of normal stresses of interest here.

In principle, any failure criterion which can be plotted in terms of principal stresses can be rotated in a similar manner and made into a three stress dimensional failure criterion.

Figure 3 is a drawing of the three dimensional failure surface for Carrara marble. This surface was developed by rotating the triaxial test results which lie on AB about the $\sigma_1 = \sigma_2 = \sigma_3$ axis. The experimental results lie between OAB and ODC and fit this surface within normal experimental scatter. The amount of scatter is shown in Figures 8, 11, and 14.

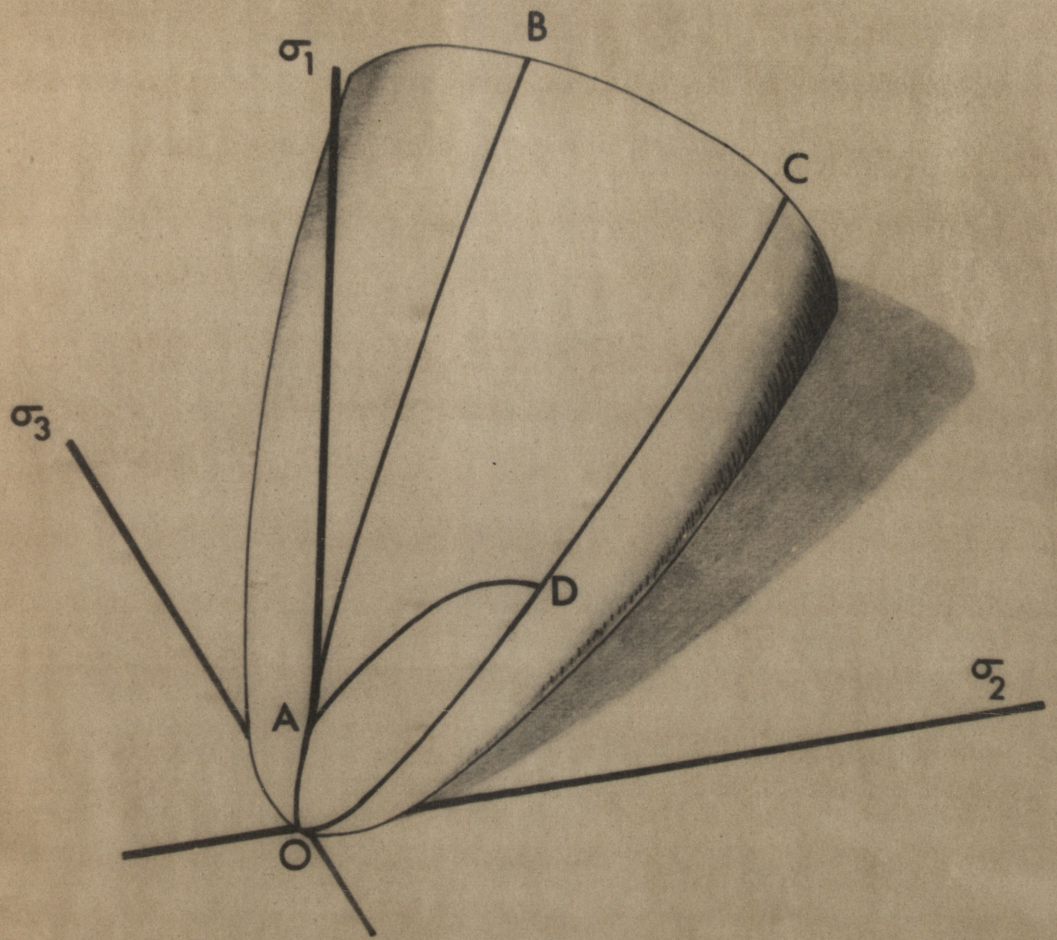

Fig. 3 Drawing of the three dimensional failure surface for Carrara marble. The conventional triaxial compression tests with $\sigma_2 = \sigma_3$ fall on A B. Extension tests with $\sigma_1 = \sigma_2$ lie on ODC. Tests in which $\sigma_3 = 0$ and σ_1 and σ_2 are varied to failure such as hollow cylinders with external pressure and axial load only lie on AD. Point A represents the unconfined compression tests. Because the convention $\sigma_1 \geq \sigma_2 \geq \sigma_3$ has been adopted, all experimental points lie on or between OAB and ODC.

Experimental Results

Because of the lack of a generally accepted means of presenting these data, the results of the experiments are given in three forms. The values of the principal stresses on the inner surface of the cylinder calculated by elastic theory for each test are given in Tables I, II, and III. Figures 4, 5, and 6 are graphs of σ_1 versus σ_2 for various ratios of σ_3/σ_2 for the three materials. In addition several sections of the failure surface for each rock type are given in Figures 7-15 along with the envelopes in the section representing three of the failure criteria which might be applicable.

Turning first to Figures 4, 5, and 6 the σ_3/σ_2 ratio of 1.0 represents the conventional triaxial compression tests. The other curves represent tests conducted on hollow cylinders with the applied pressures arranged so that $\sigma_3 < \sigma_2$ by various amounts. In practice, the experiments are performed with $P_i \neq P_e$, the principal stresses at failure are calculated and plotted and smooth curves are interpolated among the experimental results. This is a simple means of presenting the data from all of the tests on a particular experimental material on a single diagram. It is difficult to show individual test results or to compare the experimental results with the different failure criteria on these diagrams, however. Figures 7 through 15 are included to facilitate these comparisons. Figures 7, 8, and 9 are sections

Table I

Principal stresses at failure on inner surface of trachyte hollow cylinders calculated on elastic theory and type of fracture observed in each case

σ_z	σ_θ	σ_r	Type of Fracture
1.63	0	0	Fault Plane + Extension parallel to σ_z
2.29	.19	0	Conical
2.53	.34	0	Conical
3.00	.46	0	Conical
3.30	.77	0	Conical
3.51	.97	0	Conical
3.89	1.45	0	Conical
3.92	1.93	0	Conical
4.40	2.32	0	Conical + Extension parallel to σ_z
4.06	2.42	0	Collapse
3.39	2.70	0	Collapse
3.62	2.90	0	Collapse
2.76	3.38	0	Collapse
2.57	3.62	0	Collapse
2.62	3.86	0	Collapse
2.59	.17	.17	Fault Plane + Conical
3.47	.46	.17	Fault Plane + Extension normal to σ_z
3.90	.66	.17	Conical

Table I (continued)

σ_z	σ_θ	σ_r	Type of Fracture
4.69	1.14	.17	Conical
5.05	1.62	.17	Conical
5.52	2.59	.17	Conical
5.56	3.08	.17	Conical
3.19	.21	.21	Fault Planes + Conical
3.40	.16	.35	Fault Planes
4.07	.35	.35	2 Fault Planes + Extension parallel to σ_z
5.35	1.31	.35	Conical + Extension normal and parallel to σ_z
6.13	2.28	.35	Conical
4.66	.52	.52	Helical
5.30	1.00	.52	Conical + Extension normal and parallel to σ_z
6.03	1.97	.52	Conical
5.17	0.69	.69	Fault Plane + Extension parallel to σ_z
6.00	1.67	.69	Conical
6.61	1.03	1.03	Fault Plane + Helical
0	-.19	.10	Extension parallel to σ_z
.68	-.30	.59	Extension parallel to σ_z

Table I (continued)

σ_z	σ_θ	σ_r	Type of Fracture
.70	-.20	.22	Extension parallel to σ_z
.74	-.12	.07	Extension parallel to σ_z
1.13	-.43	1.31	Extension parallel to σ_z
1.42	-.06	.03	Extension parallel to σ_z
1.53	-.48	1.34	Extension parallel to σ_z
1.89	-.06	.14	Extension fracture inclined to σ_z
1.96	-.03	.12	Extension subparallel to σ_z
2.22	-.16	.52	Extension parallel perpendicular and inclined to σ_z
2.85	-.45	1.86	Extension subparallel to σ_z
3.33	-.18	1.00	Extension subparallel and subperpendicular to σ_z
4.24	-.21	1.73	Fault Plane

Table II

Principal stresses at failure on inner surface of marble hollow cylinders calculated on elastic theory and type of fracture observed in each case

σ_z	σ_θ	σ_r	Type of Fracture
0.80	0	0	Fault Plane + Helical + Extension parallel to σ_z
1.54	.46	0	Conical
2.03	.93	0	Conical
2.39	1.38	0	Conical
2.59	1.84	0	Conical
2.82	2.30	0	Conical
2.71	2.75	0	Collapse
1.11	.07	.07	Helical
1.63	.44	.07	Helical
2.14	.80	.07	Conical
3.02	1.72	.07	Conical
3.28	3.09	.07	Conical
2.13	.35	.35	Fault Plane
3.78	2.17	.35	Conical
2.38	.50	.50	Conical
3.18	.69	.69	Fault Planes
3.97	1.67	.69	Conical
4.11	1.03	1.03	Distributed

Table II (continued)

σ_z	σ_θ	σ_r	Type of Fracture
.34	-.09	.05	Extension parallel to σ_z
.79	-.09	.32	Extension parallel to σ_z
.59	-.18	.36	Extension parallel to σ_z
.69	0	.54	Extension parallel to σ_z
.57	-.15	.76	Extension parallel to σ_z
1.09	-.24	1.21	Extension parallel to σ_z
2.06	-.11	1.24	Fault Plane + Extension parallel to σ_z + Helical

Table III

Principal stresses at failure on inner surface of sandstone hollow cylinders calculated on elastic theory and type of fracture observed in each case

σ_z	σ_θ	σ_r	Type of Fracture
.49	0	0	Helical
.67	.09	0	Conical
.80	.18	0	Conical
1.08	.46	0	Conical
1.12	.77	0	Conical
1.29	.92	0	Conical
1.00	1.16	0	Collapse
1.21	1.37	0	Collapse
.73	1.45	0	Collapse
1.14	1.47	0	Collapse
.83	1.66	0	Collapse
.87	1.74	0	Collapse
.80	.07	.07	Conical
1.15	.45	.07	Conical
1.42	.62	.07	Conical
1.53	.80	.07	Conical
1.59	1.07	.07	Conical
1.85	1.33	.07	Conical
1.84	1.42	.07	Conical
1.85	1.62	.07	Conical

Table III (continued)

σ_z	σ_θ	σ_r	Type of Fracture
.98	.17	.17	Distributed
1.40	.66	.17	Conical
1.54	1.43	.17	Conical
2.10	1.62	.17	Conical
2.34	2.59	.17	Conical
1.67	.35	.35	Fault Plane
2.26	1.31	.35	Conical
2.67	2.28	.35	Distributed
1.93	.50	.50	Fault Planes
2.22	.69	.69	Helical to Distributed
2.84	1.66	.69	Distributed
2.78	1.04	1.04	Conical
.41	-.13	.29	Extension parallel to σ_z
1.07	-.18	.88	Extension parallel to σ_z

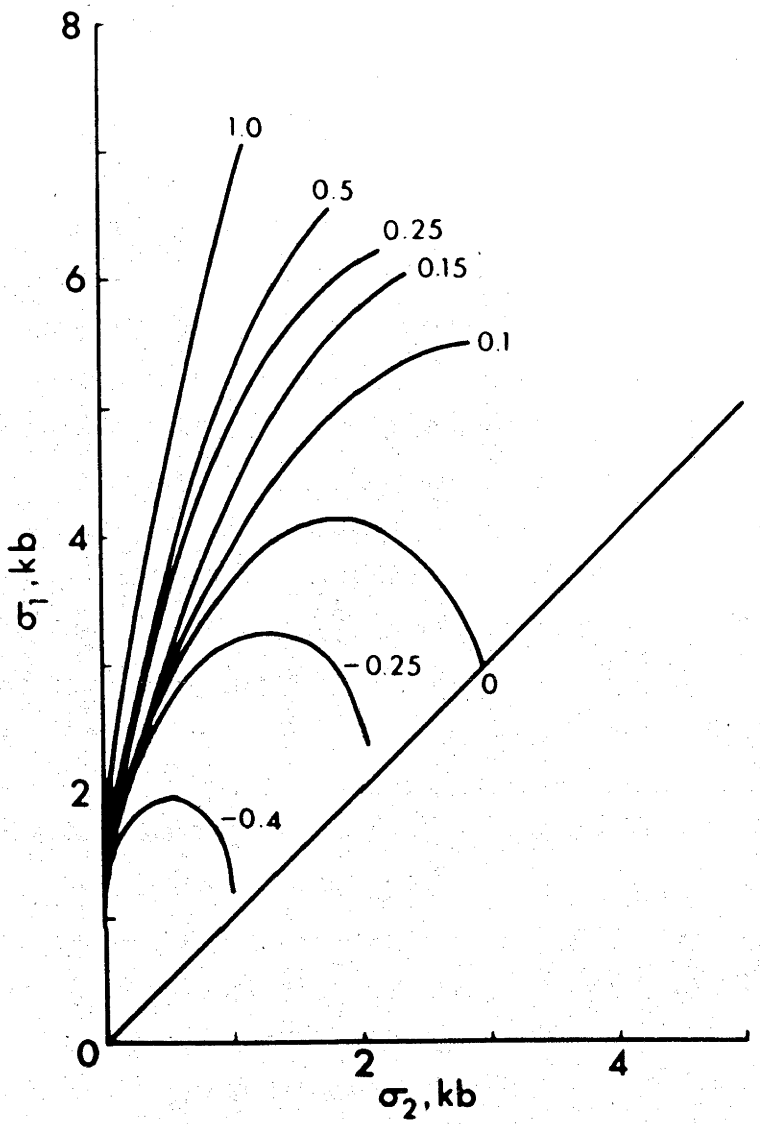

Fig. 4 Results of trachyte hollow cylinder experiments σ_1 versus σ_2 for various ratios of σ_3/σ_2.

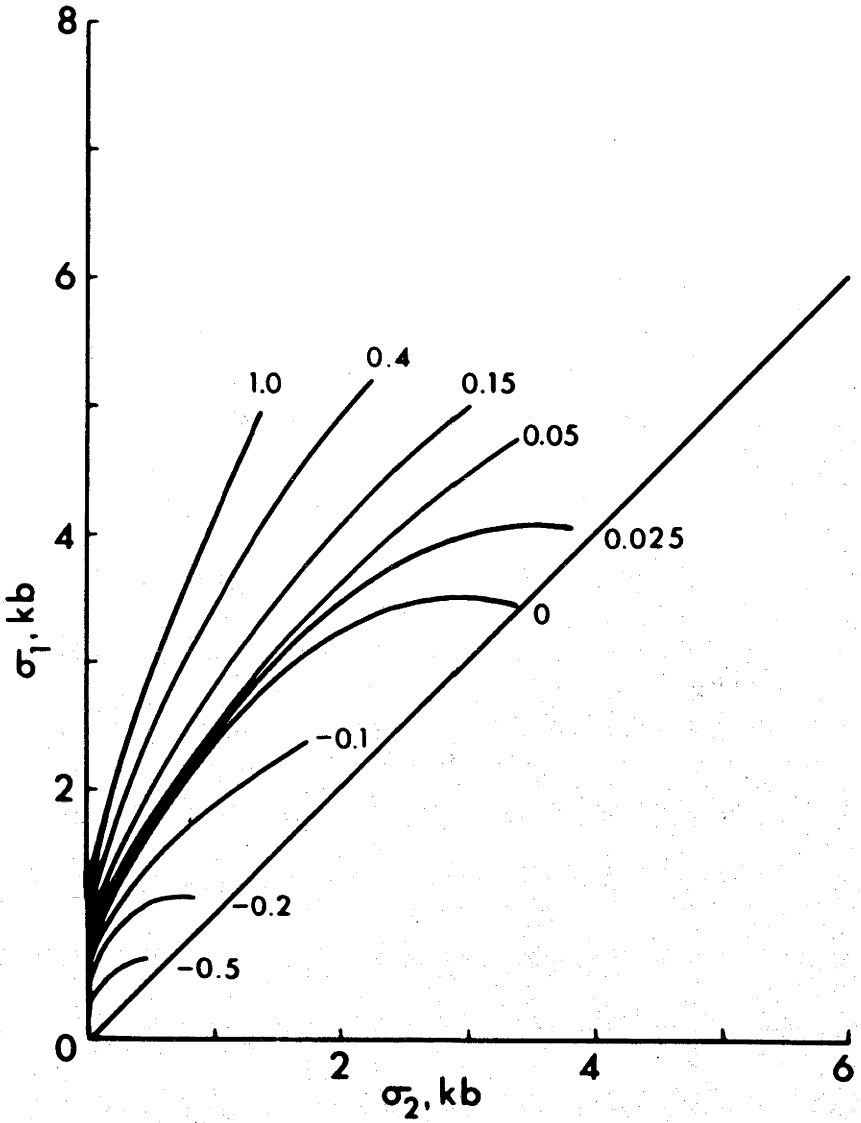

Fig. 5 Results of marble hollow cylinder experiments σ_1 versus σ_2 for various ratios of σ_3/σ_2.

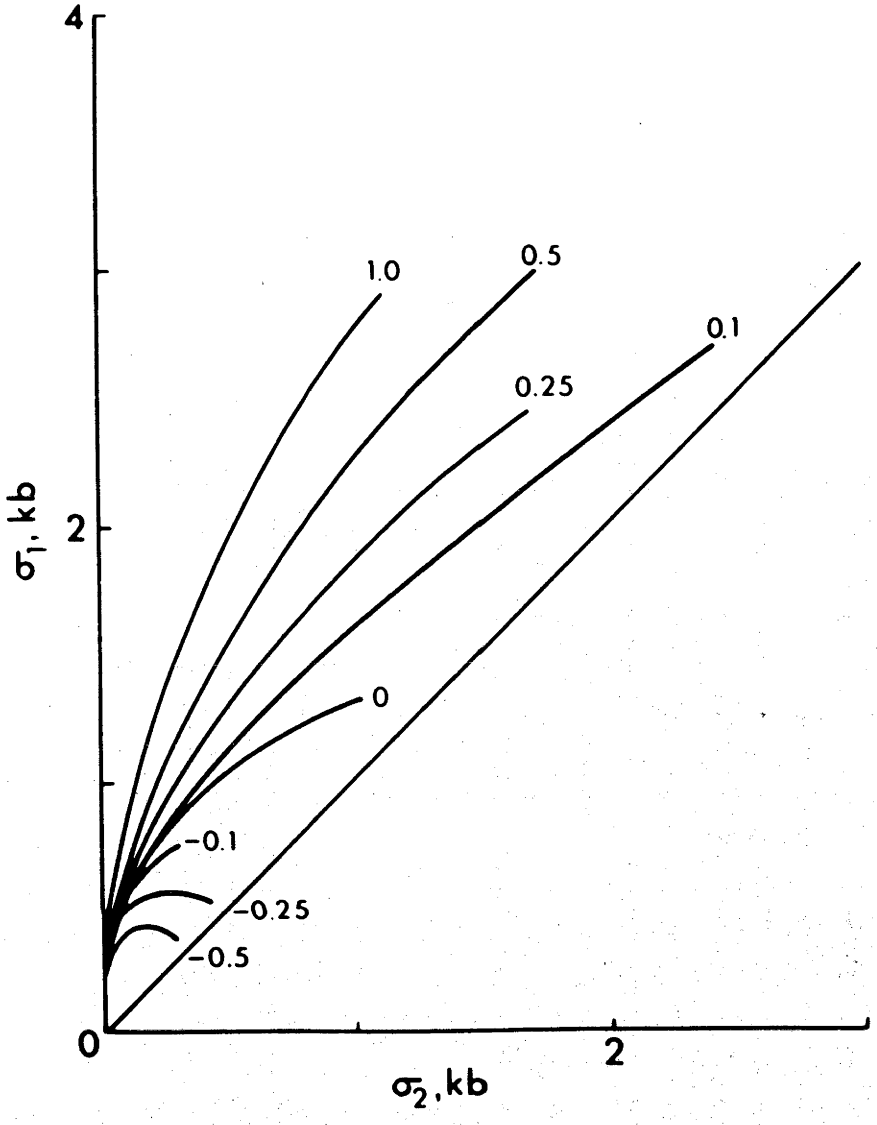

Fig. 6 Results of sandstone hollow cylinder experiments. σ_1 versus σ_2 for various ratios of σ_3/σ_2.

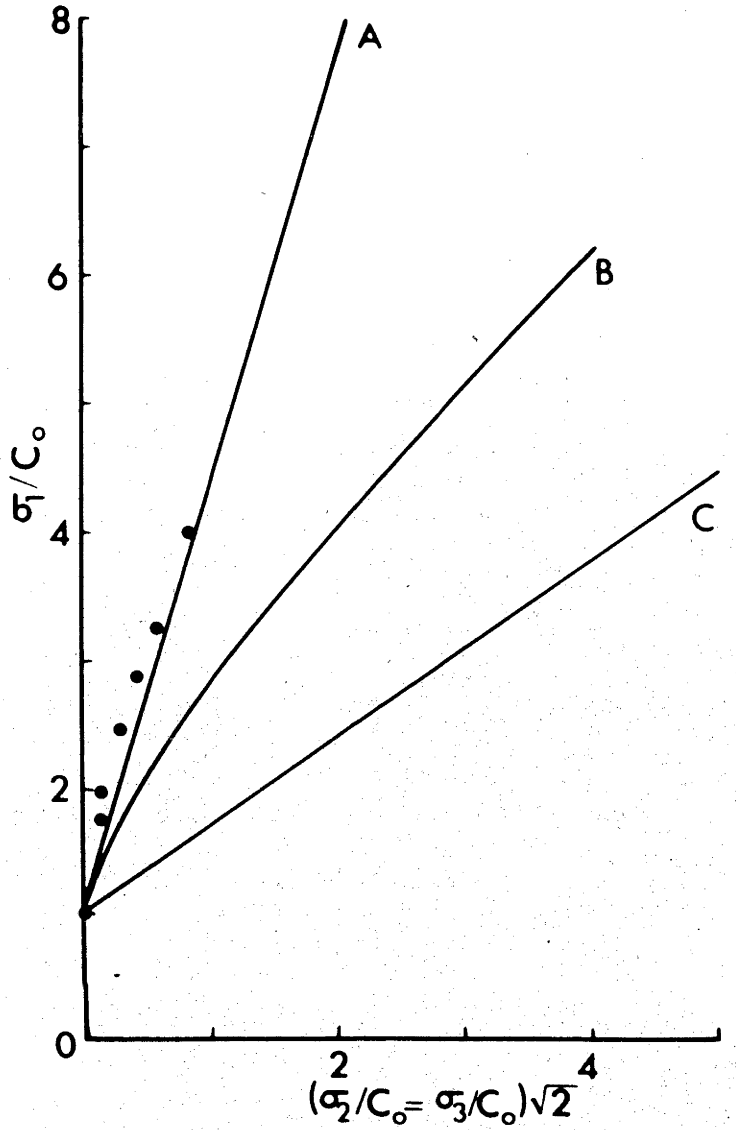

Fig. 7 Results of trachyte hollow cylinder experiments conducted with $\sigma_2 = \sigma_3$ plotted in terms of the unconfined compressive strength C_o. "A" represents the McClintock-Walsh failure criterion plotted in the $\sigma_2 = \sigma_3$ section of the failure surface with coefficient of friction $\mu = 0.80$ and the stress required to close the Griffith cracks σ_c taken equal to T_o. "B" represents the three dimensional Griffith theory failure criterion in the $\sigma_2 = \sigma_3$ section. "C" represents the distortional energy failure criterion in the $\sigma_2 = \sigma_3$ plane.

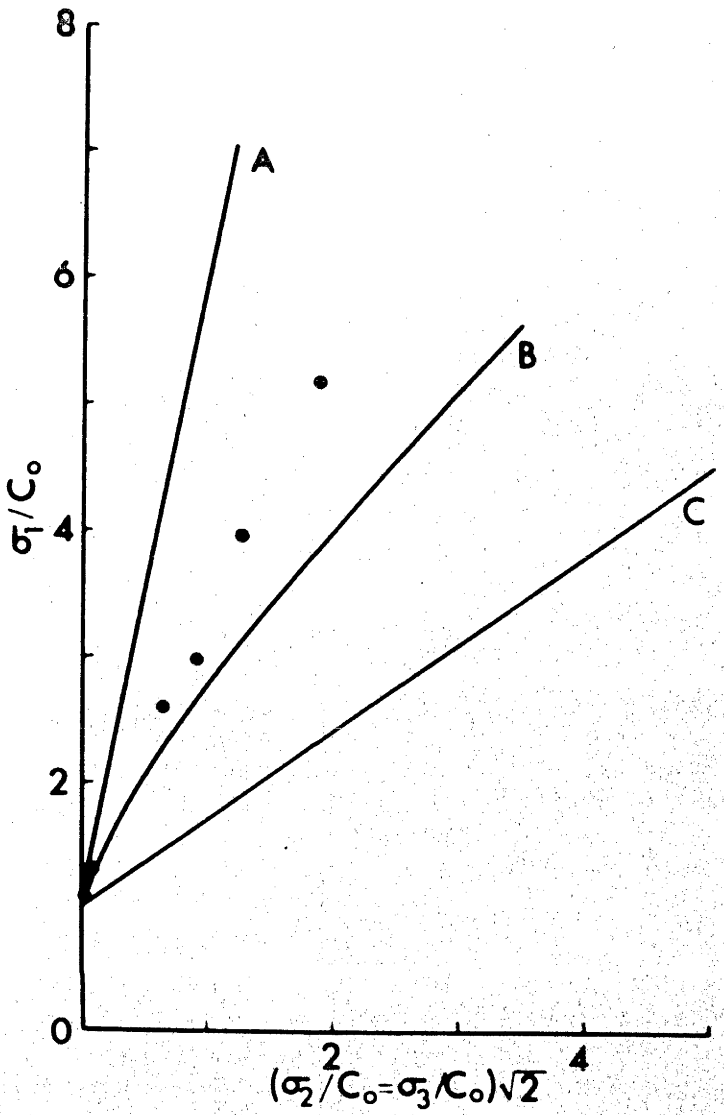

Fig. 8 Results of marble hollow cylinder experiments conducted with $\sigma_2 = \sigma_3$ plotted in terms of the unconfined compressive strength C_o. "A" represents the McClintock-Walsh failure criterion plotted in the $\sigma_2 = \sigma_3$ section of the failure surface with a coefficient of friction of 0.90 and $\sigma_c = T_o$. "B" represents the three dimensional Griffith failure criterion in the $\sigma_2 = \sigma_3$ section. "C" represents the distortional energy failure criterion in the $\sigma_2 = \sigma_3$ plane.

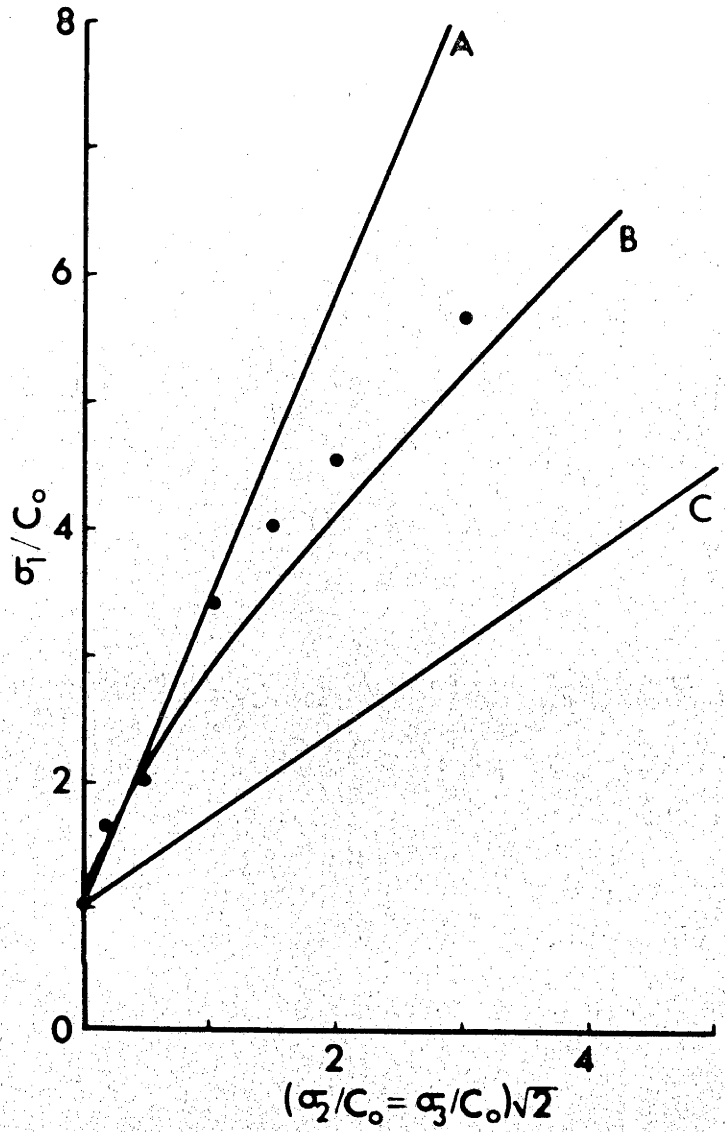

Fig. 9 Results of sandstone hollow cylinder experiments conducted with $\sigma_2 = \sigma_3$ plotted in terms of the unconfined compressive strength C_o. "A" represents the McClintock-Walsh failure criterion plotted in the $\sigma_2 = \sigma_3$ section of the failure surface with a coefficient friction of 0.66 and $\sigma_c = T_o$. "B" represents the three dimensional Griffith failure criterion in the $\sigma_2 = \sigma_3$ section. "C" represents the distortional energy failure criterion in the $\sigma_2 = \sigma_3$ plane.

in the diagonal plane of the three dimensional failure surface of each of the three rock types. This is the section which contains the usual triaxial compression tests. The experimental points are given and may be compared with curves representing the distortional energy, three dimensional Griffith and the three dimensional version of the McClintock-Walsh modification of Griffith failure criteria. None of these criteria are valid for all three of the rocks investigated. Figures 10, 11, and 12 are the oblique sections of the failure surface in which $\sigma_3 = 0$. The intersections of the same three failure criteria with the $\sigma_3 = 0$ plane are plotted in these diagrams along with results of hollow cylinder tests in which $\sigma_3 = 0$ at failure ($P_i = 0$). In addition, the triaxial test results have been rotated into this section by means of equations (6) and (7). The sandstone results given in Figure 12 show a great deal of scatter at the higher values of σ_2/C_o. These were tests in which $\sigma_\theta > \sigma_z$ at failure and the failure occurred by a sudden violent inwards collapse of the specimen walls. The failure appeared to be time dependent in these tests and the plotted stresses which are calculated on simple elastic theory are probably inaccurate.

Figures 13, 14, and 15 are oblique sections of the failure surfaces when $\sigma_3/C_o \simeq 0.1$. In these diagrams the experimental scatter is much reduced. Here again the intersections of the three theoretical failure criteria with this plane are given along with hollow cylinder test results in which $\sigma_3/C_o \simeq 0.1$ and the

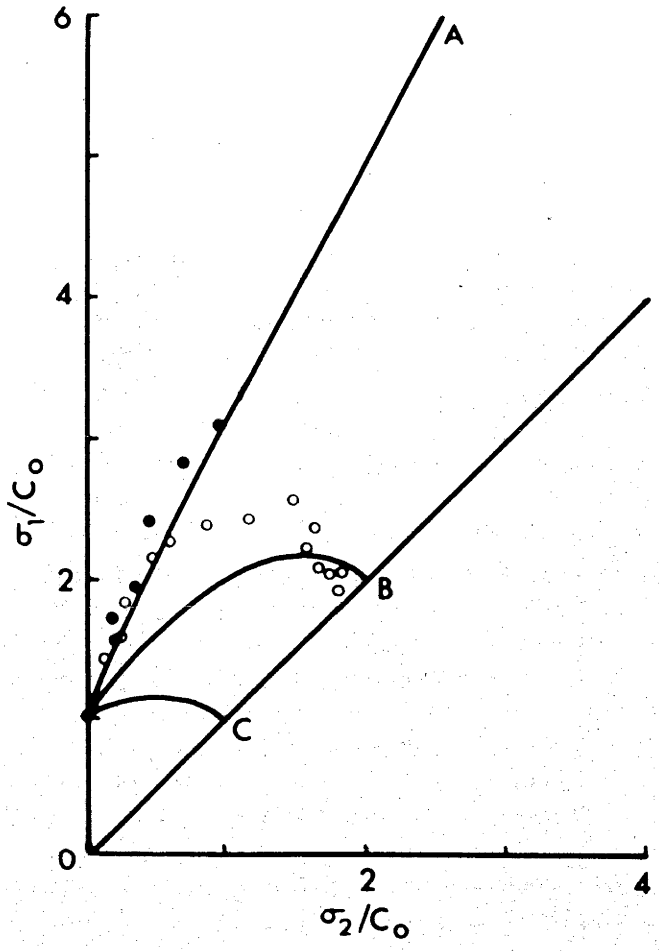

Fig. 10 Trachyte hollow cylinder tests when $\sigma_3 = 0$. ○ Hollow cylinders with internal pressure = 0, ● hollow cylinders with internal pressure = to the external pressure or $\sigma_2 = \sigma_3$ when rotated about the $\sigma_1 = \sigma_2 = \sigma_3$ axis into the $\sigma_3 = 0$ section. "A" McClintock-Walsh failure criterion rotated into the $\sigma_3 = 0$ plane, "B" three dimensional Griffith theory rotated into the $\sigma_3 = 0$ plane, and "C" distortional energy failure criterion in the $\sigma_3 = 0$ plane.

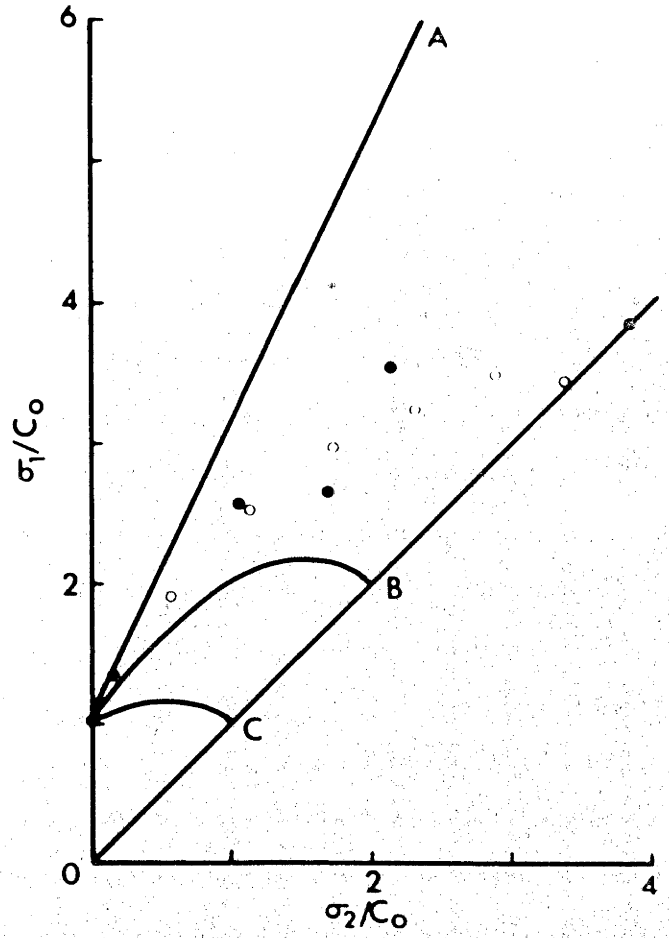

Fig. 11 Marble hollow cylinder tests when $\sigma_3 = 0$. ○ Hollow cylinders with $P_i = 0$. ● Hollow cylinders with $P_i = P_e$ or $\sigma_2 = \sigma_3$ when rotated about the $\sigma_1 = \sigma_2 = \sigma_3$ axis into the $\sigma_3 = 0$ section. "A" McClintock-Walsh failure criterion rotated into the $\sigma_3 = 0$ plane, "B" three dimensional Griffith theory in the $\sigma_3 = 0$ plane, and "C" the distortional energy failure criterion in the $\sigma_3 = 0$ plane.

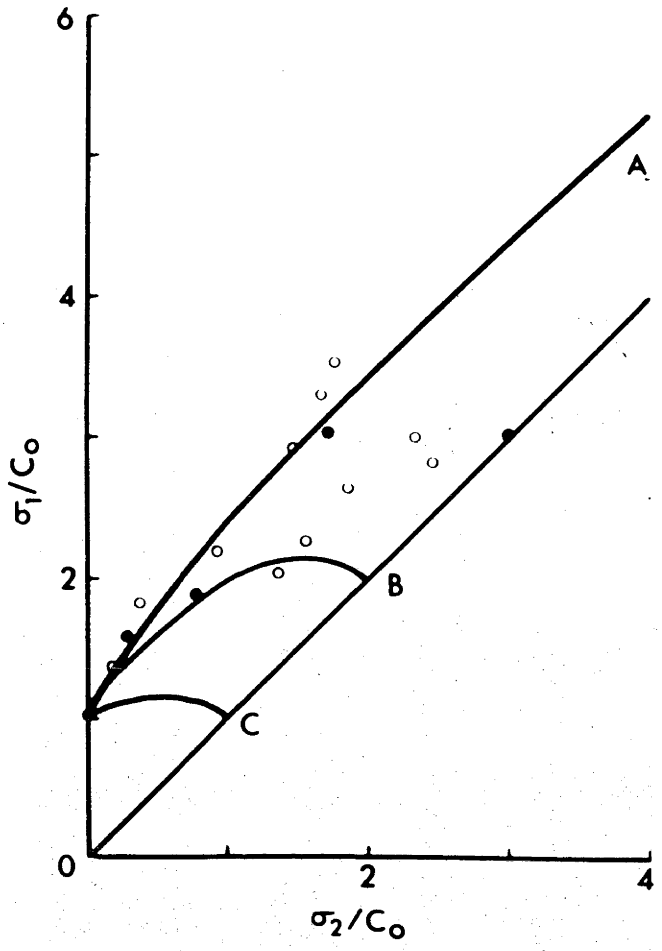

Fig. 12 Sandstone hollow cylinder tests when $\sigma_3 = 0$. ○ Hollow cylinders with $P_i = 0$. ● Hollow cylinders with $P_i = P_e$ or $\sigma_2 = \sigma_3$ when rotated about the $\sigma_1 = \sigma_2 = \sigma_3$ axis into the $\sigma_3 = 0$ section. "A" McClintock-Walsh failure criterion rotated into the $\sigma_3 = 0$ plane, "B" three dimensional Griffith theory in the $\sigma_3 = 0$ plane, and "C" the distortional energy failure criterion in the $\sigma_3 = 0$ plane.

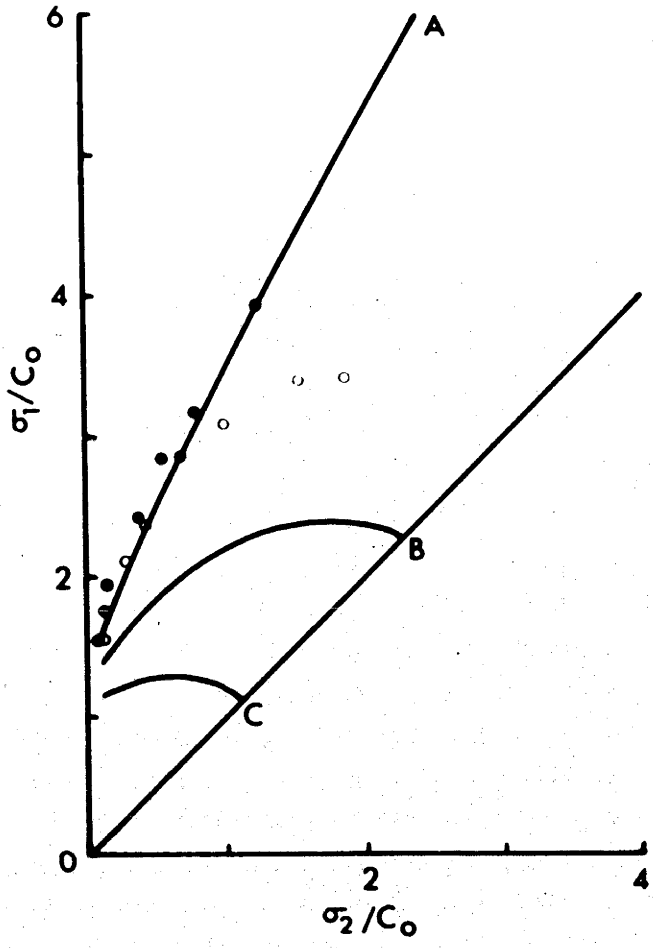

Fig. 13 Trachyte hollow cylinder tests when $\sigma_3 = 0.106\ C_o$. O Hollow cylinders with $P_i = 0.106\ C_o$. ● Hollow cylinders with $P_i = P_e$ or $\sigma_2 = \sigma_3$ when rotated about the $\sigma_1 = \sigma_2 = \sigma_3$ axis into the $\sigma_3 = 0.106\ C_o$ section of the failure surface. "A" McClintock-Walsh failure criterion rotated into the $\sigma_3 = 0.106\ C_o$ plane, "B" three dimensional Griffith theory in the $\sigma_3 = 0.106\ C_o$ plane, and "C" the distortional energy failure criterion in the $\sigma_3 = 0.106\ C_o$ plane.

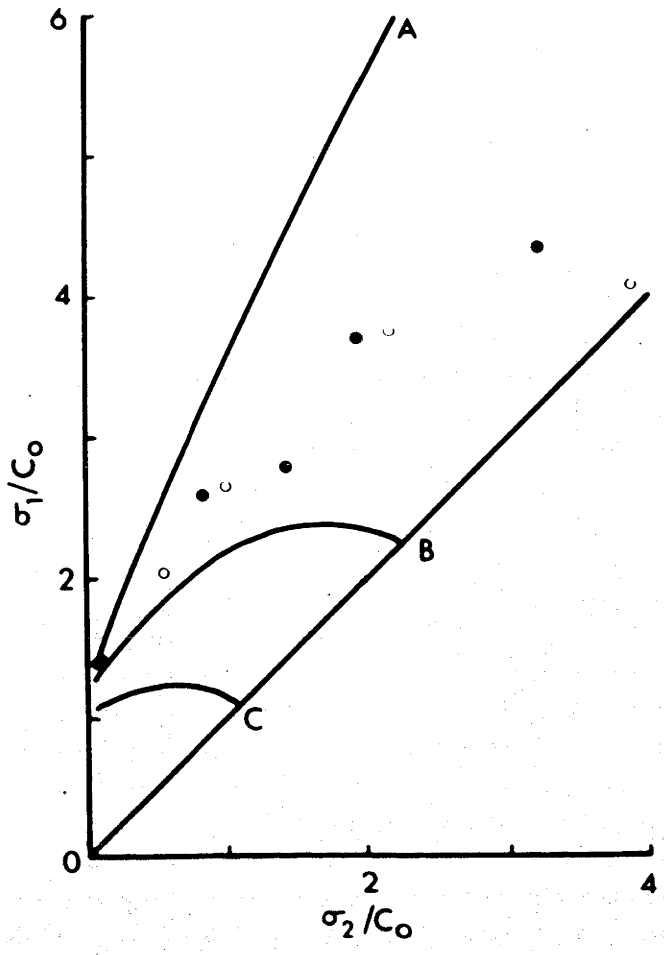

Fig. 14 Marble hollow cylinder tests when $\sigma_3 = 0.086\ C_o$. O Hollow cylinders with $P_i = 0.086\ C_o$. ● Hollow cylinders with $P_i = P_e$ or $\sigma_2 = \sigma_3$ when rotated about the $\sigma_1 = \sigma_2 = \sigma_3$ axis into the $\sigma_3 = 0.086\ C_o$ plane, "B" is three dimensional Griffith theory in the $\sigma_3 = 0.086\ C_o$ plane, and "C" is the distortional energy failure criterion in the $\sigma_3 = 0.086\ C_o$ plane.

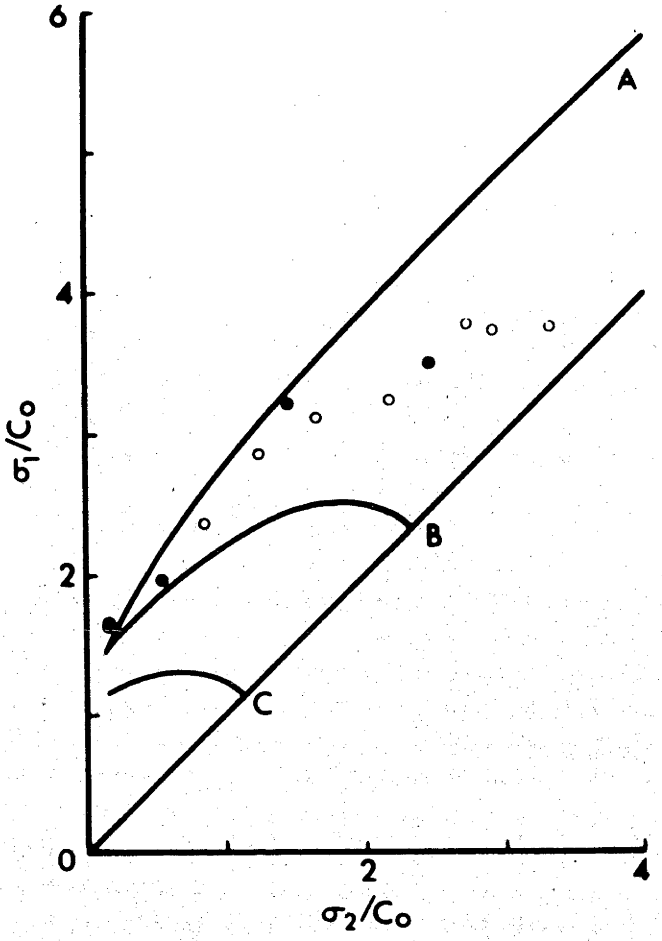

Fig. 15 Sandstone hollow cylinder tests when $\sigma_3 = 0.14\ C_o$. O Hollow cylinder tests with $P_i = 0.14\ C_o$. ●° Hollow cylinders with $P_i = P_e$ or $\sigma_2 = \sigma_3$ when rotated about the $\sigma_1 = \sigma_2 = \sigma_3$ axis into the $\sigma_3 = 0.14\ C_o$ section of the failure surface. "A" is the McClintock-Walsh failure criterion rotated into the $\sigma_3 = 0.14\ C_o$ plane, "B" is three dimensional Griffith theory in the $\sigma_3 = 0.14\ C_o$ plane, and "C" is the distortional energy failure criterion in the $\sigma_3 = 0.14\ C_o$ plane.

position of the triaxial test results when they are rotated into this same section.

Nature of the Fracture

King [1912] has given the types of fracture to be expected in hollow cylinders based on the maximum stress difference failure criterion. Robertson [1955] and Jaeger [1966] give further discussions of his treatment and Robertson loc. cit. and Jaeger and Hoskins [1966] (and in appendix 2) have compared their results of tests on hollow cylinders with external pressure and axial load with the types of failure predicted by King. Since the maximum stress difference or maximum shear stress failure criterion takes no notice of stress sign only three stress conditions and families of fracture surfaces are possible. The strength of rock specimens is considerably lower in tension than in compression, however, and in some of the experiments in this investigation in which the internal pressure exceeded the external pressure tensile stresses were developed and these governed the failure rather than the compressive or shear stresses. If the positive compressive stress sign convention is used, six different arrangements of principal stresses at failure can be written:

(1) $\sigma_z > \sigma_\theta > \sigma_r$

(2) $\sigma_r > \sigma_\theta > \sigma_z$

(3) $\sigma_\theta > \sigma_z > \sigma_r$

(4) $\sigma_r > \sigma_z > \sigma_\theta$

(5) $\sigma_z > \sigma_r > \sigma_\theta$

(6) $\sigma_\theta > \sigma_r > \sigma_z$

Combinations (1) and (2) based on King's analysis give a set of cone shaped fracture surfaces, (3) and (4) a set of equiangular spiral fractures which Robertson [1955] called hinged trap door failure, and (5) and (6) yield a set of helical fractures which give rise to the commonly observed Luder's lines on the outer surface of the specimen. Of these, combinations (1), (3), (4) and (5) were achieved in this series of tests.

Griggs and Handin [1960] recognized two types of fractures,

(a) extension fractures or the separation of a specimen across a surface perpendicular to the direction of minimum principal stress without offset parallel to the fracture surface and

(b) faults which are localized offsets parallel to a more or less plane surface of non-vanishing shear stress thats surface may be inclined at from 45° to a few degrees to the direction of maximum principal compressive stress in homogeneous materials.

In cases in which there was actual separation across a fault in these experiments these "shear fractures" were distinguished

by the presence of powdered rock on the fault surface. In some cases slickensides and fault steps were also well developed, the fault steps invariably opposing the direction of motion.

In addition experimental fractures can be divided into primary and secondary types. Primary fractures result from the stresses applied to the sample in its more or less original state and secondary fractures resulting from either continued deformation of the already failed specimen or dynamic loading due to the release of the stored elastic energy of the testing machine. In this series of tests an attempt was made to limit the development of secondary fractures by unloading the specimen as soon as there was an indication of the impending collapse of the specimen. In a few cases repeat tests were made in which total collapse was permitted allowing some direct comparisons to be made. It was not possible to control the failure of the specimens that collapsed inwardly as this was a violent, almost explosive phenomena, and complete control in any case is very difficult unless an extremely stiff testing machine is used.

A possibly separate type of secondary fracture is what Borg and Handin [1966] term a release fracture. These are extension fractures formed perpendicular to the direction of maximum compressive stress. They are thought to develop as a result of differential expansion during release of differential stress and/or confining pressure. If so, they may be associated

with the secondary changes in length of experimentally deformed rocks studied by Paterson [1963].

Tables I, II and III give the types of fractures observed in each test for each rock type for the different principal stress relationships at failure which were achieved. Figures 16, 17, 18, 19, 20 and 21 are examples of variously fractured specimens illustrating each of the major types. Transitional examples occurred when the cylinders were near to failure in both extension and compression. As an example, in a marble hollow cylinder in which the stresses on the inner surface at failure were σ_z = 2.06 kb, σ_r = 1.24 kb and σ_θ = -.111 kb, a fault plane, extension fractures perpendicular to σ_θ and helical fracture traces were all present in the cylinder after completion of the test.

The cylinders which failed by collapse deserve special mention. This was a sudden and extremely violent phenomena in all three rock types. Usually one-half to two-thirds of the height of the cylinder collapsed inwardly on equiangular spiral fracture surfaces. The hole in the remaining cylindrical portion was filled completely with densely packed powdered rock. The origin of this powdered material is of some interest. Adams [1912], Bridgman [1918] and others have observed spalling at the inner surface of a hollow cylinder subjected to external load and axial pressure. Small flakes of rock are ejected from

Fig. 16 Trachyte hollow cylinder after fault plane failure. Stresses on inner surface at failure from equations (1), (2) and (3), σ_r = 0.69 kb, σ_θ = 0.69 kb, and σ_z = 5.17 kb. Photographed against a 10 to the inch grid.

Fig. 17 Trachyte hollow cylinder after extension and fault failure showing the development of extension fractures perpendicular to the maximum principal stress. Stresses on inner surface at failure from equations (1), (2) and (3), σ_θ = -0.16 kb, σ_r = 0.52 kb, σ_z = 2.22 kb. Photographed against a 10 to the inch grid.

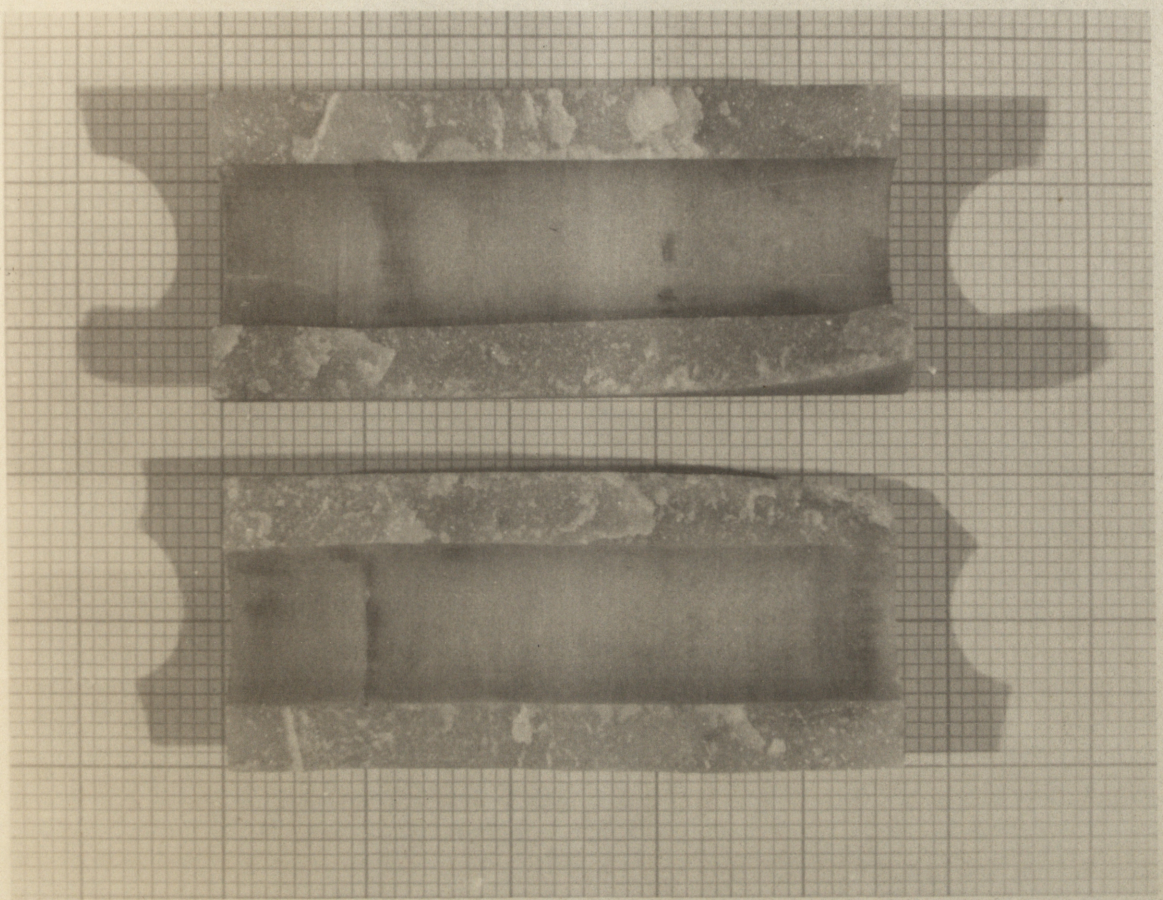

Fig. 18 Carrara marble after an extension fracture. Stresses on inner surface at failure from equations (1), (2) and (3), $\sigma_r = +0.54$, $\sigma_\theta = 0$, $\sigma_z = +0.69$. Photographed against a 10 to the inch grid.

Fig. 19 Trachyte hollow cylinder after "collapse" failure. Stresses on inner surface at failure from equations (1), (2) and (3), $\sigma_r = 0$, $\sigma_\theta = 2.9$ kb, and $\sigma_z = 3.1$ kb. End views of the two major portions recovered after the test. Photographed against a 10 to the inch grid.

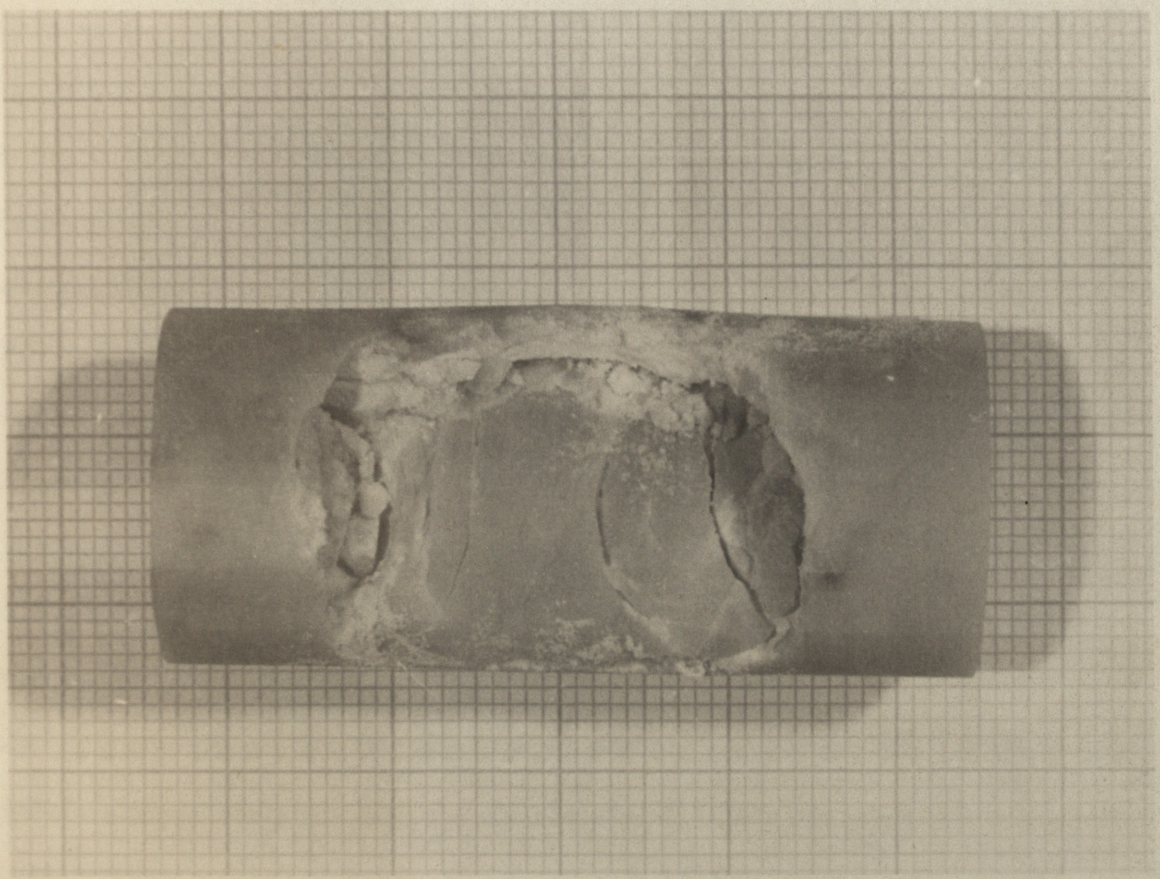

Fig. 20 Carrara marble specimen after a collapse or trap door type of failure. Stresses on inner surface at failure from equations (1), (2) and (3), $\sigma_r = 0$, $\sigma_\theta = 2.75$ kb, and $\sigma_z = 2.71$ kb. Photographed against a 10 to the inch grid.

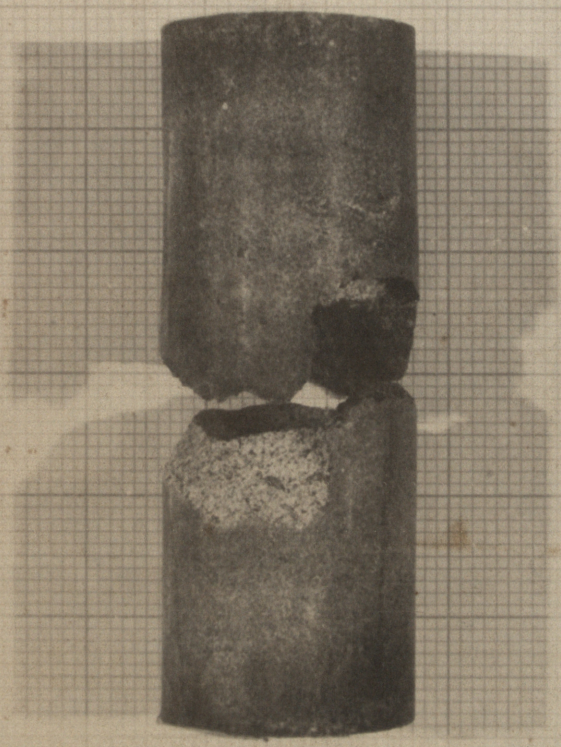

Fig. 21 Trachyte hollow cylinder after conical fault failure. Stresses on inner surface at failure from equations (1), (2) and (3), σ_r = 0.17 kb, σ_θ = 2.59 kb, and σ_z = 5.52 kb. Photographed against a 10 to the inch grid.

the inner surface of the cavity apparently with great velocity. In the case of Bridgman's experiments, this powdered material completely filled the cavity creating eventually an internal back pressure due to the increase in volume of the broken material and this internal pressure then inhibited further failure. In a few cases in the present investigation an experiment was stopped just short of failure and the specimen unloaded and inspected. Only a small amount of spalling had occurred with the dozen or so spalled particles being flake-like in shape and a few millimeters in diameter. When the specimens were subsequently reloaded they failed by collapse at only a slightly higher stress and when recovered the portion which did not collapse was tightly filled with mostly fine, approximately equi-dimensional angular particles plus a few much larger fragments. When this material was dug out of the cavity, the cavity walls were found to be unmarked over most of this area. It seems clear that the majority of the powdered material in these cases did not come from spalling but from the almost explosive disintegration of the collapsed portion of the cylinder. The elastic strain energy density in a trachyte hollow cylinder which collapsed under an external pressure of 1.38 kb was approximately 4×10^{13} ergs/cc. This may be compared with estimates of the strain energy/unit volume liberated by rock bursts in deep mines of from 0.38×10^{13} ergs/cc to 38×10^{13} ergs/cc, c.f. Duvall and Stephenson [1966].

Inward collapse of the specimens occurred when σ_θ at failure approached and became greater than σ_z. When $\sigma_z > \sigma_\theta > \sigma_r$ failure was usually on conical fracture surfaces. Minor spalling was almost always present in these tests and it occurred at the intersection of the conical faults with the inner surface of the specimen.

Several specimens were sawn in half longitudinally after testing and the failure examined in greater detail. There are three points to consider:

(1) does the failure actually start at the inner surface of the cylinder,

(2) is there evidence of non-elastic deformation and if so how far into the walls of the specimen does it proceed, and

(3) what are the characteristics of the failure traces in this surface.

In all cases when failure had not gone completely through the specimen the fractures ran from the inner surface of the hollow cylinder towards the outer surface. Where evidence of non-elastic deformation was found (twinning in the marble and grain boundary fracturing in trachyte) this deformation was always greatest at the inner wall of the hollow cylinder. Thin sections of marble and trachyte specimens were examined using a polarizing microscope and universal stage. While a detailed petrofabric analysis was beyond the scope of this project,

qualitative information on the distribution and amount of non-elastic deformation can be gained by plotting twin lamallae spacing index and percent of total grains twinned against radius for the marble hollow cylinders. This is done for a marble test specimen in Figure 22. The mechanisms of non-elastic deformation of calcite aggregates have been thoroughly studied by Turner, Griggs, Handin and their associates, c.f. Turner and Weiss [1963] for a summary of this work. At room temperature the dominant form of deformation is twin gliding on $\{01\bar{1}2\}$. These twins are easily recognized and assuming each new twin to be of approximately equal width the more heavily twinned grains have undergone the greatest deformation.

Characteristics of the fracture intersections with the saw cut surfaces were studied by grinding the surfaces, coating them with a penetrating dye and then grinding the dye coated surface carefully away leaving the fractures which the dye had penetrated visible as lines.

Comparison with Other Work

To test the possibility that these results are merely the accident of the particular materials or testing scheme used, the work of several other investigators has been replotted in the same form as the results of this investigation so that comparisons can be made.

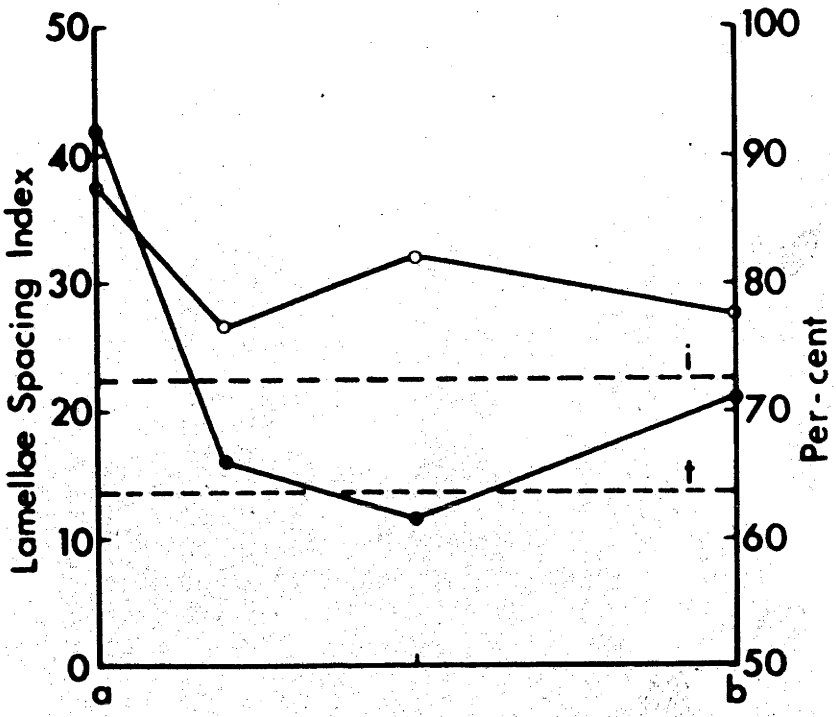

Fig. 22 O Lamellae spacing index and ● percent of grains twinned for marble hollow cylinder before and after testing. Principal stresses on inner surface at failure; σ_r = 0.35 kb, σ_θ = 2.17 kb, σ_z = 3.78 kb. a inner radius of hollow cylinder, b outer radius. i average spacing index for an undeformed specimen, t average percent of grains twinned for an undeformed specimen.

von Karman [1911] and Böker [1915] have previously worked on Carrara marble. von Karman did triaxial tests on solid cylinders and Böker did extension tests and torsion tests under confining pressure on solid cylinders. Their results are given in Figure 23 which may be compared with Figure 8. Although Böker did not do enough torsion tests to warrant drawing the σ_3/σ_2 contours with any confidence, his results are similar in form and do not contradict those from the series of tests on hollow cylinders done in this investigation.

Wu, Loh and Malvern [1963] conducted a series of tests on hollow cylinders of clay and sand similar to the present series of tests on rock. Their conclusions were that when expressed in terms of Hvorslev parameters the strength of clay was independent of the intermediate principal stress and loading path but that the strength of sand was dependent upon the intermediate stress. Data taken from their Tables II and III are plotted in Figure 24(a) and (b). The results are strikingly similar to those of this investigation. Hvorslev parameters are not applicable to tests on dry solid rock so no direct comparison with their conclusions can be drawn.

Bellamy [1960] has published results of tests performed on solid and hollow cylinders of concrete with external pressure and axial load. These are plotted in Figure 25 and are also compatible with the results of this investigation.

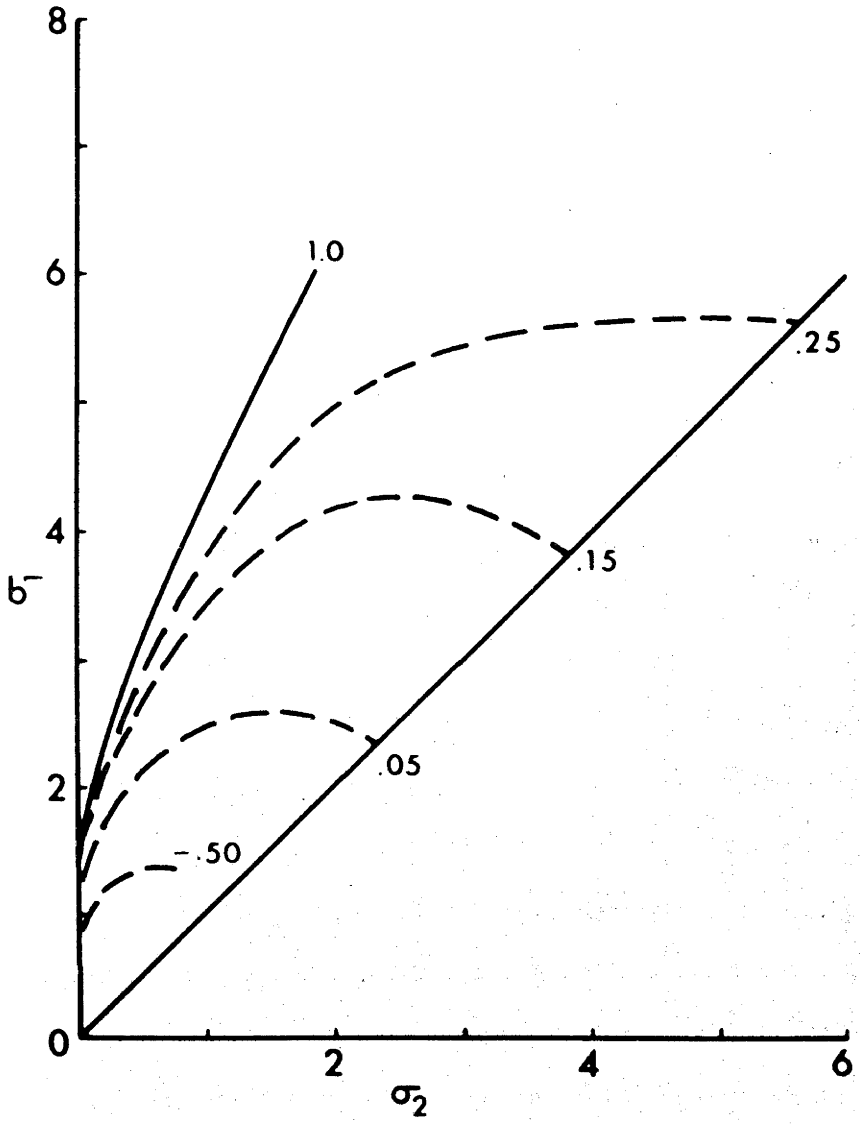

Fig. 23 Results of triaxial compression tests by von Karman and extension and torsion tests by Böker. σ_1 plotted against σ_2 for various ratios of σ_3/σ_2. Position of the dashed lines inferred only as they are interpolated between just a few scattered experimental points. Stresses are in thousands of atmospheres.

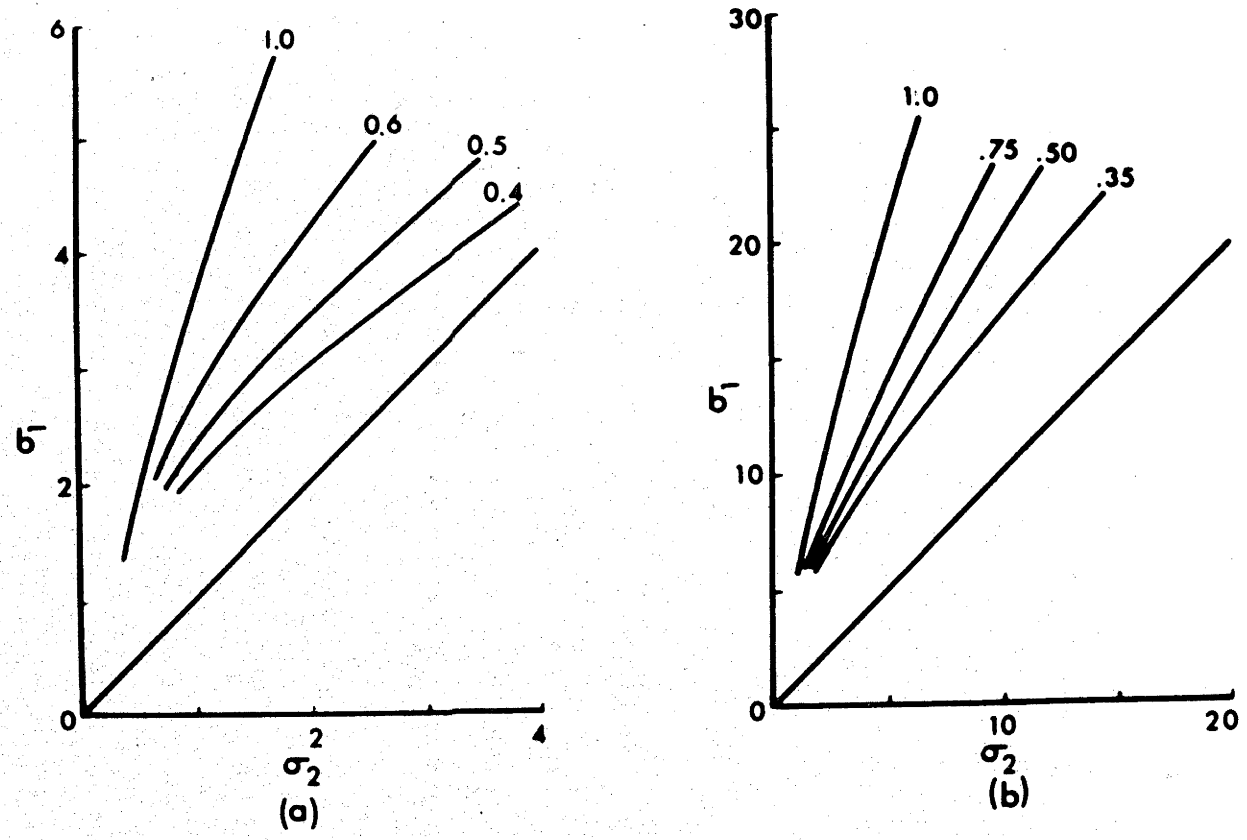

Fig. 24 Results of hollow cylinder tests by Wu, Loh and Malvern on (a) clay, batch #1 and (b) sand. σ_1 plotted against σ_2 for various ratios of σ_3/σ_2.

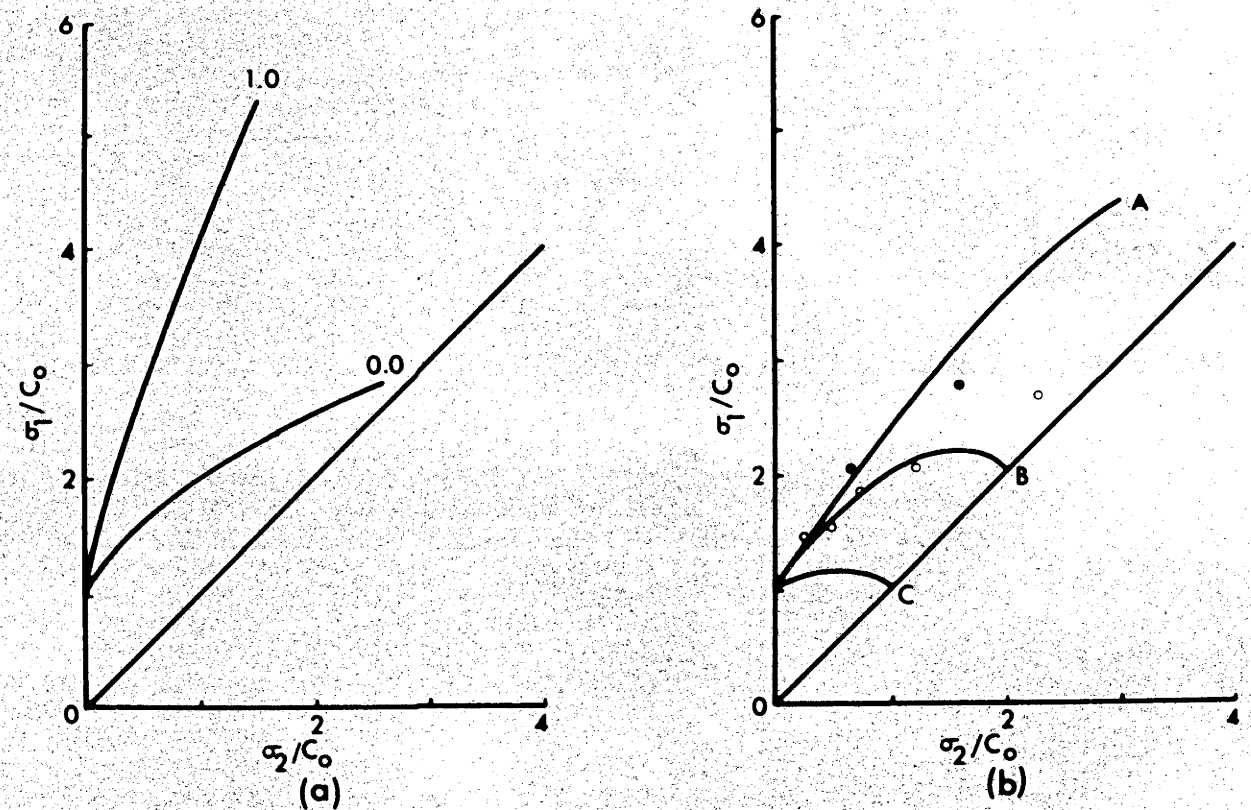

Fig. 25 Results of solid and hollow cylinder tests on concrete by Bellamy. (a) σ_1 versus σ_2 for σ_3/σ_2 ratios of 1.0 and 0.0. (b) Concrete test results when $\sigma_3 = 0$. ● Hollow cylinders with $P_i = 0$. ○ Triaxial tests with $\sigma_2 = 0$. ○ Triaxial tests with $\sigma_2 = \sigma_3$ when rotated about the $\sigma_1 = \sigma_2 = \sigma_3$ axis into the $\sigma_3 = 0$ plane. "A" McClintock-Walsh failure criterion rotated into the $\sigma_3 = 0$ plane with σ_c assumed equal to 0. "B" three dimensional Griffith theory in the $\sigma_3 = 0$ plane. and "C" the distortional energy failure criterion in the $\sigma_3 = 0$ plane.

Handin, Heard and Magouirk [1967] have recently reported the results of a series of torsion tests on thin walled hollow cylinders of limestone, dolomite and glass and compared the torsion tests with triaxial compression and extension tests. They did not find an adequate failure criterion from their results but they offer the following observation:

> "In the brittle state, the shear strength of the material does depend on the relative magnitude of the intermediate principal stress, σ_2. Over the region of mean pressure in Solenhofen limestone where faulting occurs in all three tests (2 to 3 kb), the ultimate octahedral shear strength is greater in torsion than in extension ($\sigma_2 = \sigma_1$) and less than in compression ($\sigma_2 = \sigma_3$)."

This observation is certainly in agreement with the results of the present tests on thick walled hollow cylinders.

Discussion

It seems clear that the magnitude of the intermediate principal stress has a large and regular effect on the strength of rock. None of the currently accepted failure criteria can consistently predict the failure strength of these rocks. Jaeger's [1966] recent proposal to form a failure surface by rotating the triaxial test data around the line $\sigma_1 = \sigma_2 = \sigma_3$ is reasonably well substantiated by these experiments. Mohr-Coulomb strength theory, Griffith theory in its original form and the

McClintock-Walsh modification of Griffith theory as it was originally proposed appear to be valid only for the rather special condition of $\sigma_2 = \sigma_3$. Octahedral shear stress theory even when limited to conditions of compression simply does not correspond to the present experimental values. The rotated, three stress versions of Griffith theory and modified Griffith theory more or less fit data from individual rock types but neither can be used generally.

The shape of the failure surface must ultimately be related to the microscopic mechanism of deformation and failure. The work of Griggs, Handin, and their co-workers has shown that the mechanism of failure in rocks depends not only upon the material but its stress state, strain rate and temperature as well. Neglecting the effects of strain rate and temperature, the most likely mechanism of failure for the trachyte (composed principally of silicates) at the relatively low stresses (of the order of a few kilobars) achieved in these experiments is fracturing. The McClintock-Walsh model if generalized to 3 stress dimensions is designed to describe these conditions and in fact it does conform reasonably well to the trachyte experiments. The marble and presumably the cementing material in the sandstone can deform by twinning or gliding on suitably oriented crystallographic planes as well as fracturing, however, and this mechanism is not described by any of the models. The

rotation of the triaxial test data to form a failure surface while purely an empirical procedure does in some measure take into account the mechanisms of deformation acting at higher pressures.

The possible effects of a non-elastic stress distribution can only be assessed qualitatively. The maximum stresses in a partially yielded hollow cylinder will be at the elastic-plastic boundary rather than at the inner surface. The actual stress distribution depends on both the yield criterion and the shape of the stress-strain curve for the material. The discussion given by Robertson [1955] based on a maximum shear stress failure criterion and an elastic-perfectly plastic stress-strain curve can be used as a guide. According to this solution, in the partially yielded condition the maximum tangential stress σ_θ at the elastic plastic boundary in the specimen is lower and the radial and axial stresses σ_r and σ_z are higher than the corresponding elastic solution for the stresses on the inner surface of the specimen under the same applied pressures. The effect of this on the tests in which $\sigma_\theta > \sigma_z > \sigma_r$ in Figures 10 through 15 would be to decrease σ_1 relative to σ_2 for these tests and in the case of the sandstone results to considerably decrease the amount of scatter in the data.

The stress gradients achieved in these tests appear to have little effect on rock strength in compression. In a few

cases tests were made in which $\sigma_{z_1} > \sigma_{\theta_1} > \sigma_{r_1}$ and then another test done in which $\sigma_{\theta_2} > \sigma_{z_2} > \sigma_{r_2}$ when $\sigma_{z_1} = \sigma_{\theta_2}$, $\sigma_{\theta_1} = \sigma_{z_2}$ and $\sigma_{r_1} = \sigma_{r_2}$. σ_z is a uniform stress while σ_θ and σ_r vary through the cross section of the specimen. The trachyte results with $\sigma_\theta > \sigma_z$ are indistinguishable from those in which $\sigma_z > \sigma_\theta$. In the sandstone there is considerable scatter with the $\sigma_\theta > \sigma_z$ results being generally stronger but this could well be the result of the inapplicability of the elastic stress solution to the weak and easily deformed sandstone at the pressures required to bring about this stress distribution. The results of the series of confined brazilian tests by Jaeger and Hoskins [1966] (appendix 2) are in reasonable agreement with these hollow cylinder test results especially in the case of the sandstone. The geometry of the brazilian test specimens and the stress gradients within the specimens are different than those in the hollow cylinders and for these two types of tests to agree either this amount of difference of stress gradient and specimen geometry are not very important or some coincidence has occurred.

All of the experiments reported in Tables I, II and III were performed on the same size hollow cylinders. The triaxial tests given are simply hollow cylinders tested with $P_i = P_e$. Robertson [1955] has reported hollow cylinder tests on many different rocks in which

he compared the strength of specimens with various ratios of internal to external diameter. There appear to be some systematic differences in his results with the thicker walled specimens generally the strongest. Whether this is due to the slight difference in stress gradients achieved in the tests or to the differences in surface area and/or volume of the specimens or some other factor is not yet clear.

The effect of stress gradients when one or more of the principal stresses is tensile is another matter. Jaeger and Hoskins (appendix 3 of this thesis) have suggested that stress gradients do affect the failure strength of rock in tension. In these hollow cylinder tests it was only possible for σ_θ to be tensile when σ_r and σ_z were compressive. The tensile strength was found to be dependent upon the magnitudes of these other two compressive principal stresses. In trachyte the maximum value was from a test in which σ_θ = -0.477 kb (tensile), σ_z = 1.53 kb and σ_r = 1.34 kb. This may be compared with the results of an unconfined 15° contact angle brazilian test which gave stress values at failure of σ_1 = 0.394 kb, σ_2 = 0, and σ_3 = -0.129 kb. In other words the rock in the hollow cylinder test failed at a tensile stress about 3.7 times greater than its tensile strength as determined by the commonly used brazilian test. The tensile stress at failure in the trachyte hollow cylinders tested without axial load and with internal pressure

only was -0.19 kb or about 1.5 times the brazilian value. These variations in measured tensile "strength" are in reasonably close agreement with factors that can be derived from Weibull's [1939] statistical theory of tensile strength. It might be argued that the extension fractures could have formed at a lower stress but did not propagate because of the compressive stresses, however, in the tests which gave rather high tensile strengths, failure was very definite with a sharp pressure drop and an easily audible click. There was no hint of progressive failure or weakening of the specimens during the stages of the tests just preceding failure nor was there any evidence of shear failure in the rocks when examined after the tests. Although a few strange looking fractures were found, specimens which were close to failure in both extension and compression often appeared to develop separate extension and fault or shear fracture surfaces simultaneously rather than a single set of some transitional form.

Any attempt to vary the stress gradients at failure in a hollow cylinder of a given size and wall thickness involves changing the loading sequence to failure as well. This change of loading sequence or stress path, however, may not be very important. Failure strength should be independent of stress path in a linear elastic material and Scott [1962, §8-5] quotes several references indicating that the final yield surfaces of

some presumably non-elastic clays are independent of the stress path, but no specific experiments are known establishing this for rocks.

It would appear from these tests as well as those reported by Brace [1964] that there is a smooth transition from tensile failure under combined stresses to compressive or shear failure. There are no "cut offs" or regular bulges evident in the "failure surface". It is suggested that the complete failure surface can be found by rotating the triaxial test data about the $\sigma_1 = \sigma_2 = \sigma_3$ axis. It is easy to check this procedure for any particular rock by performing tests on hollow cylinders with external pressure and axial load only. These hollow cylinder test results should fall on the triaxial curve after it has been rotated into the $\sigma_3 = 0$ section of the "failure surface".

Chapter III

ROCK FAILURE UNDER THE CONFINED BRAZILIAN TEST

The Brazilian, or indirect tensile, test, in which a disc is loaded in a diametral plane by forces applied at opposite ends of a diameter, is extended by jacketing the specimen and applying an additional confining pressure. In this way failure was studied over a range of conditions in which the least principal stress varies from tensile to compressive. The fracture is always an extension fracture in the loaded diametral plane, even if all the principal stresses are compressive. The stress analysis is based on elastic theory. Experiments were made on three isotropic rocks, and they suggest that the value of the intermediate principal stress affects the conditions for failure. The magnitude of this effect appears to be equal to that which would be predicted for these principal stress relationships from the results of the hollow cylinder tests discussed in Chapter II.

The results of these confined Brazilian tests have been published in the Journal of Geophysical Research, v. 71, no. 10, pp.2651-2659, May 15, 1966, and a reprint of the paper is included as appendix 2 to this thesis. The tests are fully discussed in the paper and as it is submitted as an integral part of the thesis there is no need to repeat the discussion here. It should be pointed out that it is difficult to imagine

a situation in which rock in either its natural state or in the conditions surrounding a man made excavation is placed in simple uniaxial tension. One or both of the other principal stresses acting will nearly always be compressive. The Brazilian test and confined Brazilian test are probably more realistic approximations to "in situ" rock failure in tension than is the uniaxial tensile test.

Chapter IV

STRESSES AND FAILURE IN RINGS OF ROCK LOADED IN DIAMETRAL TENSION OR COMPRESSION

The failure of rock materials in the form of rings subjected to line loadings on either their internal or external surfaces has been studied. Experimental results for three fine grained rocks are given and values of the tensile strengths so obtained are compared with those from direct tension, indirect tension (Brazilian) and bending tests. It is found that the calculated tensile stresses at failure for rings loaded in either fashion, and for bending tests, are considerably higher than those for direct tension or the indirect tensile test. It is suggested that this is due to the fact that in the two latter cases the stresses are uniform (or nearly so) over the section in which failure takes place, while in the three former they vary almost linearly across it. This suggests that a criterion for tensile failure must not simply involve the stresses at a point, but also their rate of change with position.

The results of this series of experiments have been published in the British Journal of Applied Physics, v. 17, pp. 685-692, 1966, and a reprint of the paper is included as appendix 3 to this thesis. The experiments are fully discussed in the paper and as it is submitted as an integral part of the thesis the discussion will not be repeated here.

Chapter V

OBSERVATIONS ON THE FAILURE OF ANISOTROPIC ROCK UNDER COMPLEX STRESSES

Introduction

A number of experiments have been made on solid and hollow cylinders of an anisotropic slate. A few diametral compression tests both unconfined and with additional confining pressure have also been conducted. The object of the experiments was to determine the mode of fracture of anisotropic rock under complex stresses and to gain some preliminary knowledge of the forces required to break this particular slate under these conditions. No attempt was made here to solve the various anisotropic elasticity problems and calculate the stresses within the specimens accurately. The corresponding isotropic stress solutions for the same specimen geometry and loading have been given in most cases but these are only intended to be used as rough guides and the values calculated should not be taken too seriously. In a few cases, because of symetry the isotropic and anisotropic solutions may coincide.

Many rocks in nature appear to be anisotropic in terms of either their elastic properties or their "strength" or both. Failure of rock in the usual rock mechanics applications more often occurs under complex polyaxial stresses rather than the

simpler uniaxial or triaxial stress systems. It seems important then to study in the laboratory the failure of anisotropic rocks under these more realistic though less well understood conditions. Very little has been done. Jaeger [1960], Donath [1963], and Hoek [1964] have tested cylinders of slate cut at different angles to their foliation in uniaxial and triaxial compression. Berenbaum and Brodie [1959], Hobbs [1962] and Pomeroy and Hobbs [1962] have tested coal under a variety of systems. Other work has been done on the deformation at high temperature and pressure of a few anisotropic rocks such as the Yule marble, Griggs and Miller [1951], Handin, Higgs and O'Brien [1960], Hasmark dolomite, Handin and Fairbairn [1955], and a phyllite, Paterson and Weiss [1966].

Experimental Material and Apparatus

A large slab of slate was collected from an abandoned quarry near Chatsbury, New South Wales. An x-ray analysis of the rock indicated that it is primarily quartz, chlorite, and muscovite with a small amount of graphite. A few grains were as large as 3 microns but most were much smaller. All of the test specimens were prepared from this single piece of rock. This slate seems to be isotropic in its plane of foliation. Cylinders arbitrarily cored in this place (with their axis parallel to the foliation) at right angles to each other show no significant difference in their strength or elastic properties.

The finish size of the solid cylinders for the compression tests cored from this rock was 7/8 inch diameter by $2\frac{1}{8}$ to $2\frac{1}{4}$ inches long. Hollow cylinders were 7/8 inch outside diameter by 23/64 inch inside diameter by $2\frac{1}{8}$ to $2\frac{1}{4}$ inches long. The diametral compression specimens were 2 inches in diameter by $1\frac{1}{4}$ inches long. All of the solid and hollow cylinders were tested with their ends lubricated with sheets of dry paper and graphite as discussed in appendix 1. A single spherical seat was used in all cases. The diametral compression specimens were loaded through platens ground to give a contact angle of 15° and these were loaded through a single cylindrical seat.

The solid and hollow cylinders were tested with their axis parallel to, perpendicular to and at 45° to the foliation of the slate. The diametral compression cylinders were cored parallel and perpendicular to the foliation. Those drilled parallel to the foliation were then tested with the loaded diameter parallel to, perpendicular to or at 45° to the plane of foliation.

The specimens were tested in simple piston and cylinder triaxial pots with additional load applied by either an Avery 50 Ton or 500 Ton testing machine. Confining pressure was developed by a manual hydraulic pump and held constant (to better than 1 per cent) throughout the test by a screw press and a needle valve. The solid and hollow cylinder compression

specimens were jacketed with soft rubber tubing and the diametral compression specimens with .003 inch thick brass.

Experimental Results

The results of these experiments are given in Tables IV, V, VI, and VII. The axial stress listed for the solid and hollow cylinders is merely the total axial force applied at failure divided by the initial cross sectional area. The (σ_θ) values given for the hollow cylinders are calculated from istropic elastic theory, c.f. Jaeger [1960] and it must be emphasized again that these are furnished only as approximations. The actual tangential stress present in an anisotropic rock around a circular hole has been estimated to be of the order of 10 per cent different from the stresses around a hole in isotropic rock (Obert and Duvall [1967, p.488]). This estimate was based on Lekhnitskii's [1963] plane stress solution for an anisotropic plate. It corresponds most closely to the cylinders with their axis parallel to the foliation.

The cylinders with their axis perpendicular to the foliation should correspond closely to the isotropic solution but the actual stress distribution in the cylinders cored at 45° to the foliation is completely unknown.

All of the compression specimens tested with their axis either parallel or perpendicular to the foliation behaved in

Table IV

Results of Confined Compression Tests on Solid Cylinders of Slate

Test No.	Angle from Core Axis to Foliation	Confining Pressure psi	Axial Stress psi
GBSA-300	0	0	35100
GBS-800	0	0	32800
GBSA-301	0	2000	45500
GBS-801	0	2000	47200
GBSA-302	0	4000	59000
GBSA-303	0	8000	78500
GBSA-304	0	12000	94600
GBSC-101	90	0	32900
GBSC-102	90	1000	38400
GBSC-103	90	3000	50600
GBSC-104	90	5000	52600
GBSC-105	90	7500	69500
GBSC-106	90	10000	76000
GBS-45-100	45	0	6400
GBS-45-101	45	2000	16720
GBS-45-102	45	4000	23950
GBS-45-103	45	8000	32200
GBS-45-104	45	12000	36900
GBS-45-105	45	12000	41500

Table V

Results of Confined Compression Tests on Hollow Cylinders of Slate

Test No.	Angle from Core Axis to Foliation	Confining Pressure psi	Axial Stress psi	(σ_θ) psi
GBSC-501	0	0	30700	(0)
GBSC-502	0	2500	39430	(6050)
GBSC-503	0	5000	50650	(12100)
GBSC-506	0	8000	60080	(19400)
GBSC-505	0	10000	47100	(24400)
GBSC-504	0	15000	18150	(36300)
GBSC-207	90	0	29000	(0)
GBSC-210	90	1000	39900	(2420)
GBSC-203	90	300	49370	(7250)
GBSC-205	90	5000	53050	(12100)
GBSC-211	90	7500	56470	(18160)
GBSC-204	90	10000	62500	(24200)
GBSC-212	90	12500	65230	(30250)
GBSC-213	90	22500	80800	(54500)
GBSH-45-200	45	0	6050	(0)
GBSH-45-201	45	2000	16720	(4860)
GBSH-45-202	45	4000	20790	(9720)
GBSH-45-203	45	8000	29130	(19440)

Table V (cont.)

Test No.	Angle from Core Axis to Foliation	Confining Pressure psi	Axial Stress psi	(σ_θ) psi
GBSH-45-204	45	12000	38670	(29200)
GBSH-45-205	45	12000	38900	(29200)

(σ_θ) is the tangential stress on the inner surface of an isotropic hollow cylinder with the same dimension and applied forces as these tests

Table VI

Results of Diametral Compression Tests on Slate

Specimen No.	Angle from Cylinder Axis to Foliation	Angle from Load to Foliation	Load at Failure lbs	Principal Stresses at the Centre of an Isotropic Disc with these Loads, psi		
				(σ_1)	(σ_2)	(σ_3)
MAR A-1	0	0	5040	3780	0	-1260
GBS A-1	0	0	4600	3450	0	-1150
GBS B-1	0	0	4950	3720	0	-1240
Avg	0	0	4865	3650	0	-1220
MAR A-2	0	90	12300	9250	0	-3075
GBS B-2	0	90	12100	9100	0	-3020
GBS A-2	0	90	13300	10000	0	-3320
Avg	0	90	12570	9450	0	-3140
MAR B-4	0	45	4250	3190	0	-1060
GBS C-1	90	0	17475	13150	0	-4360
GBS C-2	90	0	17300	13000	0	-4320
MAR C-1	90	0	17900	13450	0	-4470
Avg	90	0	17560	13200	0	-4390

Table VII

Results of Confined Diametral Compression Tests on Slate

Angle From Core Axis to Foliation	Angle from Load to Foliation	Confining Pressure psi	Differential Load at Failure lbs	Principal Stresses at the Centre of an Isotropic Disc with these Loads, psi		
				(σ_1)	(σ_2)	(σ_3)
0	90	7250	23500	(24800)	(7250)	(+1380)
0	45	7250	16600	(19730)	(7250)	(+2320)
90	0	7250	38800	(36400)	(7250)	(-2450)

a brittle, elastic manner with little or no curvature of the force-displacement record. Solid cylinders of slate cored at 45^{o} to the foliation failed in a brittle manner up to 4000 psi confining pressure with all of the visible failure on a single foliation plane. At 8000 and 12000 psi the deformation was more distributed, there was displacement on several foliation planes and the force-displacement record from the testing machine X-Y recorder is very slightly curved. Not very much can be said about the apparent behaviour of these rocks at and immediately after failure as this is a function of the relative stiffness of the testing machine.

Figures 26 and 27 show the effect of confining pressure on the axial stress at failure for the three core axis to foliation plane angles that were tested for solid and hollow cylinders.

Fracture Descriptions

In nearly all cases where the direction of the maximum principal stress is known in these experiments, the primary fracture surface appears to go through the intersection of the plane of foliation and the plane perpendicular to the direction of the maximum principal stress. A brief description of the fractures found in selected representative tests of each type is given below.

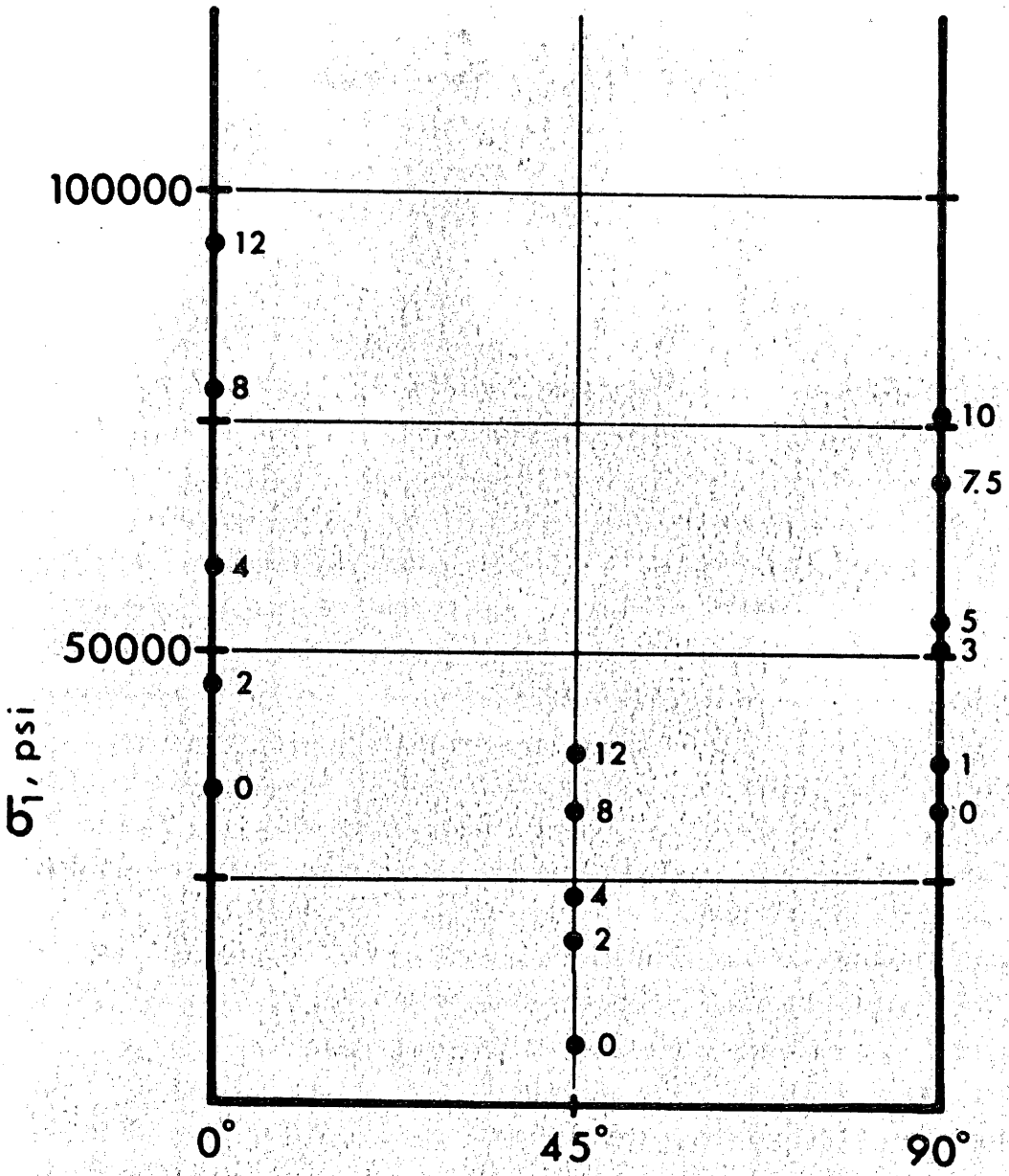

Fig. 26 Results of confined compression tests on solid cylinders of slate. Axial stress at failure versus angle from core axis to foliation. Numbers by the experimental points are the confining pressures in thousands of psi.

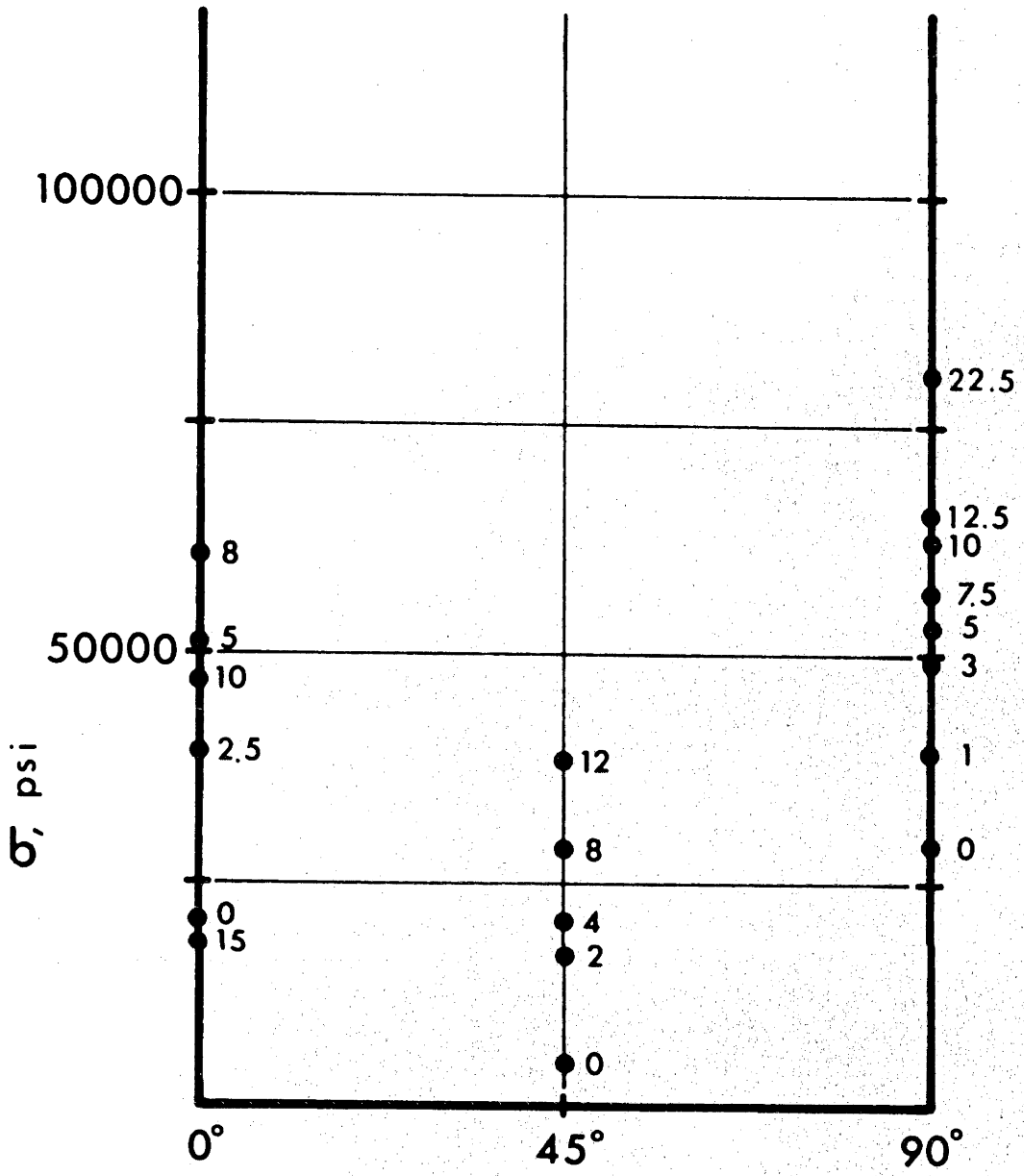

Fig. 27 Results of confined compression tests on hollow cylinders of slate. Axial stress at failure versus angle from core axis to foliation. Numbers by the experimental points are the confining pressures in thousands of psi.

Diametral Compression Tests

Typical fracture patterns from the diametral compression tests are given in Figure 28. Figure 28 (a) is the result of an unconfined test with the diametral load applied parallel to the foliation. The rock simply splits in the plane of foliation. (b) is the result of an unconfined test with the diametral load at right angles to the foliation. The rock did not fail in the diametral plane. It fractures approximately in the foliation at or near the areas of loading. Figure 28 (c) is a drawing of the surface of a specimen cored perpendicular to the foliation. It was tested unconfined and finally failed in the diametral plane at a load about $3\frac{1}{2}$ times greater than that of the specimen shown in (a). The specimen was also extensively split in the foliation planes (parallel to the face shown). The assorted fractures shown (other than the diametral crack) do not go completely through the specimen but are only $1/32$ to $\frac{1}{8}$ inch deep and then have failed in the foliation plane and flaked off of the surface. Figure 28 (d) is a specimen that has been tested unconfined with the foliation at 45° to the load. The majority of the fracture is at an angle between the foliation and the load, (approximately 20° to diametral load). Figure 28 (e) shows the fractures visible on the surface of a specimen tested with the foliation at 45° to the loaded diameter under a confining pressure of 7250 psi. Figure 28 (f) shows the

fractures visible on the surface of a specimen tested at 7250 psi confining pressure with the foliation at right angles to the loaded diameter. The suggestion from (e) and (f) is that at still higher confining pressures a plane diametral fracture might form parallel to the applied load regardless of the foliation direction. Figure 28 (g) is a drawing of the surface of a specimen cored perpendicular to the foliation that had been tested under 7250 psi confining pressure. A plane diametral fracture is formed in this case with some fine scale distributed fracturing near one of the loaded surfaces. There was no evidence of this specimen fracturing in the foliation (parallel to the surface shown).

Solid Cylinders

Drawings of representative solid cylinders of slate after failure are given in Figure 29. (a) is the result of an unconfined test with the core axis parallel to the foliation. Failure was primarily by longitudinal splitting. (b) is a 4000 psi confining compression test with the core axis parallel to the foliation. Failure is now primarily by steeply dipping shear fractures with minor longitudinal splitting. (c) is a 12000 psi confined compression test again with the core axis parallel to the foliation. The failure was on a single shear plane steeply dipping but cutting through the foliation.

Figure 29 (d) is the result of an unconfined compression test on a cylinder cored perpendicular to the foliation. Most of the failure is concentrated near one end. Fracture is mainly longitudinal splitting with a few small fractures in the foliation and at an angle to it. (e) is a 5000 psi confined compression test on a cylinder cored with its axis perpendicular to the foliation. The shear fractures intersect one end of the specimen and cut across the foliation. (f) is a 10000 psi confined compression test also on a cylinder cored perpendicular to the foliation. Again there are inclined fractures intersecting one end of the specimen. Figure 29 (g) is a drawing of a cylinder tested in unconfined compression cored with its axis at 45° to the foliation. The fracture plane is approximately 30° from the core axis. Figure 29 (h) is the result of a 4000 psi confined compression test on a core with its axis at 45° to the foliation. A single fracture plane was formed at 42° to the core axis. (i) is a drawing of a 45° specimen tested at 12000 psi confining pressure. Failure here is accurately in the foliation with one major fracture separating the specimen and several minor fracture traces, which are also accurately in the foliation, visible on the surface of the two sections.

Hollow Cylinders

Figure 30 contains drawings of several representative hollow cylinders of slate after failure. Figure 30 (a) shows

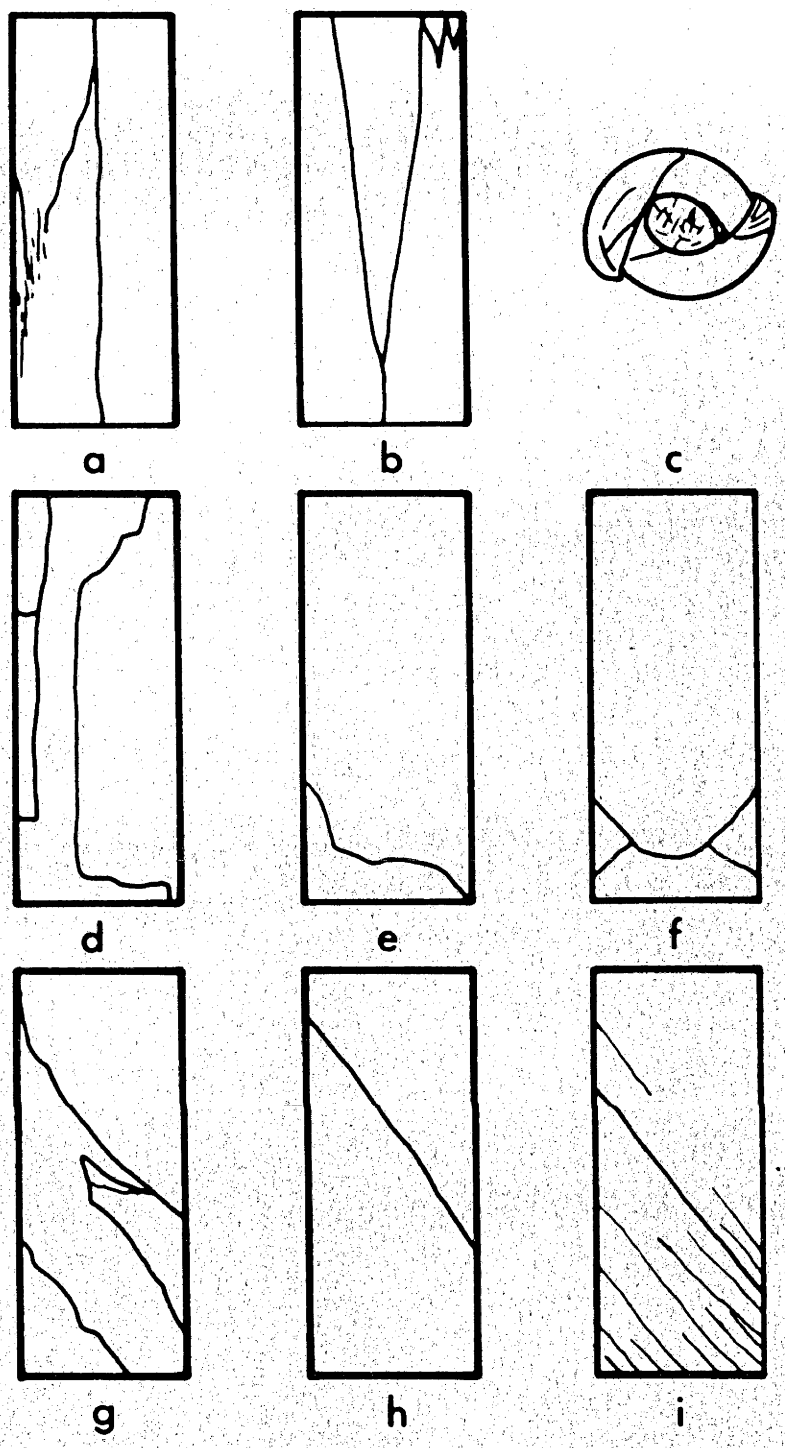

Fig. 30 Sketches of hollow cylinders of slate after failure. The results are described in the text on page 45.

the fractures visible on part of the surface of a cylinder tested in unconfined compression parallel to the foliation. The major failure is longitudinal in the foliation, splitting the specimen into halves. There is also a set of en echelon longitudinal fractures forming an inclined zone of failure in one of the halves. Figure 30 (b) shows the failure visible in a specimen tested at 5000 psi confining pressure with its core axis parallel to the foliation. The main fractures are within 10° of the core axis and there has been some sliding on these surfaces. Figure 30 (c) is the end view of a hollow cylinder with its axis parallel to the foliation that was collapsed by a confining pressure of 15000 psi. The failure was generally in the foliation. The centre hole was loosely filled with broken rock. Figure 30 (d) shows the result of an unconfined compression test on a hollow cylinder with its axis perpendicular to the foliation. Failure was primarily by longitudinal splitting with considerable associated failure in the foliation. Figure 30 (e) is a drawing of the fractures visible on the surface of a hollow cylinder with its axis perpendicular to the foliation tested at 7500 psi confining pressure. A shear surface was formed that started at one corner of the cylinder, crossed the centre hole at approximately right angles and then continued as an inclined plane. There are a few other fracture surfaces visible on the inner surface of the hollow cylinder but these

do not appear on the outer surface. Figure 30 (f) shows the fractures on the outer surface of a hollow cylinder tested to failure at a confining pressure of 22500 psi. The core axis is perpendicular to the foliation. The principal failure was a conical fracture near one end of the specimen. There was considerable fracturing visible on the inner surface of the cylinder but none of it (other than the major fracture) appeared on the outer surface. Figure 30 (g) shows the result of an unconfined compression test on a hollow cylinder cored with its axis at 45° to the foliation. The fractures range from 30° to 45° from the core axis. Figure 30 (h) shows the fracture formed in a hollow cylinder of slate tested with 2000 psi confining pressure. The core axis again is at 45° to the foliation. There is a single plane fracture inclined at 35° to the core axis. Figure 30 (i) is from a specimen tested at 12000 psi with its axis at 45° to the foliation. There is one major failure plane at 39° to the core axis and a large number of parallel planes along which there has been some movement but no actual separation.

Discussion

The fact that the strength of the hollow cylinders is in general greatly increased with increasing confining pressure is important. The maximum stresses and stress difference occur at the boundary of the hole in both the isotropic and

anisotropic solutions for stresses around a circular hole in an infinite plate. The maximum stresses and stress differences also occur at the inner surface of a thick-walled cylinder in the isotropic case and it has already been shown (Chapter II of this thesis) that failure in isotropic hollow cylinders of rock is initiated at the inner surface. One of the principal stresses on this surface is zero in a hollow cylinder and according to the Mohr failure criterion or the Griffith or modified Griffith failure theories the rock should fail at this surface at the same maximum stress as in an unconfined compression test. Since it apparently does not some reason must be found to explain the discrepancy. The actual stresses at the inner surface of a thick walled hollow cylinder of anisotropic rock are not known. The maximum differences between the isotropic and anisotropic solutions in the reasonably similar case of a hole in an infinite plate are in the range of 10 to 15 per cent. This certainly does not seem to be enough to explain the strength increases of up to 300 per cent that are observed. Another possibility is that the initial failure occurs at lower loads but the fractures do not propagate immediately through the specimen. This implies that there is enough failure at this lower load to relieve the stress concentration around the hole and change the stress distribution in the cylinder. There is not much evidence for

this. Except for the tests done at the highest confining pressures, the confined hollow cylinders appear to have failed on single shear planes or conical faults with no apparent damage to the rest of the inner surface. Failure in these tests is nearly always violent and unexpected. There is no hint of progressive weakening of the specimens except at the higher confining pressures in the 45^{o} cylinders and here considerable distributed deformation in the foliation planes is obvious with no other damage to the inner surface.

The other likely explanation is that the simple failure criteria are wrong and that there is a large and regular effect on the strength of anisotropic rock that can be ascribed to the intermediate principal stress. This is in line with the findings of Chapter II of this thesis which is based on the failure of isotropic hollow cylinders. If this is accepted it means that the fracture criteria for anisotropic rocks that have been given by Jaeger [1960], Hoek [1964], and Walsh and Brace [1964] can be valid only for the condition $\sigma_1 > \sigma_2 = \sigma_3$.

Chapter VI

AN INVESTIGATION OF THE FLATJACK METHOD OF MEASURING ROCK STRESS

A series of laboratory experiments to test the various aspects of the flatjack method of measuring rock stress have been made. The purpose of the investigation was to reproduce in so far as possible the whole procedure of the flatjack test method in the laboratory under controlled conditions with known stresses to see first how well the method measured stress and second, whether flatjacks can be used to determine "in situ" rock properties. Agreement with the known applied stresses was found to be excellent in sound rock. Problems of continued deformation after cutting the flatjack slot, differences in the values for elastic moduli determined by several methods and the relevance of these tests to the usual under ground procedure are discussed.

The results of these flatjack tests have been published in the International Journal of Rock Mechanics and Mining Sciences, vol. 3, pp. 249-264, 1966, and a reprint of the paper is included as appendix 4 to this thesis. The work is fully described and discussed in the paper and is not repeated here.

Chapter VII

AN INVESTIGATION OF BOREHOLE STRAIN ROSETTE RELIEF METHODS OF MEASURING ROCK STRESS

Full scale laboratory experiments were performed to determine the effectiveness of borehole strain rosette relief methods of measuring rock stress. The results of the experiments performed on the flattened ends of boreholes in uniaxial and biaxial stress fields have been published in the International Journal of Rock Mechanics and Mining Sciences, vol. 4, pp. 155-164, 1967. A reprint of the paper is included as appendix 5 to this thesis. The work is fully described and discussed in this paper and need not be repeated here.

Further experiments have been performed in hemispherically ended boreholes. These have not yet been published and so will be given in the sections that follow.

Strain Rosette Relief Measurements in Hemispherically Ended Boreholes

Introduction

Several techniques have now been developed throughout the world to measure rock stress. These include flatjacks c.f. Mayer *et al* [1951], Alexander [1960] and Hoskins [1966] and

appendix 4 of this thesis , curved jacks, Jaeger and Cook [1964], borehole deformation gages c.f. Hast [1958], Obert Merrill and Morgan [1962], and Leeman [1964], and strain relief on the flattened end of a borehole c.f. Mohr [1956], Leeman [1964], Hawkes and Moxon [1965] and Hoskins [1967]and appendix 5 to this thesis . None of these techniques have proven to be completely satisfactory under all conditions and the search continues for better, easier, and more universally applicable rock stress measurement methods. Leeman and Hayes [1966] for example have recently proposed a method of measuring strain relief in the walls of a borehole.

Strain rosette relief on the flattened end of a borehole is one of the more attractive of the existing rock stress measurement methods. Briefly, a diamond drill hole is drilled from an existing opening well out into the surrounding rock, the core is removed and the end of the hole ground with a specially constructed flat faced diamond bit. The face is thoroughly cleaned and dried and then a 3 element strain gage rosette is cemented to the face. A set of initial or zero strain readings are taken and then the strain gage is overcored with a thin walled diamond bit. This releases the stresses in the rock core which deforms slightly and changes the strain gauge readings. The difference between the initial and final strain readings is the elastic strain in the rock. These strains are mathematically

converted to the primary rock stresses using the elastic constants of the rock and the stress concentration factors for the flattened end of a borehole (determined by Galle and Wilhoit [1962] by three dimensional photoelasticity). A more complete description and laboratory tests of the method have been given in appendix 5 of this thesis.

There are several advantages to this technique. It can be used to take measurements at the end of a fairly long borehole well out of the area of influence of any existing major openings, only standard size (commonly BX approximately $2^3/8$ inch diameter) diamond drills and bits need to be used, and a wide variety of electric resistance strain gauges and their associated instrumentation are readily available. It has been shown, however, by Alexander [1967] and Hoskins [1967], and appendix 5 of this thesis that the method is quite sensitive to the stress component acting parallel to the axis of the borehole. While this can be taken into account in the analysis of the data, additional information such as a previous knowledge of the orientation of the principal stresses or some assumption about the exact shape of the strain relief curves for each element of the rosette is needed.

Berents and Alexander [1965] have recently proposed and used underground a modification of the technique. Instead of grinding the end of the borehole flat, it is ground to a hemispherical shape. A hemispherically ended strain relief cell

is then ~~converted~~ cemented to the face and subsequently overcored. This portion of this thesis describes the instruments and techniques necessary for deducing rock stresses from strain relief measurements made on the hemispherically ground end of a borehole. Full scale laboratory tests of the method have been performed and these are also presented.

Theoretical Considerations

No exact mathematical solution is known for the stresses and strains in the rock surrounding a hemispherically ended borehole. The solutions for a spherical cavity are well known, however, and the following analysis is based on the elastic solution for a spherical cavity given by Timoshenko and Goodier [1951]. Strains inferred from this analysis will then be compared with the measurements made on the rounded end of a borehole.

The general arrangement and coordinate system is given in Figure 31. It is assumed that all strains are measured at point A and, for these initial calculations, that one of the principal stresses in the rock mass is P_1 acting parallel to the borehole axis. The rock is considered to be an isotropic elastic continuum and compressive stresses are considered positive. The stress at A in the y direction in the borehole face due to a stress P_v applied far away from the drill hole is

$$\sigma_y = P_v \frac{27-15\mu}{2(7-5\mu)} \qquad (9)$$

where μ is Poisson's ratio. The stress at A in the x direction due to this same applied stress P_v is

$$\sigma_x = P_v \frac{15-9\mu}{2(7-5\mu)} = P_v \frac{15\mu-3}{2(7-5\mu)} \qquad (10)$$

Similarly the stresses in the borehole end face at A due to an applied stress P_h are

$$\sigma_y = P_h \frac{15-3\mu}{2(7-5\mu)} = P_H \frac{15\mu-3}{2(7-5\mu)} \qquad (11)$$

and $$\sigma_x = P_h \frac{27-15\mu}{2(7-5\mu)} \qquad (12)$$

The stresses in any direction in the borehole face at A due to a stress P_1 applied parallel to the borehole axis are

$$\sigma_x = \sigma_y = \sigma = -P_1 \frac{3+15\mu}{2(7-5\mu)} \qquad (13)$$

If the rock is linear, elastic and isotropic then the principle of superposition can be used and the total stress in the face of a hemispherically ended borehole at point A in say the y direction is

$$\sigma_y = P_v \frac{27-15\mu}{2(7-5\mu)} + P_h \frac{15\mu-3}{2(7-5\mu)} - P_1 \frac{3+15\mu}{2(7-5\mu)} \qquad (14)$$

If $P_v = P_h = P_1 = P$ or the rock stress is hydrostatic, the stress σ in the end face of the borehole in any direction is

$$\sigma = \frac{3}{2} P \qquad (15)$$

The stress distribution is generally dependent upon Poisson's ratio. Figure 32 shows the effect of Poisson's ratio on the maximum stress σ_y in the borehole face and the extent of the stress concentration into the rock for an applied stress P_v. Figure 33 shows the similar data for P_l, a stress applied parallel to the borehole axis. Figure 34 shows the stress concentration in and away from the end face of a hemispherically ended borehole in a hydrostatic stress field. The stress distribution in this particular case is independent of Poisson's ratio. In all cases the stress concentration has nearly disappeared at a distance of one diameter into the rock.

Electric resistance strain gages measure the component of strain parallel to their axis averaged over their gage length plus a generally small amount due to transverse sensitivity. The transverse sensitivity of the etched foil rosettes used in this investigation was + 0.5 per cent and this was considered small enough to disregard. The geometry of the gages was such that they covered a polar angle ψ of 0.044π steradians. The plane stress elastic stress-strain relationship on the end face of the borehole in any given radial direction r can be written

$$\epsilon_r E = \sigma_r - \mu\sigma_\theta \qquad (16)$$

where E is Young's modulus, μ again is Poisson's ratio and σ_θ is the stress normal to σ_r in the borehole face. If μ is taken = 0.20 in the stress concentration factors and the radial strain

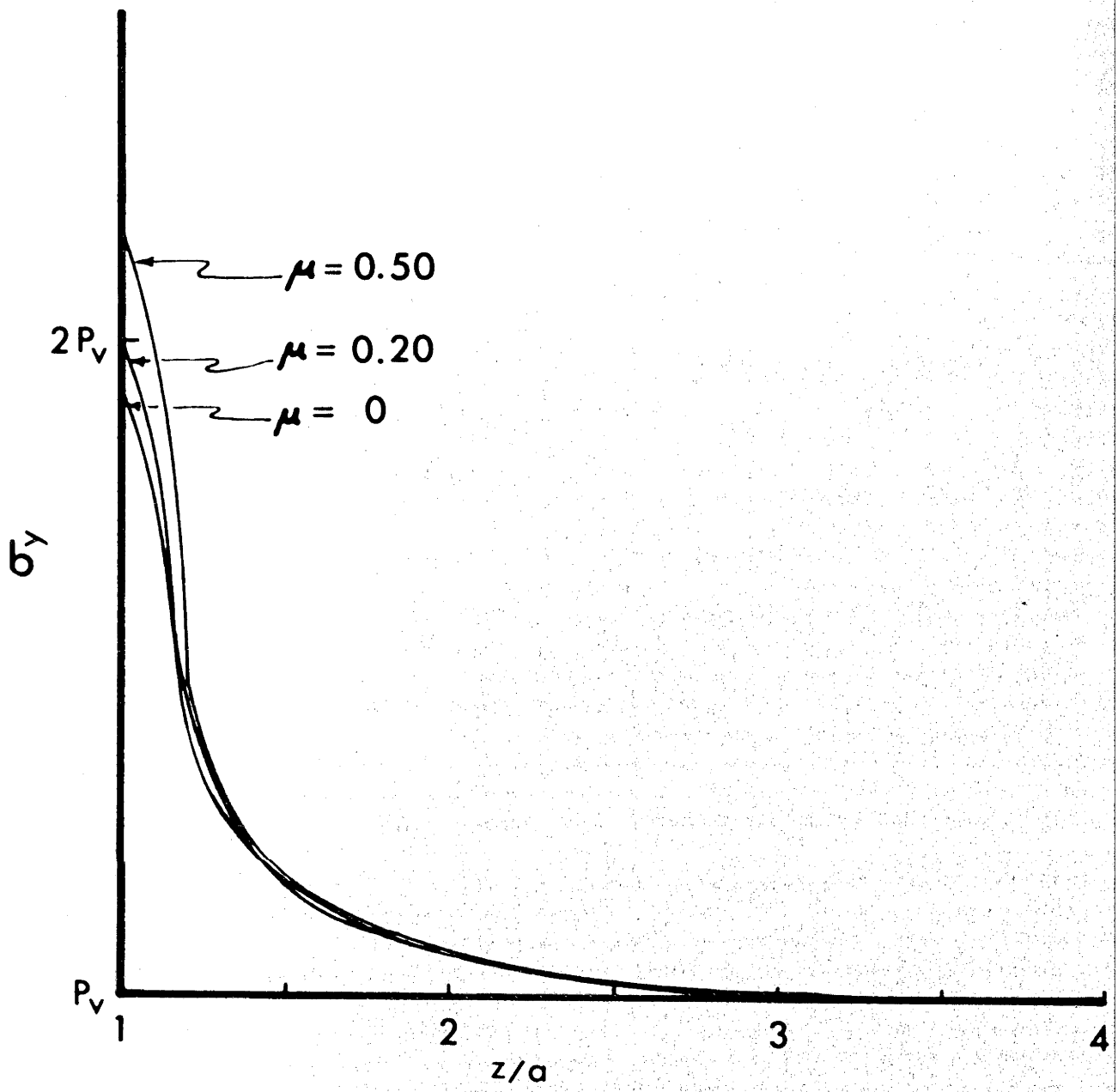

Fig. 32 Vertical stress σ_y in the rock near the end of a hemispherically ended borehole in terms of a vertical field stress P_v for Poisson's ratios of 0, 0.20 and 0.50, plotted against distance z/a from the end of the borehole.

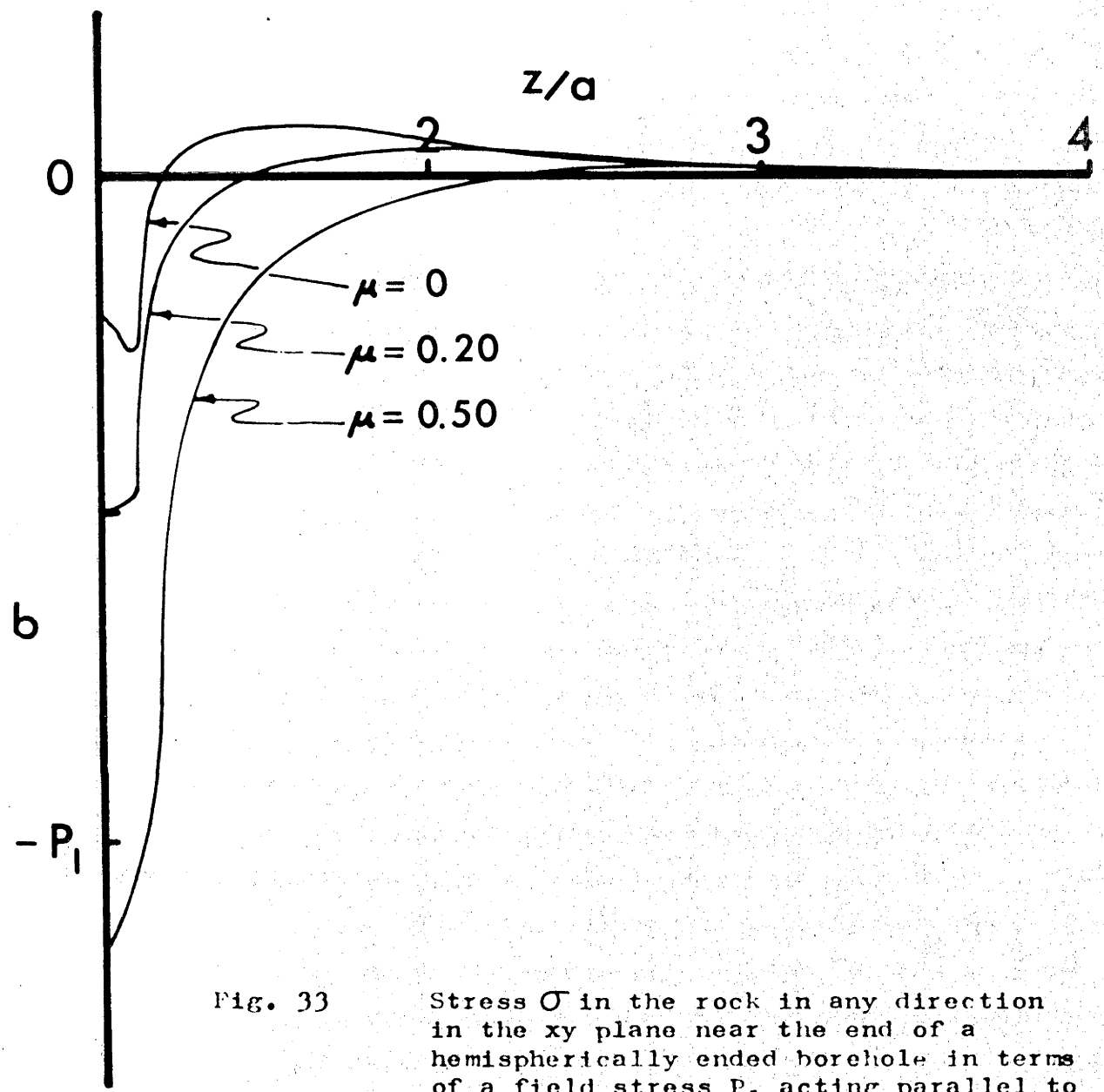

Fig. 33 Stress σ in the rock in any direction in the xy plane near the end of a hemispherically ended borehole in terms of a field stress P_1 acting parallel to the axis of the borehole, plotted against distance from the end of the borehole, z/a, for Poisson's ratios of 0, 0.20 and 0.50.

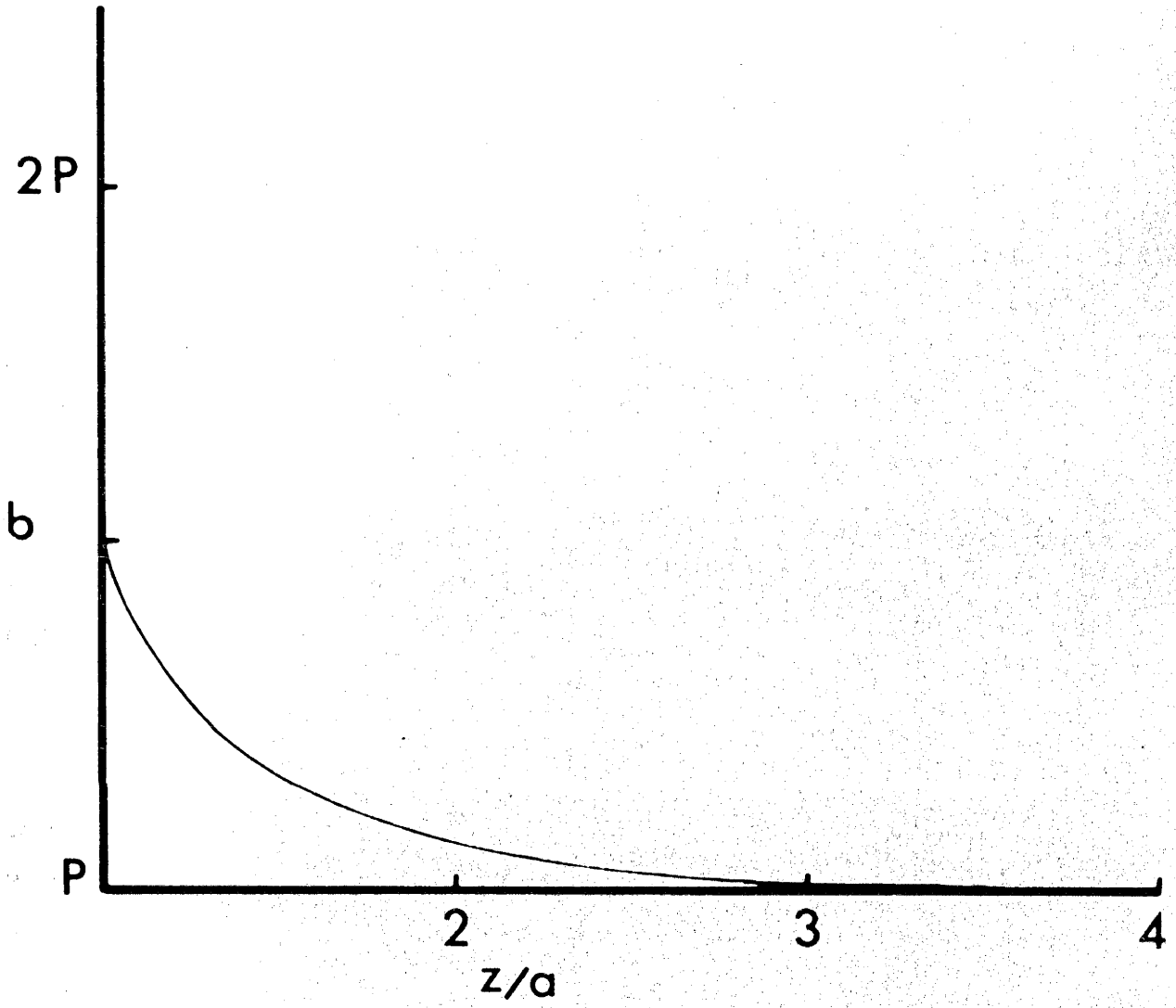

Fig. 34 Stress σ in the rock in any direction in the xy plane near the end of a hemispherically ended borehole in terms of a hydrostatic field stress P , plotted against distance from the end of the borehole.

ϵ_r is calculated in terms of the stresses σ_r', σ_θ' and σ_z' which are applied to the rock well away from the borehole, superposition of equations (9), (11) and (13) yields equation (17), the stress at infinity - strain in the face of a hemispherically ended borehole relationship when the borehole axis is parallel to one of the principal stresses.

$$\epsilon_r E = 2.0\sigma_r' - 2.0\mu\sigma_\theta' - 0.50(1-\mu)\sigma_z' \qquad (17)$$

Commonly a three strain gage rosette is used giving three different values of ϵ_r and these are solved for the three quantities ϵ_{max}, ϵ_{min}, and ϕ where ϕ is the angle from one of the gage elements to the direction of the maximum principal strain. The effect of the last term in equation (17), $- 0.50(1-\mu)\sigma_z'$ which is due to the stress acting parallel to the borehole is to decrease the estimate of ϵ_{max} and ϵ_{min} some amount depending upon the size of σ_z' but it has no effect on the calculation for ϕ. Two equations (17) are then written from the data from a single borehole, one for ϵ_{max} and the other for ϵ_{min}. A second set of measurements are then made in a hole drilled perpendicular to the first hole and in either the maximum or minimum principal strain directions as determined in the analysis of the first hole. Two more equations (17) can be written from the data from the second hole - one for ϵ_{max} and the other for ϵ_{min} in the plane perpendicular to the axis of the second borehole. In addition a ϕ_2 will be determined and this direction should be either parallel or perpendicular

to the first hole. The four equations for the principal strain in the end faces of the boreholes can then be solved by least squares for the three primary principal stresses acting in the rock.

An alternate approach, much simpler in practice, would be to do first a flat ended strain relief test and then a hemispherically ended test as close as possible to each other in the same borehole. Equations for the maximum and minimum principal strain in the end of the borehole can then be written for each test and these four equations solved for the three primary principal stresses.

Experimental Design

The biaxial loading frame used to hold and load the block of rock in which these stress measurement experiments were performed has previously been described (appendices 4 and 5 of this thesis). It was mounted on its side and arranged so that a hole could be drilled parallel to one of the applied stresses. The block of rock was loaded with large steel flatjacks on four of its surfaces. A gasoline powered portable diamond drill was used along with a BX thin walled diamond coring bit that made a hole 2.35 inches in diameter and gave a core 1.94 inches in diameter. The end of the hole was ground with a 2.35 inch diameter, hemispherically ended diamond bit. The frame, drill and rock are shown in Figure 35.

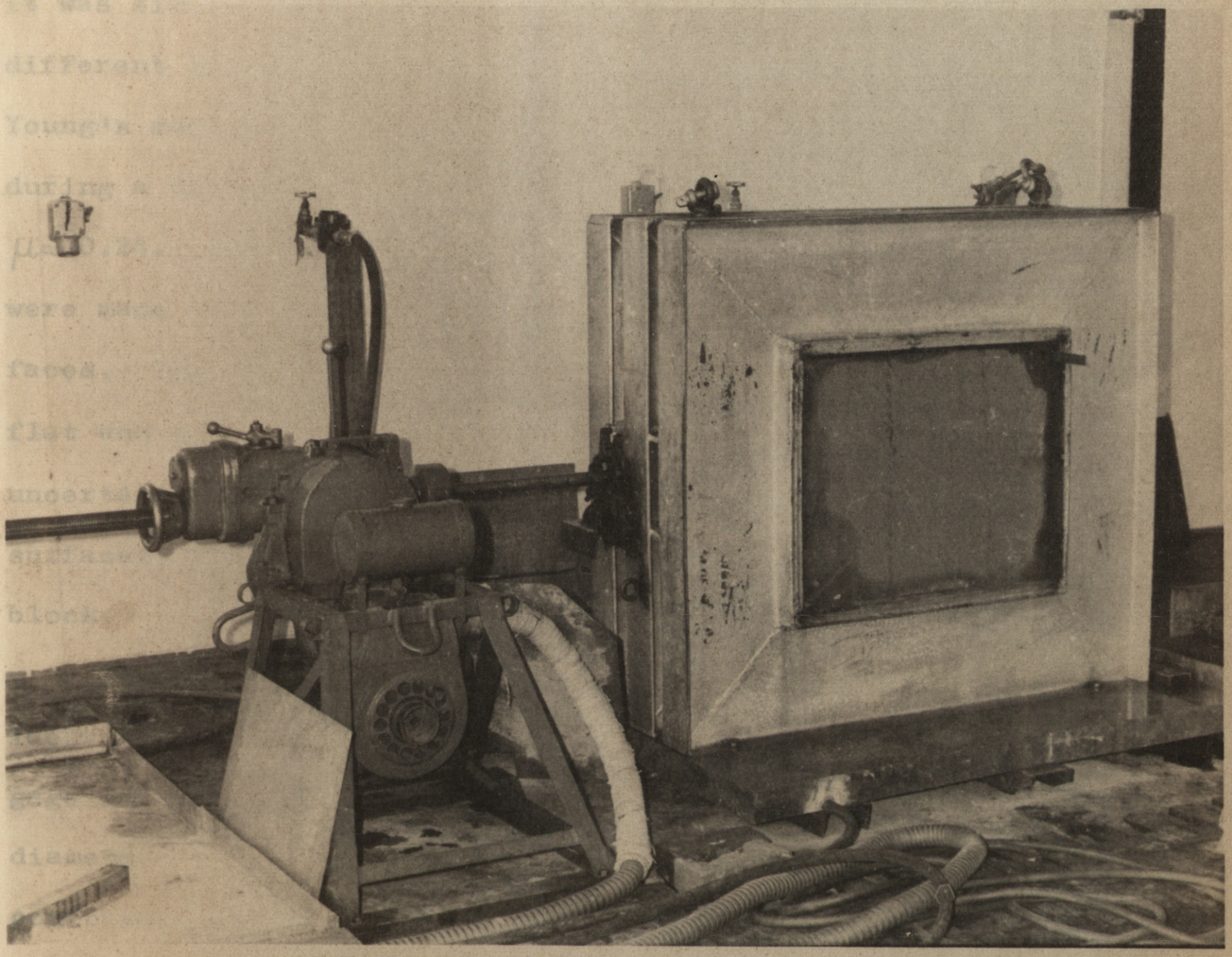

Fig. 35 General view of the strain rosette relief experimental apparatus showing the diamond drill and biaxial loading frame with a block of rock in place.

The rock was a block of a micro-syenite quarried near Bowral, New South Wales and known locally as the Bowral trachyte. It was similar in appearance and composition but had slightly different elastic properties from the blocks used previously. Young's modulus and Poisson's ratio for this block measured during a diametral compression test were $E = 6.7 \times 10^6$ psi and $\mu = 0.24$. The block was 19 x 24 x 30 in. and the measurements were made in holes collared perpendicular to one of the 19 x 24 in. faces. The block had been wire sawn and the faces then ground flat and all dimensions were ture to $\pm\frac{1}{8}$ in. Because of uncertainty concerning the stress distribution near the loaded surfaces, tests were conducted only in the middle third of the block.

The strain cells except for having a hemispherical end were identical with the flat ended cells previously used. The strain gage rosette was cemented to the inside face of a 1.360 in. diameter, $^1/16$ in. thick Perspex disc the surfaces of which conformed to the surface of a sphere with a radius of 1.175 in. The strain cell body was also Perspex. The strain gage rosette was cemented to the end disc, four-conductor cable was connected to the rosette, and the disc, cable and cell body were all fastened together with an epoxy cement. The cell body was then filled with a cold curing silicone rubber compound. The strain cell was cemented to the prepared face of the drill hole with

a quick-setting strain gage epoxy. The cable was led through the bit and drill rods and out an "O" ring packing gland on the water swivel of the drill. The cell remained connected to the strain gage instrumentation throughout the test. The strain cell was overcored in increments with strain readings taken at each increment. The strain measuring instrumentation consisted of a Philips switching and balancing unit and direct reading measuring bridge. Overall repeatability of readings with this system has been measured as ± 5 ppm by repeated readings on a rosette cemented to an unstressed block of rock.

Direct temperature compensation of the active strain gages with a dummy gage is not possible with this system, but effective compensation was achieved by allowing the drilling water to flow for some time prior to the actual overcoring until the zero strain readings had stabilized. After each drilling increment the strain gage readings were allowed to stabilize with the drilling water left running. Under these circumstances the tests can be considered to have been performed at the temperature of the drilling water and this fluctuated no more than $0.5^{\circ}C$ during any one test. Assuming a reasonable coefficient of thermal expansion of 7 ppm/$^{\circ}C$ the maximum strain induced by temperature variations is less than the basic measuring error in the instrumentation and no correction for temperature effects was considered necessary. Additional strain relief tests were

performed in which the strain cells were cemented to the stressed block of rock and the initial readings taken without turning the drilling water on. The block was then stress relieved by merely bleeding the loading jacks. Direct temperature compensation is possible under these conditions and the results are nearly indistinguishable from those determined by overcoring.

Experimental Results

A summary of the results of the tests is given in Table VIII. Agreement between the strains calculated from the applied stresses and measured elastic properties of the rock in equation (17) and the strains measured during both overcoring and pressure release cycles is quite good. Individual test results are plotted in Figures 36, 37 and 38. These look considerably rougher and show the advantage of having a series of strain gage readings to work with rather than just an initial and final value.

Conclusions

The results of these tests are encouraging. The agreement between the strains measured and those calculated on the basis of the elastic solution for a spherical cavity seems to indicate that the borehole itself does not appreciably affect the stress distribution at the end, at least not when the borehole is parallel to one of the principal stresses. This fact may also be of use in the design of underground openings.

Table VIII

Applied Stresses	Calculated ϵ_{max} and ϵ_{min}	ϵ Measured During Drilling	ϵ Measured by Bleeding Jacks
P_v = 1000 psi	ϵ_{max} = - 300	ϵ_{max} = - 295	ϵ_{max} = - 290
	ϵ_{min} = + 60	ϵ_{min} = + 65	ϵ_{min} = + 65
P_L = 1000 psi	ϵ = + 60	ϵ = + 60	ϵ = + 65
$P_v = P_L$ = 1000 psi	ϵ_{max} = - 240	ϵ_{max} = - 210	ϵ_{max} = - 220
	ϵ_{min} = + 120	ϵ_{min} = + 130	ϵ_{min} = + 115

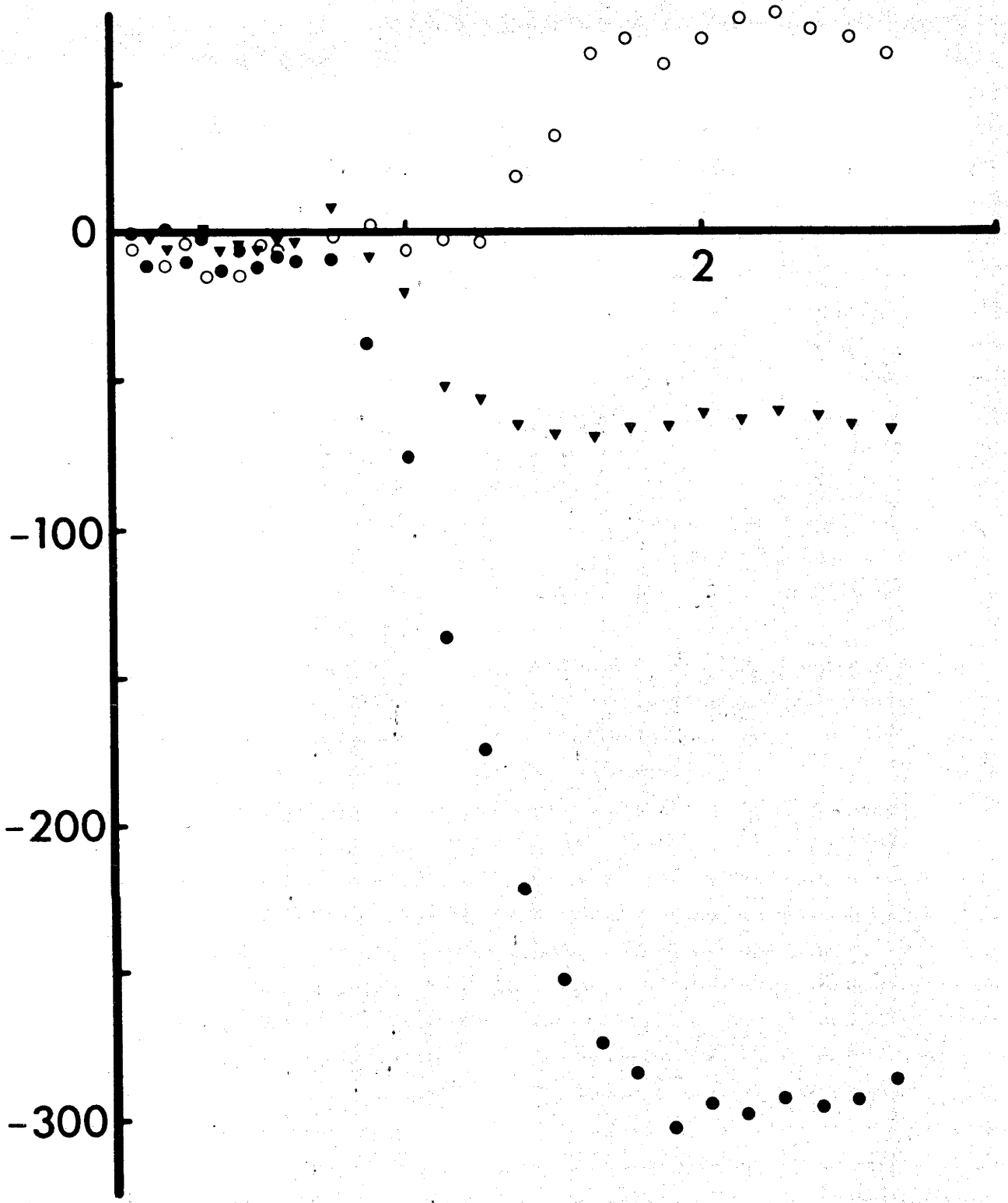

Fig. 36 Strain, ppm, on end face of a hemispherical borehole versus depth drilled, inches; vertical stress equals 1000 psi, horizontal stress equals zero, longitudinal stress equals zero. O Vertical strain gage, 45° strain gage, O horizontal strain gage.

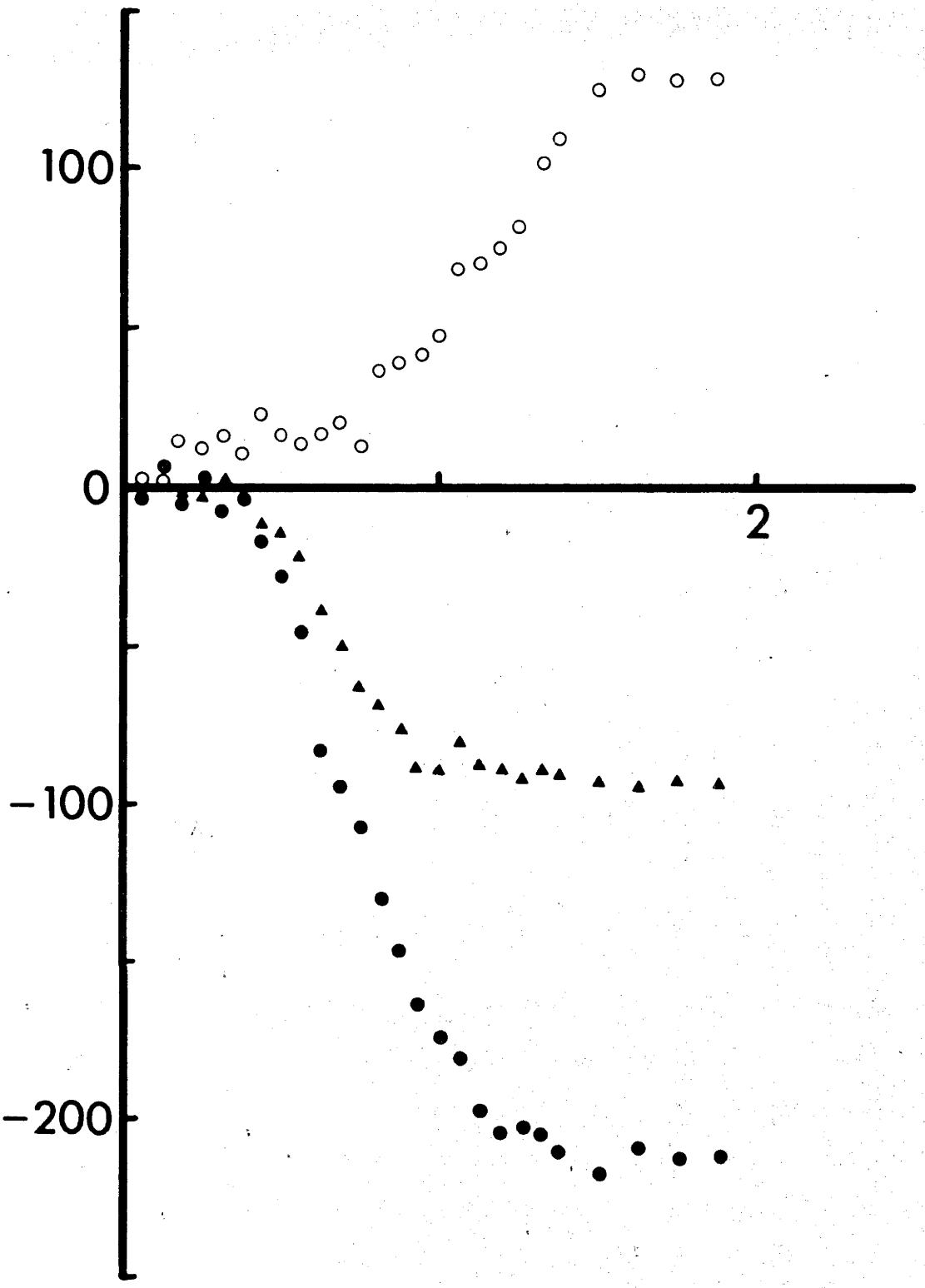

Fig. 37 Strain, ppm, on end face of hemispherical borehole versus depth drilled, inches; vertical stress equals 1000 psi, horizontal stress equals 0, longitudinal stress equals 1000 psi. ● Vertical strain gage, ▲ 45° strain gage, 0 Horizontal strain gage.

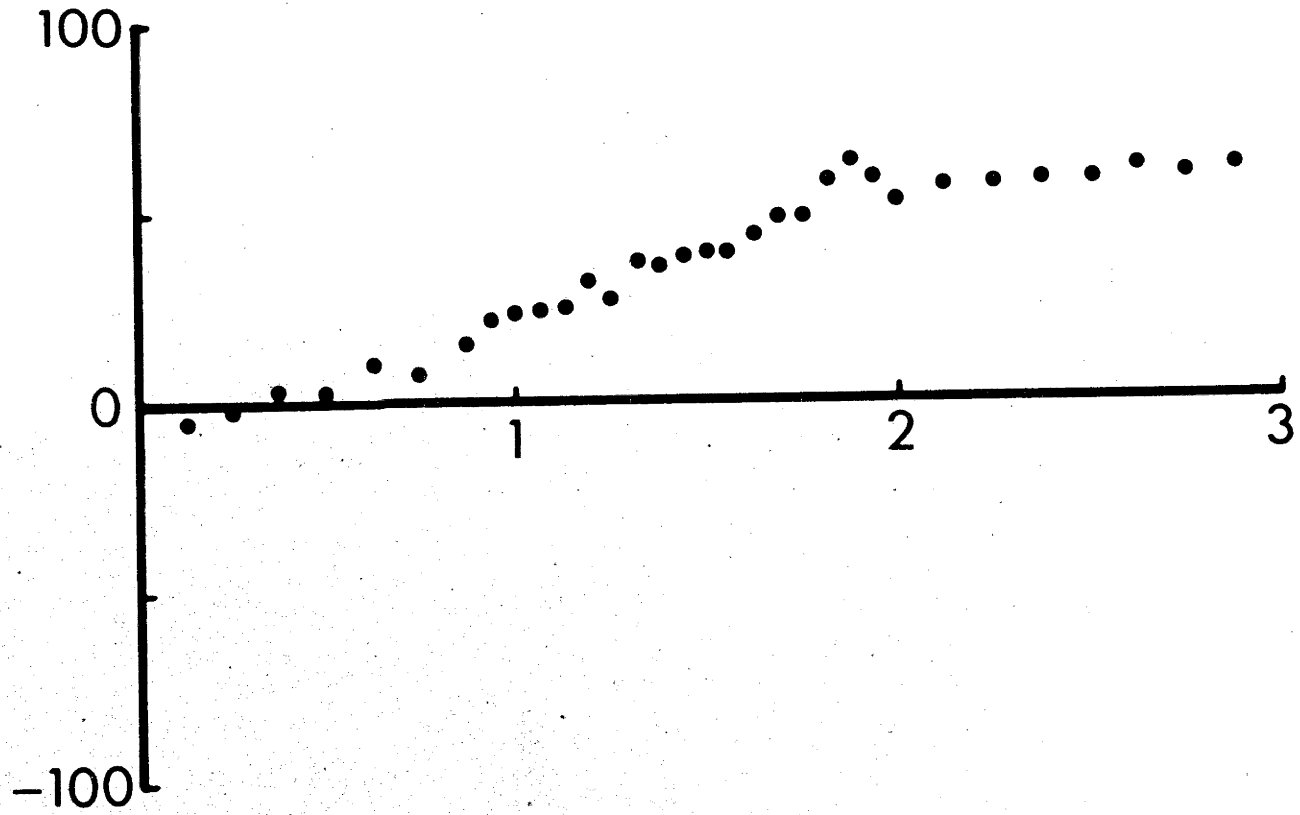

Fig. 38 Strain, ppm, on end face of hemispherical borehole versus depth drilled, inches; vertical stress equals zero, horizontal stress equals zero, longitudinal stress equals 1000 psi. ● Average of all three approximately equal strain readings.

There is at least one advantage to the hemispherically ended strain relief cells. They have a higher stress concentration factor for the stresses in the plane perpendicular to the borehole axis than do the flat-ended cells. They are also affected only about half as much by the stress acting parallel to the borehole. This means in practice that larger strains are measured in the same stress field compared to the flat ended cells and this will tend to increase the accuracy of the measurement in most cases.

Chapter VIII

LABORATORY EXPERIMENTS ON A BOREHOLE DEFORMATION GAGE

Introduction

A borehole deformation gage of the U.S. Bureau of Mines type was constructed from drawings furnished by the Snowy Mountains Hydroelectric Authority. The gage is shown schematically in Figure 39. The mechanical features of the gage have been fully described by Obert, Merrill and Morgan in [1962]. Two semi-conductor strain gages were used on the measuring cantilever in this gage instead of the four resistance strain gages used in the original U.S. Bureau of Mines design. The Bureau of Mines gage was designed to give a deformation accuracy of 50×10^{-6} inches when used in conjunction with a standard strain gage measuring bridge. The first field application of the present gage was to be at Mt. Isa, Queensland where the rock has a modulus of approximately 10×10^{6} psi. A measuring error in borehole diameter change of 50×10^{-6} inches would correspond to an error of 114 psi in a uniaxial stress field in such a rock and better accuracy than this was desired. Since the U.S.B.M. gage was designed (prior to 1962), semi-conductor strain gages have become readily available with gage factors of 50 to 60 times those of conventional resistance strain gages. It seemed an obvious step to use these

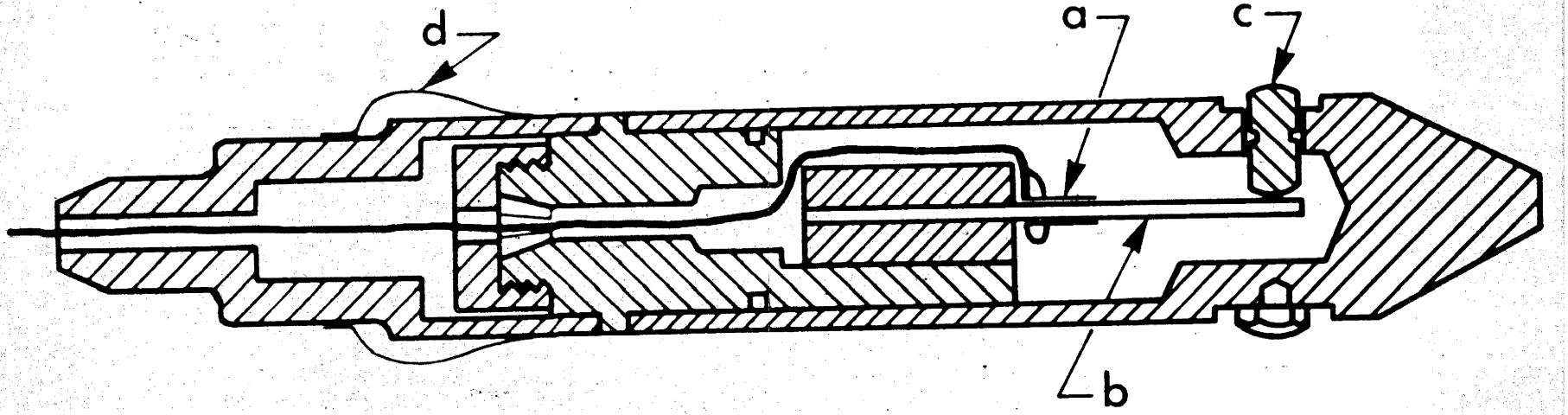

Fig. 39 Schematic section of borehole deformation gage. a, semi conductor strain gages. b. measuring cantilever, c, piston. d, leaf springs to position rear of deformation gage.

as measuring devices. There are several inherent problems with semi-conductor gages that are not important with resistance strain gages such as increased temperature sensitivity, dependence of gage factor on gage current and non-linearity of gage factor. By using semi-conductor strain gages on the top and bottom of the measuring cantilever it is possible to minimize these effects and the final sensitivity achieved was $\pm 2 \times 10^{-6}$ inches and the response was linear over the full measuring range of the instrument. This would correspond to a stress error of $\pm 4\frac{1}{2}$ psi under the same conditions as above. Figure 40 is a calibration curve for this instrument when used with a 6 volt bridge supply. The voltage inbalance in the wheatstone bridge circuit was measured with a digital voltmeter reading directly to 0.01 milli-volts. The gage was calibrated in a solidly built jig with a micrometer head reading to 0.0001 inch.

Theory

Formulae for the deformation of a circular hole based on elastic theory under conditions of both plane stress and plane strain in uniaxial and biaxial stress fields in isotropic material are given by Merrill and Peterson [1961]. Panek [1966] and Leeman [1967] have given more general solutions. The equation given by Leeman when the borehole axis is parallel to one of the principal stresses is:

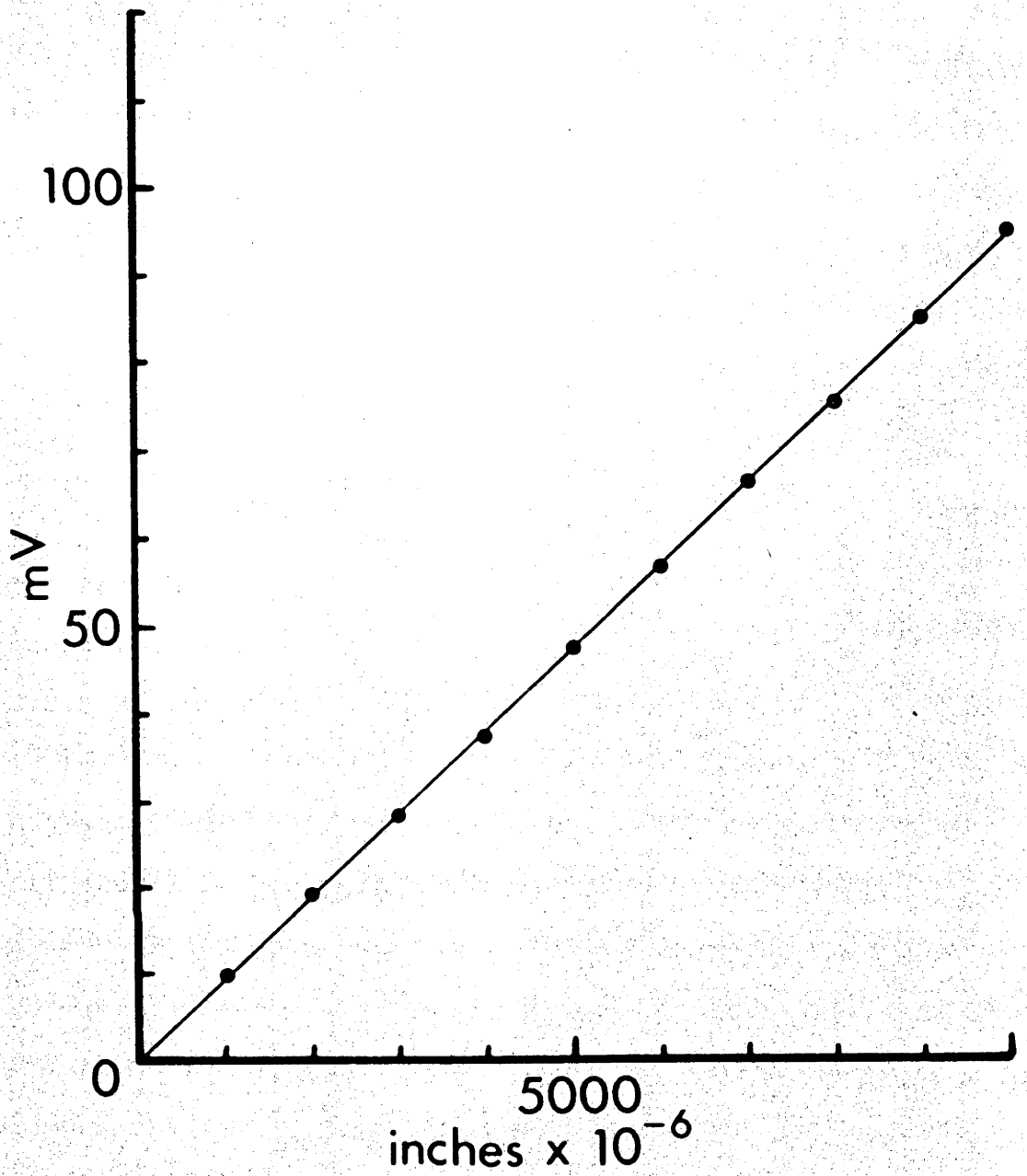

Fig. 40 Calibration curve for borehole deformation gage, milli volts versus millionths of an inch.

$$\Delta d = \frac{d}{E}\left[(\sigma_1 + \sigma_2) - \mu\sigma_3 + 2(\sigma_1 - \sigma_2)(1 - \mu^2)\cos 2\theta\right] \qquad (18)$$

where

Δd = change in borehole diameter during the stress relief

d = initial borehole diameter

σ_1, σ_2 = principal stresses acting in the plane perpendicular to the borehole axis

σ_3 = principal stress acting parallel to the borehole axis

θ = angle from the direction of measurement to the maximum principal stress in the σ_1, σ_2 plane.

E, μ = Young's modulus and Poisson's ratio for the rock.

If four borehole deformation measurements are made at different values of θ, then σ_1, σ_2, σ_3, and θ can be calculated. The U.S.B.M. analysis assumes that the effect of σ_3 is negligible and if this is so then only three borehole deformation measurements are needed to determine σ_1, σ_2, and θ.

It should be noted that σ_3 only appears as a single term multiplied by Poisson's ratio in equation (1). Poisson's ratio has been shown to be a stress dependent and somewhat difficult to specify constant for rocks c.f. Walsh [1965] and therefore σ_3 would not be determined as accurately as σ_1, σ_2, and θ in deformation measurements in a single borehole.

Experimental Materials and Procedures

A large block of micro-syenite (procured commercially and sold as the Bowral Trachyte) 19 x 24 x 30 inches was loaded in the biaxial compression frame previously described. The rock is a uniform fine grained isotropic igneous rock consisting predominantly of orthoclase and aegrine-augite 1 mm in grain size with minor amounts of quartz, calcite, and altered ferromagnesian minerals.

The EX borehole (1.465 inches diameter) in the block was collared near the centre of one of the 19 x 24 x 30 inch faces and drilled parallel to the sides of the block through a hole cut in one end of the loading frame. Stresses were applied to the rock through large flatjacks 19 x 24 inches and 19 x 30 inches acting against the frame. One of the 19 x 24 inch loading jacks was fabricated with a three inch diameter hole near its centre to allow drilling into the block parallel to one of the principal stresses and subsequent access to the hole while the rock was under load. The general arrangement was such that one principal stress was applied parallel to the borehole, another perpendicular to the borehole and the third principal stress was zero. It was not considered necessary to actually overcore the deformation gage on each test although the experimental design could have allowed this. Only one test could have been done in each block and a prohibitively large amount of experimental material would

have been required. The experimental procedure adopted was to load the block of rock to the desired stress level, insert the gage and get an initial reading, and then lower the pressure in the loading jacks in increments, reading the borehole gage at each increment until the jack pressures were zero and the rock was completely stress relieved. All of these tests were thus done on the same identical volume of rock and should be directly comparable.

Elastic Properties of the Rock

The borehole gage can only measure changes in borehole diameter in a given direction. As with any strain or deformation measuring "stress" indicator, the stresses causing this deformation must be inferred from the stress-deformation properties of the material. In the simplest case of an isotropic, elastic, continuum two such stress-deformation or elastic properties are, in general, required, Young's modulus and Poisson's ratio. As can be seen from equation (18) the accuracy of the stresses calculated from the borehole gage readings is directly proportional to the accuracy with which Young's modulus and Poisson's ratio are known. Several workers have shown that these "elastic constants" are not necessarily constants for rocks but can be dependent upon such factors as stress magnitude, mean stress, stress sign and strain rate, c.f. Cook and Hodgson [1965],

Walsh [1965], Birch [1961], Brace [1964] and Zisman [1933]. No sweeping generalizations can as yet be made as the relative effects seem to vary from rock to rock and testing procedure to testing procedure. Two methods of determining elastic moduli were tried in this investigation. Tests were made on cores in unconfined compression and by diametral compression of cylinders. Strain was measured by pairs of electric resistance strain gages mounted on opposite sides of the specimens. For these laboratory tests it was also possible to calculate elastic moduli from the deformation of the borehole as the stresses on the block were altered.

Table IX gives the moduli determined from these three types of test.

Table IX

Type of Test	E, psi	μ
Uniaxial Compression	8.2×10^6	0.27
Diametral Compression	7.4×10^6	0.22
Borehole Deformation	7.0×10^6	0.39

Experimental Results

The results of the experiments are given in Table X as borehole deformation in millionths of an inch for the various stress conditions and borehole gage orientations. Each measured deformation value given is the average of at least three separate determinations. The calculated deformations were found by substituting into equation (18) the average elastic moduli from the unconfined compression tests and the diametral compression (indirect tension) tests and the stresses that were used.

Table X

Gage Orientation From σ_1	σ_1 psi	σ_2 psi	σ_3 psi	Δd Measured in x 10^{-6}	Δd Calculated in x 10^{-6}
0	600	0	0	+ 340	+ 325
45	600	0	0	+ 133	+ 113
90	600	0	0	- 82	- 98
Any Angle	0	0	600	- 54	- 30

Chapter IX

INTRODUCTION TO THE MT. ISA EXPERIMENTS

The following chapters of this thesis contain the results of a rock mechanics investigation conducted on the 1100 copper orebody of the Mt. Isa mine, Mt. Isa, Queensland, Australia. The investigation started in September, 1965 after discussion with the engineering staff at Mt. Isa and consisted of both underground or "in situ" tests at Mt. Isa and laboratory tests on Mt. Isa rocks in Canberra.

Underground stress measurements were made in and adjacent to the 1100 copper orebody. The primary stress measurement site was in J 32 west cross cut on 14 Level. Approximate coordinates on the mine grid are 3000 north, 1650 east. The vertical depth below ground surface at this point is approximately 2180 feet. Some preliminary measurements were made in M 30 west cross cut on 13 Level, coordinates 3000 north, 2000 east, depth beneath surface approximately 1990 feet. Additional flatjacks were installed on 11 Level in L 30 west cross cut, coordinates 3000 north, 2200 east and depth beneath surface approximately 1580 feet.

All of the sites were in rock that from a mining engineering viewpoint must be considered to be extremely sound. The 13 Level and 14 Level cross cuts were approximately 14 feet on a side and

nearly square and the 11 Level cross cut was approximately 10 feet on a side. All of the cross cuts had been standing open for several years and no artificial support of any type was necessary. Extraction openings hundreds of feet on a side have been made in this mine in similar rock and these have remained open also without additional support (see Davies [1967] for a recent summary of mining techniques and conditions).

The geology of the Mt. Isa mine has been most recently described by Bennett [1965]. Briefly, Mt. Isa is a silver-lead-zinc and copper mine in a series of Precambrian silt stones, shales and bedded carbonates that strike north-south and dip 60° - 65° to the west. The dominant structural feature of the area is the Mt. Isa fault. This fault truncates the western edge of the orebodies, strikes north-south and dips 50° - 70° to the west. It has been traced about 40 miles and the relative movement is thought to have been the west side north and up. The copper and silver-lead-zinc orebodies are separate and distinct in the mine but both are confined to one formation, the Urquhardt shale. The silver-lead-zinc orebodies are restricted to relatively unaltered shale while the copper orebodies occur in zones of highly brecciated and recrystallized shales. The stress measurements in this investigation were made in and adjacent to one of the copper orebodies. The recrystallized and deformed Urquhardt shale is known locally as "silica

dolomite". This is a general term which is simply meant to cover all of the known copper host rocks. The mine geologists recognize and map four varieties of "silica dolomite", medium to coarse grained crystalline dolomite, irregularly brecciated dolomitic shale in a crystalline carbonate quartz matrix, regularly bedded but partly recrystallized shale, and fractured and brecciated siliceous shales. These four rock types are intimately associated in any part of the "silica dolomite" mass and representations and gradations of all types can be seen on any scale with irregular masses up to tens of feet on a side frequently surrounded by one of the other varieties.

There were several reasons for making the stress measurements in the "silica dolomite". This rock shows no regular continuous anisotropy. Its inhomogeneity insures that it is in a broad sense at least statistically isotropic. The surrounding shales and silt stones appear to be anisotropic in both their strength and elastic properties. Little is known of stress measurement techniques or analysis in anisotropic rock. Stable openings existed in "silica dolomite" which could be blocked off for the time required to perform the tests. The mine staff wanted to know the primary stress field in this portion of the mine to aid them in the design of the openings and mining method for the area. And finally a relatively simple petrofabric analysis could be performed on the coarsely crystalline dolomite in the

"silica dolomite" and the principal stress directions inferred from this analysis could then be compared with the stress directions measured in the "in situ" tests. The area was also well away from any major active workings in the mine. The nearest production area was about 1000 feet above and 800 feet north of the 14 Level stress measurement site. The 1100 orebody is a relatively recently discovered copper orebody in the mine and only preliminary exploration and development headings exist. During the period when the stress measurements were being made no other development openings were within 150 feet of the main stress measurement site in J 32 west cross cut on 14 Level.

The bottom of the 1100 orebody is a sharp contact with "greenstone". In this portion of the mine the contact "plane" of the greenstone and the orebody strikes north-northwest and dips east-northeast at from 10^{o} to 40^{o}. It is approximately 250 feet below the stress measurement site. It has not yet been clearly shown whether this contact is a fault or an unconformity and in fact very little is known about these "greenstones". The greenstone is exposed in the mine by only a few feet of a single heading which is 200 feet below and approximately 3500 feet north of the stress measurement site. There appears to have been considerable alteration and "shearing" at the contact and there is local enrichment of ore in the "silica dolomite" on the contact. Samples of "greenstone" both from near the contact and from diamond drill cores that had penetrated

into relatively "unaltered greenstone" were collected and tested. There were two problems here; first, openings will be made in the "greenstone" to recover the high grade ore on the contact so something of its strength needs to be known and second, there is the possibility that the primary stress field is modified near the contact of the two apparently dissimilar rock masses. The stress measurement site could be affected as it is only about 250 feet from the contact.

Above and laterally the orebody grades into dolomitized shales and relatively unmineralized "silica dolomite". The orebody limits in these directions are determined entirely by assays as all of the "silica dolomite" appears to be mineralized to some extent. As a large mass the "silica dolomite" is broadly transgressive to the surrounding shales (the general strike is about 15° different). In most recorded contacts, however, it is conformable with the undeformed shales and in many cases the contact is gradational across the bedding. The nearest known shale - "silica dolomite" contact to the 14 Level site was about 700 feet east. The main silver-lead-zinc orebodies were all at least 3500 feet north.

The laboratory work done in connection with this thesis can be separated into three distinct parts. First, the stress measurement techniques used at Mt. Isa were investigated in large blocks of sound uniform and isotropic rock under known stresses

to see if in fact these various stress measurement techniques did work at all and if so how best to analyze the results from them. This work has been reported in Chapters VI, VII and VIII and appendices 4 and 5 of this thesis. The second portion of the laboratory work involved experiments on the failure of rock under complex polyaxial stresses. Chapters II, III, IV and V and appendices 2 and 3 of this thesis contain the results of these investigations on the failure criteria of various uniform rocks.

The third section of the laboratory work was the measurement of the strength and elastic properties of the rocks collected at Mt. Isa. The Mt. Isa rocks show considerable variability in their properties even among smaller specimens prepared from the same larger single piece of rock. Tests were made on both the "silica dolomite" from the 1100 orebody and the underlying greenstone. A few tests were made on cores drilled from a block of laminated shale thats origin within the mine is not known. This work is described in Chapter XII.

Chapter X

RESULTS OF STRESS MEASUREMENT TESTS AT MT. ISA

Introduction

Three separate stress measurement techniques were used, a borehole deformation gage, strain relief on the flattened end of a borehole, and flatjacks.

The borehole deformation gage stress measurement technique has been extensively used in the United States and South Africa. The gage used at Mt. Isa was essentially a copy of the U.S. Bureau of Mines' instrument described by Obert, Merrill and Morgan [1962]. The only difference was that semi-conductor strain gages were used on the measuring cantilever instead of conventional resistance strain gages. The calibration and testing of this borehole deformation gage have been described in Chapter VIII.

In use, first an EX (1.465 inch diameter) hole is diamond drilled well beyond the proposed measurement depth. The borehole gage is inserted in this hole and accurately alligned and positioned. The EX hole and the borehole gage are then concentrically overcored with a large (6 or 8 inch diameter) diamond coring bit. This relieves the stresses in the rock surrounding the deformation gage and the EX hole changes shape

slightly. The borehole gage measures the change in length in one diameter of the hole. Three successive readings are taken with the instrument measuring three different diameters. Young's modulus and Poisson's ratio are determined in laboratory tests on the large cores recovered during the overcoring procedure and the deformation readings and moduli substituted into the elasticity equations for the deformation of a borehole to determine the principal stresses in the plane perpendicular to the axis of the borehole.

The advantages of the borehole deformation gage method of measuring rock stress are (1) it measures the stresses well away from the mine opening and (2) it is less affected by stresses acting parallel to the axis of the hole and shear stresses in the plane perpendicular to the hole than is the borehole strain rosette relief technique. In theory, Leeman [1967], Panek [1966], measurements in two boreholes not at right angles are sufficient to determine the primary principal stress field and no previous knowledge of principal stress directions is required. The disadvantages of the method are (1) large diameter diamond core drilling equipment is necessary (2) the method is difficult if not impossible to use in jointed or fractured rock (3) laboratory determined values of the elastic constants are required and the stresses calculated are directly proportional to these laboratory values and (4) the measurements are made at separate isolated points in the rock mass and then later combined in the stress

calculation. Only a few cubic inches of rock are involved in each measurement and any chance minor variance occurring at that point in the stress field or the properties of the rock directly affects the deformation measured and the stresses calculated.

Strain rosette relief on the flattened end of a borehole procedure was identical to that described in appendix 5. Briefly, the technique involves cementing an electric resistance strain gage rosette to the center of the flattened end of a BX borehole. Initial readings are taken and then the strain gage rosette is overcored in closely spaced increments with a thin walled BX diamond bit. Strain gage readings are taken at each increment. When there is no further change in strain gage readings (usually after about 2 inches of strain relief drilling) the rosette is considered fully strain relieved and the test halted. From the strain gage rosette readings the principal strains in the end of the drill hole and their orientation are determined. The elastic constants of the rock are determined by separate laboratory tests. The procedure used in this investigation was to cut the core stub recovered with the strain cell into brazilian test specimens about two inches in diameter and one inch thick. From strain measurements made on the faces of the Brazilian specimen loaded in diametral compression, the elastic moduli were determined using the formulae derived by Hondros [1959]. The magnitude of the stress acting parallel to the

borehole axis which has been shown to have a large effect on the strains measured with this technique can be found either by making similar strain rosette relief measurements in a second hole drilled in one of the principal strain directions determined in the first hole, or by comparing the strain rosette relief measurements with measurements made by some other technique such as the borehole deformation gage method which is affected relatively less by the stress parallel to the borehole.

The main advantages of this technique are

1. measurements can be made well away from the mine opening in presumably more solid rock, and
2. only standard size diamond drilling apparatus (in this case BX which is about $2\frac{3}{8}$ inches diameter) is used.

The disadvantages are

1. some initial knowledge or assumption of principal stress directions is required,
2. the stresses calculated are directly proportional to the laboratory determined elastic moduli,
3. the strain cells are single use throw-away items and several are required for the complete determination of the stresses in any one area, and
4. strain gage measurements are precise measurements of small electrical quantities. The electronic

instrumentation that is required to make these measurements is delicate, temperamental and expensive and there are practical difficulties in adequately preparing and inspecting the rock face at the end of a drill hole, properly cementing a strain gage to this face and maintaining and operating the instrumentation in an underground environment.

Flatjack theory, general procedure, the results of some laboratory tests, and a general discussion of the method are given in appendix 4. The detailed drilling and installation procedure used at Mt. Isa was identical to the procedures used by the Snowy Mountains Hydroelectric Authority and described by Alexander [1960]. Briefly, measuring points are installed, a slot is diamond drilled midway between these measuring points (six overlapping BX diamond drill holes are used to make a slot 13 inches deep by 13 inches long by approximately $2\frac{3}{8}$ inches high) and the measuring points move a little closer together. A flat hydraulic jack is grouted into the slot and the jack pressurized in steps until the measuring pins are forced back into their preslot positions. The hydraulic pressure required (with a minor correction for slot dimensions and the effect of the biaxial stress) is the average stress in the rock from 0 to 12 inches into the face, in the direction normal to the jack. From the graphs of measuring pin movement versus slot size, time and jack pressure, values for the "in situ" elastic modulus during

both loading and unloading of the rock are attained along with an "in situ" creep curve.

The advantages of the flatjack method are

1. it is direct, no laboratory modulus determinations are necessary,
2. the equipment used is simple and relatively robust, being entirely mechanical and hydraulic,
3. some of the "in situ" rock properties are determined during the test as well as a stress value, and
4. several cubic feet of rock are involved in each stress measurement making minor inhomogeneities in the rock relatively less important in this technique compared with the borehole deformation gage or borehole strain relief techniques.

The disadvantages of flatjacks are all related to the fact that the flatjacks only measure the stresses in the rock at the surface of the mine opening. This rock may be fractured due to either the blasting done in driving the opening or the excess rock stress caused by the presence of the opening.

The stresses in the walls of an underground opening depend upon the relative magnitudes and the direction of action of the primary rock stresses and upon the properties of the rock. If the rock can be considered an isotropic elastic continuum and the mine opening is driven parallel to one of the primary

principal stress directions the analysis is relatively simple. Alexander [1960] gives and discusses the procedures used in these conditions. If the mine opening is not parallel to one of the primary principal stresses the analysis is much more complicated. Hiramatsu and Oka [1962] have given the theory for the stresses round a circular opening in a general stress field and they give some three dimensional photoelastic test results for approximately square or rectangular openings. It is extremely difficult in practice, however, to calculate the directions and magnitudes of the primary principal stresses with any confidence from flatjack measurements alone.

No one of these three methods can be considered completely reliable on its own. There are serious disadvantages to each technique. The approach adopted in this investigation was to try all three techniques and compare their results. I felt that a reasonably consistent pattern of results from a limited number of each of the three stress measurement techniques would be more believable than a great number of internally consistent results from any single technique.

Results of the Borehole Deformation Gage and Borehole Strain Rosette Relief Tests

Borehole deformation gage measurements were made in three horizontal north-south drill holes, one at the 13 Level site

and two at the 14 Level site. An attempt was made to take measurements in a hole inclined upwards at 45° to the west at the 14 Level site but none of the tests in this hole were successful. Twelve individual tests were completed and the results are given in Table XI. These results have been combined by the usual rosette analysis techniques to find the directions and magnitudes of the maximum and minimum borehole deformations in the vertical east-west plane six and a half feet north of the 13 Level M 30 W cross cut, six feet south of the 14 Level J 32 W cross cut, eight feet north of the 14 Level J 32 W cross cut and twelve feet north of the 14 Level J 32 W cross cut. The elastic moduli were determined in uniaxial and triaxial compression tests on small ($^7/_8$ inch diameter by two to two and one half inches long) cores drilled from the large core near each point of measurement and in the directions of the measurements. These values are given in Table XII. Stress values can be calculated at this stage if the rather stringent conditions of plane stress or plane strain are assumed. This is the procedure given by Merrill and Peterson [1961] and these values are also given in Table XII.

The borehole strain rosette relief tests were made in two holes in the J 32 W cross cut on 14 Level. The first hole was drilled horizontally towards the south. Three successful measurements were made, one each at approximately five, ten,

Table XI

Borehole Deformation Gage Results

Depth ft.in.	Angle of Measurement From Vertical Plunging	Borehole Deformation inches x 10^6
13 Level Horizontal Hole Drilled Towards the North		
1-8	0°	4000
5-7	0°	490
6-7	90°	1350
7-7	45° W	500
14 Level Horizontal Hole Drilled Towards the South		
3-5	0°	350
4-1	0°	850
5-0	90°	720
5-8	57° E	1350
6-6	0°	650
14 Level Horizontal Hole Drilled Towards the North		
3-2	0°	1020
3-11	72° E	675
7-5	90°	675
8-1	57° E	1250
9-0	0°	720
12-1	0°	720
12-8	38° W	520

Location	Δd_{max} x 10^{-6} ins	Δd_{min} x 10^{-6} ins	ϕ	E psi x 10^6	μ	Plane Strain σ_{max} psi	Plane Strain σ_{min} psi	Plane Stress σ_{max} psi	Plane Stress σ_{min} psi
L3 Level 6' N of M 30 W cross cut	2000	495	44° W	11.0	0.15	10570	4800	10300	4700
14 Level 6' S of J 32 W cross cut	1400	-40	47° W	10.4	0.15	7700	2465	7525	2415
14 Level 8' N of J 32 W cross cut	1325	20	43° W	12.1	0.15	8360	2840	8160	2775
14 Level 12' N of J 32 W cross cut	875	520	41½° W	10.9	0.15	4000	2650	3915	2600

ϕ is the angle from vertical to Δd_{max}

and fifteen feet from the side of the opening. The measurements at fifteen feet are about one diameter from the cross cut and so can be considered to be out of the zone of influence of the cross cut for practical purposes. The strain measurements indicated that the maximum principal stress in the east-west vertical plane plunged at about 45° to the east. A second measurement hole was drilled upwards towards the east at about 45° or in the direction of the minimum principal strain measured in the first hole. Two successful measurements were made in this hole, one at five feet and the other at 13 feet 9 inches. Because of the angle of the hole the deepest measurement was only about nine feet from the surface of the cross cut and was therefore still well within the stress concentration zone surrounding the cross cut. The individual results are given in Table XIII as the maximum and minimum principal strains and their orientation. The technique which I had hoped to use to analyze these test results was to combine the maximum and minimum measured strains from tests in each hole made outside of the stress concentration zone around the cross cut into four equations of the type

$$\epsilon_{max} E = 1.56\sigma_{max} - 1.56\mu\sigma_{min} - 1.04(1-\mu)\sigma_L$$

and solve these four equations for the three unknown principal stresses. Since the deepest measurements in the inclined hole were still within the stress concentration zone this was not possible. If the equations given by Leeman [1964] are used,

$$\left[(520 \times 10^{-6})/1.465\right]\left[10.9 \times 10^{6}\right] = (\sigma_{max} + \sigma_{min}) - 2(1-(.15)^2)$$

$$(\sigma_{max} - \sigma_{min}) - .15\sigma_L$$

These have been solved by least squares and the results and their probable errors using the methods of analysis given by Smart [1958] are

$$\sigma_{max} = 3220 \pm 340 \text{ psi}$$

$$\sigma_{min} = 2050 \pm 340 \text{ psi}$$

$$\sigma_L = 1900 \pm 560 \text{ psi}$$

with the maximum stress plunging towards the east at approximately 45°. Implicit in this analysis is the assumption that one of the primary principal stresses at Mt. Isa, σ_L, acts horizontally and in a north-south direction.

The north-south stress must increase from zero at the wall of the opening to nearly its primary value at one opening diameter into the rock. As a reasonable approximation to the variation of this "radial" stress with distance from the opening I have used Savin's [1961] mathematical solution for the stress in an elastic plate under equal biaxial stresses in the vicinity of a nearly square hole. The increase in stress is approximately linear out to a depth of one hole diameter. Using the value 1900 psi for the north-south stress at twelve feet six inches, and assuming the linear variation out to one opening diameter or fifteen feet, the σ_{NS} stress can be calculated for each

measurement depth and if this is done both the borehole gage combinations and the strain rosette relief measurements can be solved individually, for the maximum and minimum strains at each point of measurement. This has been done and the values are plotted in Figure 41. The estimated stresses then, about one opening diameter into the rock in the vertical east-west plane and north-south and horizontal are

$$\sigma_{max} = 3130 \text{ psi}$$
$$\sigma_{min} = 1800 \text{ psi}$$
$$\sigma_{NS} = 2375 \text{ psi}$$

with the maximum principal stress dipping to the east at about 45°.

The results of the strain rosette relief tests in the inclined hole are much more difficult to handle. I have somewhat arbitrarily assumed that the longitudinal stress in this hole (the minimum stress measured in the horizontal holes) also increases linearly from zero at the surface of the opening to its full value one opening diameter into the rock, and have calculated the stresses given in Table XIII using these values for the longitudinal stress in the equations. The directions and magnitudes of the principal strains indicated by the strain gage rosettes are almost certainly affected by the shear stresses existing in the rock near the opening, however, so these results are not considered very reliable.

Table XIII

Results of the Borehole Strain Relief Tests
Horizontal Hole Drilled Towards the South

Depth ft.in.	ϵ_{max} ppm	ϵ_{min} ppm	ϕ Plunging Towards	σ_{max} psi	σ_{min} psi	σ_{ζ} psi
5-1	595	195	76° E	5290	2910	880
10-0	320	115	39° E	3900	2750	1750
15-3	226	- 90	42° E	3370	1450	2675
			Inclined Hole (43° up from horizontal due East)			
5-3	755	35	56° N	6270	3580	445
13-9	67	- 102	55° N	1180	70	1165

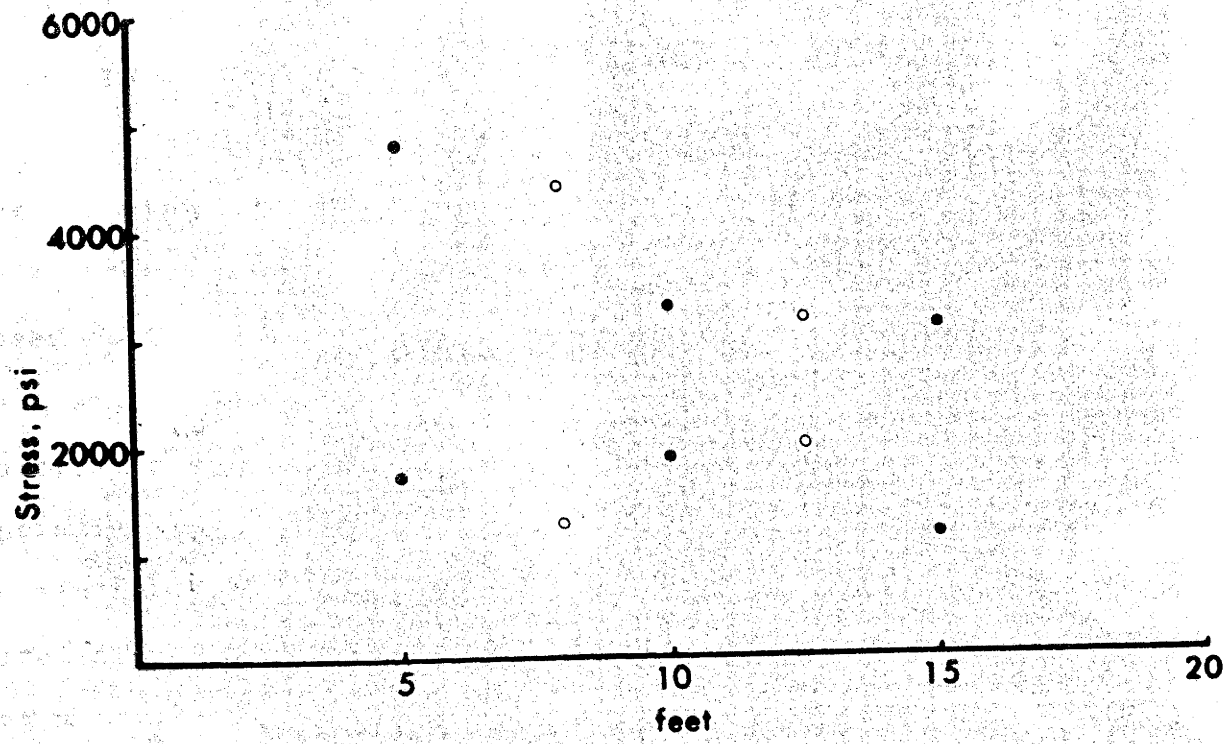

Fig. 41 Variation of measured maximum and minimum principal stresses with distance from the J 32 west cross cut on 14 Level. All values shown were determined in horizontal north south boreholes. O Borehole deformation gage results. ● Strain rosette relief results.

Results of the Flatjack Tests

A total of 18 flatjack tests were completed, six at each of the 11, 13, and 14 Level sites. The results are summarized in Table XIV. The flatjacks, of course, give only the stresses near the surface of the openings. These openings are not parallel to any of the principal stress directions inferred from the borehole deformation gage and borehole strain rosette relief tests so the simple analysis method given by Alexander [1960] can not be expected to work here. Hiramatsu and Oka [1962] have given a three dimensional photoelasticity solution for the stresses on the surface of a nearly square hole in a general three dimensional stress field. Figure 42 is a cross cut outline photograph of the 14 Level cross cut and it can be seen that it is approximately a square with rounded corners. Using Hiramatsu and Oka's analysis and the stresses and stress directions inferred from the borehole deformation gage and strain rosette relief measurements, the stresses in the positions and directions in the roof and walls of the cross cut corresponding to the flatjack measurements for the 14 Level site have been calculated. These values are listed in Table XIV opposite the 14 Level measurements as the calculated stresses. Considering the uncertainties and approximations involved in the analysis the agreement between the measured and calculated stresses is good. Four of the calculated values agree within 200 to 300 psi and

Table XIV

Summarized Results of the Flatjack Tests

Location of Jack	Direction of Stress Measured	Modulus x 10^6 psi Average of 6 in. and 10 in.	Stress, psi Average of 6 in. and 10 in.	Calculated Stress
11 Level-back	Transverse to cross cut axis	8.64	1815	-
11 Level-back	NE-SW	6.73	1990	-
11 Level North Wall	45° dipping East	8.99	1345	-
11 Level North Wall	45° dipping West	5.05	670	-
11 Level South Wall	Horizontal	7.13	2545	-
11 Level South Wall	Vertical	10.13	3895	-
13 Level North Wall	Vertical	7.60	1190	-
13 Level North Wall	45° dipping East	7.84	3335	-
13 Level North Wall	45° dipping West	6.62	1325	-

Table XIV (cont.)

Location of Jack	Direction of Stress Measured	Modulus x 10^6 psi Average of 6 in. and 10 in.	Stress, psi Average of 6 in. and 10 in.	Calculated Stress
13 Level-back	Parallel to cross cut axis	11.33	1965	-
13 Level-back	Transverse to cross cut axis	9.29	5150	-
13 Level-back	NW. SE	5.25	1178	-
14 Level South Wall	Vertical	6.90	2000	3168
14 Level South Wall	Horizontal	8.07	2540	2228
14 Level South Wall	45° dipping West	11.30	2260	2060
14 Level South Wall	45° dipping East	9.50	3072	3310
14 Level-back	Transverse to cross cut axis	5.24	2887	2665
14 Level-back	NW-SE	5.97	1290	2410

the other two are each about 1100 psi higher than the measured stresses. Both of these two disagreeing flatjack tests gave low values for the "in situ" modulus of the site which probably means that the rock at these sites was fractured and this could in turn mean that these sites were to some extent stress relieved.

There is certainly some general agreement then between the three stress measurement techniques. Further work needs to be done to more firmly establish the directions of the principal stresses and the magnitude of the north-south stress. It should be made clear that all of the above work has proceeded on an initial assumption that one of the principal stresses does set in a north-south and horizontal direction. The fact that the three different stress measurement techniques agree though each is affected differently by shear stresses acting in their plane of measurement suggests that any shear stresses present must have a small magnitude and therefore that the stress measurements were made in approximately principal stress directions.

Measurements of Dolomite Twin Lamellae

A preliminary study was made of the orientation of dolomite twin lamellae in oriented specimens of "silica dolomite" from the 1100 orebody. One suite of three orthogonal thin sections was taken from the oriented borehole deformation gage core 8 feet north of the 13 Level M 30 W cross cut and another suite of

three orthogonal thin sections was taken from oriented strain rosette relief core 5 feet south of the 14 Level J 32 W cross cut. Once the dolomite "C" axes and twin lamellae are measured (on a petrographic microscope equipped with a universal stage) it is possible (following Turner and Weiss [1963]) to determine the directions of maximum and minimum principal stresses that would give the maximum critical resolved shear stress in the twin plane for each deformed grain. If a large number of grains are measured and the inferred maximum and minimum principal stress directions plotted on an equal area net it is sometimes possible to estimate the directions and relative magnitudes of the principal stresses that were acting when the dolomite was deformed. The measurements that were made are given in Figures 43, 44, 45, 46, 47 and 48. No detailed interpretation seems possible. The two samples differ and similar work in another portion of this mine suggests still another stress distribution (private communication from K. Rosengren, [1966]). The most that can be said is that a north-south horizontal principal stress direction is the only direction that does not conflict with any of the dolomite deformation lamellae measurements.

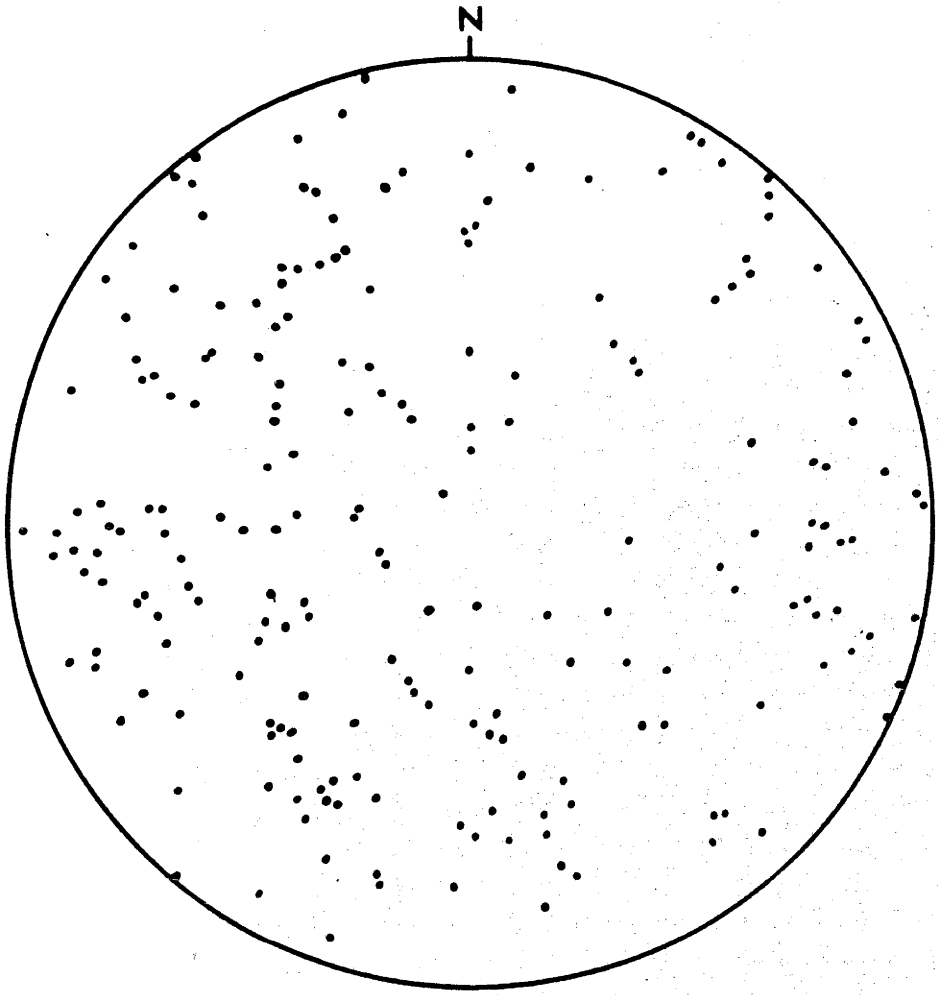

Fig. 43 Lower hemisphere, equal area projection presentation of dolomite "C" axis orientations. Sample taken from oriented core 8 feet north of the 13 Level M 30 west cross cut.

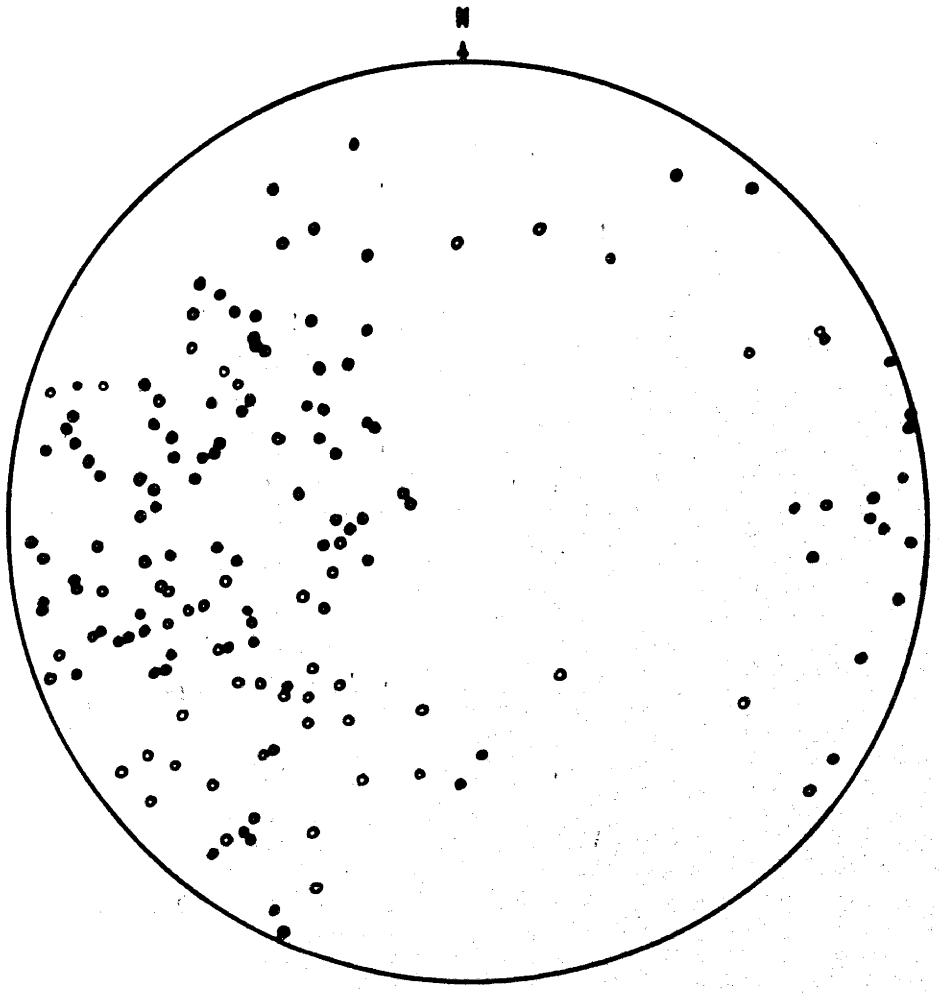

Fig. 44 Lower hemisphere, equal area projection presentation of maximum principal stress directions determined from measurements of dolomite twin lamellae. Sample taken from oriented core 8 feet north of the 13 Level M 30 west cross cut.

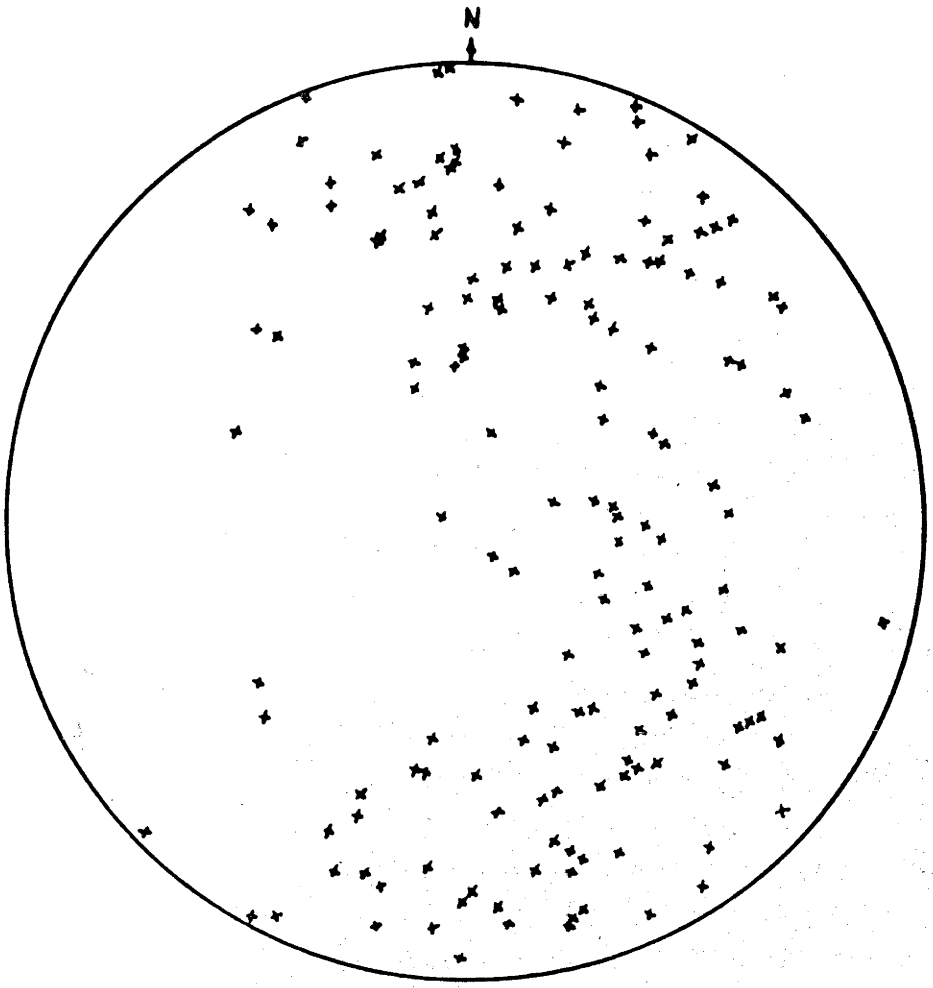

Fig. 45 Lower hemisphere, equal area projection presentation of minimum principal stress directions determined from measurements of dolomite twin lamellae. Sample taken from oriented core 8 feet north of the 13 Level M 30 west cross cut.

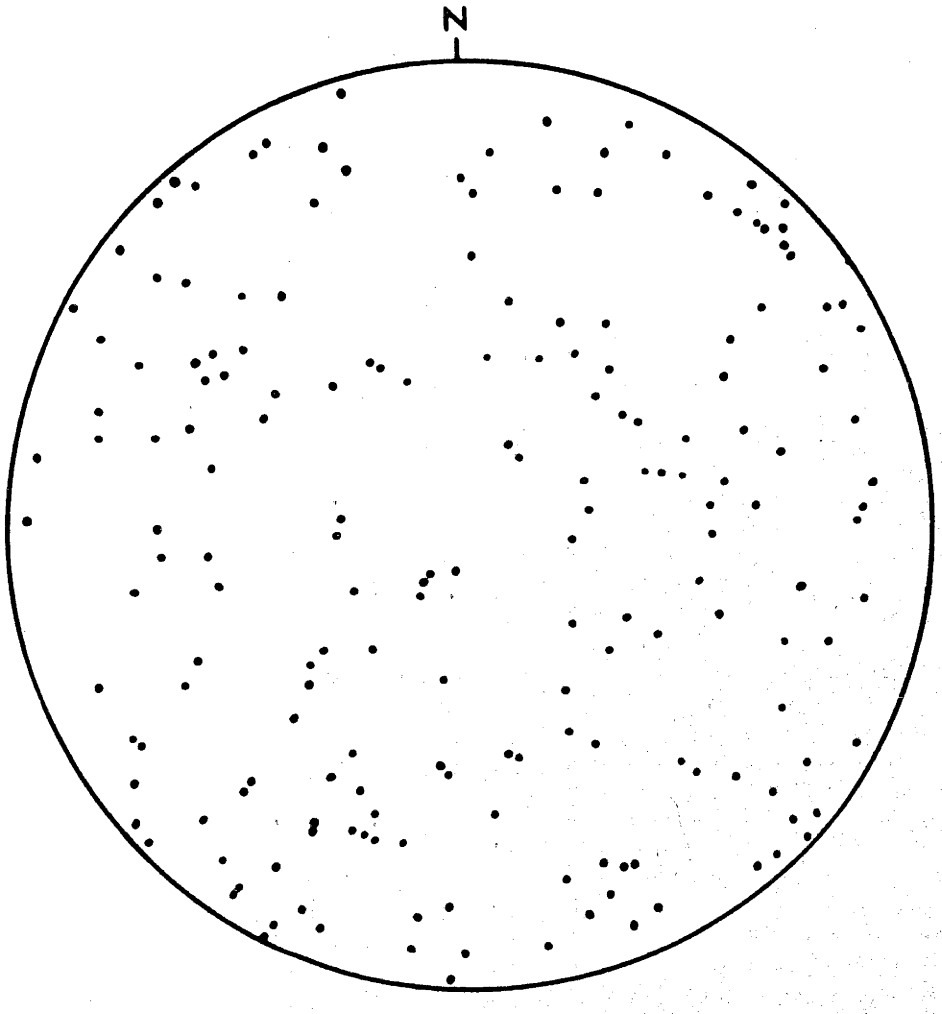

Fig. 46 Lower hemisphere, equal area projection presentation of dolomite "C" axis orientations. Sample taken from oriented core 5 feet south of the 14 Level J 32 west cross cut.

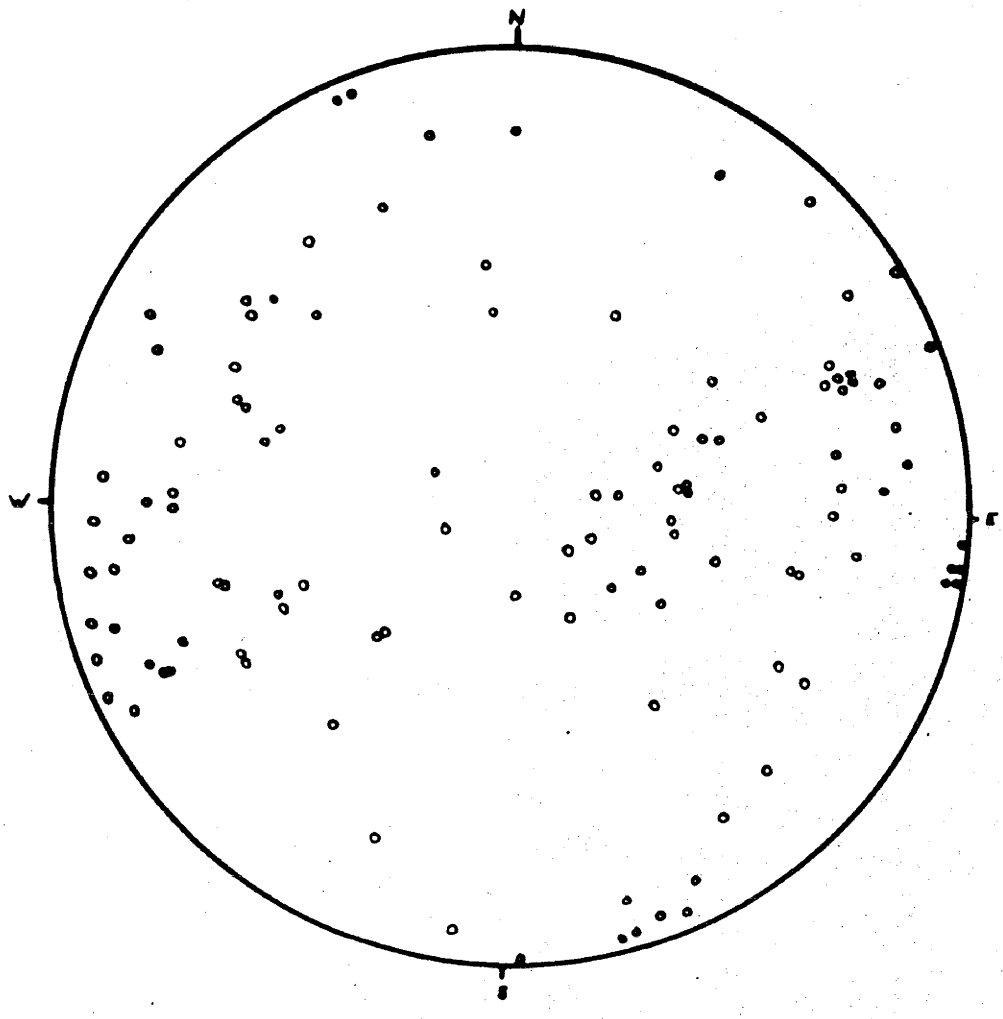

Fig. 47 Lower hemisphere, equal area projection presentation of maximum principal stress directions determined from measurements of dolomite twin lamellae. Sample taken from oriented core 5 feet south of the 14 Level J 32 west cross cut.

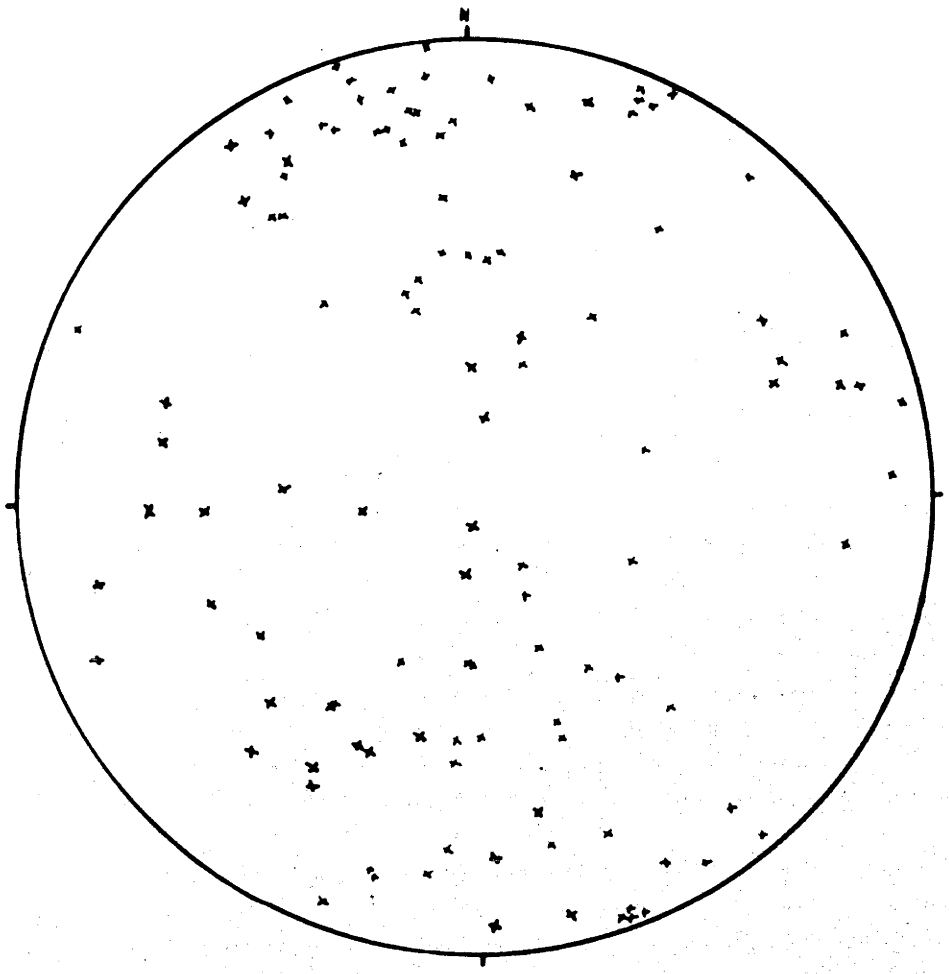

Fig. 48 Lower hemisphere, equal area projection presentation of minimum principal stress directions determined from measurements of dolomite twin lamellae. Sample taken from oriented core 5 feet south of the 14 Level J 32 west cross cut.

Chapter XI

COMPARISON OF IN SITU AND LABORATORY MEASURED VALUES OF DEFORMATION MODULI ON ROCKS FROM MT. ISA

A number of "in situ" and laboratory measurements of deformation moduli were made during the course of this project. Each flatjack test can yield four separate "in situ" measurements of modulus. One modulus can be attained from the jack pressure-pin displacement records when the flatjack is being pressurized. Another modulus comes from the pin displacements during slot cutting once the stress normal to the flatjack has been determined. Both moduli can be determined for the two pairs of measuring pins, six and ten inches apart. The relevant elastic theory was given by Alexander [1960] and has been discussed in appendix 4. It is necessary to have a value for Poisson's ratio to solve the equations and 0.15 was used in the calculations as it was the mean of the laboratory determinations that were made on rock from this same area in connection with the borehole deformation gage and borehole strain rosette relief tests.

The four different values of modulus that can be calculated for each flatjack need not necessarily be equal. The relationships of these various modulus measurements to each other and to

laboratory determined values are examined in some detail in appendix 4. The individual values from the underground tests are listed in Table XV. There are a total of 33 measurements with a mean of 7.9×10^6 psi.

There are 46 laboratory measurements of elastic modulus which were made in unconfined compression on 7/8 and $2\frac{1}{4}$ inch cores drilled at different directions into the six and eight inch core recovered from the borehole deformation gage tests. These values are listed in Table XVI. There are also 5 measurements of Young's modulus and Poisson's ratio made by diametral compression of cylinders cut from the core recovered with the borehole strain rosette relief tests and their values are given in Table XVII. Strain in 44 of the cores tested in unconfined compression was measured by two mechanical extensometers fixed on opposite sides of the cores. The cores were loaded in an Amsler 10000 lb. capacity testing machine to a stress of approximately 5000 psi. All of the tests reported are the average of at least two loading cycles. None of the cores were tested to destruction. Two cores were tested using electric resistance strain gages on opposite sides to measure the rock strain. Most of the tests gave a linear stress-strain curve over this range with only a small amount of hysteresis. The mean value of Young's modulus determined in the laboratory tests was 11.6×10^6 psi and the mean value of Poisson's ratio for

Table XV

In Situ Deformation Moduli Determined from the Flatjack Tests

All Values in psi x 10^6

Flatjack Location and Number	Six Inch Pins			Ten Inch Pins			Total Mean
	Slot Cutting	Jack Pressure	Mean	Slot Cutting	Jack Pressure	Mean	
11 Level							
Jack 1	6.8	5.0	5.9	12.3	11.5	11.9	8.6
Jack 2	7.9	6.3	7.1	6.3	6.4	6.3	6.7
Jack 3	10.7	7.7	9.2	9.8	7.9	8.8	9.0
Jack 4				4.7	5.4	5.1	5.1
Jack 5	5.9	5.6	5.8	8.2	8.8	8.5	7.1
Jack 6	9.1	9.1	9.1	11.2	11.2	11.2	10.1
13 Level							
Jack 1	9.5	5.9	7.7	9.0	6.0	7.5	7.6
Jack 3	7.4	6.6	7.0	8.6	8.9	8.7	7.8
Jack 4	5.3	3.9	4.6	8.6	8.8	8.7	6.6

Table 11 (cont.)

Flatjack Location and Number	Six Inch Pins			Ten Inch Pins			Total Mean
	Slot Cutting	Jack Pressure	Mean	Slot Cutting	Jack Pressure	Mean	
Jack 5				14.0	8.7	11.3	11.3
Jack 6	6.9	6.3	6.6	12.8	11.2	12.0	9.3
Jack 7	5.3	6.0	5.7	4.7	5.0	4.8	5.3
14 Level							
Jack 1	4.9	4.0	4.4	10.5	8.2	9.4	6.9
Jack 2	9.8	6.7	8.2	9.4	6.4	7.9	8.1
Jack 3				12.1	10.5	11.3	11.3
Jack 4	10.1	8.8	9.5	10.8	8.4	9.6	9.5
Jack 5	5.8	4.4	5.1	5.9	4.9	5.4	5.2
Jack 6	4.6	7.7	6.2	4.8	7.9	5.8	6.0

Table XVI

Results of Laboratory Elastic Modulus Determinations - Uniaxial Compression of Cores Drilled from Borehole Deformation Gage Core

Specimen No.	Direction of Core Axis	Modulus x 10^6 psi
V4-1	Vertical	4.4
V4-2	Vertical	12.1
V4-3	Vertical	1.8
V4-4	Vertical	16.3
V4-5	Vertical	11.5
H4-1	Horizontal, East-West	9.5
H4-2	Horizontal, East-West	11.6
H4-3	Horizontal, East-West	8.8
45° W-4-1	Dipping 45° to West	19.2
45° W-4-2	Dipping 45° to West	11.6
45° W-4-3	Dipping 45° to West	13.9
45° W-4-4	Dipping 45° to West	20.0
45° W-4-5	Dipping 45° to West	12.2
45° E-4-2	Dipping 45° to West	10.2
45° E-4-3	Dipping 45° to East	5.9
45° E-4-4	Dipping 45° to East	8.7
45° E-4-5	Dipping 45° to East	8.1
45° E-4-6	Dipping 45° to East	10.5
V2-7-1	Vertical	13.7
V2-7-2	Vertical	13.7

Table XVI (cont.)

Specimen No.	Direction of Core Axis	Modulus x 10^6 psi
V2-7-3	Vertical	13.2
H2-7-1	Horizontal, East-West	11.8
H2-7-2	Horizontal, East-West	11.5
H2-7-3	Horizontal, East-West	11.7
45° E2-7-1	Dipping 45° to West	12.1
45° E2-7-2	Dipping 45° to West	11.6
45° E2-7-3	Dipping 45° to West	12.8
45° W2-7-1	Dipping 45° to East	11.4
45° W2-7-2	Dipping 45° to East	10.2
45° W2-7-3	Dipping 45° to East	12.0
V2-9-1	Vertical	11.9
V2-9-2	Vertical	10.9
V2-9-3	Vertical	11.9
H2-9-1	Horizontal, East-West	11.4
H2-9-2	Horizontal, East-West	11.6
H2-9-3	Horizontal, East-West	7.7
H2-9-4	Horizontal, East-West	11.1
45° E2-9-1	Dipping 45° to West	12.5
45° E2-9-2	Dipping 45° to West	11.3
45° E2-9-3	Dipping 45° to West	12.0
45° E2-9-4	Dipping 45° to West	11.5

Table XVII

Results of Laboratory Elastic Modulus Determination - Diametral Compression of Cylinders Recovered from Borehole Strain Rosette Relief Tests

Specimen No.	Young's Modulus x 10^6 psi	Poisson's Ratio
SG2-L-1	11.1	0.28
SG4-L-1-1	11.4	0.10
SG4-L-1-2	11.3	0.11
SG8(b)L-2-1	11.5	0.13
SG8(b)L-2-2	11.0	0.12

the tests in which this was determined was 0.15. The specimens which gave a modulus of 15 x 10^6 psi or more contained a noticeably larger proportion of sulphide minerals. This was not expected, however, Clark [1966] gives a modulus for a specimen of massive pyrite from Noranda, Ontario of approximately 24 x 10^6 psi. He gives moduli for various dolomites as 10 x 10^6 to 13 x 10^6 psi and quartzites as approximately 14 x 10^6 psi. The quartzite and pyrite values quoted by Clark were determined by dynamic techniques and these generally yield slightly higher moduli than do static tests. Two different Australian quartzites were tested using the same techniques and equipment as the Mt. Isa tests and these gave moduli of 9.0 x 10^6 and 11.5 x 10^6 psi.

There are a number of ways in which these results can be graphically presented. Figure 49 is a histogram comparing the "in situ" or flatjack moduli with the laboratory moduli. The frequency is given as the per cent of the total measurements for each type. The laboratory values give a reasonably normal distribution about the mean value; the "in situ" measurements do not. It is tempting to consider the flatjack moduli distribution that is shown as being the sum of two normal distributions, one for relatively sound rock and the other for fractured rock. There are some traps here, however. Each flatjack is represented on this diagram by two measurements, the average of the moduli determined across the six inch pins

and the average of the moduli determined across the ten inch pins. These are plotted separately in Figure 50 (a) and (b). While each set of values retains a semblance of a bimodal distribution about the mean, there are certainly more high moduli among the ten inch measurements and more low moduli among the six inch measurements. The six inch measurements being closer to the slot will be relatively more affected by any fracturing or loosening of already existing fractures caused by drilling a narrow slot in the existing stress field. It could be argued that measurements on the ten inch pins give high moduli and measurements on the six inch pins give low moduli and that very little is learned about the relative modulus of flatjack sites unless these are averaged and a single value plotted for each site. This has been done in Figure 51 and the trouble now is that there are not enough values plotted to tell what the distribution is. Another possible argument is that the moduli measured on the ten inch pins should be used as it is affected relatively less by the loosening of the rock close to the slot and it therefore better represents the rock conditions before the slot was drilled. Obviously more "in situ" modulus measurements by flatjacks or some different method such as plate bearing or borehole expansion tests are needed before this problem can be conclusively resolved.

Another pertinent graph is the relationship of flatjack modulus to the stress measured by the flatjack. One laboratory flatjack test reported in appendix 4, which was done in a very weak, low modulus and irregular concrete block, indicated a higher stress than was actually applied. If this is a general conclusion then the low modulus sites underground should yield high stress values and these flatjack stress results would not mean very much. On the other hand, areas of high stress undrground would be more likely to fracture and relieve the stresses present to some degree so that (assuming that the modulus is related to fracturing) low modulus sites should yield the lower stress values. Figure 52 shows the relationship. It is probably best not to draw sweeping conclusions from diagrams that look like this but certainly it can be said with some safety that there is no clear tendency for flatjack sites with a low modulus to yield high stresses.

From all of the above it is concluded that the "in situ" modulus of the "silica dolomite" at the sites tested ranges from approximately 5×10^6 psi to 12×10^6 psi with a mean value of about 8×10^6 psi. The mean of the laboratory determined values was 11.6×10^6 psi for specimens taken from the same area. Because of the low stresses and relatively strong minerals present, the difference in moduli is considered to be due to the presence of more small scale fracturing in the

approximately two cubic feet of rock involved in the "in situ" measurement than in the approximately two cubic inches of rock in the laboratory tests. The laboratory test specimens are not fair samples of the mass of rock as the weakest sections will have already failed during the collection and preparation of the specimens. The "in situ" measurements of modulus reported here are not completely fair samples of the rock mass either. The procedure in flatjack site selection is to take great care to find the soundest possible rock and put the flatjacks there. This makes the interpretation of the flatjack results simpler but it must be remembered that the moduli determined by flatjacks under these conditions are only an upper limit on the "in situ" modulus of the larger body of rock.

Chapter XII

RESULTS OF LABORATORY STRENGTH TESTS ON MT. ISA ROCKS

A fairly large number of strength tests were made on rock specimens collected at Mt. Isa. The majority of these tests were triaxial compression tests on cores of "silica dolomite". A few indirect tension and confined hollow cylinder tests were also made on this material. A lesser number of confined compression and indirect tension tests were made on altered greenstone collected close to the contact and a specimen of "shale" marked H104 and furnished by the Rock Mechanics section. A few confined compression tests were also made on cores of "unaltered greenstone" also furnished by the Rock Mechanics section. As would be expected those materials show considerable variation in their mechanical properties from specimen to specimen. The individual values are listed in Tables XVIII, XIX, XX, XXI, and XXII and the "silica dolomite" triaxial tests are plotted in Figure 53. Figure 54 is a strength versus foliation angle diagram for altered greenstone at several confining pressures. The stresses given for the indirect tension tests and hollow cylinder tests were calculated on the basis of linear isotropic elastic theory. In the case of the anisotropic greenstone and shale specimens this is obviously inaccurate but

Table XVIII

Results of Triaxial Compression Tests on Mt. Isa Silica Dolomite

Specimen No.	σ_3, psi	σ_1, psi
M30-600	0	33100
M30-601	0	30900
M30-602	0	25850
M30-A3	0	43500
T31E 200-1	0	37400
T31E 100-2	0	55500
W22E 395-3	0	29780
W22E 100-2	500	53000
T31E 300-2	500	46100
M31 A1	500	39300
M30 A6	500	38250
M30 A2	1000	49100
M30 A8	1000	54100
W22E 400-3	1500	44500
M30 A4	1500	37100
M30 A-7	1500	52500
T31E 100-1	1500	62900
M30 A-11	2000	55600
W22E 300-1	3000	66600
W22E 400-2	3000	54500

Table XVIII (cont.)

Specimen No.	σ_3, psi	σ_1, psi
T31E 200-1	3000	49200
M30 A5	3000	40500
M30 A10	3000	62700
W22E 400-1	3850	64350
W22E 500-2	3850	75040
T31E 400-1	3850	83140
M30-603	5000	70000
M30-604	5000	74400
M30-605	5000	74400
MI-800	5000	72200
T31E 300-1	5300	75900
M30 A9	5300	72700
W22E 395-1	6750	51550
W22 N2 700-1	6750	69950
T31E 100-3	8200	77700
W22E 100-1	8200	84000
M30 A12	8200	82900
M30 606	10000	88800
M30 607	10000	78500
M30 608	10000	87300
W22E 300-2	11100	106100

Table XVIII (cont.)

Specimen No.	σ_3, psi	σ_1, psi
W22E 500-1	11100	98300
T31E 400-2	11100	111900
T31E 200-2	14000	131800
W22E 395-2	14000	88800
M30 609	15000	97200
M30 610	15000	106700
M30 611	15000	105600

Table XIX

Results of Confined Hollow Cylinders and Brazilian Tests on Mt. Isa Silica Dolomite

Specimen No.	σ_1, psi	σ_2, psi	σ_3, psi
M1 500	31000	0	0
M1 501	35800	0	0
M1 502	22400	0	0
M1 503	57200	2420	0
M1 504	44900	2420	0
M1 505	53600	2420	0
M1 506	64030	7260	0
M1 507	61230	7260	0
M1 508	67130	7260	0
M1 509	76850	12100	0
M1 510	66550	12100	0
M1 511	71650	12100	0
M1 512	82600	24200	0
M1 513	87400	24200	0
M1 514	87100	24200	0
M1 515	113700	48400	0
M1 516	102700	48400	0
M1 517	10270	48400	0
T31E 300	6450	0	- 2150

Table XX

Results of Confined Compression Tests on Altered Greenstone

Specimen No.	Foliation Angle From Core Axis	σ_3 psi	σ_1 psi	Fracture Angle From Core Axis
M1GSH-1	75°	0	26000	39°
M1GSH-2	90°	1000	26700	23°
M1GSH-3	75°	2000	37200	50°
M1GSH-4	70°	5000	39500	32°
M1GSH-5	80°	14000	79000	36°
M1GSV-1	10°	0	22400	34°
M1GSV-2	10°	1000	26300	25°
M1GSV-3	10°-15°	2000	30000	23°
M1GSV-4	10°	5000	36000	30°
GS-1	15°	3000	25900	25°
GS-2	10°-20°	1500	19200	20°
GS-3	15°	3840	28340	18°
GS-4	25°	6740	35800	28°
GS-5	20°-25°	14000	46700	25°
GS-6	30°	14000	47950	30°
V-1 (axis Vert. in Space)	20°	14000	55400	20°
V-2 "	20°	14000	46300	20°
V-3 "	20°	6740	35990	30°
V-4 "	20°	0	15300	20°

Table XX (cont.)

Specimen No.	Foliation Angle From Core Axis	σ_3 psi	σ_1 psi	Fracture Angle From Core Axis
E-1 (axis E-W in Space)	24°	14000	46100	37°
E-3 "	30°	10380	45480	30°
E-4 "	40°	6740	35400	25°
E-5 "	40°	0	15960	27°
E-8 "	34°	3840	27790	24°
E-9 "	30°	21350	65800	31°

Table XXI

Results of Confined Compression Tests on "Unaltered Greenstone"

Specimen No.	Foliation Angle From Core Axis	σ_3 psi	σ_1 psi	Fracture Angle From Core Axis
T28E Dec 1 466'-1	subparallel	0	21300	Shattered
T28E Dec 1 466'-2	?	5000	71400	20°
T28E Dec 1 552'-1	40°	2000	10850	40°
T28E Dec 1 552'-2	40°	5000	17900	40°
T28E Dec 1 608'-1	?	5000	20300	26°
T28E Dec 1 608'-2	?	10000	24000	30° and 0.9°
S10E Dec 1 1536'-1	?	1000	34100	0° to shattered
S10E Dec 1 1536'-2	?	5000	67200	0° and 90°
R6E Dec 1 1479'-1	25°	0	6980	0°-20°

Table XXII

Results of Confined Compression and Brazilian Tests on H104 Shale

Specimen No.	σ_3, psi	σ_1, psi
	Cylinders Parallel to Foliation	
HA 4	0	80100
HA 8	1500	83200
HA 7	3480	101840
HA 6	6750	122950
HA 10	6750	122850
HA 5	9650	129250
HA 3	11600	139400
HA 2	12550	147750
HA 1	14000	149800
HA 9	14000	154900
	Cylinders Perpendicular to Foliation	
HA 1	0	45400
HP 5	0	46500
HP 8	750	89650
HP 4	3480	103040
HP 3	6750	117250
HP 9	8700	128200
HP 7	11600	13320
HP 2	14000	148100
HP 6	14000	150000

Table XXII (cont.)

Specimen No.	(σ_3) psi	(σ_1) psi
	Diametral Compression Parallel to Foliation	
HA 14	(- 2790)	(8370)
HA 15	(- 2670)	(8010)
	Diametral Compression Perpendicular to Foliation	
HA 11	(- 2680)	(8040)
HA 12	(- 4175)	(12525)
HA 13	(- 2880)	(8640)
	Diametral Compression 45° to Foliation	
HA 16	(- 2040)	(6120)
HA 17	(- 2510)	(7530)

Note: (σ_1) and (σ_3) values were calculated from formulae based on linear isotropic elasticity. They are given here only as a means of comparing the behaviour of the rock in various directions relative to its foliation

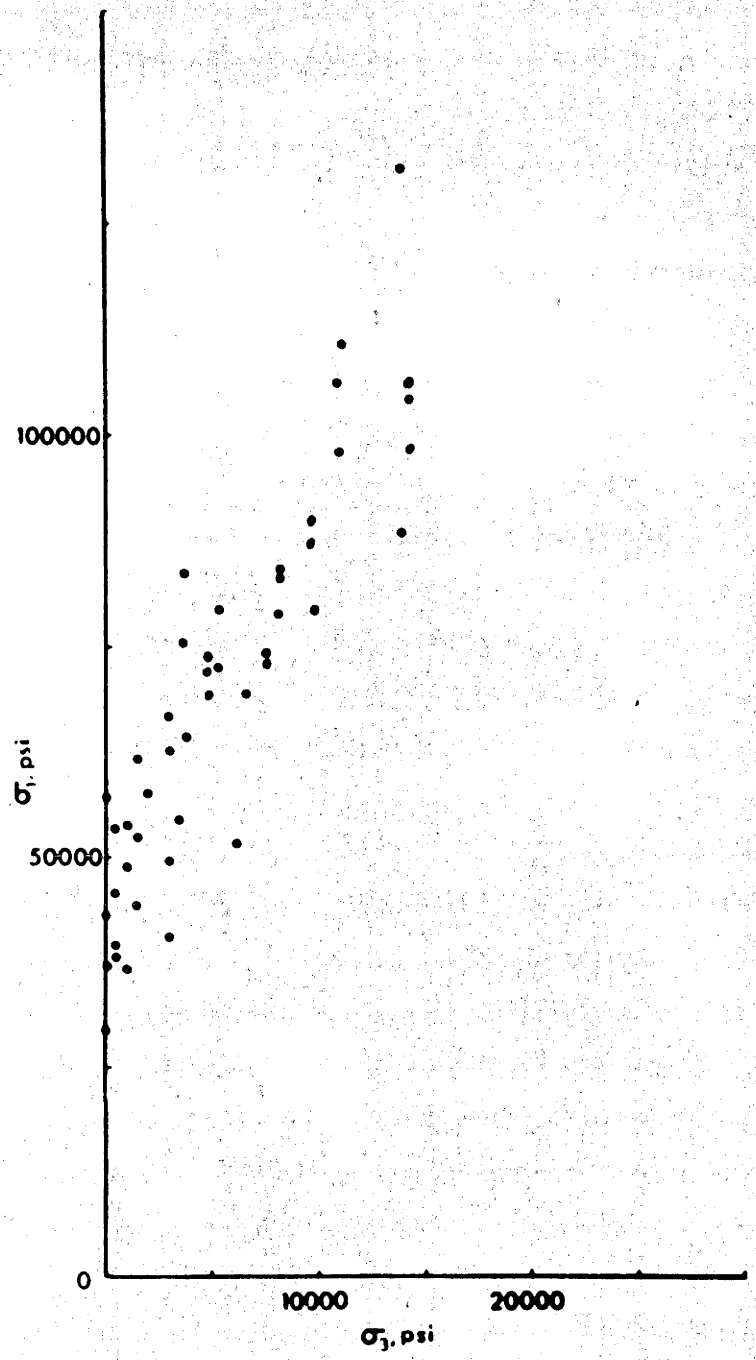

Fig. 53 Principal stress relationships at failure for Mt. Isa "silica dolomite" triaxial tests.

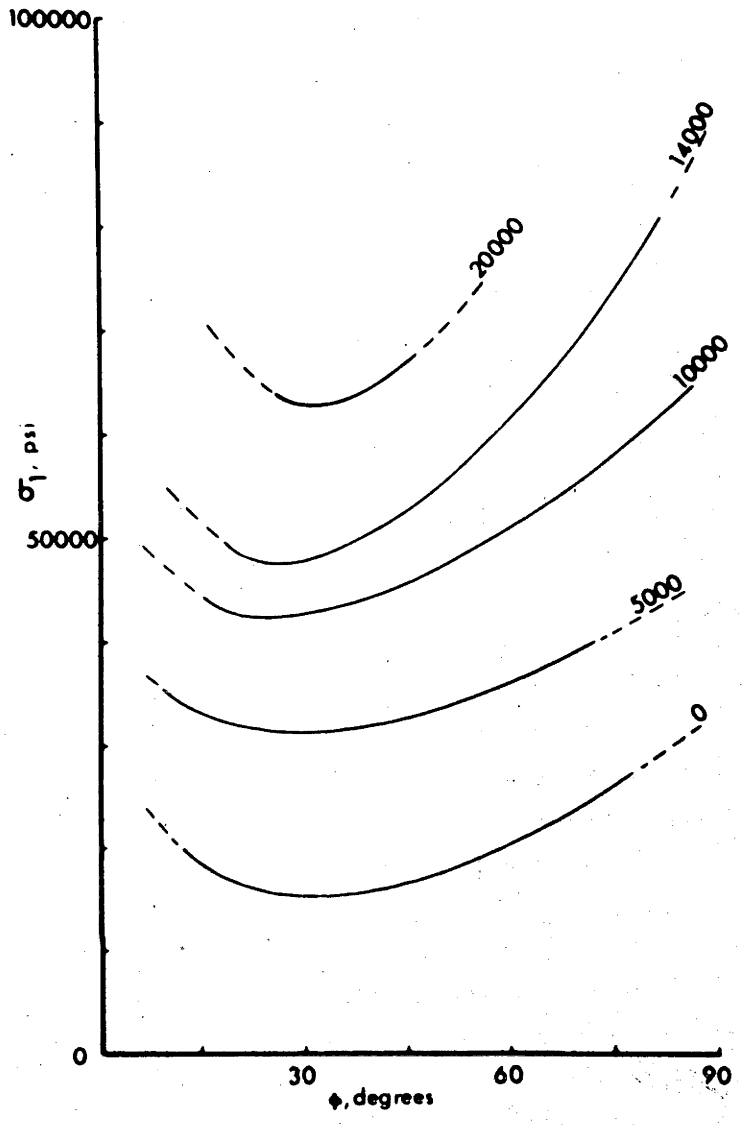

Fig. 54 Differential stress at failure versus angle from foliation to core axis for altered greenstone triaxial tests at several confining pressures.

as there is no anisotropic solution available this is the best that can be done at present and can serve perhaps at least as a rough guide.

Jaeger [1966] has proposed developing a three dimensional failure surface for any given rock by rotating the triaxial test data about the $\sigma_1 = \sigma_2 = \sigma_3$ axis. This has tentatively been verified on several isotropic and uniform rock materials in Chapter II. This criterion can be simply checked by comparing the results of tests on hollow cylinders of rock subjected to external pressure and axial load with triaxial test data from the same rock rotated into the $\sigma_3 = 0$ principal stress plane, since the hollow cylinders fail with one principal stress on the inner surface = 0. This has been done on cores cut from a selected place of "silica dolomite" which seemed to be fairly uniform and the results are given in Figure 55. The correlation seems to be very good. This idea is best not carried too far yet as the stresses at failure in the hollow cylinder are calculated on the basis of linear elastic theory which may not be valid at the point of failure in all cases. However, for the essentially brittle silica dolomite at the pressures expected around underground openings at Mt. Isa this is probably a better failure criterion than the Mohr or modified Griffith theories.

BIBLIOGRAPHY

Adams, F.D., An experimental contribution to the question of the depth of the zone of flow in the earth's crust, Journal of Geology, 20, 97-118, 1912.

Alexander, L.G., Field and laboratory tests in rock mechanics. Third Australian-New Zealand Conference on Soil Mechanics and Foundation Engineering, 161-168, 1960.

Alexander L., Discussion to paper by E.S. Barnes in Stress and Failure Around Underground Openings, University of Sydney 1967.

Bellamy, C.J., On the strength of concrete under combined stress, University of Sydney, School of Civil Engineering, Research Report no. R-23, 29, 1960.

Bennet, E.M., Lead-zinc-silver and copper deposits of Mt. Isa in Geology of Australian Ore Deposits, 233-246, 1965.

Berents, H.P. and Alexander L.G., Rock stress measurements and drilling techniques, Contracting and Construction Equipment, 19, 1, 64-66 1965.

Birch, F., The velocity of compressional waves in rocks to 10 kilobars, Part 2, J. of Geophysical Research, 66, 2199-2224, 1961.

Böker, R., Die Mechanik du bleibenden Formanderung in kristallinisch aufgebauten Korpem, Verhandel. Deut. Ing. Mitt. Forsch., 175, 1-51, 1915.

Borg, I. and Handin. J., Experimental deformation of crystalline rocks, Tectonophysics, v. 3, no. 4, 251-367, 1966.

Bowden, F. and Taber, D., The Friction and Lubrication of Solids, Part II, Oxford, 1964.

Brace, W.F., An extension of Griffith theory of Fracture to rocks, J. of Geophysical Research, 65, 3477-3480, 1960.

Brace, W.F., Brittle fracture of rocks, State of Stress in the Earth's Crust, American Elsevier, 1964.

Bridgman, P.W., The failure of cavities in crystals and rocks under pressure, The American Journal of Science, 4th Series, no. 268, 243-268, 1918.

Broms, B.B. and Casbarian, A.O. and Broms, B.B. and Jamal, A.K., Triaxial tests on thin-walled tubular samples, Proceedings of the 6th Int. Conf. on Soil Mech. and Foundation Engineering, 1, 179-187, 1965.

Clark, S., Handbook of Physical Constants, G.S.A. Mem. 97, 1966.

Cook, N.G.W. and Hodgson, K., Some detailed stress strain curves for rock. J. of Geophysical Research, 70, 2883-2888, 1965.

Davies, E., Mining practice at Mt. Isa Mines Ltd., Australia, Trans. Inst. of Min. and Met., 76, A14-A40, 1967.

Duvall, W., and Stephenson, D., Seismic Energy Available from Rockbursts and Underground Explosions, Trans. of the S.M.E., 232, 235-240, 1965.

Galle, E.M. and Wilhoit, J.C., Stresses around a wellbore due to internal pressure and unequal principal geostatic stresses, Soc. Petrol. Eng. Jl., 2, 145-155 1962.

Grassi, R.C. and Cornet, I., Fracture of gray cast-iron tubes under biaxial stresses, Journal of Applied Mechanics, Trans. AS.M.E., 71, 178-182, 1949.

Griggs, D. and Handin, J., Observations on fracture and a hypothesis of earthquakes, Geol. Soc. Amer. Mem. 79, 347-364, 1960.

Griggs, D. and Miller, W., Deformation of Yule marble, Part I, Geol. Soc. of America Bull., 63, 853-862, 1951.

Handin, J., Higgs, D.V. and O'Brien, J.K., Torsion of Yule marble under confining pressure, Geol. Soc. Amer. Mem. 79, 245-274, 1960.

Handin, J., Heard, H.C. and Magouirk, J.N., Effects of the intermediate principal stress on the failure of limestone, dolomite and glass at different temperatures and strain rates, J. of Geophysical Research, 72, 611-640, 1967.

Hast, N., The Measurement of rock pressure in mines, Sveriges Geologiska Undersokning Sec. C, Arsbok 52, no. 3,1958.

Hawkes, I. and Moxon S., The measurement of in-situ rock stress using the photoelastic gage and the core-relief technique, Int. J. Rock Mech. Min. Sci., 2, 905-919, 1965.

Hill, R., The Mathematical Theory of Plasticity, Oxford, 1950.

Hiramatsu, Y. and Oka, Y., Stresses around a shaft or level excavated in ground with a three-dimensional stress state, Kyoto University, Faculty of Engineering Mem. 24, 56-76, 1962.

Hobbs, D.W., The strength of coal under biaxial compression, Colliery Engineering, 39, 285-290, 1962.

Hondros, G., The evaluation of Poisson's ratio and the modulus of materials of a low tensile resistance by the Brazilian (indirect tensile) test with particular reference to concrete. Aust. J. of Appl. Sci., 10, 243-268, 1959.

Jaeger, J.C., The frictional properties of joints in rock, Geofis. Pura e Appl., 43, 148-161, 1959.

Jaeger, J.C., Elasticity, Fracture and Flow, Methuen, 1962.

Jaeger, J.C., Fracture of rocks, in Tewksbury Symposium on Fracture (1963), 268-283, Engineering Faculty, University of Melbourne, 1965.

Jaeger, J.C., Brittle Fracture of Rocks, in Eighth Symposium on Rock Mechanics, University of Minnesota, 1966.

Jaeger, J.C. and Cook, N.G.W., Theory and application of curved jacks for measurement of stress, in State of Stress in the Earth's Crust, Elsevier, 1964.

Jaeger, J.C. and Hoskins, E., Stresses and failure in rings of rock loaded in diametral tension or compression, Brit. Journal of Applied Physics, 17, 685-692, 1966(a).

Jaeger, J.C. and Hoskins, E., Rock Failure under the confined Brazilian test, J. of Geophysical Research, 71, 10, 2651-2659, 1966(b).

Joplin, G.A., Petrography of Australian Igneous Rocks, Angus and Robertson, 1964.

Karman, Th. von, Festigskeitsversuche unter allseitigem Druck, Zeits, Venein. Deutsch Ing., 55, 1749-1757, 1911.

King, L.V., On the limiting strength of rocks under conditions of stress existing in the earth's interior, Journal of Geology, 20, 119-138, 1912.

Leeman, E., The measurement of stress in rock, Parts I and II, J.S. Afr. Inst. Min. Metall., 65, 2, 45-114 1964.

Leeman, E., The borehole deformation type of rock stress measuring instrument, Int. J. of Rock Mech. and Min. Sci., 4, 23-44, 1967.

Leeman, E. and Hayes, D.J., A technique for determining the complete state of stress in rock using a single borehole, Proceedings of the First Congress of the Int. Soc. of Rock Mechanics, 2, 17-24 1966.

MacGregor, C.W., Coffin, L.F. Jr. and Fischer, J.C., Partially plastic thick-walled tubes, Journal of the Franklin Inst., 245, 135-158, 1948.

Marin, J., New evaluations for multiaxial stress properties of ceramic materials, Proc. of the Soc. for Exp. Stress Analysis, XXII, 1, 162-170, 1966.

Mayer, Habib and Marchand, Underground rock pressure Testing, International Conference about Rock Pressure and Support in Workings, Liege, 1951.

McClintock, F.A., and Walsh, J.B., Friction on Griffith cracks under pressure, Proc. of Fourth U.S. Nat. Congress on Applied Mechanics, 1015-1021, 1962.

Merrill, R. and Peterson, J., Deformation of a borehole in rock, U.S.B.M.R.I. 5881, 1961.

Mohr, F., Measurement of Rock Pressure Mine and Quarry Engineering, 22, 178-189, 1956.

Murrell, S.A.F., A criterion for brittle fracture of rocks and concrete under triaxial stress and the effect of pore pressure on the criterion, in Rock Mechanics ed. by C. Fairhurst, Pergamon, 563-577, 1963.

Murrell, S.A.F., The effect of triaxial stress systems on the strength of rocks at atmospheric temperatures, Geophys. Journal, 10, 231-283, 1966.

Nadai, A., Theory of Fracture and Flow of Solids, 1, McGraw-Hill, 1950.

Obert, L. and Duvall, W., Rock Mechanics and the Design of Structures in Rock, Wiley, 1967.

Obert, L., Merrill, R. and Morgan, T., Borehole Deformation Gage for Determining the Stress in Mine Rock, U.S.B.M.R.I. 5978, 1962.

Obert, L., and Stephenson, D.E., Stress conditions under which core disking occurs, Soc. Mining Eng. Trans., 232, 237-234, 1965.

Panek, L., Calculation of the average ground stress components from measurements of the diametral deformation of a drill hole, U.S.B.M.R.I. 6732, 1966.

Paterson, M.S., Secondary changes of length with pressure in experimentally deformed rocks, Proc. of the Roy. Soc., Series A, 271, 57-87, 1963.

Paul, B., A modification of the Coulomb-Mohr theory of fracture, Journal of Applies Mechanics, Trans. A.S.M.E., 28, 259-268, 1961.

Pomeroy, C.D. and Hobbs, D.W., The fracture of coal specimens subjected to complex stresses, Steel and Coal, 1124-1133, 1962.

Robertson, E.C., Experimental study of the strength of rocks, Bull. of the G.S.A., 66, 1275-1314, 1955.

Savin, G., Stress Concentration Around Holes, Pergamon Press, 1961.

Scott, R.F., Principles of Soil Mechanics, Addison-Wesley, 1963.

Smart, W. M., Combinations of Observations, Cambridge Press, 1958.

Taylor, G.I. and Quinney, H., The plastic distortion of metals, Phil. Trans. Roy. Soc. of London, Series A, 230, 323-362, 1931.

Timoshenko, S. and Goodier, J.N., Theory of Elasticity, McGraw-Hill, New York 1951.

Turner, F.J. and Weiss, L., Structural Analysis of Metamorphic Tectonites, McGraw-Hill, 1963.

Walsh, J., The effect of cracks on the uniaxial elastic compression of rocks, J. of Geophysical Research, 70, 399-411, 1965.

Walsh, J., The effect of cracks in rocks on Poisson's ratio, J. of Geophysical Research, 70, 5249-5258, 1965.

Walsh, J. and Brace, W., A fracture criterion for brittle anisotrppic rock, J. of Geophysical Research, 69, 3449-3456 1964.

Weibull, W., A Statistical theory of the strength of materials, Ingvetensk, Akad. Handl. no. 151, 1939.

Wu, T.H., Loh, A. and Malvern, L., Study of the failure envelope of soils, J. of the Soil Mechanics and Foundation Division, Proc. of the A.S.C.E., 89, no. S.M. 1, 145-181, 1963.

Zisman, W., Comparison of statically and seismologically determined elastic constants of rocks, Proc. of the National Acad. of Sciences, 19, no. 7, 680-686, 1933.

Appendix 1

EXPERIMENTS ON THE EFFECT OF END LUBRICANTS ON THE MEASURED STRENGTH OF ROCK TESTED IN TRIAXIAL COMPRESSION

Introduction

It has long been known that the geometry and the materials of the platens of a testing machine can affect the measured strength of rock compression specimens. Perry [1897] and Unwin [1899] gave early arguments as to whether masonry and stone compression blocks should be tested between bare steel platens or if they should be tested between sheets of millboard or lead. Filon [1901] solved the elasticity problem for compression or tension of an unconfined cylinder with free or restrained ends and Balla [1960] obtained an elastic solution for a cylinder in triaxial compression. Hill [1950] gives a solution for the plastic compression of a cylinder between "rough" and "smooth" surfaces.

Very little experimental work appears to have been done on the effect of end lubrication for rock materials although several investigators have worked on soils and metals. Rowe and Barden [1964] and Blight [1965] have made extensive experiments which demonstrate the importance of loading triaxial soil samples through lubricated and/or matched end pieces if

uniform stresses and strains in the specimen are desired. Similar results were obtained by van Rooyen and Backofen [1960] for the plastic compression of aluminium, copper, and iron.

Rocks are seldom either perfectly elastic or perfectly plastic and the characteristics of any given rock change with the magnitude of the confining pressure so it would seem that some experimental work is justified to establish the effectiveness of some of the various lubricants that might be used and further to simply see what effect these lubricants have on the measured strengths of various types of rocks. The specific problem in regard to this thesis was to find a lubricant suitable for use with the hollow cylinder tests described in Chapter II. Under certain loading conditions the hollow cylinders failed by an inward radial collapse. Friction between the ends of the specimen and the platens or anvils seemed to affect this collapse. Since it was thought desirable to do all of the tests under the same end conditions, a lubricant was needed that would not inhibit these radial displacements and also not affect the basic strength of the hollow cylinders under other loading conditions. The standards of comparison were tests in which the specimen ends were in direct contact with dry hardened steel end pieces of the same diameter.

The paper used in the paper and graphite lubricated tests was ordinary porous "Roneo" duplicating paper. The paper was cut to the same diameter as the rock specimen and powdered graphite generously sprinkled on one side. The graphite was thoroughly rubbed into the paper. The graphite impregnated side of the paper was placed against the steel anvil and the clean side of the paper against the rock. Both ends of the rock cylinders were lubricated.

Other lubrication methods investigated included;

(a) simply smearing "Moly Pad" (molybdenum disulphide in a viscous binder) on the ends of the specimens,

(b) using successive layers of grease, sheet latex, grease, and 0.2 mm brass shim in an arrangement similar to that used by Gramberg [1965], and

(c) using a sheet of 0.1 mm teflon at each end of the specimen. In addition a few tests were done with dry latex and also with approximately 1 mm thick lead sheets at the specimen ends.

Experimental Results

The results of these tests are summarized in Tables I, II, III and IV.

Table I

Trachyte

No. of Tests	End Conditions	Confining Pressure kb	Average Maximum Stress At Failure kb
6	Bare	0	1.67
3	Paper and Graphite	0	1.69
3	Moly Pad	0	1.74
2	Latex and Brass	0	1.74
2	Teflon	0	1.64
2	Dry Latex	0	1.05
2	Lead	0	0.96
3	Bare	0.50	4.68
3	Paper and Graphite	0.50	4.67
3	Bare	1.00	6.52
3	Paper and Graphite	1.00	6.47

Table II

Sandstone

No. of Tests	End Conditions	Confining Pressure kb	Average Maximum Stress At Failure kb
3	Bare	0	0.41
3	Paper and Graphite	0	0.40
2	Bare	0.28	1.34
2	Paper and Graphite	0.28	1.35

Table III

Carrara Marble

No. of Tests	End Conditions	Confining Pressure kb	Average Maximum Stress kb
4	Bare	0	0.84
4	Paper and Graphite	0	0.79
1	Bare	0.17	1.51
1	Paper and Graphite	0.17	1.49
2	Bare	0.28	1.90
2	Paper and Graphite	0.28	1.88
1	Bare	0.35	2.05
1	Paper and Graphite	0.35	2.09

Table IV

Lithographic Limestone

No. of Tests	End Conditions	Confining Pressure kb	Average Maximum Stress kb
3	Bare	0	2.27
3	Paper and Graphite	0	2.15
1	Bare	0.50	3.87
1	Paper and Graphite	0.50	3.86

BIBLIOGRAPHY FOR APPENDIX 1

Balla, A., A new solution to the stress conditions in triaxial compression, Act. Tech. Hung., 28, 349-388, 1960.

Blight, G.E., Shear stress and pore pressure in triaxial testing, Journal of the Soil Mechanics and Foundations Division, A.S.C.E. 91, No. SM6 Proc. Paper 4540, 25-39, 1965.

Rowe, P.W. and Barden, L., Importance of free ends in triaxial testing, Journal of the Soil Mechanics and Foundations Division, A.S.C.E. 90, No. SM1 Proc. Paper 3753, 27 pp., 1964.

Filon, L.N.G., On the elastic equilibrium of circular cylinders under certain practical systems of load, Philosophical Transactions of The Royal Society of London, Series A, 198, 147-233, 1902.

Gramberg, J., Axial cleavage fracturing, a significant process in mining and geology, Engineering Geology, 1, 31-72, 1965.

Hill, R., The Mathematical Theory of Plasticity, Oxford, 1950.

Perry, J., Applied Mechanics, Cassell and Co., London, 1897.

Unwin, W.C., The Testing of Materials of Construction, Longmans, Green and Co., London, 1899.

van Rooyen, G.T. and Backofen, W.A., A study of interface friction in plastic compression, Int. Journal of Mech. Sci., 1, 1-27, 1960.

Appendix 2

ROCK FAILURE UNDER THE CONFINED BRAZILIAN TEST

J. C. JAEGER
AND
E. R. HOSKINS

A Reprint from

MAY 15, 1966

Journal of Geophysical Research

VOLUME 71 NUMBER 10

PUBLISHED BY
THE AMERICAN GEOPHYSICAL UNION

JOURNAL OF GEOPHYSICAL RESEARCH VOL. 71, NO. 10 MAY 15, 1966

Rock Failure under the Confined Brazilian Test

J. C. JAEGER AND E. R. HOSKINS

Department of Geophysics Australian National University, Canberra

The Brazilian, or indirect tensile, test, in which a disk is loaded in a diametral plane by forces applied at opposite ends of a diameter, is extended by jacketing the specimen and applying an additional confining pressure. In this way failure may be studied over a range of conditions in which the least principal stress varies from tensile to compressive. The fracture is always an extension fracture in the loaded diametral plane, even if all principal stresses are compressive. The stress analysis is based on elastic strain theory. Experiments were made on three rock types, and they suggest that the value of the intermediate principal stress affects the conditions for failure. This effect is of the same order of magnitude as that shown by experiments on hollow cylinders with axial loading and external confining pressure.

1. INTRODUCTION

The indirect tensile, or 'Brazilian,' test has been much used in the testing of concrete [*Hondros,* 1959] and has been applied to rocks and coal [*Berenbaum and Brodie,* 1959; *Hobbs,* 1965]. In it, a circular cylinder of radius R is compressed in a diametral plane by line loads W per unit length (as in Figure 1*a*, except that this is drawn for a distributed loading). In this case, linear elastic theory [*Timoshenko,* 1934, section 33] shows that there is a uniform tensile stress

$$W/\pi R \qquad (1)$$

across the diametral plane. Measurement of W at failure thus gives the tensile strength of the material immediately. Tensile strengths measured in this way are reproducible and in reasonable agreement with values obtained in uniaxial tension. For this reason the test is, in principle, a very interesting one because its results are obtained from the elastic theory of a quite complicated system. In all cases (in isotropic materials) failure is by an extension fracture in the diametral plane.

Jaeger [1965] suggested that if an additional confining pressure is applied to the specimen, the transition from tensile to compressive values of the least principal stress could be studied, and he gave a few measurements which suggested that the σ_1, σ_3 values for failure with σ_3 compressive were close to those obtained from the triaxial test. This situation with applied hydrostatic pressure and loading in a diametral plane will be described as the 'confined Brazilian test.'

Our primary object in this paper is to discuss further the theory of the Brazilian test, both confined and unconfined, which is done in sections 2 and 6, and also to describe experiments on three types of rock, sections 3 and 4. The nature of the fracture is described in section 5. The experiments suggest that for σ_3 compressive there is a small but systematic difference from the triaxial results.

Since failure in these experiments takes place under three unequal principal stresses, they have some relevance to general criteria for failure and, in particular, to the influence of the intermediate principal stress on failure. Throughout this paper compression will be reckoned positive and $\sigma_1 \geq \sigma_2 \geq \sigma_3$.

Most measurements on brittle fracture of rocks have been made under conditions in which the stress is (approximately) homogeneous and is measured directly. The systems in which the stress is homogeneous are uniaxial tension or compression, the triaxial test in which $\sigma_1 > 0$ and $\sigma_2 = \sigma_3 \geq 0$, and the case of extension in the triaxial test in which $\sigma_1 = \sigma_2 > 0$ and $\sigma_3 \leq 0$. The only information about the effect of the intermediate principal stress obtainable from these systems is given by the remark of *Brace* [1964] that it is probably negligible because in some cases the same values for failure were found under the conditions $\sigma_1 > 0$, $\sigma_2 = \sigma_3 = 0$ and $\sigma_1 = \sigma_2 > 0$, $\sigma_3 = 0$.

For a full examination of the fracture of rocks with unequal principal stresses it is neces-

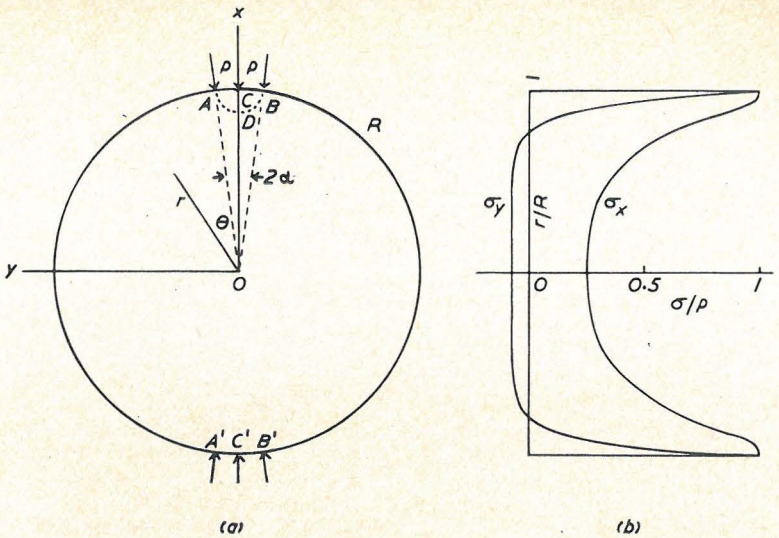

Fig. 1. (*a*) Brazilian test with loading over an angle 2α; (*b*) Principal stresses σ_x and σ_y on the loaded diameter CC' of (*a*).

sary to use more complicated systems in which the stresses are inhomogeneous. In such cases fundamental new difficulties arise: (1) the stresses are not directly measurable but have to be calculated on the assumptions of the theory of elasticity (in some cases elastic-plastic theory has to be used), (2) since the stresses are inhomogeneous, stress gradients exist which may well affect failure, (3) the effect of end conditions or friction at platens may be of enhanced importance. It may well be that, as suggested by *King* [1912], the conditions of failure depend on the boundary conditions, so that each geometry would have its own criterion of failure.

The simplest possible result which could be hoped for is that each material would have its own fracture surface

$$\sigma_1 = f(\sigma_2, \sigma_3) \qquad (2)$$

and that brittle fracture would occur when the stresses at some point of the body first satisfy this relation. This surface could be mapped by experiments with different specimen geometries and conditions of loading. Thus the triaxial test gives a curve on this surface, extension in the triaxial test another, and the confined Brazilian test another, while more complicated systems such as torsion with axial load and confining pressure [*Handin et al.*, 1960; *Böker*, 1915] or hollow cylinders with axial load and internal and external pressure [*King*, 1912; *Robertson*, 1955] allow portions of the surface to be mapped. In this way it should be possible to check conclusively the important result (which follows from discussion of the Mohr envelope) that the intermediate principal stress has no effect, so that (2) reduces to

$$\sigma_1 = f(\sigma_3) \qquad (3)$$

From this point of view it is important to study the same rock under as many experimental conditions as possible. If these results were consistent there would be a strong presumption of the existence of a characteristic fracture surface (2). If they were inconsistent, reasons for this, such as the effects of stress gradients on failure or the inadequacy of the theory of elasticity for calculating stresses in material close to failure, must be sought. There is, in fact, evidence of inconsistencies in tensile strengths determined by different methods [*Berenbaum and Brodie*, 1959; *Durelli and Parks*, 1962; *Jaeger and Hoskins*, 1966].

The confined Brazilian test gives failure under conditions in which σ_3 is small relative to σ_2 and its results may be interpreted as showing an increase of strength with σ_2. It is therefore desirable to see whether its results are consistent with measurements for the case $\sigma_2 = 0$, which

may be achieved with hollow cylinders stressed with an axial load and external hydrostatic pressure. For this reason, experiments were made with this system which are reported in section 7. These are not intended to be a complete study but to show reasonable consistency between the two systems.

2. The Confined Brazilian Test

In the original form of the Brazilian test, line loads W per unit length are applied to a cylinder of radius R and the principal stresses at the center of the cylinder, calculated on elastic theory, are

$$\sigma_1 = 3W/\pi R, \quad \sigma_2 = 0, \quad \sigma_3 = -W/\pi R \quad (4)$$

In this case there is a stress concentration where the load is applied, and to avoid this several authors [*Hondros*, 1959; *Fairhurst*, 1964] have suggested using a distributed loading. Hondros has given formulas for the stresses at any point for the case of pressure p applied over two diametrically opposite arcs ACB and $A'C'B'$ of angular width 2α of the surface (Figure 1*a*). If α is small this is equivalent to line loads

$$W = 2\alpha pR \quad (5)$$

Throughout this work the angle $2\alpha = 15°$ will be used, and for this case the values of the stresses σ_x and σ_y along the diameter $C'C$ are shown in Figure 1*b*. It appears that σ_y is tensile and nearly constant over rather more than half this diameter, and the stresses at the center O are given by

$$\sigma_1 = 0.948W/R \qquad \sigma_2 = 0$$
$$\sigma_3 = -0.311W/R \quad (6)$$

which differs only slightly from the simple results (4), so that we shall continue to use the latter.

If an additional hydrostatic pressure H is applied to the whole surface of the cylinder, the stresses at the center of the cylinder become

$$\sigma_1 = H + 3W/\pi R, \qquad \sigma_2 = H,$$
$$\sigma_3 = H - W/\pi R \quad (7)$$

so that they are connected by a relation

$$\sigma_1 - 4\sigma_2 + 3\sigma_3 = 0 \quad (8)$$

and the results may be interpreted as giving the section of the surface (2) which specifies fracture with the plane (8) instead of, for example, with the plane $\sigma_2 = \sigma_3$ in the ordinary triaxial test.

A more refined discussion of the stresses is necessary and will be given in section 6; for example, it is not clear that failure is initiated at the center of the cylinder where the stresses are given by (7). Meantime, the experimental results given in section 4 will be reduced using (7).

3. Apparatus and Materials

Specimens are 5 cm in diameter and ~~12.5~~ 3.7 cm long, surface-ground and jacketed in copper 0.012 cm thick. They are tested in an ordinary triaxial pot 9.8 cm in diameter with a cylindrical seat having hardened platens ground to give an angle of contact of 15°. This system is extremely simple but is not an accurate one because the testing machine measures the sum of the hydraulic load on the piston and the load on the specimen and at high confining pressures the latter may be as little as one-quarter of the former. The fact that σ_3 in (7) is obtained by subtraction of two quantities which may be nearly equal reduces the accuracy further. To eliminate the effect of friction, the load on the specimen at failure is taken from the testing machine record; this implies that the confining pressure has to be kept as nearly constant as possible before and during stressing. It is controlled manually by a bleed value and a screw press and can be controlled to better than 1%.

Conventional triaxial compression tests were also made on 12.5 × 5 cm cylinders of all materials.

Materials for such experiments must be fine-grained, homogeneous, and isotropic. Anisotropy is readily detected in the unconfined Brazilian test, and the fine-grained siltstone previously used was rejected because of it. Wombeyan marble which had also been used was rejected because of variations in grain size. The materials finally chosen were three commercially obtainable building stones. For this reason it was necessary to cut all specimens from a single block, so that the number of experimental runs was limited. The rock types used were

1. Bowral trachyte, an even-grained igneous

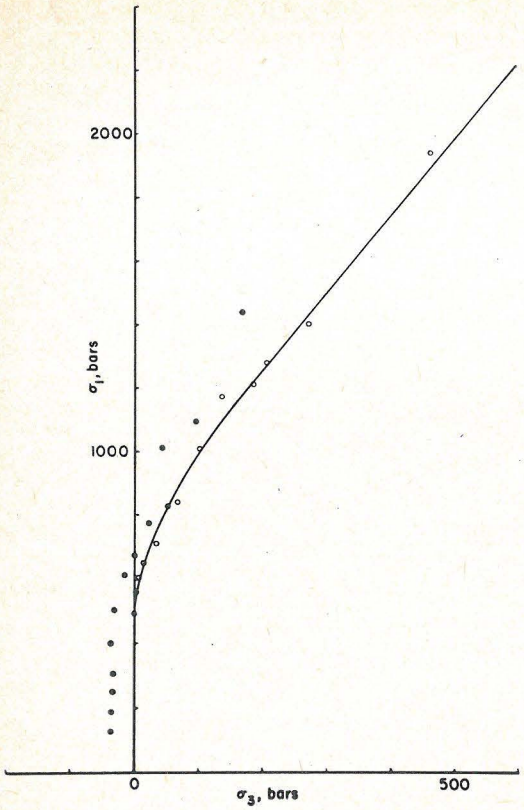

Fig. 2. Variation of σ_1 with σ_3 for Gosford sandstone at the center of the disk in the confined Brazilian test (dots). Open circles represent values for the triaxial test.

rock consisting predominantly of orthoclase 1 mm in grain size with minor quartz, calcite, and altered ferromagnesian minerals. The amount of alteration and the grain size vary between specimens and may account for some of the experimental scatter.

2. Gosford sandstone, a very uniform, fine-grained, rather weakly cemented quartz sandstone.

3. Fine-grained Carrara marble. This material was used, despite the fact that under certain conditions it will become plastic, because it fails relatively slowly and so may be used to give some indication of the mechanism of failure.

4. Experimental Results

Values of σ_1 and σ_3 at failure calculated from (7) for the three materials at various confining pressures are shown in Figures 2 to 4. The values at zero hydrostatic pressure are the mean of five experiments; all other points represent single experiments and so indicate the amount of scatter occurring.

In all cases the points for the confined Brazilian test fit reasonably well to the curves for the triaxial test, but there is a consistent tendency for them to lie higher. This is best seen for the Gosford sandstone, Figure 2, which is the best experimental material. This effect may be attributed to the effect of the intermediate principal stress on fracture and will be further discussed in sections 6 and 7. The results for Carrara marble are more difficult to interpret because plastic phenomena are probably involved in some of them.

5. The Nature of the Fracture

In all cases in which σ_3 is tensile for the

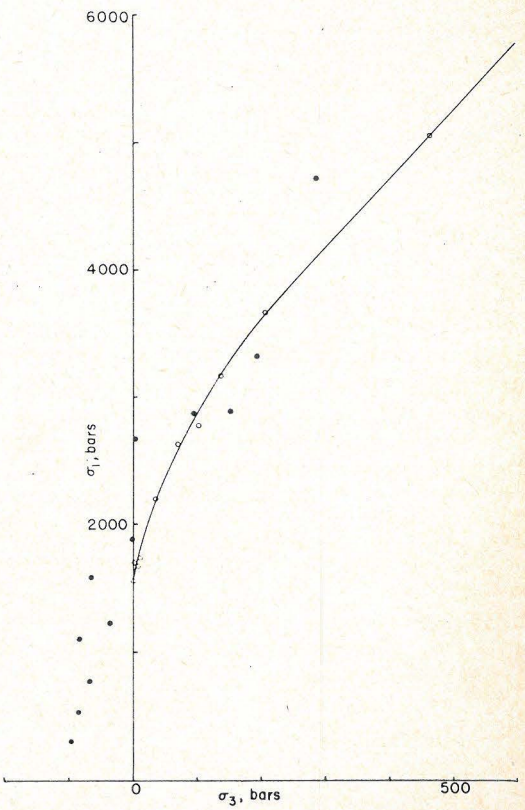

Fig. 3. Variation of σ_1 with σ_3 for Bowral trachyte at the center of the disk in the confined Brazilian test (dots). Open circles represent values for the triaxial test.

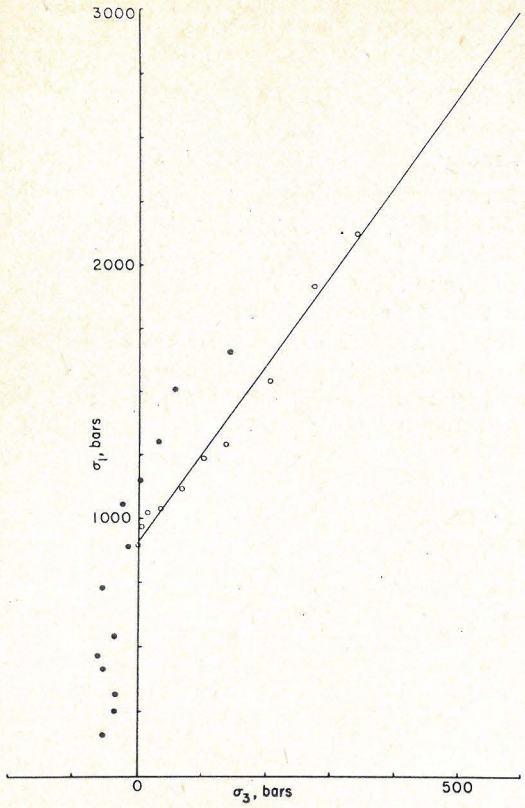

Fig. 4. Variation of σ_1 with σ_3 for Carrara marble at the center of the disk in the confined Brazilian test (dots). Open circles represent values for the triaxial test.

trachyte and sandstone the failure may be described as an extension fracture in the diametral plane CC', Figure 1*a*. In the marble and sandstone specimens, the fracture does not always extend to the loaded surfaces. Sometimes in the stronger and more brittle trachyte, wedges are formed at the loading surface. Some workers, e.g., *Hiramatsu et al.* [1954], regard such wedges as having been produced by an initial shear failure close to the loaded area, the extension fracture being produced subsequently when these wedges were forced into the material. This cannot be the primary means of failure, however, as the wedges are not formed in every case, and it seems more likely to us that such wedges are produced by continued loading (or release of elastic energy stored in the testing machine) after an initial extension failure has almost entirely separated the specimens into two half-cylinders.

In the present experiments, great care has been taken to load the specimens slowly and to release the load immediately when there is any indication of failure. The specimens are subsequently coated with penetrant dye and the surface is ground off, leaving the traces of any internal cracks. In this way, specimens have been observed in which there are cracks in the interior which do not penetrate to the outer surface; in other specimens they may run only to one platen. Commonly, they will begin along the diametral plane and run to one edge of the outer loaded area. The experimental indications are that failure begins as an extension fracture in the interior of the disk and propagates to the surface.

If all three principal stresses in the interior of the disk are compressive, the situation is not so clear. Certainly, as confining pressure is increased, some point will be reached for each type of rock where the stress differences in the neighborhood of the platen will be great enough to cause plastic flow in this region, rendering the strictly elastic solution for the stresses meaningless. The problem is too difficult to study on an elastic-plastic basis and so is best approached experimentally.

Carrara marble was used as an experimental material because it has the property of failing slowly, so that cracking is more readily observed. However, it becomes plastic at low confining pressures (of the order of 200 bars) in triaxial compression tests. In the unconfined Brazilian test no evidence of plastic deformation (twinning, or blueing under X-ray irradiation) was found at loads of 80% of those necessary to cause failure. However, when the confining pressure is above about 70 bars, the crack pattern as revealed by penetrating dye suggests a slip line network (in the sense of *Nadai* [1950]) in the region near the platen, say $r/R > 0.8$, $-7.5° < \theta < 7.5°$.

Macroscopic fracture, however, still begins near the center of the disk, and it is possible that in this case the fracture is an intrusion fracture in the sense of *Brace* [1964], the material intruded being plastically deformed marble.

The sandstone fails in extremely fine extension cracks in the diametral plane up to confining pressures of approximately 350 bars, where slip line fields similar to those noted in

the marble become apparent. This is well above the confining pressure (170 bars) above which all three principal stresses in the interior of the disk are compressive.

The maximum confining pressure used with the trachyte (1380 bars) was not sufficient to cause a regular slip line field to become evident with the penetrant dye. Some subsidiary fracturing was observed, but this may be a secondary effect.

This observation, that with concentrated loading what are apparently extension fractures in a plane perpendicular to the least principal stress may occur under conditions in which all principal stresses are compressive, may be relevant to the failure of pebbles in an aggregate under confining pressure.

6. The Stresses in the Brazilian Test on Two-Dimensional Elastic Theory

Hondros [1959] has given formulas for all stress components in polar coordinates for the system of Figure 1*a* with plane stress. On the loaded diameter CC', $\theta = 0$ (Figure 1*a*), σ_r and σ_θ are shown in Figure 1*b* calculated for $\alpha = 7.5°$. At $r = 0$, $\sigma_\theta = -0.081p$ and $\sigma_r = 0.248p$, which are very close to the values (4) for concentrated loading. σ_θ is negative for $0 < r/R < 0.8$, approximately, and as $r \to R$ both σ_r and σ_θ tend to p. The stress difference

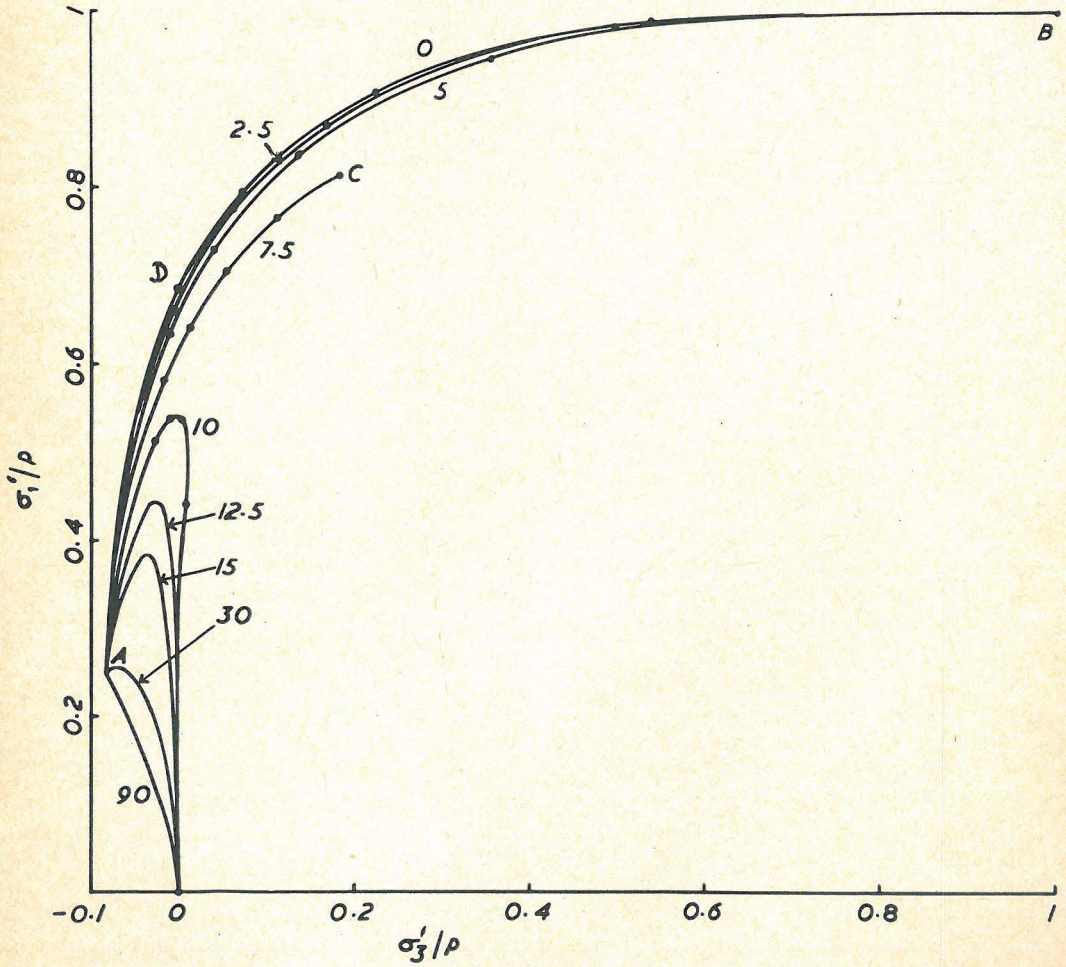

Fig. 5. Variation of the principal stress σ_1' with σ_3' along various radii in the system of Figure 1*a* with plane stress. Numbers on the curves are values of θ. Dots on the curves are at values 0.8, 0.85, 0.9, 0.95, 1 of r/R.

$\sigma_r - \sigma_\theta$ has its maximum value near the point D, $r/R = 0.87$ (Figure 1*a*), as might be expected from the theory for a semi-infinite solid with a strip load.

The principal stresses at any point in the plane of the disk can be calculated from Hondros's formulas. They will be denoted by σ_1' and σ_3' to avoid confusion with the three-dimensional case, and their variation with r/R along the radii $\theta = 0°$, 2.5°, 5°, 7.5°, 10°, 12.5°, 15°, 30°, and 90° is shown in Figure 5. In all cases when $r = 0$ the stresses are given by the point A, $\sigma_1' = 0.248p$, $\sigma_3' = -0.081p$. As r increases to R they tend to B (p, p), if $0 < \theta < 7.5°$; to C $(0.818p, 0.182p)$, if $\theta = 7.5°$; and to zero if $\theta > 7.5°$. To show how the stresses vary near the loaded region, dots are shown on some of the curves at the values 0.8, 0.85, 0.9, 0.95, and 1 of r/R.

It follows that for a given σ_3' the values of σ_1' and $\sigma_1' - \sigma_3'$ in the plane of the disk are greatest when $\theta = 0$, so that failure may be expected to occur on this diameter. Considering the variation of σ_1' with σ_3' on the diameter $\theta = 0$, the portion AD, $0 < r < 0.8R$, of the curve representing this corresponds very closely to the parabolic locus to be expected from Griffith theory which passes through the points $\sigma_1' = 3T_0$, $\sigma_3' = -T_0$, and $\sigma_1' = 8T_0$, $\sigma_3' = 0$, where T_0 is the tensile strength. In the present case, with $T_0 = 0.081p$, this parabola would pass through the point $\sigma_1' = 0.67p$, $\sigma_3' = 0$, and it is a little lower than the curve AD. In fact, if $\alpha = 8°$, the two curves are almost identical. Thus on Griffith theory the whole of the region $0 < r < 0.8R$ comes simultaneously very close to failure as the load is increased. On the other hand, the region DB, $0.8R < r < R$, lies below the Griffith parabola, so that failure should not take place in this region. *Fairhurst* [1964] has pointed out that, because the ratio of compressive to tensile strength of 8:1 predicted by Griffith theory is rather low, the curve AD should lie below the failure curve and conditions for failure would be expected to be attained at the center first.

In three dimensions, with confining pressure H, the principal stresses will be $\sigma_1' + H$, H, and $\sigma_3' + H$ and if $0 < r/R < 0.8$ so that $\sigma_3' < 0$ these will be, in order of magnitude, σ_1, σ_2, and σ_3. If $r/R > 0.8$, σ_3' is positive and $\sigma_3' + H$ is the intermediate principal stress. This case will not be considered here because it is not relevant to the type of failure under consideration, though it will affect plastic conditions near the loaded area if these should occur.

When failure occurs, the stresses $\sigma_1 = \sigma_1' + H$ and $\sigma_3 = \sigma_3' + H$ on the loaded diameter can be calculated from the values in Figure 1*b*. Some values for Bowral trachyte corresponding to some of the points in Figure 3 are shown in Figure 6 and are compared with the σ_1 and σ_3 values for failure in the triaxial test. For the unconfined Brazilian test, $H = 0$, the whole of the curve lies well below the triaxial curve, and an extension failure at the origin would be expected. The same applies to the confining pressure $H = 140$ bars.

If the confining pressure is held constant at a higher value, e.g., $H = 465$ bars, and the load W is increased, the curve representing

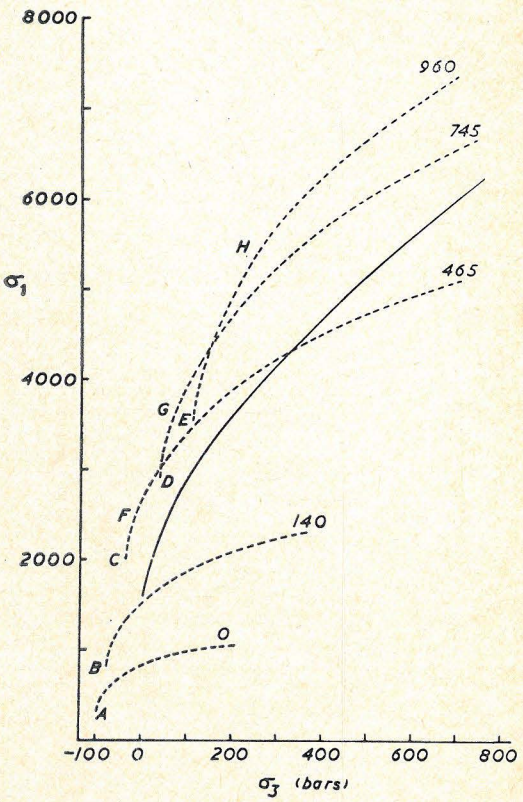

Fig. 6. Dotted curves: variation of σ_1 with σ_3 on the loaded diameter in the confined Brazilian test, numbers on the curves are values of the confining pressure in bars. Full curve: variation of σ_1 with σ_3 in the triaxial test. Material: Bowral trachyte. Stresses are in bars.

stresses in the loaded diameter will pass through the triaxial curve, ultimately reaching the position CF when fracture occurs. In the discussion of section 4 and in Figure 3 the stresses at the center of the disk, calculated from the simple formula (4), were used. These are represented by the points A, B, C, D, and E in Figure 6. From the present discussion it seems likely that a better representation of the conditions of failure would be obtained by drawing an envelope which would touch the dotted curves of Figure 6 near the points A, B, F, G, and H, respectively. This envelope does not differ greatly from the curve ABCDE previously used. Failure might be expected to begin at the points, such at F, G, and H, at which any curve touches this envelope, and these points correspond to intermediate positions on the diameter, say $r/R < 0.5$.

7. Hollow Cylinders with Axial Load and External Hydrostatic Pressure

To test the consistency of the results of the confined Brazilian test with this system, we measured the stresses at failure of a number of cylinders 12.5 cm long, 2.5 cm outside diameter, 1.25 cm inside diameter, and encased in rubber jackets. These specimens were taken from blocks of the material different from those used for the Brazilian tests, so that complete agreement cannot be expected.

For a hollow cylinder of external radius b and internal radius a, with hydrostatic pressure H applied to its outside surface and axial pressure P, the principal stresses at the inner surface are, for the relative values of P and H used here,

$$\sigma_1 = P \quad \sigma_2 = 2b^2H/(b^2 - a^2) \quad \sigma_3 = 0$$

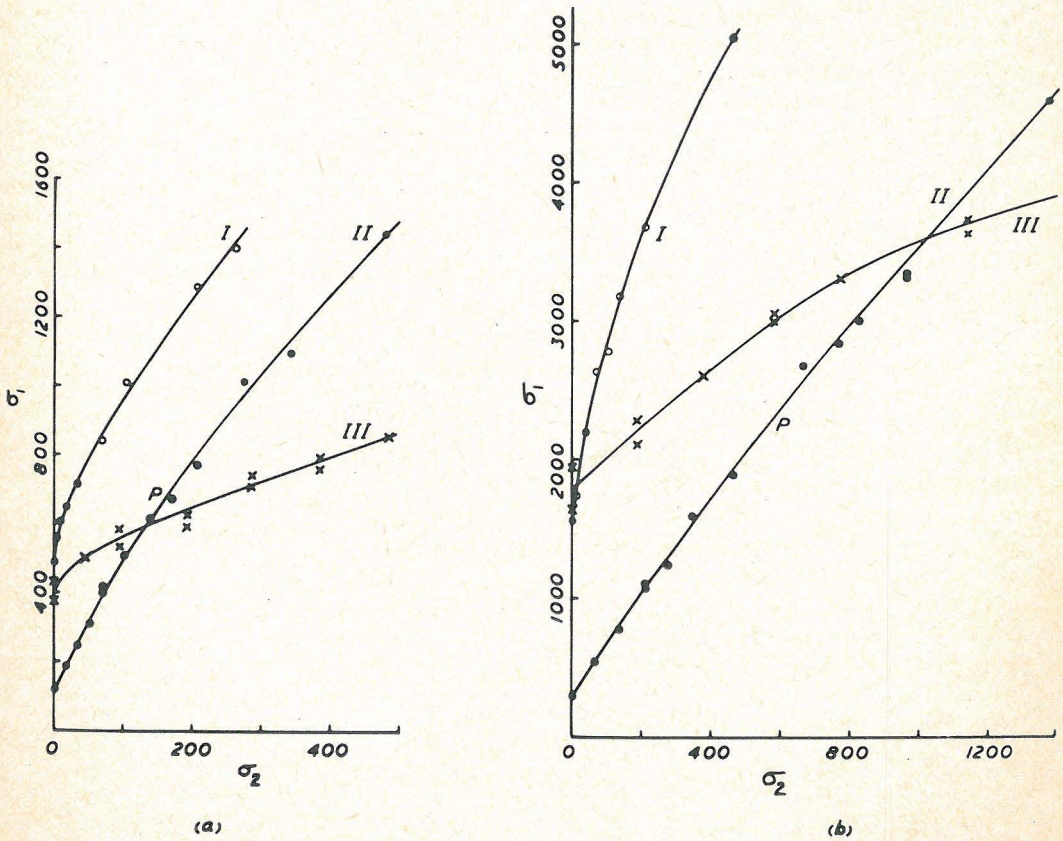

Fig. 7. (a) Gosford sandstone: (b) Bowral trachyte. Curves I (open circles), triaxial test with $\sigma_2 = \sigma_3$. Curves II (dots), confined Brazilian test with $\sigma_3 = (4\ \sigma_2 - \sigma_1)/3$: the points P on these curves correspond to $\sigma_3 = 0$. Curves III (crosses), hollow cylinders with $\sigma_3 = 0$. Stresses are in bars.

In all cases H was held fixed and P increased to failure, which took place on a circular cone with axis along the axis of the cylinder.

The results for Gosford sandstone and Bowral trachyte are shown in Figure 7, curves III, with the results for triaxial tests for comparison, curves I. The most obvious interpretation is that $f(\sigma_2, \sigma_3)$ for $\sigma_3 = 0$ increases slightly with σ_2.

The variation of σ_1 with σ_2 for the Brazilian test is shown in curves II. If these curves were consistent with curves III on the hypothesis of equation 2, they should cross them at the points P at which $\sigma_3 = 0$. This is seen to be nearly the case for the sandstone. For the trachyte, which is a more variable material and for which the points of Figure 3 show a large scatter near $\sigma_3 = 0$, there is a 25% discrepancy.

There is thus no gross disagreement with the hypothesis that these two tests show effects of σ_2 on failure of the same order of magnitude. The effect could be attributed to stress gradients or to the failure of elastic theory in both materials and both tests, but the conditions in the two systems are so different that this seems less probable.

Acknowledgment. We are indebted to Mrs. T. Chamalaun for the calculations leading to Figure 5.

References

Berenbaum, R., and I. Brodie, Measurement of the tensile strength of brittle materials, *Brit. J. Appl. Phys., 10,* 281–286, 1959.

Böker, R., Die Mechanik der bleibenden Formänderung in kristallinisch aufgebauten Körpern, *Verhandel. Deut. Ing. Mitt. Forsch.,* 175, 1–51, 1915.

Brace, W. F., Brittle fracture of rocks, in *State of Stress in the Earth's Crust,* edited by W. Judd, pp. 111–180, Elsevier Publishing Company, New York, 1964.

Durelli, A. J., and V. Parks, Relationship of size and stress gradient to brittle fracture stress, *Proc. Fourth U. S. Nat. Congr. Appl. Math.,* 931–938, 1962.

Fairhurst, C., On the validity of the Brazilian test for brittle materials, *Intern. J. Rock Mech. Mining Sci., 1,* 535–546, 1964.

Griggs, D., and J. Handin, Observations on fracture and a hypothesis of earthquakes, *Geol. Soc. Am., Mem. 79,* 347–364, 1960.

Handin, J., D. V. Higgs, and J. K. O'Brien, Torsion of Yule marble under confining pressure, *Geol. Soc. Am., Mem. 79,* 245–274, 1960.

Hiramatsu, Y., M. Nishihara, and Y. Oka, A discussion on the methods of tension test of rock, *Nippin Kogyo Kaishi (J. Mining Met. Inst. Japan), 70,* 285–289, 1954.

Hobbs, D. W., An assessment of a technique for determining the tensile strength of rock, *Brit. J. Appl. Phys., 16,* 259–268, 1965.

Hondros, G., The evaluation of Poisson's ratio and the modulus of materials of a low tensile resistance by the Brazilian (indirect tensile) test with particular reference to concrete, *Australian J. Appl. Sci., 10,* 243–268, 1959.

Jaeger, J. C., Fracture of rocks, in *Tewksbury Symposium on Fracture* (1963) pp. 268–283. Engineering Faculty, University of Melbourne, 1965.

Jaeger, J. C., and E. R. Hoskins, Stresses and failure in rings of rock loaded in diametral tension or compression, *Brit. J. Appl. Phys.,* in press, 1966.

King, L. V., On the limiting strengths of rocks under conditions of stress existing in the earth's interior, *J. Geol., 20,* 119–138, 1912.

Nadai, A., *Theory of Fracture and Flow of Solids,* McGraw-Hill Book Company, New York, 1950.

Robertson, E. C., Experimental study of the strength of rocks, *Bull. Geol. Soc. Am., 66,* 1275–1314, 1955.

Timoshenko, S., *Theory of Elasticity,* McGraw-Hill Book Company, New York, 1934.

(Manuscript received December 13, 1965; revised February 18, 1966.)

Reprinted from

British Journal of Applied Physics

The Institute of Physics and The Physical Society

Printed in Great Britain by Adlard & Son, Ltd., Dorking

BRIT. J. APPL. PHYS., 1966, VOL. 17

Stresses and failure in rings of rock loaded in diametral tension or compression

J. C. JAEGER and E. R. HOSKINS

Department of Geophysics, Australian National University, Canberra, Australia

MS. received 25th November 1965

Abstract. The failure of rock materials in the form of rings subjected to line loadings on either their internal or external surfaces is studied. Formulae for the stresses and some numerical values are given. Experimental results for three fine-grained rocks are given and values of the tensile strengths so obtained are compared with those from direct tension, indirect tension (Brazilian) and bending tests. It is found that the calculated tensile stresses at failure for rings loaded in either fashion, and for bending tests, are considerably higher than those for direct tension or the indirect tensile (Brazilian) test. It is suggested that this is due to the fact that in the two latter cases the stresses are uniform (or nearly so) over the section in which failure takes place, while in the three former they vary almost linearly across it. This suggests that a criterion for failure must not simply involve the stresses at a point, but also their rate of change with position.

1. Introduction

The conventional methods of measuring tensile and compressive strengths of rocks and of studying criteria for their failure involve the use of uniform uniaxial stress with a superposed confining or hydrostatic pressure (Brace 1964). In these, except for end effects, the stresses are known and uniform throughout the volume being tested. Historically, two systems have been extensively used which involve non-uniform stresses which have to be calculated by assuming that the theory of elasticity holds until failure takes place — these are torsion (Handin, Higgs and O'Brien 1960) and bending (Berenbaum and Brodie 1959). It is well known that these give anomalous results, for example the older text books (Morley 1923) use the term modulus of rupture for the 'tensile strength' as deduced from bending experiments to indicate that this may not be the same as the uniaxial tensile strength.

Recently the so-called Brazilian, diametral compression, or indirect tensile test has been extensively used as a measure of tensile strength because of its simplicity compared with the direct tensile test. It gives very reproducible results which do not differ greatly from those obtained in uniaxial tension. However, it involves a more sophisticated application of the theory of elasticity than do bending and torsion tests. In its simplest form (figure 1(*a*)), a circular cylinder of radius b is compressed between flat platens which provide compressive load W per unit length at the ends of a diameter AA′ (Berenbaum and Brodie 1959). In this case the stresses on the diameter AA′ (the x axis) at distance x from the origin are (compression being reckoned positive)

$$\sigma_y = -W/\pi b, \qquad \sigma_x = \frac{W}{\pi b}\left\{\frac{4}{(1-x^2)/b^2)} - 1\right\}. \tag{1}$$

Thus, in theory, there is a uniform tensile stress across the whole of the loaded diameter AA′.

In order to avoid the unknown effects of the stress concentration at the platens A, A′, Hondros (1959) proposed that the load be applied over narrow arcs of angular width 2α on the surface (figure 1(*b*)), and he gave the elastic theory for radial pressure p applied over these arcs. In the whole of the calculations and experiments in the present paper Hondros's convenient value $\alpha = 7{\cdot}5°$ has been used. Values of the tensile strength obtained from

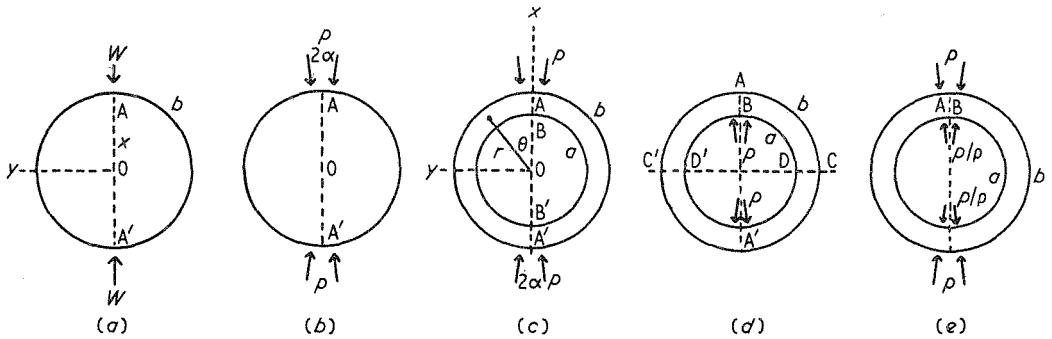

Figure 1. The various systems considered.

experiments with flat platens and with contact over an arc of 15° are in good agreement, their difference being of the order of 10% or less.

In these experiments it is not clear whether the extension failure which extends over the whole plane AA′ is initiated at the centre where the tensile stress is $W/\pi b = 2p\alpha/\pi$ or at the highly stressed regions near the platens. Presumably in order to ensure that failure is initiated at the centre, it has been proposed to drill a small hole at the centre (Hobbs 1965). The effect of a small hole at $x = 0$ in the stress field (1) is to give a maximum tangential stress $-6W/\pi b$ in the circumference of the hole where it meets the diameter OA. Since in fact the load W at failure is not greatly affected by a small central hole, tensile strengths determined by the disk-with-hole method will be much greater than those from the solid disk (Hobbs 1965).

The object of this paper is to give a fairly complete analysis, both theoretical and experimental, of the stresses in a ring loaded symmetrically over small arcs of its surface. The case of external loading (figure 1(*c*)) is considered in §2. Internal loading (figure 1(*d*)), which is quite practicable experimentally, is discussed in §3; and a combination of the two (figure 1(*e*)), which applies a localized squeeze to the ring, in §4. Experimental results are described in §5. These results are discussed with reference to criteria and mechanism of failure in §7.

Methods for the calculation of stresses in a ring were set out by Filon (1924) but he does not give explicit formulae and his numerical results are confined to the case of point loading on the inner boundary. Hobbs (1965) gives only formulae for σ_θ for point loading on the outer boundary. In view of the general importance of the problem the full results are given in the Appendix.

2. A hollow circular cylinder loaded over opposite arcs of its outer surface

The situation is that of figure 1(*c*) in which a cylinder of external radius b and internal radius a is loaded by radial pressure p applied over the arcs $-\alpha < \theta < \alpha$ and $\pi - \alpha < \theta < \pi + \alpha$ of its outer surface.

Formulae for the stresses in polar coordinates at any point r, θ are given in the Appendix. In figure 2 the tangential stress σ_θ across the cross section AB, $\theta = 0$, for the case $\alpha = 7{\cdot}5°$ is plotted as a function of r/b for various values of the ratio $\rho = a/b$. Compression is reckoned positive. The tensile stress has its maximum value at the inner surface $r = a$, $\theta = 0$, and its value here is $pf(\rho)$ where $f(\rho)$ is given in table 1. As $\rho \to 0, f(\rho) \to 0{\cdot}492$.

Table 1. Stress concentration factors

ρ	0·1	0·2	0·3	0·4	0·5	0·6	0·7	0·8	0·9
$f(\rho)$	0·524	0·622	0·804	1·112	1·643	2·636	4·799	10·98	44·3
$g(\rho)$	0·182	0·231	0·323	0·482	0·761	1·296	2·504	6·10	26·3
$h(\rho)$	0·009	0·039	0·105	0·241	0·522	1·136	2·671	7·62	37·4

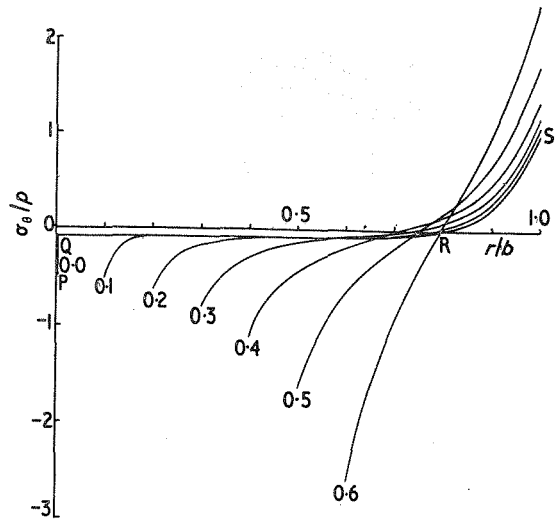

Figure 2. The variation of tangential stress σ_θ over the loaded diameter AB of figure 1(*c*). Numbers on the curves are values of the ratio $\rho = a/b$.

In an experiment with small values of α, the load W per unit length applied along the x axis is $2pb\alpha$ so that the tensile stress at failure is $Wf(\rho)/2ab$. A graph of $f(\rho)$ is given by Hobbs (1965, figure 2).

In this case and in those of §3 the maximum tensile stress occurs at a point of pure tension, the other principal stresses being zero.

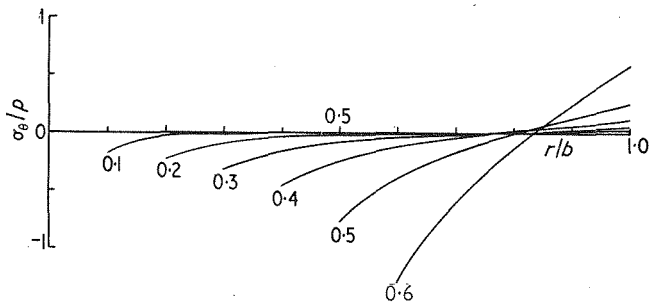

Figure 3. The variation of tangential stress σ_θ over the diameter CD in figure 1(*d*). Numbers on the curves are values of the ratio $\rho = a/b$.

3. A hollow cylinder loaded over opposite arcs of its inner surface

The cylinder $a < r < b$ is loaded by pressure p over the regions $-\alpha < \theta < \alpha$, $\pi - \alpha < \theta < \pi + \alpha$ of its inner surface $r = a$ (figure 1(*d*)). Formulae for the stresses in polar coordinates are given in the Appendix. It appears that for moderate values of ρ the greatest tensile stresses occur on the diameter CD, $\theta = 90°$. The variation of σ_θ with r/b for $\alpha = 7{\cdot}5°$ and $\theta = 90°$ is shown in figure 3 for various values of $\rho = a/b$. The maximum tensile stress occurs at the point D on the inner surface and may be written $pg(\rho)$ where values of $g(\rho)$ are given in table 1.

Tangential tensile stresses also occur across the outer portion of the diameter AB reaching a maximum value at the point A which may be written $ph(\rho)$ where $h(\rho)$ is given in table 1.

It appears from table 1 that if $\rho < 0{\cdot}6$, $g(\rho) > h(\rho)$ so that failure would be expected to take place on the diameter C′D′DC perpendicular to the direction of the load and this is observed experimentally. If the stress concentration near the point of loading had any

important influence on failure it would be expected to favour failure along the diameter AA'. The fact that failure is not associated with the region of loading makes this system a good one experimentally since the method of applying the load, whether over an arc or by contact with a round bar, is unimportant.

It follows from table 1 that if $\rho > 0{\cdot}6$, $g(\rho) < h(\rho)$ so that failure should take place on the diameter AB. The use of such thin rings seems undesirable both because of the large values of the functions in table 1 and because of the increased importance of flaws in the material. However, samples with $\rho = 0{\cdot}75$ usually broke along both diameters AB and CD into four pieces. This might, of course, be a secondary effect.

4. A hollow cylinder loaded over opposite arcs of both surfaces

Results for this case can be written down by combining those of the previous sections. In particular the case in which there is pressure p over the arcs $-\alpha < \theta < \alpha$ and $\pi - \alpha < \theta < \pi + \alpha$ of the outer surface and pressure p/ρ over the same arcs of the inner surface has some affinities with both diametral compression of the solid cylinder and the squeezing of a rectangular bar between localized forces applied to two opposite faces (Filon 1903).

Calculation shows that in this case there are tangential tensile stresses across part of the section AB. For $\rho = 0{\cdot}5$ about two thirds of this region has σ_θ tensile and the maximum tensile stress is $0{\cdot}21\,p$.

5. Experimental

Tests were made on three fine-grained materials, Carrara marble, 'Gosford sandstone', a fine-grained, rather weakly cemented quartz sandstone, and 'Bowral trachyte', an even-grained igneous rock consisting predominantly of orthoclase 1 mm in grain size, with minor quartz, calcite and altered ferromagnesian minerals.

In all cases the length of the cylinders was one inch and the external diameter two inches. A range of internal diameters from $a/b = 0{\cdot}1$ to $0{\cdot}6$ was used with external loading, and from $0{\cdot}4$ to $0{\cdot}6$ for internal loading. For external loading, the specimen was compressed between hardened platens ground to a radius of one inch for a width of $0{\cdot}261$ inch. For internal loading, since, as remarked in §3, the exact shape of the loaded area does not matter, stresses were applied by two circular rods of as large diameter as possible (to minimize bending) pulled apart in a testing machine.

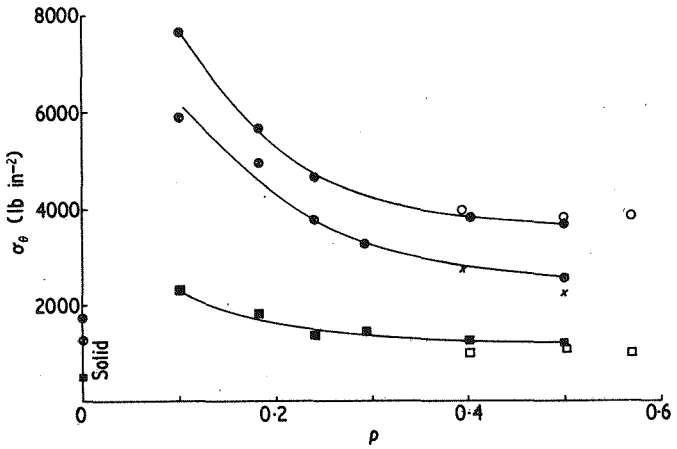

Figure 4. The variation of maximum calculated tensile stress at failure with $\rho = a/b$. Full circles: Bowral trachyte with external loading. Open circles: Bowral trachyte with internal loading. Crosses in circles: Carrara marble with external loading. Crosses: Carrara marble with internal loading. Full squares: Gosford sandstone with external loading. Open squares: Gosford sandstone with internal loading. Units are lb in^{-2}.

The maximum tensile stresses at failure, calculated using the values $f(\rho)$ and $g(\rho)$ given in table 1 are shown in figure 4. All points are the mean of at least three measurements. Values for solid cylinders are shown on the line $a/b = 0$. It appears that the calculated tensile strengths decrease fairly sharply as ρ increases from 0·1 to 0·4 and that, while the variation, both for internal and external loading, is much less in the region from 0·4 to 0·6, the values in this region are substantially greater than those for solid cylinders.

In all cases fractures were apparently extension fractures—for external loading in the plane AA′, and for internal loading in the plane CC′.

The sandstone and trachyte behaved as ideal brittle substances, failing quite suddenly. They would hold loads slightly less than those necessary to cause failure for hours.

The marble was used because it has the useful property of failing slowly so that some indication of the mechanism of failure can be obtained. The stresses shown in figure 4 are those corresponding to complete failure. However, for external loading, cracks can be observed in marble at the inner surface under substantially lower loads. These cracks do not propagate so that complete failure does not occur.

6. The variation of the principal stresses across the plane on which failure takes place

In discussing theories of failure it is convenient to plot stresses on a σ_1, σ_2 diagram. In the present case σ_r is always the greatest principal stress and σ_θ the least, compression being reckoned positive. In figure 5, the variation of σ_r/p and σ_θ/p across the planes in which failure takes place is plotted for each of the cases considered here. Curve I is for the solid cylinder, curve II for the region AB of the cylinder with $a = \frac{1}{2}b$ and external loading, curve III is for the region DC of the cylinder with $a = \frac{1}{2}b$ and internal loading, curve IV is for the region AB of figure 1(*e*) with loading on both surfaces and $a = \frac{1}{2}b$.

7. Discussion

Considering first the solid cylinder with loading over the region $\alpha = 7{\cdot}5°$, the tensile stress over the loaded diameter is given by the curve QRS of figure 2 and is seen to be very nearly constant over half the radius. The variation of σ_θ with σ_r is shown in curve I of figure 5 and it appears that the portion QR of this lies very close to the Griffith parabola

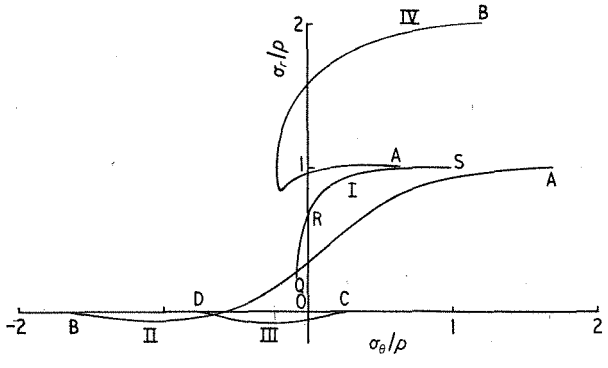

Figure 5. Principal stresses on various surfaces plotted against one another. I, the radius OA of a solid cylinder loaded externally. II, the radius BA of a hollow cylinder loaded externally. III, the radius DC of a hollow cylinder loaded internally. IV, the radius BA of a hollow cylinder loaded as in figure 1(*e*).

(for which OR would be 2·67 times the ordinate of Q) while the portion RS, corresponding to the region near the platen, lies below it. This suggests that on the Griffith criterion the whole of the region QR is very near to the condition of failure so that this probably takes place here and not near the platen. The point has been made by Fairhurst (1964) who also

points out that the Griffith criterion gives too low a ratio of compressive to tensile strength so that failure would be more likely to be initiated near Q. The question of the mechanism of failure has been confused by the fact that in some cases wedges are observed leading from the platens, and these suggest that failure might have been initiated at the platens. However, these wedges are probably a secondary effect produced during catastrophic failure, and in slow testing of marble it is easily possible to produce cracks which run from the interior to one platen only and also to show that there is no other evidence of failure (e.g. twinning) near the platens.

The effect of a small central hole may be seen from figure 2. If it is very small, a very shallow stress concentration PQ results. Even if $\rho = 0{\cdot}1$ the stress concentration does not penetrate beyond $b/5$. This shallow stress concentration explains the rapid fall of the curves of figure 4 up to $\rho = 0{\cdot}4$—if failure does take place at the inner surface the crack does not propagate. As remarked in §5 such cracks can be observed in marble.

For larger holes, $\rho > 0{\cdot}4$, the variation of stress is completely different from that in the solid cylinder and tends to the almost linear variation from tension to compression also observed in bending of a beam. The same remark applies to the case of internal loading (figure 3). The $(\sigma_r, \sigma_\theta)$ curves (figure 5, curves II and III) for these cases are completely different in type from curve I. The criterion of failure can only be satisfied at a point; it cannot be approached over a whole region.

On the other hand the system of figure 1(*e*) in which the ring is compressed between localized loads $W = 4atp$, where t is the thickness of the specimen (in this case $\frac{1}{2}b$), shows a variation of σ_θ and σ_r (figure 4, curve IV) which is of the same type as curve I. In this case a maximum tensile stress of $1{\cdot}26\ W/\pi t$ is attained, which is of the same order as that given by (1). Numerical values for the stresses in a rectangular bar compressed between concentrated loads applied on opposite faces do not appear to have been given although the theory has been set out by Filon (1903). For comparison with other methods a number of measurements have been made and reduced according to the formula $1{\cdot}26\ W/\pi t$. These are listed in table 2 under 'pinching' and may be expected to be an underestimate.

Table 2. Comparison of values obtained by different methods

Units are lb in^{-2}

	Gosford sandstone	Carrara marble	Bowral trachyte
Direct tension	520	1000	1990
Brazilian (15° contact)	540	1265	1740
Pinching	450	670	1090
Disk with hole $\rho = 0{\cdot}5$ external loading	1200	2500	3500
Disk with hole $\rho = 0{\cdot}5$ internal loading	1100	2300	3700
Bending: 3 point loading	1140	1710	3650

Values of calculated tensile stresses at failure for the three materials considered and various experimental situations are listed in table 2. It appears that they fall into two sets differing by a factor of around two.

In sum, it is suggested that tests may fall into three classes:

(i) Those in which the criterion of failure is nearly satisfied over a surface or volume of the body. These include uniaxial and triaxial testing, the Brazilian test, and compression of a rectangular bar between line loads.

(ii) Those involving non-uniform stresses in which the criterion for failure in the tensile region is only approached at a point. These include bending of beams and stressing of disks of moderate thickness. Results from these need not agree with those from tests involving uniform stresses.

(iii) Those involving stress concentrations such as the disk with a small hole. These may be meaningless since, even if failure occurs at the stress concentration, it may not propagate.

Acknowledgments

We are greatly indebted to Mrs. T. Chamalaun for programming the formulae of the Appendix for the computer and calculating the values of figures 2 and 3.

Appendix

Elastic stresses in a circular ring due to symmetrical normal loading at its surface

We consider plane stress in the circular ring $a < r < b$ caused by unit normal pressure applied over symmetrical arcs of angular width 2α at its surface, the remainder of the surface being unstressed.

The normal stress N at the surface is then given by

$$\left.\begin{aligned} &N = 1, \quad -\alpha < \theta < \alpha, \quad \pi - \alpha < \theta < \pi + \alpha \\ &N = 0, \quad \text{elsewhere} \end{aligned}\right\} \tag{2}$$

which may be represented by the Fourier series

$$N = \sum_{n=-\infty}^{\infty} A_n \, e^{2in\theta} \tag{3}$$

where

$$\left.\begin{aligned} A_0 &= 2\alpha/\pi \\ A_n &= A_{-n} = (\sin 2n\alpha)/n\pi. \end{aligned}\right\} \tag{4}$$

Filon (1924) has discussed the problem using a stress function but the stresses are most simply calculated by the use of the complex variable. In the form of this analysis used by Stevenson (1945) and briefly summarized by Jaeger (1962) the stresses are determined from two analytic functions $\phi'(z)$ and $\chi''(z)$ of the complex variable $z = re^{i\theta}$ by the formulae

$$\sigma_r + \sigma_\theta = 4\mathscr{R}\{\phi'(z)\} \tag{5}$$

$$\sigma_\theta - \sigma_r + 2i\tau_{r\theta} = 2\{\bar{z}\phi''(z) + \chi''(z)\} \, e^{2i\theta} \tag{6}$$

where a 'bar' denotes the conjugate complex and primes denote differentiation. $\phi'(z)$ and $\chi''(z)$ are given by Laurent series whose coefficients are determined by the boundary conditions at $r = a$ and $r = b$.

The formulae given apply, of course, to all cases in which the load is represented by a Fourier series of type (3) with $A_n = A_{-n}$ and not merely to the specialized values (4).

For the case of external loading as in figure 1(*c*), writing $\rho = a/b$ and

$$\Delta_n = \{(1 - \rho^{4n})^2 - 4n^2 \rho^{4n-2}(1 - \rho^2)^2\}^{-1} \tag{7}$$

$$U_n = 1 - \rho^{4n} + 2n(1 - \rho^2) \tag{8}$$

$$V_n = 1 - \rho^{4n} + 2n\rho^{4n}(1 - \rho^2) \tag{9}$$

$$W_n = 1 - \rho^{4n} + 2n\rho^{-2}(1 - \rho^2) \tag{10}$$

$$X_n = 1 - \rho^{4n} + 2n\rho^{4n-2}(1 - \rho^2). \tag{11}$$

It is found that

$$\phi'(z) = \tfrac{1}{2}A_0/(1 - \rho^2) + \sum_{n=-\infty}^{\infty}{}' A_n X_n \Delta_n \rho^{2n}(z/a)^{2n} \tag{12}$$

$$\chi''(z) = A_0(z/a)^{-2}/(1 - \rho^2) - \sum_{n=-\infty}^{\infty}{}' 2nA_n V_n \Delta_n \rho^{2n-2}(z/a)^{2n-2} \tag{13}$$

where the prime after the signs of summation denotes that the term $n = 0$ is omitted.

From these, the components of stress can be written down by (5) and (6). They give, writing

$$R = r/a \tag{14}$$

$$\sigma_r + \sigma_\theta = 2A_0/(1 - \rho^2) + 4 \sum_{n=1}^{\infty} A_n \Delta_n \rho^{2n} \{X_n R^{2n} - W_n R^{-2n}\} \cos 2n\theta \tag{15}$$

$$\sigma_\theta - \sigma_r = 2A_0 R^{-2}/(1 - \rho^2) + 4 \sum_{n=1}^{\infty} nA_n \Delta_n \rho^{2n} \{X_n R^{2n} + W_n R^{-2n} - V_n \rho^{-2} R^{2n-2} - U_n \rho^{-2} R^{-2n-2}\} \cos 2n\theta \tag{16}$$

$$\tau_{r\theta} = 2 \sum_{n=1}^{\infty} nA_n \Delta_n \rho^{2n} \{X_n R^{2n} - W_n R^{-2n} - V_n \rho^{-2} R^{2n-2} + U_n \rho^{-2} R^{-2n-2}\} \sin 2n\theta \tag{17}$$

For the case of *internal loading* as in figure 1(*d*) the corresponding results are

$$\sigma_r + \sigma_\theta = -2A_0 \rho^2/(1 - \rho^2) - 4 \sum_{n=1}^{\infty} A_n \Delta_n \{U_n \rho^{4n} R^{2n} - V_n R^{-2n}\} \cos 2n\theta \tag{18}$$

$$\sigma_\theta - \sigma_r = -2A_0 R^{-2}/(1 - \rho^2) + 4 \sum_{n=1}^{\infty} nA_n \Delta_n \{W_n \rho^{4n} R^{2n-2} + X_n R^{-2n-2} - U_n \rho^{4n} R^{2n} - V_n R^{-2n}\} \cos 2n\theta \tag{19}$$

$$\tau_{r\theta} = 2 \sum_{n=1}^{\infty} nA_n \Delta_n \{W_n \rho^{4n} R^{2n-2} - X_n R^{-2n-2} - U_n \rho^{4n} R^{2n} + V_n R^{-2n}\} \sin 2n\theta. \tag{20}$$

References

Berenbaum, R., and Brodie, I., 1959, *Brit. J. Appl. Phys.*, **10**, 281–7.

Brace, W. F., 1964, *State of Stress in the Earth's Crust*, Ed. W. R. Judd (New York: Elsevier), p. 111.

Fairhurst, C., 1964, *Int. J. Rock. Mech. Mining Sci.*, **1**, 535–46

Filon, L. N. G., 1903, *Phil. Trans. Roy. Soc. Lond.*, A, **201**, 63–155

—— 1924, *Inst. Civil Engrs.*, Selected Engineering Papers, No. 12.

Handin, J., Higgs, D. V., and O'Brien, J. K., 1960, *Geol. Soc. Amer. Memoir.*, **79**, 245–74

Hobbs, D. W., 1965, *Brit. J. Appl. Phys.*, **16**, 259–68.

Hondros, G., 1959, *Aust. J. Appl. Sci.*, **10**, 243–68.

Jaeger, J. C., 1962, *Elasticity Fracture and Flow*, 2nd edn (London: Methuen).

Morley, A., 1923, *Strength of Materials*, 6th edn (London: Longmans-Green).

Stevenson, A. C., 1945, *Proc. Roy. Soc. Lond.* A, **184**, 129–79.

Int. J. Rock Mech. Min. Sci. Vol. 3, pp. 249–264. Pergamon Press Ltd. 1966. Printed in Great Britain

AN INVESTIGATION OF THE FLATJACK METHOD OF MEASURING ROCK STRESS

E. R. HOSKINS
Australian National University, Canberra, Australia

(*Received* 24 *May* 1966)

Abstract—A series of laboratory experiments to test various aspects of the flatjack method of measuring rock stress have been made. Agreement with the known applied stresses is found to be excellent in sound rock. Problems of continued deformation after slot cutting or creep, differences in the values for elastic moduli determined by various methods and the relevance of these tests to the usual underground procedures are discussed.

1. INTRODUCTION

THE well-known flatjack method of measuring rock stress has been in use in mines and underground construction projects since before 1951[1], [2]. Its supposed merits and faults have been discussed at some length by ALEXANDER, JAEGER, MERRILL, and PANEK [3]–[10]. Because anomalous stresses have frequently been measured by flatjacks, doubt has been cast on the whole procedure, in particular the question of allowance for time-procedure deformations or creep. The purpose of this investigation was to reproduce in so far as possible the whole procedure of the flatjack test method in the laboratory under controlled conditions with known stresses to see first, just how well the method measured stress and how creep affects this measurement and second, whether flatjacks can be used to determine *in situ* rock properties. The results of six tests carried out on two types of rock and concrete uniaxial and biaxial stress conditions are described. Problems of continued deformation after slot cutting or creep, differences in elastic moduli determined by various methods, and the relevance of these laboratory tests to those usually carried out underground are discussed.

2. EXPERIMENTAL PROCEDURE

Blocks of rock and concrete 19 × 24 × 30 in. were procured and loaded in uniaxial or biaxial compression. Two different loading frames were used. The first, shown in Fig. 1(a), applied only a uniaxial stress. It consisted of two end plates held a fixed distance apart by rods. The end plates were $\frac{3}{4}$-in. thick mild steel plates with three 12 in. × 5 in. × 30 lb I-beam sections 24 in. long welded to the outside faces of the plates to minimize bending. The I-beams were stiffened by welding $\frac{1}{2}$-in. thick plates cut to shape into the webs at each end of each beam. Eight 2-in. diameter threaded rods and bolts were used to tie the two end plates together. Large flat hydraulic jacks, 19 × 24 in. were used to load the rock and these acted against the relatively rigid frame.

The second loading frame shown in use in Fig. 1(b), could apply either uniaxial or biaxial stress. It was a box-shaped device also fabricated from 12 in. × 5 in. × 30 lb I-beams welded to $\frac{3}{4}$-in. thick internal liner plates. Again the I-beams were stiffened by $\frac{1}{2}$-in. thick pieces of steel plate cut to shape and welded into the webs. During construction great care

was taken to ensure that the frame was not warped by excessive welding heat and when completed all dimensions were true to better than $\pm \frac{1}{16}$ in.

Loads were applied to the ends and sides of the test blocks in the biaxial frame also by large (19 × 24 and 19 × 30 in.) flatjacks. The blocks were positioned in the frame and loaded to the intended pressure by the large flatjacks. This pressure was then held constant for the duration of the test. Two measuring pin holes 1 in. diameter, 6 in. deep and 6 in. apart were drilled on opposite sides of the centreline of the proposed flatjack slot. Six-inch long by $\frac{1}{2}$-in. diameter measuring pins were cemented into these holes with a sand–cement grout. The measuring pins were held in a jig to ensure that they remained parallel while the grout hardened. The heads of these measuring pins protruded $\frac{1}{2}$-in. above the rock surface. Sixteen other $\frac{1}{4}$-in. high measuring points were cemented with an epoxy resin to the face of the rock in the array shown in Fig. 2. It was felt that the additional points might provide useful information but it was not considered wise to drill the rock full of holes on the neighbourhood of the jack.

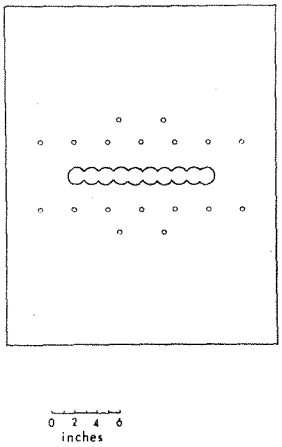

FIG. 2. Layout of slot and measuring points on face of the blocks.

Measurements were taken with a Huggenberger deformeter of the position of these points as soon as the cement and epoxy had hardened urements were repeatedand these meas several times to firmly establish the zero position of the loaded block. A flatjack slot was then diamond drilled 13 in. long and 13 in. deep with an EX bit (o.d. 1·465 in.). A row of ten overlapping holes was required. A complete set of measurements were taken after the completion of each hole. The slot was left open while deformation readings were taken for three to four days. A 12 × 12-in. flatjack was then grouted into the slot with its edge flush with the rock surface. Three to four days were allowed for the grout to harden before the jack was pressurized. The flatjack pressure was increased in appropriate steps with a set of measurements taken at each step until all combinations of measuring points were forced back to their initial or pre-slot values. The flatjack pressure was then released again in steps to zero. Two to four cycles were run over a period of several days and a mean cancellation pressure determined. In two of the experiments the jack was held at pressure for an extended time. The cancellation pressure was corrected according to the theoretical considerations discussed in a following section and these corrected values compared with the known applied

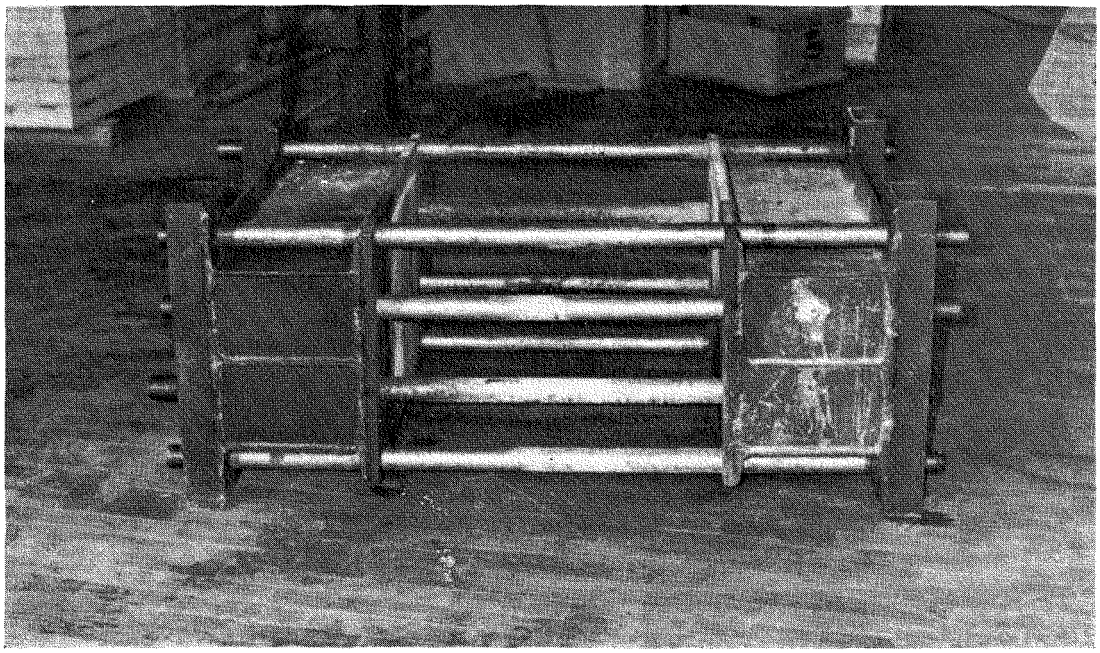

FIG. 1(a). View of uniaxial compression frame.

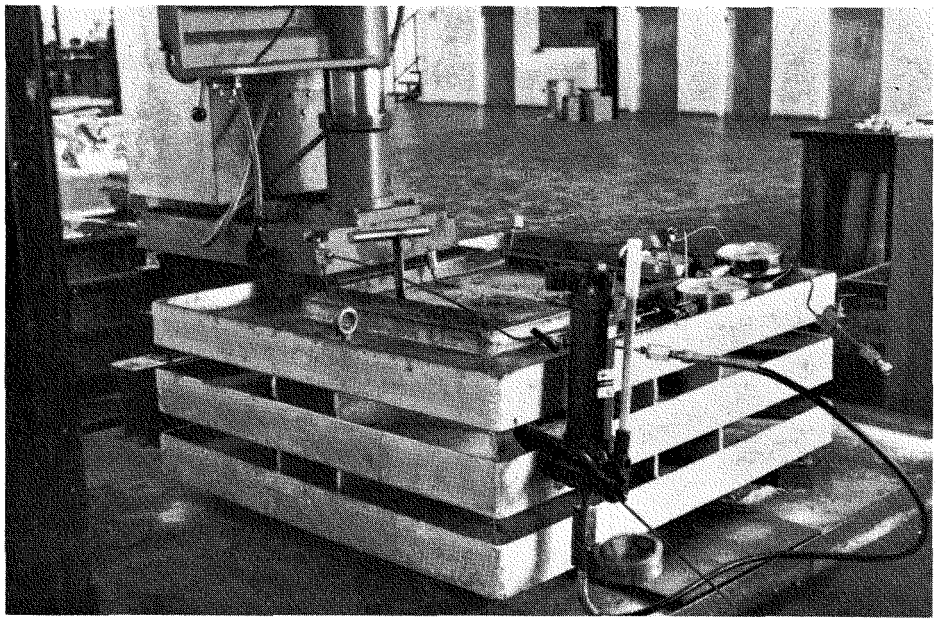

FIG. 1(b). View of biaxial compression frame with B trachyte block.

facing page 250 R.M.

FIG. 6. Concrete specimen from weak end of Block B, 2 in. diameter and 4·5 in. long.

loads on the block. The cores recovered from slot cutting were laboratory tested to determine their strength and elastic properties.

Except for the additional measuring points cemented to the rock face the experimental design was chosen to agree as far as possible with the procedures used underground by the Snowy Mountains Hydroelectric Authority which are described by ALEXANDER *et al.* [3], [4].

3. EXPERIMENTAL MATERIALS

Blocks of marble, trachyte and concrete were used in the investigation. The blocks of rock were procured commercially and had been wire sawn to rough dimensions and then ground to finish size. All sides were smooth and the dimensions were accurate to $\frac{1}{8}$ in. The blocks of rock were sound and free from joints. The concrete blocks were prepared in the laboratory.

Confined compression tests were made on specimens prepared from the cores recovered during the drilling of the flatjack slots. The results of these tests are plotted in Figs. 3–5 as ultimate strength against confining pressure. The apparatus used in these tests consisted of a 500 ton Avery testing machine, a Hart hydraulic pressure bench and a simple triaxial cell with a spherical seat. This apparatus has been fully described by PATTERSON [11]. The test specimens had a length-to-diameter ratio of about $2\frac{1}{2}$:1. The ends were machine ground with a diamond wheel and were flat and parallel to better than 0·0001 in. The specimens were air dried and jacketed with soft rubber tubing.

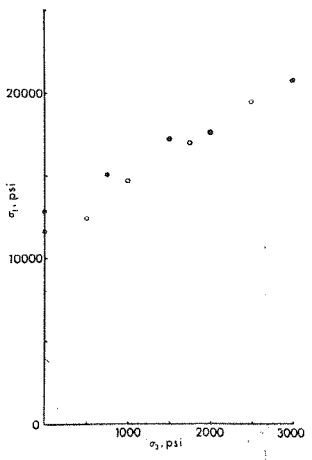

FIG. 3. Wombeyan marble. Principle stress relationships at failure for triaxial compression tests. Circles represent tests on cores from Block A and dots tests on cores from Block B.

Modulus of elasticity and Poisson's ratio determinations were made on cores prepared in the same manner as those used for the strength tests. Measurements of the elastic properties were made on unconfined compression specimens under quasi-static loading conditions. In all tests except those made on the poorer quality concrete cores, deformation was measured with electric resistance strain gauges bonded directly to the specimen. Read-out instrumentation consisted of a Philips strain bridge and ten-channel switching and balancing unit. Deformation of specimens from the weak concrete block, one of which is shown in Fig. 6,

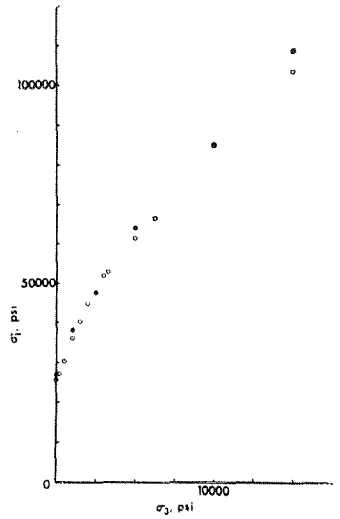

FIG. 4. Trachyte. Principal stress relationships at failure for triaxial compression tests. Circles represent tests on cores from Block A and dots tests on cores from Block B.

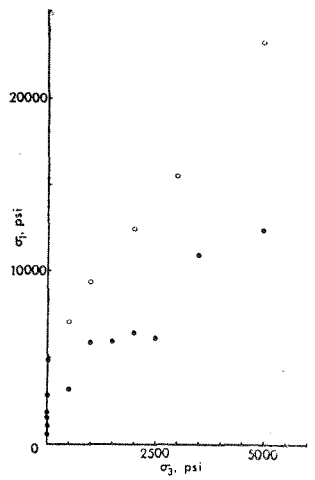

FIG. 5. Concrete. Principal stress relationships at failure for triaxial compression tests. Circles represent tests on cores from Block A and dots tests on cores from Block B.

was measured with either Huggenberger mechanical extensometers mounted on the specimen or when this was not possible with 0·0001-in. dial gauges between the testing machine plattens.

3.1 *Wombeyan marble*

The Wombeyan marble used in this investigation was obtained from the same quarry as that described by PATTERSON [11]. According to Patterson the rock is silurian and has probably been affected by several orogenies. Fabric analysis and compression tests on oriented cylinders by Patterson have shown no measurable anisotropy. The marble is

fairly coarse grained and the grain size varies from 0·05 to 5 mm. The average grain size in these two blocks was about 2 mm. Figure 7 is a stress–strain curve from a typical unconfined compression test on this marble.

3.2 *Bowral trachyte*

The two blocks of trachyte came from quarries near Bowral, New South Wales. This is an even-grained apparently isotropic igneous rock consisting predominantly of orthoclase with minor quartz, calcite and altered ferromagnesian minerals. Grain size is approximately 1 mm. Figure 8 is a stress–strain curve from a typical unconfined compression test on this trachyte.

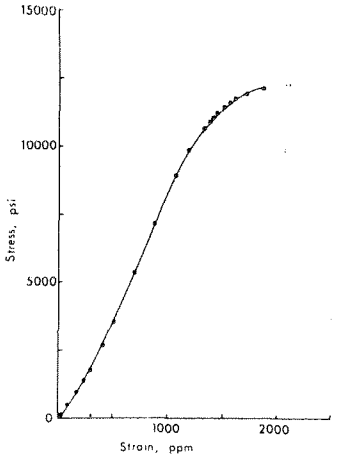

FIG. 7. Wombeyan marble. Typical stress–strain curve in uniaxial compression.

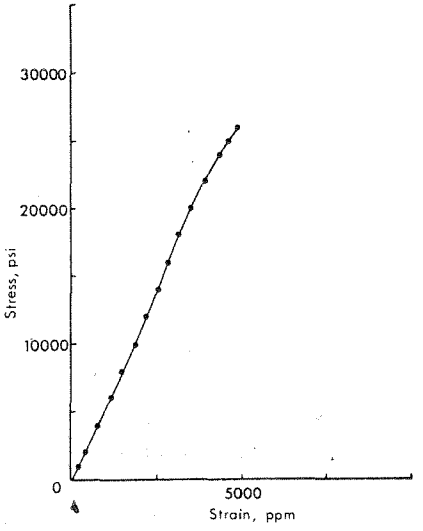

FIG. 8. Trachyte. Typical stress–strain curve in uniaxial compression.

3.3 *Concrete*

These blocks were mixed and cast in the laboratory for this project. The mixture used in block A was in the volumetric ratio of three size 4 marble chips (approximately $\frac{1}{2}$-in. diameter) to one and one-half size 2 marble chips (approximately $\frac{1}{4}$ in. diameter) to two builder's sand to one cement to three-quarters water. No allowance was made for moisture in the aggregate. The block was 90 days old when the test commenced.

Block B is the result of an attempt to make the weakest, most creep prone and irregular block that would hold together well enough to complete a flatjack test. The mix was in the volumetric ratio of three size 4 marble chips to three-quarters builders sand to three-quarters cement to one-half water. There was a considerable amount of segregation in the mold. One end of the block was a 'no fines' mix for about 8 in. The concrete appeared to be progressively stronger towards the other end. Twelve 6-in. deep by 2-in. diameter holes were drilled into the top face at the weak end and these were later filled with a sand-cement grout. The block was approximately six months old when tested. The unconfined compression strength varied from 600 to 3000 psi and the modulus of elasticity from $0{\cdot}3 \times 10^6$ psi to $4{\cdot}2 \times 10^6$ psi in the cores tested. The range in modulus is graphically shown in Fig. 9 along with a typical stress–strain curve from a specimen taken from the A concrete block.

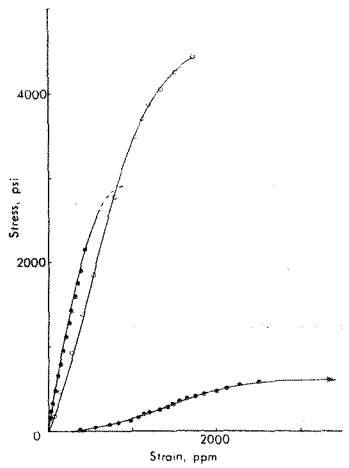

FIG. 9. Concrete. Stress–strain curves in uniaxial compression. Circles represent a test on a typical specimen from Block A. Dots represent extreme specimens tested from Block B.

4. SENSITIVITY

The Huggenberger deformeter is graduated in 0·0001 in. and under laboratory conditions can be read to the nearest 0·00005 in. The instrument, however, is temperature sensitive and must be frequently calibrated on an Invar bar standard. Readings repeated over several days on measuring points on an unstressed block of trachyte indicate that the overall accuracy including operator error is approximately $\pm$ 0·0001 in. The maximum total deformation measured across the slot for the blocks tested varied from 0·0031 to 0·0099 in. and the stress error equivalent to a reading error of $\pm$ 0·0001 in. was therefore 1–3 per cent. The hydraulic pressure gauges used were graduated in intervals ranging from 10 to 100 psi, and they were read to the nearest one quarter of a division. Their accuracy is $\pm$ 2 per cent so that the maximum error was $\pm$ 5 per cent.

5. THEORETICAL CONSIDERATIONS

ALEXANDER [3] has given the formulae for the displacements in the flatjack test based on elasticity theory assuming an elliptical slot and plane stress. These are:

$$W_0 = \frac{Sc}{E}\left\{(1-\mu)\left(\sqrt{1+\frac{Y^2}{C^2}}-\frac{Y}{C}\right)+(1+\mu)\Big/\sqrt{1+\frac{Y^2}{C^2}}\right\} \tag{1}$$

$$W_1 = \frac{SY_0}{E}\left\{-2\mu\left(\sqrt{1+\frac{Y^2}{C^2}}-\frac{Y}{C}\right)+(1+\mu)\Big/\sqrt{1+\frac{Y^2}{C^2}}\right\} \tag{2}$$

$$W_2 = -W_1\left[\frac{Q}{S}\right] \tag{3}$$

$$W_j = \frac{PC_0}{E}\left\{(1-\mu)\left(\sqrt{1+\frac{Y^2}{C_0^2}}-\frac{Y}{C_0}\right)+(1+\mu)\Big/\sqrt{1+\frac{Y^2}{C_0^2}}\right\} \tag{4}$$

$$W = W_0 + W_1 + W_2 \tag{5}$$

and at cancellation pressure

$$W = W_j \tag{6}$$

where:

$2W$ = displacement across open slot
$2W_j$ = displacement caused by raising jack pressure
$2W_0$ = displacement during slot cutting due to an infinitely thin slot
$2W_1$ = displacement due to finite slot width
$2W_2$ = displacement due to biaxial stress
S = rock stress normal to the jack
Q = rock stress parallel to the jack
C = half length of the slot
C_0 = half length of the jack
Y = distance of measuring point from the major axis of the slot
Y_0 = half width of slot
P = jack pressure
E, μ = Young's modulus and Poisson's ratio for the rock.

Substituting the appropriate dimensions into equations (1)–(6) and assuming a Poisson's ratio of 0·2 we find that

$$S = 0{\cdot}853P + 0{\cdot}056Q. \tag{7}$$

Thus the cancellation pressure P depends on the dimensions of the slot and flatjack, the biaxial stresses and to a small degree on Poisson's ratio. It is independent of the modulus of elasticity of the rock. Further manipulations of the equations can lead to estimates of the *in situ* rock modulus, however. In terms of the displacements which occur when the slot is drilled

$$E = [11{\cdot}02S - 0{\cdot}62Q]/W \tag{8}$$

and in terms of the displacements which occur when the flatjack is pressurized

$$E = 9{\cdot}4P/W_j. \tag{9}$$

In this investigation Poisson's ratio was measured on specimens taken from each block of rock and the appropriate value inserted in the equations.

A different approach has been suggested by JAEGER[12]. If the jack is composed as is usual of flat plates edge welded together, a region δ near the edge (of the order of $\frac{1}{4}$ in. wide) is inoperative so that the rock stress might be expected to be

$$S = P_c (C_0 - \delta)/C \tag{10}$$

where P_c is the cancellation pressure. With the usual slot and jack dimensions then

$$S = 0{\cdot}88\, P_c \tag{11}$$

which may be compared with equation (7).

6. RESULTS

The results of the experiments are summarized in Table 1. The calculated stresses and cancellation pressures are given for the embedded measuring pins on the centreline of the jack. The difference between the calculated stresses and the applied normal stress (excepting the B concrete block) ranges from $-$ 1·5 per cent to $+$ 5·5 per cent. Since this is approximately the measuring error of the deformeter and pressure gauges it may be concluded that the flatjacks in these cases do accurately measure the normal stress.

TABLE 1. SUMMARIZED RESULTS OF FLATJACK TESTS. (All stresses and pressures in psi)

Block	Applied stress: Normal to jack	Applied stress: Parallel to jack	Cancellation pressure	Calculated stress	Error (%)
A marble	500	0	610	515	+ 3
B marble	750	0	980	790	+ 5
A trachyte	1000	0	1310	1055	+ 5·5
B trachyte	1700	1000	1850	1675	− 1·5
A concrete	750	500	860	760	+ 1
B concrete	250	0	620	530	+ 112

The corrections for slot shape and biaxial stress given in the preceding section apply only to measuring points which are on the centreline of the slot, however the cancellation pressures for all combinations of the measuring points shown in Fig. 2, numbered from right to left, are given in Table 2. Positions one, two, eight and nine are on the ends of the slot and outside the ends of the slot and underwent very small deformations. They are also outside of the active portion of the flatjack. Combinations three, four, five, six and seven which, however, are more centrally located gave reasonably uniform results. Points four and six which are 10 in. apart show no systematic difference from the other measurements which were made on points 6 in. apart. There was no evidence of tilting of the embedded measuring pins. Graphical records of two typical tests, B marble and B trachyte, are given in Figs. 10 and 11. The displacements of the central embedded measuring points (number 5 in Table 2) are shown during slot cutting, creep and jack pressurizing.

TABLE 2. CANCELLATION PRESSURE (in psi) FOR MEASURING POSITIONS SHOWN IN FIG. 2. POSITIONS ARE NUMBERED FROM LEFT TO RIGHT

	1	2	3	4	5	6	7	8	9
A marble	420	380	650	600	610	600	590	350	320
B marble	1040	1000	970	1080	980	970	1090	1130	1130
A trachyte	1135	1315	1315	1280	1310	1320	1235	1210	1030
B trachyte	2425	1790	1750	1820	1850	1860	1790	1900	2075
A concrete	1060	900	860	900	860	910	850	960	980
B concrete	460	640	630	670	620	690	630	670	675

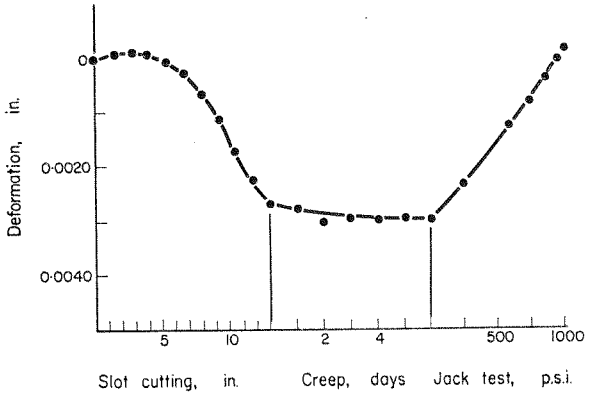

FIG. 10. Wombeyan marble. Flatjack test record for centrally located, embedded measuring points, 6 in. apart. Block B.

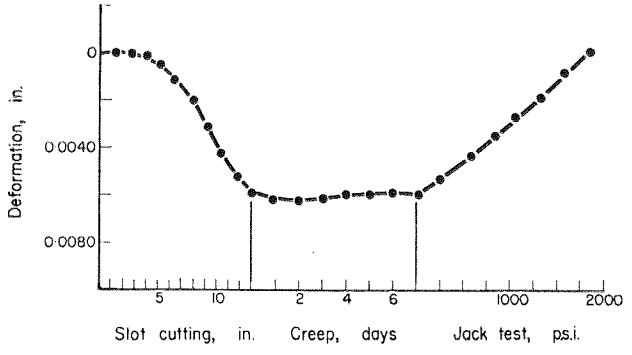

FIG. 11. Trachyte. Flatjack test record for centrally located, embedded measuring points, 6 in. apart. Block B.

7. THE PROBLEM OF CREEP

Deformation across the slot continued for several days after the slot and been drilled in the marble and concrete test blocks. This time-dependent deformation will herein be called creep for lack of a more precise term. This has been noted by ALEXANDER [3] in underground tests who ascribes it to jointing and says that it is notably absent in some cases. None of the blocks used in this investigation were jointed, however, so absence of obvious jointing is not necessarily an assurance against creep.

Stated simply, the problem in practice is whether to raise the flatjack pressure high enough to cancel all, none, or some portion of the observed creep deformation. This cannot be resolved without taking into consideration the time allowed for creeping under the various conditions that exist during the course of a flatjack test and the rate at which stresses are applied to the rock under these conditions. This implies that we know the deformation vs. time or creep rate law acting under each of these conditions, also whether or not the creep is recoverable and if so the various rates of creep recovery.

Deformation both elastic and non-elastic begins as soon as the first hole of the flatjack slot is drilled. This deformation increases as the slot is lengthened by each succeeding drill hole. When the slot is completed the purely elastic portion of the deformation ceases (assuming that the applied stresses do not change) but the time-dependent deformation continues. When the flatjack is grouted into the slot, the problem changes. Creep may continue but at a different rate as it is necessary to compress the grout. The creep rate will also be different with each level of pressure in the flatjack.

Creep in rock is a complex phenomena that is not at all well understood. The term is here being used in its most general sense to include all time-dependent deformation. Some of the mechanisms involved include twinning, translation gliding, intergrannular slip, fracturing, and slip on pre-existing fracture surfaces (GRIGGS [13] ROBERTSON [14], [15] and FRIEDEL [16]. Each of these mechanisms will have its own deformation vs. time characteristic and each will assume a differing relative importance depending upon the material and the state of stress. All of these mechanisms probably occur to some degree during a flatjack test in any rock but fracturing and slip on pre-existing fractures might be expected to predominate because of the relatively low mean stresses developed. A good deal of experimental data for the creep of limestone and marble is reported in the literature along with a somewhat lesser amount of creep data for igneous rocks and concrete; cf. MICHELSON [17], [18]; GRIGGS [13]; LOMNITZ [19]; EVANS [20]; ROSS [21]; HARDY [22]; ROBERTSON [14], [15] and PRICE [23]. The experiments described in the literature were all performed under relatively simple stress systems, confined or unconfined compression, bending and torsion. Various empirical creep-rate laws have been derived from these data. None of this information, however, is directly applicable to the problem of creep around flatjack slots.

All investigations have found that creep rate is strongly dependent upon stress. The stress field around the slot is not accurately known even if the applied stresses are known. The only solutions available are for the elastic stress distributions assuming plane stress around simple shapes such as an ellipse or an oval. While the solution for an ellipse given by ALEXANDER [3] appears to be adequate to describe the elastic displacement of the measuring points which are some distance from the actual boundaries of the slot, the majority of the creep, regardless of the mechanisms involved, should take place in the areas of high stress differences which are immediately adjacent to the more irregularly shaped slot shown in Fig. 2. It would be extremely difficult to quantitatively predict the effect of creep on flatjack test results from the available laboratory determined creep-test data. The experiments performed in this investigation, however, offered an opportunity to measure the sum of these effects under conditions that closely approximated underground tests.

Creep of the marble and concrete blocks with open completed slots is shown in Fig. 12. The deformation, $2W$ is the change in distance between the centrally located, embedded measuring pins. The creep rates of both marble blocks and the A concrete block are reasonably well described by the logarithmic relationships indicated. The creep rate of the B concrete block appears to follow an exponential relationship over the time interval tested. One

of the principal mechanisms of creep in concrete is thought to be the movement of water out of sub-microscopic bundles of fibrous cystals (Ross [21]). Since this is not an important mechanism in the creep of rock it is dangerous to attempt to use experiments on concrete to gain information concerning rock creep. Nevertheless, the form of the results of the tests on the A concrete block is indistinguishable from the tests on marble blocks. There was no significant creep in the two tests on trachyte blocks.

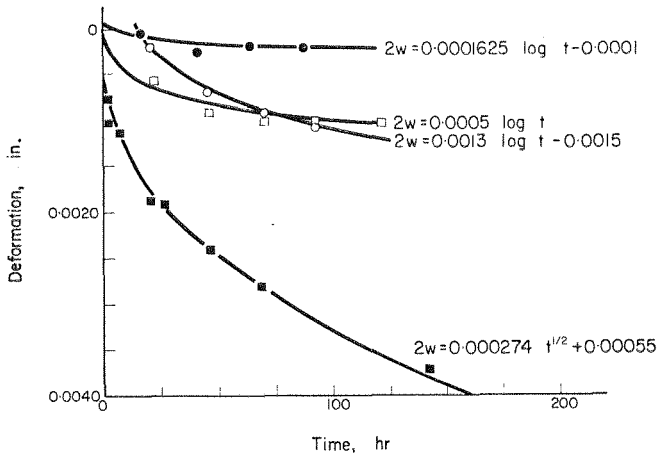

FIG. 12. Creep curves. Records of movement of the centrally located, embedded measuring points after the slot was completely drilled and before the jack was installed. ○ A marble, ● B marble, □ A concrete, ■ B concrete.

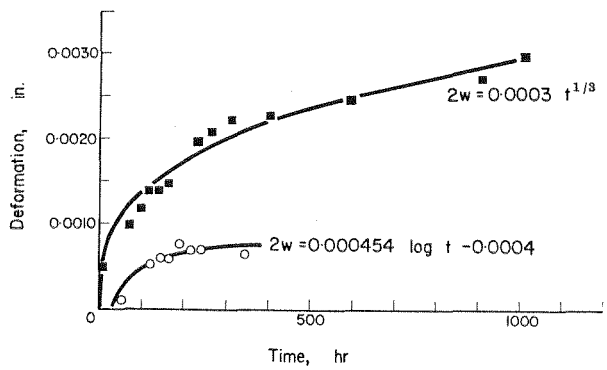

FIG. 13. Creep curves. Records of movement of the centrally located embedded measuring points with pressure in the flatjack. ○ A marble with 500 psi stress applied to the block and 600 psi pressure in the jack. ■, B concrete with 250 psi stress applied to the block and 400 psi pressure in the jack.

Creep-rate curves for the A marble and B concrete blocks with pressurized flatjacks are shown in Fig. 13. Again the marble can be represented by a logarithmic relationship while the B concrete creep rate is best described by an exponential equation.

PANEK and STOCK [10] recommend either of two procedures to correct for creep during a flatjack test and state that they should yield equivalent results. The first method they call a 'slow test' and involves holding the "jack pressure near the existing ground stress for several days, until the time-dependent strain component has been recovered". In their second method or 'rapid test' they "add up all time strains observed from the start of drilling the slot until

the first pressuring cycle, and deduct this from the strain change that is to be annulled". They do not make a correction for slot shape or presence of a biaxial stress. Alexander at least in his early work followed the first procedure (usually allowing one day for creep with jack pressure) and did correct for slot shape.

The method used in this investigation was to rather quickly raise the flatjack pressure high enough to cancel all of the observed deformation and then correct this pressure for slot shape by equation (7). These are the results given in Table 1 as the calculated stresses. It would appear from the results of the trachyte blocks which are not complicated by creep effects, that a correction for slot shape is required. Applying this procedure to the other test blocks gives uniformly good results, excluding the weak B concrete block. It should be noted that creep deformation amounted to 24 per cent of the total deformation measured in the A marble and A concrete blocks, 10 per cent of the total deformation in the B marble block and 47 per cent of the total deformation in the B concrete block.

The assumption implied by this method of treating the creep problem is that the creep deformation is wholly due to progressive, small-scale inter-grannular fracturing and then slip on the suitably oriented fracture surfaces. Jack pressure merely reversed the direction of slip on these fracture surfaces and there is no significant time delay in recovering the deformation once the pressure is sufficient to cause movement. This asumption is obviously not valid in the case of the B concrete block where mechanisms of creep other than fracturing are presumed to be acting.

8. ELASTIC MODULI

Elastic moduli were determined for the test blocks by several methods: first, by strain-gauge measurements on cores taken from the slot, second by deformation measurements made during slot cutting using equation (8) and third by Jack pressure-displacement values using equation (9). The values are compared in Table 3. It is immediately apparent that the methods do not always agree. The blocks tested in uniaxial compression, A marble, B marble, A trachyte and B concrete show a higher modulus from core specimens than they do from slot deformation or jack pressure–displacement measurements. The two blocks tested in biaxial compression, B trachyte and A concrete, show an equal or lower modulus in core specimens than they do from slot deformation or jack pressure–displacement curves. ALEXANDER [3], ALEXANDER *et al.* [4], and TINCELIN [2] have previously noted differences between the moduli measured in the laboratory on core specimens and those measured *in situ*. These workers have ascribed the differences to the presence of 'tight' or 'open' jointing. While jointing undoubtedly affects the *in situ* measurements, the blocks of rock used in this investigation had no jointing in the usual sense at all. A more detailed investigation of the various methods used to calculate the moduli is required to satisfactorily explain the differences apparent in Table 3.

The first method of determining the modulus of elasticity, the use of electrical resistance strain gauges bonded to the surface of an unconfined compression specimen is quite well known. The assumptions are that stresses and strains in the specimen are uniform and that the material has no time-dependent deformational properties. In practice, of course, these assumptions are seldom completely satisfied. With careful specimen preparation the effects of non-uniform stress and strain near the loaded surfaces and bending can be minimized. Strains dependent upon time are generally not important for fresh solid-rock specimens stressed below their yield point during the period covered by the usual laboratory test. A considerable amount of time-dependent deformation or creep is included, however, in

the measurements made in this investigation on the poorer quality concrete. The Young's modulus determined by this method for this material and given in Table 3 is therefore lower than any instantaneously determined value by an unknown amount.

Equation (8) yields an unloading modulus from displacements measured while the slot is being drilled. Since it takes from 2 to 4 hr to drill the slot, an unknown amount of creep is included in the total slot deformation $2W$. Portions of this creep occur during and after one hole, two holes, three holes . . . etc., have been drilled. Equation (8) can therefore, by this argument, be expected to yield a lower value for the modulus than any more rapidly determined value such as the strain-gauge measurements on cores which are normally

TABLE 3. COMPARISON OF ELASTIC MODULI DETERMINED *in situ* AND FROM CORE SPECIMENS

	Young's modulus × 10^6 psi			Poisson's ratio
	Slot closure	Jack displacement	Cores in compression	Cores in compression
A marble	5·0	3·9	8·9	0·22
B marble	6·2	5·9	8·7	0·30
A trachyte	5·2	5·5	6·4	0·30
B trachyte	6·1	6·0	6·0	0·33
A concrete	4·3	3·5	3·0	0·15
B concrete	1·0	1·3	0·33–4·2	Not determined

completed in 20–30 min. The deformation $2W$ used in equation (8) is the total movement between the two measuring points. The rock between these points is not uniformly stressed. The variation can be from relatively low compressive stresses near the measuring points to stresses near failure in tension at the edge of the slot. Examination of Figs. 7 and 9 show that for marble and concrete the modulus of elasticity varies markedly with stress level in an unconfined compression test. Recent work by COOK and HODGSON [24] and WALSH [25] also on unconfined compression specimens examines this non-linearity of elastic 'constants' in much greater detail. The modulus is generally less at low and high stresses. In addition it is well known from the work of BIRCH [26], BRACE [27], and FANG [28], that the elastic constants of rock have a strong dependence on mean stress. The mean stress near the surface of the slot between the measuring points is lower (compression being reckoned positive) than it is away from the slot and near the measuring points. Thus while it is not possible to quantitatively evaluate these factors it can be seen that they all would tend to give lower moduli than would the more conventionally measured laboratory tests using the straight-line portion of the stress–strain curve from unconfined compression tests. Some of these effects are reduced when the slot is in a biaxial stress field. The zone of tensile stress near the slot is reduced or eliminated and the mean stress increased. In addition the fact that this is an unloading modulus determined during a 'minor stress cycle' in the sense of COOK and HODGSON [24] would tend to give a slightly higher modulus than would a reloading modulus determined during the 'major stress cycle'. All of these factors then—creep, stress level, mean stress, presence of a biaxial stress and the amount of hysteresis in the stress–strain curve of the material, must be evaluated before the modulus determined from the slot displacements can be compared with the modulus determined from a laboratory test on a piece of core.

These same factors must also be evaluated to resolve the differences between the modulus determined by equation (9) from the slope of the jack pressure–displacement curve and the core modulus.

This is the value usually reported by Alexander and his-co-workers as the *in situ* modulus. The advantage of using this equation is that jack pressure can be raised more quickly than the slots can be drilled so that the relative amount of time-dependent deformation included in the measurement is reduced. Also during this portion of a flatjack test zones of tensile stresses are eliminated and the mean stress in the rock between the measuring points is increased. At cancellation pressure the rock should be in a reasonably uniform biaxial stress field.

9. RELEVANCE TO UNDERGROUND TESTS

It is important to relate these experiments to underground flatjack tests as they are usually performed. First it can be said with some certainty that carefully done flatjack tests in sound rock should yield a good estimate of the rock stress normal to the jack. In less sound rock, perhaps irregularly stressed, with a large creep component (as in concrete test block 'B') the stress estimate may be less reliable. The rock at most underground test sites will probably fall somewhere between the two extremes tested and a certain amount of judgement will inevitably be required to interpret the results.

Second, the accuracy attained in these laboratory tests is likely to be much better than that attained underground even in sound rock. There is a certain amount of technique involved in using the deformeter and the usual underground conditions of poor light and awkward positions do nothing to improve one's technique. A consistency reading accuracy of $\pm$ 0·0002 in. is probably the best that can be hoped for with the deformeter under field conditions. The hydraulic pressure gauges used in these experiments were of 8 in. diameter, carefully calibrated, and selected for the proper range of expected pressure. These gauges are cumbersome, expensive and relatively vulnerable to damage and so are generally not used underground. They are replaced in some cases apparently by gauges as small as 3 in. diameter [10] and these smaller gauges must have a greater range to cope with unknown pressures and thus an even lesser sensitivity. Perhaps a reasonable estimate of the best consistently attainable underground accuracy would be 15–20 per cent.

These experiments were performed in blocks of rock that were isotropic and, compared with most mine rocks homogeneous and fine grained. No theoretical or experimental analyses have yet been made for underground stress measurements in anisotropic rock.

The results of a series of flatjack tests gives only the stresses near the surface of an underground opening. Usually the quantities wanted for design purposes are the primary stresses far removed from the influence of the opening. To get these primary stresses from flatjack results, stress concentration factors are found (generally by photoelastic analysis) for the particular shaped opening where the flatjack tests were conducted. A group of simultaneous equations containing the flatjack results and the stress concentration factors are solved to find the stresses parallel, vertical, and transverse to the opening (c.f. ALEXANDER, [3]). If this is done for openings at three different orientations, the direction and magnitude of the three principal stresses can be determined. No case is known as yet in which the analysis has been carried this far. The most common practice seems to be to find the orthogonal stresses vertical, parallel and transverse to the axis of the opening [3], [4] and [7] and base design considerations on these values.

It seems obvious that if creep is measured around a flatjack slot a comparable amount of

creep must occur after a mine opening is made in the same rock. This creep may be accompanied by a relaxation of stress around the mine opening rendering the stress concentration factors determined by a purely elastic analysis invalid. Under these circumstances the flatjacks would still at least approximately yield the stresses on the surface of the opening, which is after all where rock failure will most likely occur. Perhaps the most interesting information would be the stress–strain–time relationships around the open slot and the pressurized flatjack.

Several investigators have proposed using installed flatjacks to monitor changes in rock stress due to mining activities or to monitor readjustment of rock stress around an opening over several years time, [3]; [10]; [2]: MAYER *et al.* [1] and JAEGER [5] have made tests on blocks of concrete and rock in testing machines which can be interpreted to give some idea of the effectiveness of a flatjack as a stress monitor for rapid, elastic stress changes. Jaeger's conclusions were that if uniformly loaded the flatjacks did accurately respond to changes in rock stress under these conditions. Similar tests have been conducted on marble and trachyte blocks as a part of this investigation and this conclusion is supported. The problem with long-term flatjack monitoring tests is in separating rock movement due to creep at constant stress from rock movement due to changes in stress. If this problem is not resolved in each particular case the flatjacks will not be effective stress monitors.

Acknowledgements—This investigation was suggested by Professor J. C. JAEGER who has given continuous encouragement and support. The author has been privileged to see recent unpublished work of the Snowy Mountains Hydroelectric Authority. The research was supported by an Australian National University Research Scholarship and a National Science Foundation Fellowship held by the author.

REFERENCES

1. MAYER A, HABIB P. and MARCHAND R. Underground rock pressure testing, *Proceedings of the International Conference on Rock Pressure and Support in Workings*, Liège (1951).
2. TINCELIN O. Research on rock pressure in the iron mines of Lorraine, *Proceedings of the International Conference on Rock Pressure and Support in Workings*, Liège (1951).
3. ALEXANDER L. G. Field and Laboratory tests in rock mechanics, *Proceedings of the Third Australian–New Zealand Conference on Soil Mechanics and Foundation Engineering*, pp. 161–168 (1960).
4. ALEXANDER L. G., WOROTNICKI G. and AUBREY K. Stress and deformation in rock and rock support, Tumut 1 and 2 underground power stations, *Proceedings of the Fourth Australian–New Zealand Conference on Soil Mechanics and Foundation Engineering*, pp. 165–178 (1964).
5. JAEGER J. C. Disc. Tech. Session 9, *Proceedings of the Third Australian–New Zealand Conference on Soil Mechanics*, pp. 5–9 (1960).
6. JAEGER J. C. Theory and application of curved jacks for measurement of stresses, *State of Stress in the Earth's Crust*, Elsevier (1964).
7. MERRILL R. H., WILLIAMSON J., RAPCHAN D. and KRUSSE G. *Stress Determination by Flat Jack and Borehole Deformation Methods*, USBMRI 6400 (1964).
8. MERRILL R. H. *In situ* determination of stress by relief techniques, *State of Stress in the Earth's Crust*, Elsevier (1964).
9. PANEK L. A. Measurement of rock pressure with a hydraulic cell, *Trans. Am. Inst. Min. Engrs* **220**, 287–290 (1961).
10. PANEK L. A. and STOCK J. A. *Development of a Rock Stress Monitoring Station Based on the Flat Slot Method of Measuring Existing Rock Stress*, USBMRI 6537 (1964).
11. PATTERSON M. S. Experimental deformation and faulting in Wombeyan marble, *Bull. geol. Soc. Am.* **69**, 465–476 (1958).
12. JAEGER J. C. Private communication (1966).
13. GRIGGS D. T. Creep of rocks, *J. Geol.* **47**, (3) 225–251 (1939).
14. ROBERTSON E. D. Creep in Solenhofen limestone, *Rock Deformation*, G.S.A. Memoir 79, 227–244 (1960).
15. ROBERTSON E. C. Viscoelasticity of rocks, *State of Stress in the Earth's Crust*, Elsevier (1964).
16. FRIEDEL J. *Dislocations*, Pergamon Press, Oxford (1964).
17. MICHELSON A. A. The laws of elastic–viscous flow—I, *J. Geol.* **25**, 405–410 (1917).
18. MICHELSON A. A. The laws of elastic–viscous flow—II, *J. Geol.* **28**, 18–24 (1920).

19. LOMNITZ C. Creep measurements in igneous rocks, *J. Geol.* **64**, (5) 473–479 (1956).
20. EVANS R. H. Effect of rate of loading on some mechanical properties of concrete, *Mechanical Properties of Non-Metallic Brittle Materials*, Butterworths (1958).
21. ROSS A. D. The elasticity, creep and shrinkage of concrete, *Mechanical Properties of Non-Metallic Brittle Materials*, Butterworths (1958).
22. HARDY H. R. Time dependent deformation and failure of geologic materials, *Colo. Sch. Mines Q.* **54**, (3) 134–175 (1959).
23. PRICE N. J. A study of the time–stress behaviour of coal measure rocks, *Int. J. Rock Mech. Min. Sci.* **1**, 271–303 (1964).
24. COOK N. G. W. and HODGSON K. Some detailed stress–strain curves for rock, *J. geophys. Res.* **70**, 2883–2888 (1965).
25. WALSH J. B. The effect of cracks on the uniaxial elastic compression of rocks, *J. geophys. Res.* **70**, (2) 399–411 (1965).
26. BIRCH F. The velocity of compressional waves in rocks to 10 kilobars—II, *J. geophys. Res.* **66**, 2199–2224 (1961).
27. BRACE W. F. Brittle fracture of rocks, *State of Stress in the Earth's Crust*, Elsevier (1964).
28. FANG WEI-CHIN, Investigations of the elastic properties of rocks under high isostatic pressures, *Wo Li Haueh Pao*, (Chinese) **11**, (1) 28–46 (1962). Edited Translation by Foreign Technology Division, Air Force systems Command, Wright Patterson Air Force Base, Ohio.

Int. J. Rock Mech. Min. Sci. Vol. 4, pp. 155–164. Pergamon Press Ltd. 1967. Printed in Great Britain

AN INVESTIGATION OF STRAIN ROSETTE RELIEF METHODS OF MEASURING ROCK STRESS

E. R. HOSKINS

Department of Geophysics and Geochemistry, Australian National University, Canberra, Australia

(*Received* 18 *September* 1966)

Abstract—Full-scale laboratory experiments have been performed to determine the effectiveness of borehole strain rosette relief methods of measuring rock stress. The effect of the stress acting parallel to the borehole axis cannot be neglected when analysing the data. The stress distribution in the block of rock used in these experiments seems to conform closely to the three-dimensional photoelastic pattern for stresses around the flattened end of a borehole, determined by Galle and Wilhoit. It appears that independent information concerning the orientation of at least one of the principal stress directions is necessary before this type of borehole strain relief technique can be used. If the direction of one of the principal stresses is known, the effect of the stress acting parallel to the borehole axis on the measured strains taken into account, and the elastic moduli of the rock determined under stress conditions similar to those acting during the strain relief test, the method of strain rosette relief on the flattened face of a borehole gives a good estimate of the rock stress.

INTRODUCTION

STRAIN rosette relief methods were probably the first techniques to be used to attempt to measure rock stresses underground. The earliest known worker was LIEURANCE in 1933 [1]. MOHR [2] reported using this method in 1956 and OLSEN [3] summarized his own work extending back to 1947 in 1957. Recently, LEEMAN [4, 5] and ALEXANDER [6] have described modifications to the method. The technique is also well established in the general field of experimental stress analysis [7].

Briefly, the technique involves fixing a strain rosette to a prepared surface of stressed rock and then cutting or drilling a channel around the rosette to a depth sufficient to completely release the elastic strain in the rock and allow it to deform the rosette. The deformation of the rosette is measured, the elastic moduli of the rock determined and the stress in the rock face calculated according to the theory of elasticity.

Lieurance cemented measuring points into the wall of a drainage tunnel and used a mechanical strain gauge with a 20 in. gauge-length to make the deformation measurements. The stress relief was accomplished by drilling an overlapping series of holes to form a square channel completely around the measuring station. ROBERTS *et al.* [8], briefly mention the use of photoelastic disks to determine 'elastic rebound' in rock, the technique being described in more detail by HAWKES and MOXON [9]. All other workers appear to have used bonded electric resistance strain gauge rosettes and accomplished the stress relief by overcoring the rosette with a diamond coring bit. Once the stresses in the rock face have been determined, stress concentration factors are assumed for the shape of the opening and the primary rock stresses are calculated.

The technique described by LEEMAN [4, 5], advances the method by installing the strain gauge rosette on the flattened face of a borehole. This borehole can be made deep enough to

avoid the rather uncertainly stressed area influenced by the driving and presence of the mine opening. The gauge is overcored and the direction and magnitude of the principal stresses in the borehole face determined using elastic theory. These stresses are then multiplied by a stress concentration factor for the end of a borehole which has been determined by three-dimensional photoelastic analysis, to find the primary rock stresses. LEEMAN's analysis [4] assumed that the stress acting parallel to the borehole axis would not significantly affect the stress measurements. This seemed contrary to calculations based on the three-dimensional photoelasticity study of the problem by GALLE and WILHOIT [10], and it was the purpose of this investigation to experimentally examine this question in particular and the method in general to determine how well the technique actually measures rock stress.

STRESSES AND STRAINS AT THE END OF A BOREHOLE

No exact mathematical solution is known for the stresses and deformation in rock surrounding the flattened end of a borehole. A three-dimensional 'frozen stress' photoelastic study has been made by GALLE and WILHOIT [10] and LEEMAN [4] has reported confirming their results both photoelastically (referring to unpublished work by Hoek) and with strain gauges on blocks of steel, granite and araldite. Galle and Wilhoit give fairly complete results for stresses and their analysis has been accepted and used in this investigation. Portions of their data have been replotted in a more convenient form for this problem in Figs. 1 and 2. The usual cylindrical co-ordinate system of r, θ and z is employed with the

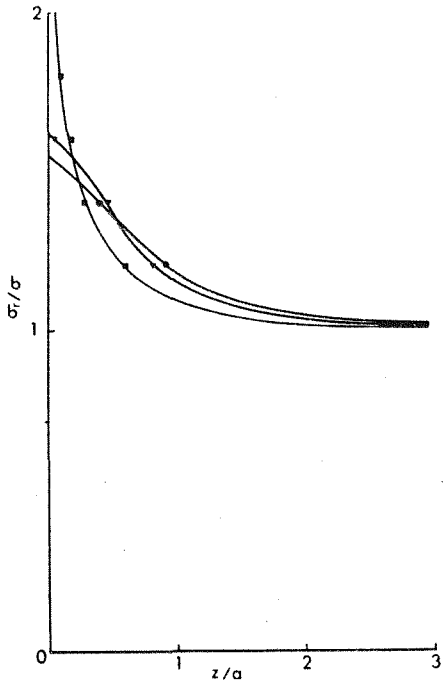

FIG. 1. Ratio of stress σ_r on end face of borehole to an applied stress σ in the same direction for radii

● $r = 0$;
▲ $r = 0{\cdot}5a$;
■ $r = a$

plotted against distance from the end of the borehole. [Data replotted from GALLE and WILHOIT [10] Fig. 7(b).]

z-axis coinciding with the axis of the borehole. The radius of the borehole is a. Compressive stress will be reckoned positive throughout this paper. Figure 1 shows the variation of σ_r for $\theta = 0°$ in terms of a stress σ applied at a great distance from the hole and normal to its axis, with the distance into the rock from the flattened face. Curves are given for the radii $r = 0$, $r = 0{\cdot}5a$, and $r = a$. Figure 2 is a similar set of curves for the case when the applied stress σ acts parallel to the axis of the borehole. The radial stress σ_r for $\theta = 0°$ at

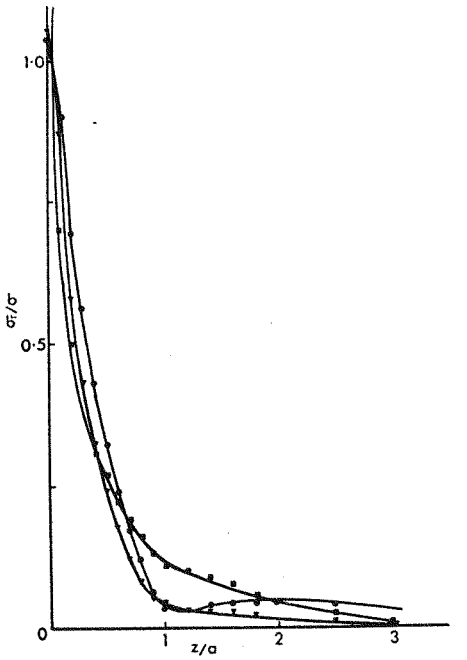

FIG. 2. Ratio of radial stress σ_r on end face of borehole to an applied stress σ parallel to the borehole. For radii

● $r = 0$;
▲ $r = 0{\cdot}5a$;
■ $r = a$

plotted against distance from the end of the borehole. [Data replotted from GALLE and WILHOIT [10] Figs 6(b), 7(b) and 9(b)].

the centre of the flattened face is 1·56 times the stress applied parallel to the face at some distance from the borehole. The radial stress σ_r at $\theta =$ any angle at the centre of a flat face is $-$ 1·04 times the stress applied normal to the face. GALLE and WILHOIT [10] include sufficient information to determine the stresses on the face of the borehole for any given loading condition as long as the axis of the borehole is parallel to one of the principal stresses.

Strain gauges measure the component of strain parallel to their axis averaged over their gauge length plus a generally small amount due to transverse sensitivity. The transverse sensitivity of the etched foil rosettes used in this investigation was + 0·5 per cent, and was considered small enough to disregard. The geometry of the gauges was such that they measured only average radial strains from $r/a = 0$ to $r/a = 0{\cdot}2$. The elastic stress–strain relation-

ship for radial strain on the end of the borehole assuming plane stress can be written:

$$\epsilon_r E = \sigma_r - \mu\sigma_\theta \tag{1}$$

where E and μ are Young's modulus and Poisson's ratio. In terms of the stresses σ_r', σ_θ' and σ_z' applied to the rock well away from the borehole and assuming a stress concentration factor of 1·56 for stresses parallel to the face and −1·04 for the stress normal to the face, the stress at infinity – strain on the borehole face relationship can be given as:

$$\epsilon_r E = 1{\cdot}56\sigma_{r'} - 1{\cdot}56\mu\sigma_{\theta'} - 1{\cdot}04(1-\mu)\sigma_{z'}. \tag{2}$$

Each of the three strain gauges in the rosette is affected by all three of the applied principal stresses.

EXPERIMENTAL DESIGN

The apparatus used to hold and load the rock specimens was the biaxial loading frame previously described by HOSKINS [11]. It was mounted on its side and a 3-in. diameter hole cut in one end. The rock could be loaded with large flatjacks on the ends and top and bottom. Two sides were unstressed. One of the end jacks was fabricated with a 3-in. hole in the middle to allow drilling through that end. Figure 3 is a general view of the apparatus showing the block of rock and the drill in place. The drilling was accomplished with a gasoline powered portable diamond drill. A thin-walled diamond bit was used which gave a hole diameter of 2·35 in. and a core diameter of 1·94 in. The end of the hole was ground with a flat-faced diamond bit.

The rock was a block of trachyte quarried near Bowral, New South Wales. It consists predominantly of orthoclase 1 mm in grain size with minor quartz, calcite and altered ferromagnesian minerals. The block was 19 × 24 × 30 in. and the hole was collared in one of the 19 × 24 in. faces. The faces of the block were wire sawn and then ground flat and the dimensions were true to $\pm \frac{1}{8}$ in. It was theoretically possible to conduct tests at intervals over nearly the full 30-in. block length, but because of uncertainty concerning stress distribution near the ends of the rather squat block only those tests conducted in the middle third of the block will be discussed here.

The strain cells, one of which is shown after testing in Fig. 4, were constructed with a Perspex body. The strain gauge rosette (Baldwin Lima Hamilton FAR 50–12–45) was cemented to the inside face of a 1·360-in. diameter, $\frac{1}{16}$-in. thick Perspex disk. Four-conductor cable was solder-connected to the terminals of the rosette and the cable and disk cemented to the strain cell body as a unit. The body was then filled with a cold-curing silicone rubber compound to completely waterproof and encapsulate the strain gauge rosette. The strain cell was cemented to the face of the drill hole with Philips quick hardening epoxy strain gauge cement. The cable was fed through the bit and drill rods and out a packing gland on the water swivel of the drill. It remained connected to the strain gauge instrumentation throughout the test. The strain cell was overcored in $\frac{1}{16}$-in. increments with strain reading taken at each increment. The quantity of drilling water used and the drilling water temperature were measured.

Strain measuring instrumentation consisted of a Philips 10-channel switching and balancing unit and direct reading measuring bridge. Overall repeatability of readings with this system was determined to be ± 5 ppm by repeated readings on a gauge cemented to an unstressed block.

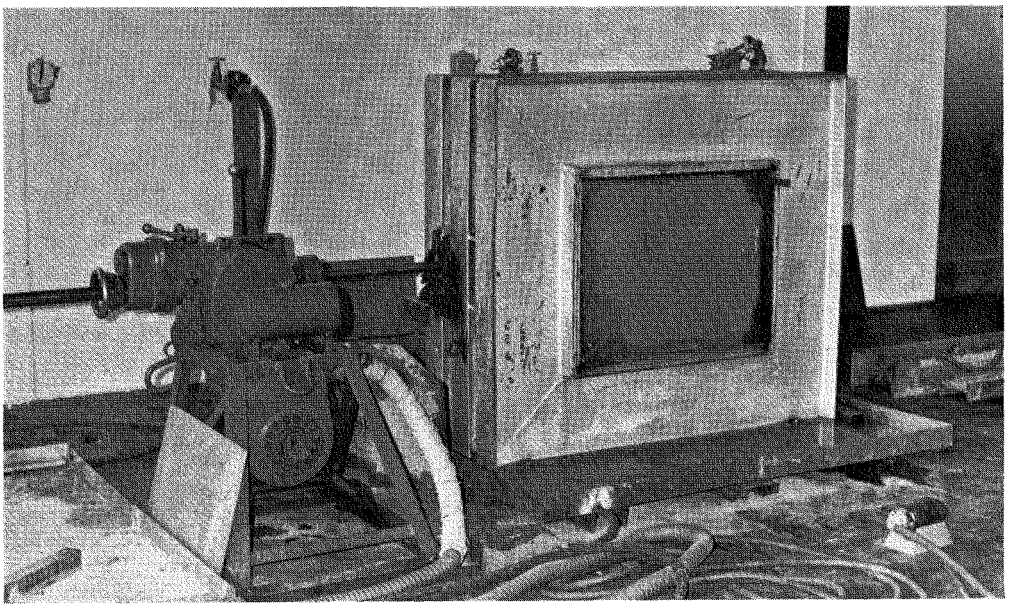

FIG. 3. General view of the apparatus showing the diamond drill and biaxial loading frame with the block of rock in place.

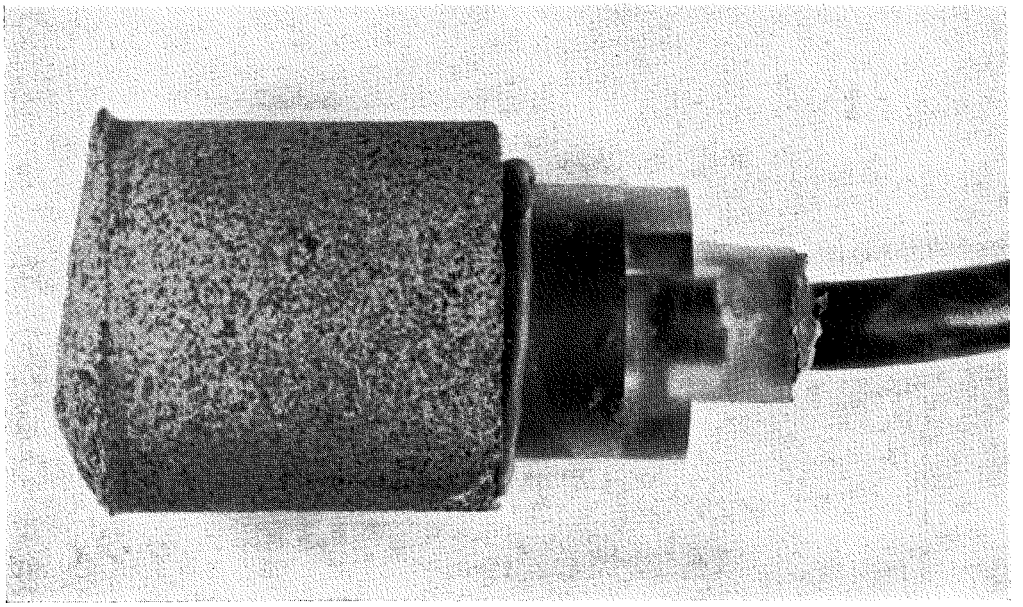

FIG. 4. Strain cell cemented to rock core after a strain relief test.

Direct temperature compensation of the active strain gauges with a dummy gauge is not possible with this system, but effective compensation was achieved by allowing the drilling water to flow for some time prior to actual overcoring until drift in the strain gauge readings had ceased. This usually took 10–15 min. After each drilling increment the strain gauge readings were allowed to stabilize with the drilling water left running if they showed any tendencies to drift. Under these conditions the tests can be considered to have been conducted at the temperature of the drilling water and this fluctuated no more than 0·5°C during any one complete test. Using a reasonable coefficient of thermal expansion for an igneous rock of 7 ppm/°C from CLARK [12], the maximum error introduced by temperature variations is less than the basic measuring error of the instrumentation and no correction for temperature effects was considered necessary.

EXPERIMENTAL RESULTS

Results of three of the tests are given in Figs. 5–7. Figure 5 shows the curves of strain relief with overcoring depth when the stresses applied to the block are: vertical = 1000 lb/in^2, longitudinal = 0 and horizontal = 0 Figure 6 shows the strain relief pattern when the applied stresses are: vertical = 1000 lb/in^2, longitudinal = 1000 lb/in^2 and horizontal = 0. The differences are apparent and significant even though the stresses applied in the plane

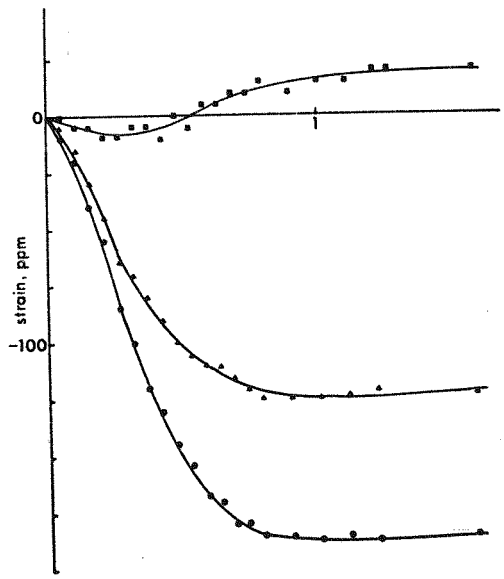

FIG. 5. Strain on end face of borehole vs. depth of relief z/a; vertical stress equals 1000 lb/in^2, horizontal stress equals zero, longitudinal stress equals zero.

● Vertical strain gauge;
▲ 45° strain gauge;
■ Horizontal strain gauge.

of the gauge are the same. Figure 7 is the strain relief pattern for a test in which the only applied stress was parallel to the borehole and equal to 1000 lb/in^2. Subtraction of the values shown in Fig. 7 from the corresponding values in Fig. 6 yields Fig. 8 which may be compared with the results of the uniaxial test shown in Fig. 5.

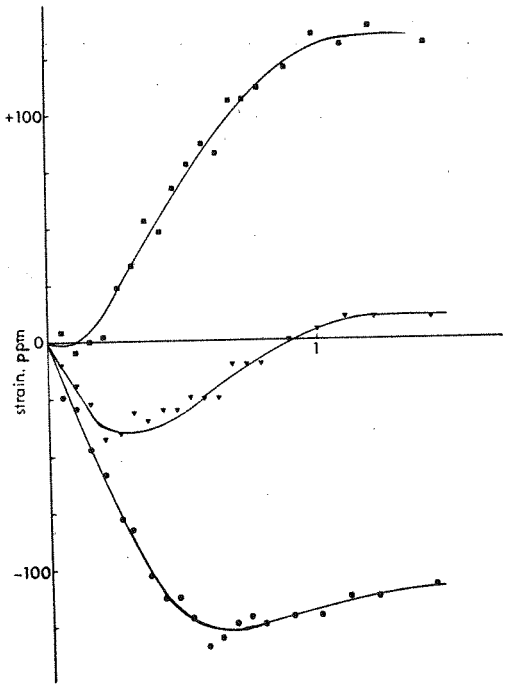

FIG. 6. Strains on end face of borehole vs. depth of relief, z/a; vertical stress equals 1000 lb/in^2, horizontal stress equals zero, longitudinal stress equals 1000 lb/in^2.

● Vertical strain gauge;
▲ 45° strain gauge;
■ Horizontal strain gauge.

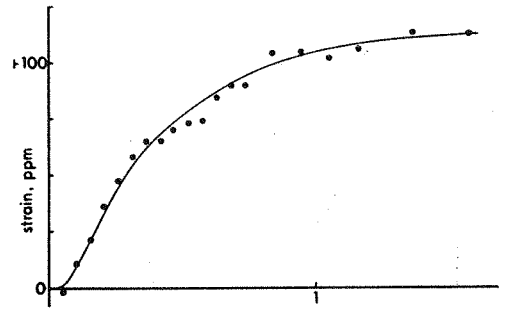

FIG. 7. Strains on end face of borehole vs. depth of relief, z/a; vertical stress equals zero, horizontal stress equals zero, longitudinal stress equals 1000 lb/in^2. Averages of all three approximately equal strain readings.

Leeman converted measured strain into rock stresses in the end face of the borehole by means of the following relationships:

$$\sigma_x = [E/(1-\mu^2)]\,[\epsilon_x + \mu\epsilon_y]$$
$$\sigma_y = [E/(1-\mu^2)]\,[\epsilon_y + \mu\epsilon_x] \quad . \tag{3}$$

He then used a stress concentration factor of 1·53 to find the primary stresses in the rock away from the borehole [4, 5]. Using this method of analysis and values of $7{\cdot}4 \times 10^6$ lb/in^2

and 0·223 for Young's modulus and Poisson's ration, the strains from the test with only an applied vertical stress of 1000 lb/in^2 in the plane of the gauge would indicate rock stresses of 955 lb/in^2 vertical compression and 85 lb/in^2 horizontal compression which should be acceptable accuracy. The strain values from the test in which the applied stresses were 1000 lb/in^2 vertical and 1000 lb/in^2 parallel to the borehole analysed in this manner, however, would

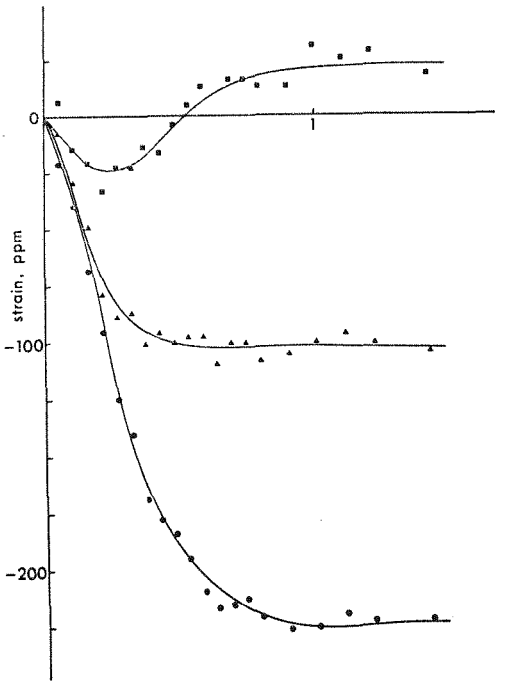

FIG. 8. The result of subtracting the values in Fig. 7 from each of those given in Fig. 6 at each depth of stress relief.

● Vertical gauge;
▲ 45° gauge;
■ Horizontal gauge.

indicate primary rock stresses of 385 lb/in^2 vertical compression and 530 lb/in^2 horizontal tension. If the strain gauge rosette is solved for the maximum and minimum principal strains and their orientation in the plane of the rosette by any of the standard techniques [13], and these values substituted into equations (2) (replacing ϵ_r, σ_r', and σ_θ' by ϵ_{max}, ϵ_{min}, σ_{max}, and σ_{min} as appropriate) along with the known longitudinal stress of 1000 lb/in^2, the principal stresses indicated in the block are 1060 lb/in^2 vertical compression and 160 lb/in^2 horizontal compression. This, of course, is impossible in the practical situation as in general the longitudinal stress will not be known, but it indicates how well the stresses in the rock correspond to the photoelastic solution. A similar effect can be achieved by graphically subtracting the results of the test with only a longitudinal stress shown in Fig. 7 from the test with combined stresses. This has been done in Fig. 8 and these strain values yield estimates of the rock stress of 1100 lb/in^2 vertical compression and 190 lb/in^2 horizontal compression.

The tests consistently indicate a small horizontal compressive stress although none was ever applied. This may be due to friction effects of the loaded surfaces as suggested by

LEEMAN [4], uncertainty in the proper value of Poisson's ratio to use in reducing the data, or measurement errors in the magnitude of the horizontal strain component since the horizontal strain was only 4–5 times the basic reading error of the measuring system in some of these tests.

DISCUSSION

From these experimental results it is clear that measurement of stress underground by strain relief techniques at the flattened end of a bore hole is not, in general, a simple straightforward process. In the first place, the effect of a stress acting parallel to the borehole axis is not negligible unless the stress in that direction is negligible. The effect of this longitudinal stress is always to reduce the estimate of compressive stresses acting in the plane of the gauge and in fact can even falsely indicate the presence of tensile stresses in this plane when none actually exist.

A second problem is that the stress concentration factors determined by GALLE and WILHOIT [10] are valid only when the borehole axis coincides with one of the principal stress directions. VAN HEERDEN [14] describes tests in which boreholes were drilled into steel cubes at various angles up to 25° from the principal directions. Strain gauge rosettes were cemented to the end faces of these holes and the cubes loaded in uniaxial compression. He found errors introduced up to 27·9 per cent assuming a stress concentration factor of 1·5 at the end of the borehole.

If the direction of one of the principal stresses can be found, measurements made on the end of a borehole drilled in this direction will yield the other principal stress directions. A second measuring hole then drilled in one of these principal directions will yield enough equations of the type given in equation (2) to solve for the magnitudes of the three principal stresses. (Four equations can be written, one for the maximum and minimum principal strain in each borehole face.)

It is tempting to assume that one of the principal stresses acts vertically. FAIRHURST [15], however, has pointed out that this may not in general be a valid assumption. There have not as yet been enough complete underground stress determinations reported to warrant making any general assumptions of this nature.

JAEGER and COOK [16] have described a technique for determining principal stress directions. It consists essentially of placing a cylindrical pressure cell in a borehole and pressurizing the cell until the rock around it has failed. The cell and surrounding fractured rock is then overcored with a large diameter bit and the orientation of the rock fractures measured. The fractures are presumed to be perpendicular to the direction of least principal stress. The method is simple and direct but it requires that the rock be isotropic in terms of its tensile strength as well as its elastic properties.

A third problem is the question of how to determine the elastic moduli of the rock. The particular block of rock used in these experiments appears to be unusually sound, free from flaws of any description, and uniform in grain size and composition throughout. No better experimental rock material could be expected. Modulus determinations were made in cores taken from the rock (length/diameter 2·6/1) in unconfined compression. Longitudinal strain was determined by averaging the readings of 3 electric resistance strain gauges bonded to the rock and equally spaced about the circumference. Transverse strain was determined by averaging the results from two gauges placed perpendicular to the core axis at its midheight and together covering about 40 per cent of the circumference. All strain gauge readings were corrected for transverse sensitivity using the numerical factors and methods given by WU [17].

Repeated loading cycles were made to 20 per cent of the unconfined compressive strength of this rock. Ends of the specimens were lapped flat and parallel to better than 0·0001 in. The specimens were loaded through a spherical seat. Tests were conducted both with dry, bare, unlubricated end conditions and with the specimen ends lubricated with paper and graphite. All tests (within the strain measuring repeatability of $\pm$ 5 ppm) yielded identical, linear, stress–strain curves with no initial curvature or hysteresis evident. Typical test results are shown in Fig. 9. The values of the elastic moduli determined by these methods were, Young's modulus = 8·28 $\times$ 10^6 lb/in^2 and Poisson's ratio = 0·272.

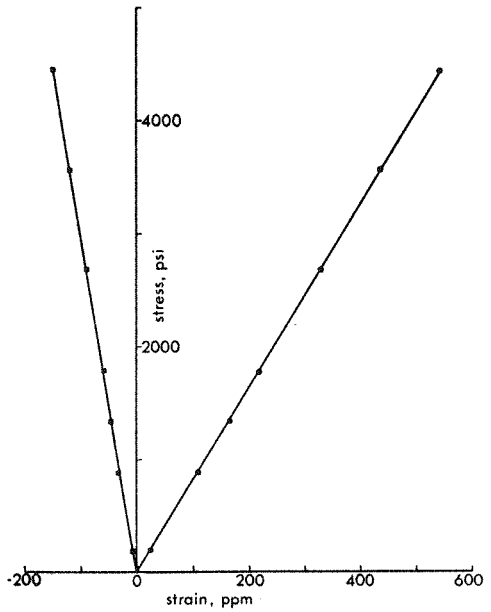

FIG. 9. Stress–strain curves for trachyte in unconfined compression.
● Axial strain,
■ Circumferential strain.

The rock in a strain relief test usually undergoes tensile strains in at least one direction. To test the possiblity of differing elastic moduli under combined tensile and compressive forces, the moduli were also determined on specimens prepared from the strain relieved rock cores and loaded in diametral compression. The elastic theory has been set out by HONDROS [18]. Strain was measured with small foil strain gauges (gauge length/specimen diameter = 0·06/1) placed on both faces of the specimen. Plain stress conditions were assumed. The rock was loaded with platens ground to give a 15° arc of contact and a cylindrical seat was used with its axis of rotation perpendicular to the core axis. The moduli determined by this method were Young's modulus = 7·4 $\times$ 10^6 lb/in^2 and Poisson's ratio = 0·223. Since the strains induced by the overcoring procedure were in the main tensile in these experiments the values of the elastic moduli determined by the diametral compression tests were used to convert strain gauge readings from the strain cells to stresses. There is an additional practical advantage here in that diametral compression specimens are easily prepared from the strain relief cores so that modulus measurements can be made directly on the particular volume of rock in question. The moduli determined by the diametral compression

tests also, when used in equations (2) or (3), yield stress values more closely approximating the applied stresses in these experiments than did the elastic moduli determined in unconfined compression.

Acknowledgements—This research has been supported by an Australian National University Research Scholarship and a National Science Foundation Fellowship held by the author. The author has been privileged to see recent unpublished work by the Snowy Mountains Hydroelectric Authority and the Rock Mechanics Section of Mt. Isa Mines Ltd., Professor J. C. JAEGER of the Australian National University has given his continuous encouragement and support.

REFERENCES

1. LIEURANCE R. S. *Stresses in Foundation at Boulder Dam*, Tech. Memo. 346, U.S. Bureau of Reclamation Denver, 12 pp. (1933).
2. MOHR H. F. Measurement of rock pressure, *Mine Quarry Engng* **22**, 178–189 (1956).
3. OLSEN O. J. Measurement of residual stress by the strain relief method, *Color. Sch. Mines*, **52**, 185–204 (1957).
4. LEEMAN E. R. The measurement of stress in rock, Parts I, II, and III, *Jl S. Afr. Inst. Min. Metall.* **65**, 45–114; 254–285 (1964).
5. LEEMAN E. R. Rock stress measurements using the trepanning stress-relieving technique, *Mine Quarry Engng* **30**, 250–255 (1964).
6. ALEXANDER L. G. Private communication (1965).
7. HETENYI M. *Handbook of Experimental Stress Analysis*, Chap. 11, Wiley, New York (1950).
8. ROBERTS A., EMERY, C. L., CHAKRAVARTY P. K., HAWKES I. and WILLIAMS F. T. Photoelastic coating technique applied to research in rock mechanics, *Trans. Inst. Min. Metall.* **65**, 408–418 (1965).
9. HAWKES I. and MOXON S. The measurement of *in-situ* rock stress using the photoelastic gauge and the core-relief technique, *Int. J. Rock Mech. Min. Sci.* **2**, 905–919 (1965).
10. GALLE E. M. and WILHOIT J. C. Stresses around a wellbore due to internal pressure and unequal principal geostatic stresses, *Soc. Petrol. Eng. Jl.* **2**, 145–155 (1962).
11. HOSKINS E. R. An investigation of the flatjack method of measuring rock stress, *Int. J. Rock Mech. Min. Sci.* **3**, 249–264 (1966).
12. CLARK S. P. *Handbook of Physical Constants Revised Edition*, Memoir 97 of the Geological Society of America, Chap. 7, pp. 78–93 (1966).
13. JAEGER J. C. *Elasticity, Fracture and Flow*, Chap. 10, 2nd edn. Methuen, London (1962).
14. VAN HEERDEN W. L. Contribution to Discussion of a paper by E. R. Leeman, The measurement of stress in rock, *Jl. S. Afr. Inst. Mid, Metall.* **65**, 418–423 (1965).
15. FAIRHURST C. Measurement of *in situ* rock stresses with particular reference to hydraulic fracturing, *Rock Mech. Eng. Geol.* **II**, 129–147 (1964).
16. JAEGER J. C. and COOK N. G. W. Theory and application of curved jacks for measurement of stresses, in *State of Stress in the Earth's Crust*, pp. 381–395, Elsevier, New York, (1964).
17. WU C. T. Transverse sensitivity of bonded strain gages, *Exp. Mech.* **2**, (1962).
18. HONDROS G. The evaluation of Poisson's ratio and the modulus of materials of a low tensile resistance by the Bazilian (indirect tensile) test with particular reference to concrete, *Aust. J. Appl. Sci.* **10**, (3), 243–268 (1959).